

https://dspace.org/

Electrical transient interaction between transformers and the power system: case study of an onshore wind farm

Banda, Cedric Amittai

2016

http://hdl.handle.net/10539/22657

Banda, Cedric Amittai (2016) Electrical transient interaction between transformers and the power system: case study of an onshore wind farm, University of the Witwatersrand, <http://hdl.handle.net/10539/22657>

Downloaded from a DSpace repository. https://dspace.org/

Electrical Transient Interaction between Transformers and the Power System: Case Study of an Onshore Wind Farm

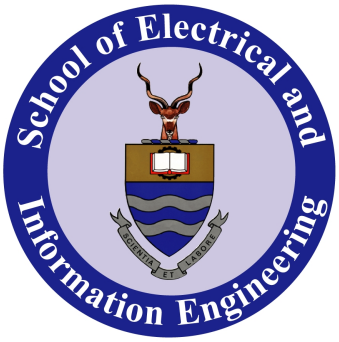

Cedric Amittai Banda

EPPEI CENTRE FOR HVAC

Faculty of Engineering

University of the Witwatersrand

A dissertation submitted to the Faculty of Engineering and the Built Environment, University of the Witwatersrand, in fulfilment of the requirements of the degree of

Master of Science in Electrical Engineering

June 2016

Declaration

I declare that this dissertation is my own unaided work. It is being submitted for the Degree of Master of Science in Engineering in the University of the Witwatersrand, Johannesburg. It has not been submitted before for any degree or examination in any other University.

Signature 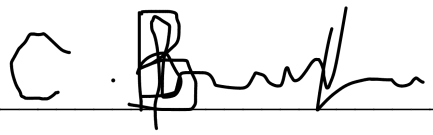

Signed this on the 10th day of June 2016

This is for the Bandas: Daniel, Pam, Nisbert and Theresa. We finally here!

Acknowledgements

I would like to express my deepest gratitude to my supervisor and mentor, Dr. John M. Van Coller, for his excellent guidance, caring, patience, and providing me with an excellent atmosphere for doing research. Would like to acknowledge the contributions of Eskom Power Plant Engineering Institute (EPPEI) for funding of the Masters Program. Without EPPEI this would not have been possible. Would also like to gratefully acknowledge the contributions of Lee Mbenge and Jorge Del Porzo from Actom Distribution Transformers for allowing me to do my research at Actom and all the different transformers we tested. Lastly would like to thank my friends for being with me through all the tough times.

Abstract

Through the Renewable Energy Independent Power Producer Procurement Program (REIPPPP) the South African government has awarded opportunities for growth of renewable energy through bidding rounds. Round 1 saw a total capacity of 397 MW being awarded to independent power producers (IPP). Subsequently Rounds 2, 3 and 4 each had a total capacity of 333 MW auctioned. The advent of renewables on the market has brought upon its own associated problems with regards to power quality issues and failure of HV equipment. This thesis will address transformer failures that occurred at an onshore wind farm. The nature of the transformer failures suggest transient overvoltages are mainly to blame. A comparison between transformer failures in South African and Brazil suggest a common failure mechanism. The failure starts with an inter-turn insulation failure which propagates to an inter-layer insulation. In worst cases the failure mode results in a puncture through the LV-HV barrier and punctures through the LV winding. An extensive literature review was performed to find appropriate methods to predict and explain the failure mode in wind turbine LV-MV step-up transformers. Of the different models which were reviewed the most notable was the Multi-conductor Transmission Line (MTL) model which was chosen as the preferred model due to its ability to predict the inter-turn/inter-layer voltage stresses. Verification of the developed MTL model by the author was then compared to published results of an MTL model of a disc winding transformer. The results of the comparison revealed a relatively good agreement between the developed model and the published model. The application of the MTL model to represent the voltage stresses in transformer windings was then extended to two specially constructed wind turbine step-up transformer prototypes. The prototypes differed in the winding arrangement of the MV coil. The other used two separate MV coils separated by an oil gap whereas the other had a single MV coil. To validate the model accuracy, a comparison of measured results versus those obtained analytically was done for the two prototypes. The analytical and measured results also had a relatively good agreement for the two prototypes considered. Measurement of

switching surges was done on-site at the wind farm to understand the nature of the transients. Using analysis tools such as FFT and frequency domain severity factor it was possible to understand the impact the nature of these transients would pose on the transformer insulation. Different mitigation techniques which can be used to alleviate the transient overvoltages to within safe levels were investigated. The most notable protection device considered was the RL choke device which offered a significant reduction of the pre-strikes and is virtually transparent under power frequency operation.

Contents

Contents v

List of Figures ix

List of Tables xiii

List of Acronyms xiii

1 Introduction 1

1.1 Case Study: Brazil experience 2
1.2 Case study: South African experience 6
1.3 Research Motivation and research questions 9
1.4 Contributions 9
1.5 Dissertation Outline 10
1.6 Conclusion 10

2 Literature Review 11

2.1 Chapter Overview 11
2.2 Transformers and Circuit Breaker Induced Transients 11
2.3 Difficulties in High Frequency modelling 13
2.4 Unified terminal and internal transformer model 14
2.5 Discussion and Conclusion 14

3 Transformer Modelling 16

3.1 Chapter Overview 16
3.2 Existing Transformer Models 16
3.3 Black Box Model 17
3.3.1 Admittance Matrix by Measurements 18

3.3.2 Black Box model admittance matrix derived from White Box model . . 19
3.4 White Box models . . . 19
3.4.1 RLC ladder Network model . . . 19
3.4.2 Multi-transmission Line (MTL) model . . . 21
3.5 Grey Box models . . . 24
3.5.1 Generic Phase Model of the Transformer . . . 25
3.6 Discussion on appropriate model to address the research questions and Conclusion 27

4 Parameter Determination 28
4.1 Chapter Overview . . . 28
4.2 MTL Model flowchart . . . 28
4.3 Parameter extraction . . . 29
4.3.1 Calculation of the C (capacitance) matrix . . . 30
4.3.2 Calculation of the G (conductance) matrix . . . 32
4.3.3 Calculation of the R (resistance) matrix . . . 33
4.3.4 Calculation of the L (inductance) matrix . . . 34
4.4 Conclusion . . . 35

5 Model Verification 36
5.1 Chapter Overview . . . 36
5.2 Parameters of the transformer winding . . . 36
5.3 Model comparison and verification . . . 38
5.3.1 Sweep Frequency response of turn 20, turn 40 and turn 60 . . . 38
5.4 Discussion . . . 42
5.5 Conclusion . . . 44

6 Resonance Analysis: Verification of High Frequency Model of Transformer 45
6.1 Chapter Overview . . . 45
6.2 Test Equipment and Measurement of Resonance . . . 45
6.3 Stacked core transformer prototypes . . . 48
6.3.1 Split round winding prototype transformer . . . 48
6.3.2 Single round winding prototype transformer . . . 50
6.4 Comparison of Measured and Calculated Results . . . 51
6.4.1 Split round winding prototype transformer . . . 51
6.4.2 Non-split round winding prototype transformer . . . 55
6.4.2.1 Full layer measurements . . . 55
6.4.2.2 Start to middle of winding measurements . . . 58

6.5 Comparison of the Resonance Performance of Split and Non-Split MV Windings 59
6.6 Discussion and Conclusion 61

7 Switching Surges and Severity Factors 63
7.1 Chapter Overview 63
7.2 Measurement of Switching Transients 64
7.2.1 Energizing the transformer on no-load 64
7.2.2 Disconnection of the transformer on no-load 69
7.2.3 Frequency domain analysis 69
7.3 Severity Factor 72
7.3.1 Implementation and analysis of the Frequency Domain Severity Factor (FDSF) 72
7.4 Discussion and Conclusion 76

8 Insulation Co-ordination 77
8.1 Chapter Overview 77
8.2 Insulation coordination 77
8.3 Design Insulation Level (DIL) 78
8.4 Mitigation techniques against fast transients 79
8.4.1 Traditional methods of suppressing fast transients 79
8.4.1.1 RC Snubbers 80
8.4.1.2 Surge Capacitors 81
8.4.1.3 Surge Arresters 81
8.4.2 RL Choke device 81
8.5 Special winding designs 90
8.6 Discussion and Conclusion 90

9 Conclusions, Future Work and Recommendations 91
9.1 Chapter Overview 91
9.2 Assessment of the outcome of the research questions 91
9.2.1 Research Question 1 91
9.2.2 Research Question 2 92
9.2.3 Research Question 3 92
9.2.4 Research Question 4 92
9.3 Future work and recommendations 93
9.3.1 Time Domain Severity Factor (TDSF) 93
9.3.2 Condition monitoring 95

Appendix A - (Supplement of Chapter 4) **96**
.1 Calculation of Capacitance Matrix 96
.2 Parameters of Split MV winding Transformer 101
.3 Parameters of Non-split MV winding Transformer 102

Appendix B - Publications **103**
.4 List of attached publications 103

References **140**

List of Figures

1.1 Failed SE Ipatinga 1 Autotransformer 230/161/13.8 kV (courtesy of Angelica da Costa Oliveira Rocha) . . . 4
1.2 TresMarias Substation: Failed 25 MVA, 13.8/289 kV step-up transformer (courtesy of Angelica da Costa Oliveira Rocha) . . . 5
1.3 TresMarias Substation: Failed 25 MVA, 13.8/289 kV step-up transformer (courtesy of Angelica da Costa Oliveira Rocha) . . . 5
1.4 Failed winding with inter-turn insulation severely damaged (courtesy of Transformer Manufacturer) 6
1.5 Burn through the HV to LV barrier (courtesy of Transformer Manufacturer) . . . 7
1.6 Burning of first layer of LV foil winding (courtesy of Transformer Manufacturer) . . . 7

3.1 Black Box model of a transformer (measurement procedure for the jth column of the admittance matrix from [1]) . . . 18
3.2 RLC ladder network model of transformer winding from [2] . . . 20
3.3 Multi-conductor Transmission Line model . . . 21
3.4 Generic phase model of a transformer adapted from [3] . . . 25
3.5 Grey box test set-up layered modelling approach adapted from [4] . . . 26

4.1 MTL model flow chart adapted from [5] . . . 29
4.2 Parameters needed for computation of fast transients . . . 30
4.3 tan δ versus frequency (10 kHz $< f <$ 1 MHz) . . . 33

5.1 Measurement setup of a core-type transformer winding adapted from [5]. . . . 37
5.2 Comparison between developed MTL model and Sun et. al MTL model (adapted from [5]) : Amplitude of transfer function between turn 20 of Figure 5.1 and input. . . . 39
5.3 Comparison between developed MTL model and Sun et. al MTL model (adapted from [5]) : Amplitude of transfer function between turn 40 of Figure 5.1 and input. . . . 40

5.4 Comparison between developed MTL model and Sun et. al MTL model (adapted from [5]) : Amplitude of transfer function between turn 60 of Figure 5.1 and input. 41
5.5 Magnitude of transfer function of turn 20 relative to the input (taking into account proximity effects) 43

6.1 Test equipment used 46
6.2 Test Setup 46
6.3 Test equipment setup 47
6.4 Axisymmetric view of the first prototype transformer. 49
6.5 Split round winding prototype transformer. 49
6.6 Axisymmetric view of the second prototype transformer 50
6.7 Non-split round winding prototype transformer 50
6.8 Resonance voltage ratio across Layer 1 [measured between tap 1 and tap 2 of Figure 6.4] versus calculated. 51
6.9 Resonance voltage ratio across Layer 15 [measured between tap 32 and tap 33 of Figure. 6.4] versus calculated. 52
6.10 Resonance voltage ratio across Layer 1 [measured between tap 33 and tap 34 of Figure. 6.4] versus calculated. 52
6.11 Resonance Voltage Ratio (RVR) distribution in layers 1 - 4 53
6.12 Resonance Voltage Ratio (RVR) distribution in layers 5 - 8 53
6.13 Resonance Voltage Ratio (RVR) distribution in layers 9 -12 54
6.14 Resonance Voltage Ratio (RVR) distribution in layers 13 - 16 54
6.15 Resonance voltage ratio (RVR) across layer 4 [measured between tap 6 and tap 7 of Figure. 6.6] versus calculated. 55
6.16 Resonance voltage ratio (RVR) across layer 5 [measured between tap 7 and tap 8 of Figure. 6.6] versus calculated. 56
6.17 Resonance voltage ratio (RVR) across layer 6 [measured between tap 8 and tap 9 of Figure. 6.6] versus calculated. 56
6.18 Resonance voltage ratio (RVR) across layer 7 [measured between tap 9 and tap 10 of Figure. 6.6] versus calculated. 57
6.19 Resonance voltage ratio (RVR) across layer 8 [measured between tap 10 and tap 11 of Figure. 6.6] versus calculated. 57
6.20 Resonance voltage ratio (RVR) across the start to middle of layer 2 [measured between tap 2 and tap 3 of Figure. 6.6] versus calculated. 58

6.21 Resonance voltage ratio (RVR) across the start to middle of layer 3 [measured between tap 4 and tap 5 of Figure. 6.6] versus calculated. 59
6.22 Comparison of the sweep frequency response of layer 1 for the transformers in Figures 6.5 and 6.7. 60
6.23 Comparison of the sweep frequency response of layer 15 for the transformers in Figures 6.5 and 6.7. 60
6.24 Comparison of the sweep frequency response of layer 16 for the transformers in Figures 6.5 and 6.7. 61

7.1 Measurement setup on a wind turbine transformer (Pad-mounted Transformer). 64
7.2 Block diagram of test setup. 65
7.3 Measured pre-strike behaviour at 12:45 66
7.4 Measured pre-strike behaviour at 13:13 66
7.5 Time expansion of measured pre-strike behaviour at 13:13 67
7.6 Measured pre-strike behaviour at 13:15 67
7.7 Time expansion of measured pre-strike behaviour at 13:15 68
7.8 Measured pre-strike behaviour at 13:26 68
7.9 Measured waveform during transformer disconnection 69
7.10 FFT analysis for the measured transient at 12:45 70
7.11 FFT analysis for the measured transient at 13:13 70
7.12 FFT analysis for the measured transient at 13:15 71
7.13 FFT analysis for the measured transient at 13:26 71
7.14 Magnitude spectrum for transient signal in Figure 7.8 and standard lightning and chopped lightning waveforms. 73
7.15 Comparison of ESD for transient signal in Figure 7.8 and ESD for standard test waveforms in Figure 7.14 74
7.16 FDSF for the measured transient in Figure 7.4. 74
7.17 FDSF for the measured transient in Figure 7.6. 75
7.18 FDSF for the measured transient in Figure 7.8. 75

8.1 RC Snubber network 80
8.2 Physical realization of VFT suppressing devices installed on a transformer . . . 82
8.3 Impedance vs Frequency plot of RL choke device adapted from [6] 83
8.4 FDSF for the measured transient in Figure 7.4 before and after RL choke device installation. 84
8.5 FDSF for the measured transient in Figure 7.6 before and after RL choke device installation. 84

8.6 FDSF for the measured transient in Figure 7.8 before and after RL choke device installation. 85
8.7 RL choke device implementation in ATP DRAW 85
8.8 50 Hz transparency of RL choke device 86
8.9 Unprotected terminal phase voltages measured using the setup in Figure 7.1 . . 87
8.10 Protected terminal phase voltages using choke device to suppress the measured transients in Figure 8.9 87
8.11 Unprotected terminal phase voltages measured using the setup in Figure 7.1 . . 88
8.12 Protected terminal phase voltages using choke device to suppress the measured transients in Figure 8.11 88
8.13 Unprotected terminal phase voltages measured using the setup in Figure 7.1 . . 89
8.14 Protected terminal phase voltages using choke device to suppress the measured transients in Figure 8.13 89

9.1 Prototype transformer to be tested 94
9.2 Final prototype transformer 94

3 Capacitance top view 97
4 Prototype transformer 98

List of Tables

1.1 Part winding resonance of the winding 8

3.1 Selection criteria used to pick the proper model 27

5.1 Main Parameters of the winding 37

8.1 Factors for conversion to one-minute (r.m.s.) power frequency level adapted from [7]. 78

8.2 Test voltage levels and the impulse ratios adapted from [7], [8]. 78

1 Calculated Capacitors for Transformer with split MV winding shown in Figure 6.5 in Chapter 6.3.1 99

2 Calculated Capacitors for Transformer with non-split MV winding shown in Figure 6.7 in Chapter 6.3.2 100

3 2700kVA three phase 33000/690V Dyn11 three limb mitre core transfomer with split MV winding shown in Figure 6.5 in Chapter 6.3.1 101

4 2700kVA three phase 33000/690V Dyn11 three limb mitre core transfomer with non-split MV winding shown in Figure 6.7 in Chapter 6.3.2 102

List of Acronyms

ANNs	Artificial Neural Networks
ATP	Alternative Transient Program
BIL	Basic Insulation Level
CFM	Constrained Fitting Methods
CI	Chopped Impulse
DGA	Dissolved Gas Analysis
DIL	Design Insulation Level
EMTP	ElectroMagnetic Transients Program
ESD	Energy Spectral Density
FA	Furan Analysis
FDSF	Frequency Domain Severity Factor
FRA	Frequency Response Analysis
FRP	Fast Residue Pertubation
LI	Lightning Impulse
LTAC	Line terminal AC withstand test
MV	Medium Votage
MTL	Multi-conductor Transmission Line
RAF	Resonance Amplification Factor
RVR	Resonance Voltage Ratio
SDP	Semi-Definite Programming
SI	Switching Impulse
SIL	Switching Impulse Level
TDSF	Time Domain Severity Factor
TRV	Transient Recovery Voltage
VCB	Vacuum Circuit Breaker
VFT	Very Fast Transients
UFM	Unconstrained Fitting Methods
WG	Working Group

Chapter 1

Introduction

The global energy crisis and pressure from environmentalists with regards to global warming has put pressure on governments to find green sources of energy. Renewable energy provides an alternative to alleviate this energy demand. In South Africa the coastal regions along the Eastern and Western Cape are blessed with high wind speeds allowing construction of wind farms a feasible option. This has resulted in wind farms being constructed such as Coega, Cookhouse, Jeffreys Bay and Sere wind farm [9]. The wind turbine models being used is either the Vestas or the Siemens type. Due to different operators who have been tasked with running of these wind farms, at the present moment there is no strict guideline which governs how the wind farms are operated. A persistent problem with wind generation is when the wind speed decreases below a threshold value for electricity generation, the wind turbine tend to consume power from the grid. A common technique to alleviate this problem is to disconnect the wind turbine transformer from the grid. This is accomplished by switching either the MV or LV circuit breaker. When the wind speed is sufficient to allow generation of electricity, the wind turbine transformer is switched back into the grid. The constant switching of wind turbine transformers presents voltage transients problems which have been found to cause transformer insulation failure. Vacuum circuit breakers are a commonly used switching device used in Medium Voltage (MV) networks [10]. However the constant switching of vacuum circuit breakers [11], [12] can result in voltage transients which may lead to re-ignitions or re-strikes (which occur during contact opening) and pre-strikes (which occur during contact closing). In wind farms, due to the high capacitance collector cable network there is a high probability that system-initiated transients will contain oscillatory voltage waveforms at the transformer terminals [13], [14]. These voltage transients to which the transformer is exposed to contains a spectrum of superimposed oscillations with different frequency components and may exhibit high du/dt values and be repetitive in nature. As such any manufactured transformer has a

natural resonant frequency where if excited will result in [4]:

- The voltage distribution across the winding being non-uniform.
- The currents or voltages inside the winding reach values greater than the steady state proportion of a harmonic excitation signal.

In transformers resonance can be classified as either being internal or external (terminal) resonance. Internal winding resonance occurs when a frequency component of the incoming transient matches one of the several natural resonant frequencies of the transformer winding. This can then lead to the development of very high internal voltages inside the transformer. These internal voltages can exceed the insulation withstand capability of the transformer by resonant voltage build-up. The effect of resonant voltage build-up can be shown in [15] where it signifies the constant increase in voltage as resonance occurs. Also a flashover can occur from the windings to the core or in between the turns [16]. If the transient is repetitive accelerated ageing of the insulation could occur reducing the insulation withstand capability. However it should be noted that internal winding resonances will not necessarily result in immediate breakdown, but may result in partial discharges, which will further aid in insulation degradation and ultimately failure [11]. Terminal resonance occurs due to cable and transformer interaction such that the natural frequency of the supplying cable matches the natural frequency of the transformer [17]. Hence the adjacent network becomes of importance to the transient interaction i.e. the length of transformer feeder lines will directly influence the dominating frequency of the oscillatory transients. In offshore wind farms this is common with wind turbine transformers where energization may result in cable transformer resonant transients with the supplying cable [18].

1.1 Case Study: Brazil experience

A number of transformer failures occurred in the Brazilian transmission system which was reported by [19], [20]. The failures occurred over a period of ten years. Different cases were investigated and documented. Only the cases where the transformers failed due to either transient overvoltages or frequent switching will be reviewed. The importance of this review is the experience gained by Brazilian utilities apply to the South African experience which will be presented in Section 1.2. The following cases are presented [19]:

Case 1 :Insulation failures occurred on two 400 MVA 500/345/13.8 kV auto-transformers in 1995. The cause of the failure was unknown and the transformers failed a few days from each other. An intensive investigation was carried out by the utility to explain the cause of failure.

The common thinking after the exhaustive investigation yielded that the transformers failed due to the occurrence of internal overvoltages. The development of the internal overvoltages was attributed to the frequent switching operations at the substation.

Case 2: A flashover occurred on the LV side bushing of a 55 MVA 230/138/13.8 kV transformer during a no-load switching event. The flashover lead to the formation of a short-circuit to earth. The switching was done on the HV side of the transformer using a bus tie breaker. The LV side of the transformer which was operating in an open condition had no protection installed i.e. lightning arresters or RC snubbers. An investigation was carried out to determine the root cause of the failure. The investigation attributed the failure to a dominant frequency of the transient voltage occurring on the HV side being close to one of the calculated winding resonant frequencies. Hence internal winding resonance occurred.

Case 3: Insulation failures in single phase transformers have been documented since 555 MVA step-up transformer banks started their operation in 1988. The failure mechanism involved short-circuits between turns in the HV winding, between HV and LV windings, and LV winding to ground. Sweep frequency response measurements showed that the winding natural resonant frequencies coincided with one or more of the dominant frequency of the incoming transient voltage. This resulted in local amplification of the voltage between turns leading to the short circuit conditions that caused dielectric failure on the 16 kV terminals.

Case 4: In 1994 a 378 MVA 13.8/550 kV step-up transformer failed. An analysis was carried out by different engineers from the utility and research centres to try and explain the phenomena surrounding the failure. After simulations and extensive field measurements the failure was attributed to very fast transients generated to due switching operation in the 550 kV GIS.

Figures. 1.1, 1.2 and 1.3 show the failure mechanism for some of the documented case studies. A common criteria from the Brazilian experience that will relate to the South African is:

- Transformers were exposed to frequent switching by circuit breakers.
- The constant switching of transformers by circuit breakers generated transient voltages on transformer terminals.
- The transient voltages were composed of a spectrum of superimposed oscillations with different frequency components.
- Internal winding resonance most probable cause of transformer failures exposed to frequent



Figure 1.1: Failed SE Ipatinga 1 Autotransformer 230/161/13.8 kV (courtesy of Angelica da Costa Oliveira Rocha)

switching.

- Failure mechanism occurred between turn-turn, between disks or layers, between HV and LV winding and LV winding to ground.



Figure 1.2: TresMarias Substation: Failed 25 MVA, 13.8/289 kV step-up transformer (courtesy of Angelica da Costa Oliveira Rocha)



Figure 1.3: TresMarias Substation: Failed 25 MVA, 13.8/289 kV step-up transformer (courtesy of Angelica da Costa Oliveira Rocha)

1.2 Case study: South African experience

The investigated transformer was a 2.7 MVA 0.690/33 kV step up wind turbine transformer. The transformer had a history of being constantly switched on the MV side. During low wind speeds, the transformer was de-energized by switching the vacuum circuit breaker (VCB) on the MV side. When the wind speeds picked up to allow generation of electricity, the transformer was energized by switching the VCB on the MV side.



Figure 1.4: Failed winding with inter-turn insulation severely damaged (courtesy of Transformer Manufacturer)

Figure 1.4 shows the failed transformer unit when it was unwound at the transformer factory. The failed transformer showed a burn in the first layer with the inter-turn insulation severely damaged. There was substantial distortion of the first and second layer of the MV winding as seen in Figure 1.4 . Further examination of the winding revealed a burn through the MV to LV winding barrier had occurred as can be seen in Figure 1.5.
The fault was also sufficient to cause a puncture through the first layer of the LV foil winding as shown in Figure 1.6. It interesting to note that from Figure 1.4, it is difficult to predict if the failure started as an inter-turn or inter-layer fault due to the burning of the oil paper insulation. However the failure mechanism had sufficient magnitude to cause substantial distortion of the first two layers and create a puncture through the LV foil winding.

Part winding resonance tests were conducted on one of the undamaged windings of the wind turbine transformer. The goal was to determine the winding's natural resonant frequencies by measurements. As previously mentioned, dangerous overvoltages can be imposed on the transformer terminals. For the impinged voltage to be of concern, it must in addition to

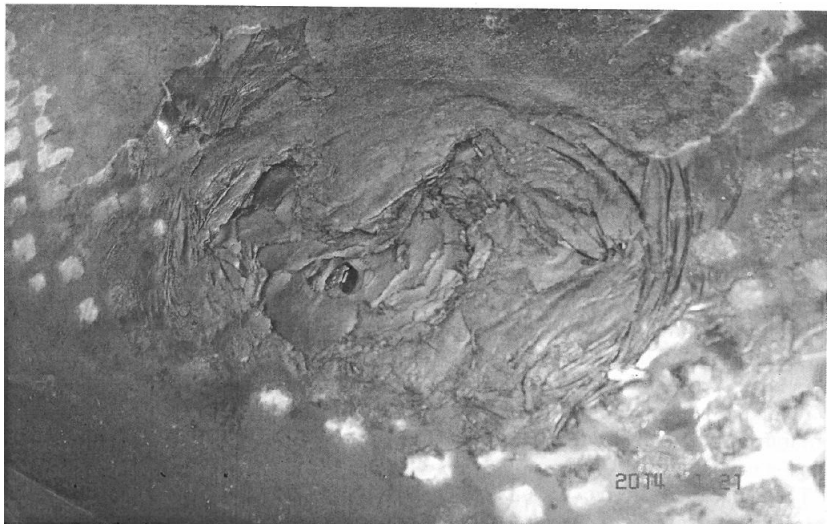

Figure 1.5: Burn through the HV to LV barrier (courtesy of Transformer Manufacturer)



Figure 1.6: Burning of first layer of LV foil winding (courtesy of Transformer Manufacturer)

having a dominant frequency component, be of sufficient magnitude that will match a peak in the transformer voltage transfer from the given terminal to some internal point along the winding [4]. The method used is a common technique known as sweep frequency response. Measurements were done by exciting the winding with a variable frequency sinusoidal voltage and recording the maximum amplitude between two layers for a frequency range of 50 Hz to 2 MHz. A ratio known as the Resonance Amplification Factor (R.A.F) was used which is

defined as the voltage between points of resonance at a certain frequency divided by the 50 Hz voltage at the same point. The results are shown in Table 1.1. It should be noted that for the determination of resonant frequencies using the RAF method, the input voltage should be kept fairly constant. From Table 1.1 at 660 kHz the amplification factor of 2.5 was recorded

Table 1.1: Part winding resonance of the winding

Point in Winding	**Frequency**	**R.A.F**
Start of winding (between 2 layers)	536 kHz	1.15
Middle of winding (between 2 layers)	1.17 MHz	0.67
End of winding (between 2 layers)	181 kHz	0.95
End of winding (between 2 layers)	660 kHz	2.5*
End of winding (between 2 layers)	1.32 MHz	0.67

between the last and second last layer of the HV winding. This could result in internal winding resonance if closing transients that matched this frequency component occurred

Further fault analysis was also carried out to investigate other failure modes that could have contributed to the damaged transformer. The following were considered as other possible factors:

1. Lightning discharges into the 33 kV cable grid: Although possible for a lightning stroke hitting the overhead lines and generating a lightning impulse on the line, which would propagate through the extensive cable network to the point of transformer failure. No cable or cable terminal faults close to the wind turbine were reported. Furthermore, no lightning activity was reported during period of transformer failures.

2. Part-winding resonance of the winding with the supply cable (Terminal resonance): part winding resonance with the supply cable is also unlikely as the shortest cable first resonant frequency is more than an order below the first resonant frequency of the winding.

3. Inadequate system insulation of the Transformer (poor insulation coordination): the insulation system of the transformer withstood the routine induced over voltage test IEC60076 and complied with the impulse test to IEC 60076.

4. Switching of magnetizing current at no load.

For this research switching surges and resonance phenomena will be investigated. It should be noted that frequently switched transformers are more prone to failure than rarely switched transformers.

1.3 Research Motivation and research questions

The motivation for this research is to be able to determine the root cause of transformer failures especially in instances where they are exposed to frequent switching. The aim being to suggest proper insulation coordination studies such that the transformers are well insulated for any particular switching event. This should be done by devising suitable measurement and analytical techniques to address the engineering problem at hand. Hence the following will constitute research questions to be addressed in this thesis:

Research question 1. *What are the methods available in literature that can be used to properly characterize a high frequency model of a transformer?*

Research question 2. *In literature the Multi-conductor Transmission Line (MTL) model is used for the computation of the inter-turn voltages. Can the model be extended for the computation of inter-layer or layer voltages using appropriate matrix reduction techniques? i.e. grouping the total number of turns in a layer winding to represent the voltage distribution in that layer.*

Research question 3. *The MTL model is a commonly used model for the calculation of voltage distribution within transformer windings. Can the MTL model be applied for any transformer winding geometry? i.e. either split MV winding or non-split MV winding.*

Research question 4. *In literature different methods are proposed for the mitigation of fast transients brought about by transformer circuit breaker interaction. The protection methods range from the use of RC snubbers, surge capacitors and surge arrestors, to RL choke devices. Hence, what are the limitations of using these protection methods to curb the development of resonant overvoltages inside transformer windings? What appropriate protection methods can be used to co-ordinate with the insulation level of the transformer for protection against switching surges?.*

1.4 Contributions

The scientific content covered in this dissertation will focus on addressing the mentioned industry problems by proposing both an experimental and theoretical approach. Hence the research findings should be able to make sound engineering investments and economic contributions to the industry. Particularly where it concerns the integration of renewable energy to the existing grid. This is an important topic at the moment with different utilities particularly investing in renewable energy projects. The key findings and contributions of this work are summarised as follows:

1. Application of the improved MTL model with the matrix reduction method to model the sweep frequency response of a layer type of winding.
2. A high frequency model of transformer using MTL model valid from 1 kHz to 10 MHz.
3. The advantages and disadvantages of having a non-split MV winding as opposed to a split MV winding with respect to resonant points of the winding.
4. It is intended that this research will aid in coordinating the protection measures with the insulation level of the transformer.
5. It is intended that the MTL model particularly referred to as the white box model be implemented by transformer manufacturers during the design stage.

1.5 Dissertation Outline

This dissertation outline is as follows: Chapter 2 reviews the existing literature such that the problem is contextualised within the framework of existing works. Different transformer models are explored in Chapter 3, with the aim of finding the best model to describe the reviewed transformer failures. Chapter 5 provides a platform for verification of the chosen high frequency model of a transformer by comparing the developed work with results obtained in a research journal. Chapter 6 extends the application of the chosen high frequency model in Chapter 5 to resonant voltage modelling in two transformer prototypes. Chapter 7, addresses the measurement and analysis of switching surges to assess if a transformer is protected against a particular switching event. Chapter 8 summarizes the main findings of this research and proposes several mitigation techniques against switching transients. Chapter 9 reviews if the research questions set out in Chapter 1 were addressed and possibilities for further extension of this work is also discussed.

1.6 Conclusion

This chapter has introduced the motive for conducting the research, which is based on a number of transformer failures at the investigated wind farm. Initial literature review, reveals certain similarities between the transformers that failed in South Africa and Brazil. The shortfalls and the need to validate previous work on transformer related failures due to fast transients, leads to the construction of the research questions, which form the foundation of this thesis.

Chapter 2

Literature Review

2.1 Chapter Overview

In this chapter, existing work which has been published in research journals and conference papers will be reviewed. The goal being to find the appropriate research methods and models that will aide in addressing the research questions mentioned in Chapter 1.

2.2 Transformers and Circuit Breaker Induced Transients

In [21], the circuit breaker pre-strike effect that occurs during energization of an unloaded transformer was investigated. It is a well known phenomenon that the switching of highly inductive loads such as transformers can result in the generation of re-strikes or pre-strikes. The fast transients generated by switching of the circuit breaker propagate through the cable towards the transformer terminals. Due to differences in impedances a mismatch occurs and reflection and absorption occurs at the transformer terminals [21]. The voltage oscillations that propagate along the winding are continuously superimposed by new voltage surges emanating from the circuit breaker. In this short instance the voltage waveforms along the windings can have different amplitude and rate of rise [21]. As the distribution of these switching surges are non-linear, generation of high inter-turn overvoltages may result which stress the thin insulation and accelerate its failure. The effect of pre-strike was also investigated in depth by the authors in [22], [23] and [24] leading to the development of first transient switching surge protection device. Although it was initially conceived for purposes of protecting motors, its application has been further extended to transformers. Different protection methods will be investigated in this research including application of surge arresters, surge capacitors, RC snubbers and RL choke devices.

The problem presented by voltage transients measured on the transformer terminals is the difficulty in trying to predict their distribution along the windings. The work of Popov et. al in [21] addressed that. This was done by analysing the effects of pre-strikes on a prototype three phase distribution transformer with installed measuring points along the transformer winding and also for the different phases. The test transformer with the installed measuring points had the tank and the oil removed for ease of access to the windings. Modelling of the transformer was done by using lumped parameters extracted from telegrapher's equations in discrete form. It should be noted that successful modelling of transformers using transmission line equations has been applied in [5], [16], [25], [26] to describe the wave propagation in large shell type transformers. However several challenges still exist with transformer modelling which include [21]: (i) Information about the transformer geometry and dimensions of the windings may not be known. (ii) Proper modelling of transformers based on transformer geometry and type of windings is difficult to obtain. (iii) Consideration of the frequency dependent losses is still a major problem.

In [27], a method of trying to apply the black-box transformer models to white box transformer models was investigated. This was done by firstly determining the three different models used in transformer modelling. These are:

1. **Transmission line models:** This is one of the white box models used for the computation of very fast transients and voltage propagation studies within the winding [16], [26], [28], [29], [30], [31]. However they have several shortcomings which include: (i) They require detailed information about the transformer geometry. (ii) Not easily integrated into EMTP type of software which may be crucial for insulation coordination studies.

2. **Lumped parameter models:** This is another type of white box model and as such can be utilized for the computation of the internal voltage distribution within the transformer windings. It can also be extended to studying transformer interaction with the surrounding power system. The lumped parameter models find application in the simulation of lightning impulses as shown in [32], [33], [34], [35], [36],[37] and [38] and may also find application in the simulation of switching surges as shown in [39], [40], [41], [42]. The advantage of lumped parameter models is they can easily be integrated into EMTP type of software. However the major drawback is they still rely on the intricate details of the transformer geometry for proper modelling.

3. **Black box models:** Are mainly used to study the interaction of the transformer with the surrounding power system and for the computation of transferred overvoltages between HV and LV winding. Black models can easily be integrated into EMTP type of software.

However since this model portrays the terminal behaviour of the transformer with the power system, it can not be used for the propagation of transient voltages along the winding.

From the reviewed models above, it is clear that presently there is no unified model that links the white box models with the black box models without requiring the intricate design details of the transformer. Hence the drawback that still exist is the need to use the terminal voltages computed from the black box model and apply them as inputs for any of the white box models. In [27], complete unification of the black-box models with the white box model is still under investigation.

2.3 Difficulties in High Frequency modelling

EMTP like software packages offer black box models for simulating the transformer response with the surrounding power system. However a major drawback is the inability to correctly represent the transformer behaviour during a transient state [43]. As the transformer frequency response is characterised by several resonant points. It is necessary to be able to depict this behaviour. Hence more appropriate methods are employed which constitute fitting the measured admittance matrix of the transformer versus frequency to obtain a high frequency model of the transformer as done in [1]. The challenges with establishing a model by measurement are

1. **Repeatability of the measured waveforms:**. Few authors who have investigated black box models have not shown that the results can be reliably reproduced for a larger frequency ranges i.e. up to 10 MHz.

2. **Fitting methods:** The use of numerical fitting methods to rationally approximate the calculated transformer admittance matrix to the measured admittance matrix does not usually result in a good agreement [43]. Hence it is not easy to solve a constrained mathematical problem that will yield an optimum solution necessary to fit the curves.

A comparison of the different fitting methods which can be categorized as Unconstrained Fitting Methods (UFM) and Constrained Fitting Methods (CFM) were investigated in [43]. Depending on the number of poles, the Semi-Definite Programming (SDP) method a type of CFM can be used if the poles are less than 50. If the fitting obtained by SPD does not yield the required results and there is a loss of accuracy. Then the Fast Residue Perturbation (FRP) which is a type UFM method may be used with poles up to 120. However it should be noted that not all measured data can be accurately fitted using either SDP or the FRP method [43]. This usually

occurs if the measurement procedure was not performed accurately. The error introduced by the measurements changes the measurement data of the passive component (transformer) to act as non-passive one [43]. Hence performing the measurements accurately is essential to get the right output from the fitting methods.

2.4 Unified terminal and internal transformer model

As previously discussed black box models are usually used to study the terminal behaviour of transformer with surrounding power system. However the distribution of the terminal voltages along the winding is usually done using white box models as shown in [5], [25], [29], [44]. To address the short coming, Gustavsen in [45], [46], proposed a modified black box model which allows investigating voltage transfers from the transformer terminals to chosen nodes along the winding. In this respect, a black box model can still find application to study the terminal interaction of the transformer and the power system using EMTP like software. The overvoltages generated can then be used to address along which nodes dielectric stresses are likely to occur.

In [47], an investigation into overvoltages generated during cable-transformer interactions was performed. The modified black box model described in [45] was used to study the internal and external overvoltages generated during energization of a 100 MVA, 69 / 218.5 kV step up transformer. Time domain simulations were performed using EMTP-RV software (an electromagnetic transient program) to study the response of the internal nodes when both the HV and LV terminals were excited by a lightning impulse. Severity factors were then used in the assessment of the dielectric severity supported by the internal nodes when subjected to a transient wave at the terminals. Only the Time Domain Severity Factor (TDSF) was only considered by the author in [47]. The Frequency Domain Severity Factor (FDSF) was not taken into account. The results obtained revealed that whilst connecting a cable to the LV terminal does reduce the magnitude of the overvoltages due to cable transformer resonance. It impacts negatively on the internal nodes as the overvoltages generated do exceed the winding's specified Basic Insulation Level (BIL).

2.5 Discussion and Conclusion

The literature review has yielded some positive results which can find application to the research questions mentioned in Chapter 1. To address the cause of transformer failures the following

important findings which were reviewed in the literature survey will find application in the later chapters.

- High frequency modelling of transformers can be done both internally and externally in the assessment of overvoltages. Hence what remains is finding the appropriate model to describe the transformer behaviour when subjected to steep transients. This is covered in Chapter 3, Transformer Modelling.
- Circuit breaker induced transients can cause development of resonance be it internally or externally. Hence measurement and analysis of the nature of switching transients is crucial. This is covered in Chapter 7 using FFT and FDSF as analysis tools. FDSF is an analysis technique to assess the severity supported by the transformer at its terminals when excited by a transient waveform. A protected transformer will have FDSF values less than unity whilst a transformer which is at risk will have FDSF values which are greater than unity.
- Different mitigation techniques for protection against circuit breaker induced transients are investigated in Chapter 8.4 with the aim of finding the best protection method.

Chapter 3

Transformer Modelling

3.1 Chapter Overview

A high frequency model of a transformer is crucial for analysis of the internal transformer response to externally applied fast transients. Proper modelling will ensure computation of either the internal stresses within the winding or the terminal stresses impinged on the transformer terminals. The aim of this chapter is to present the different types of models used in modelling transformers. The overall goal being to find an appropriate model that can be used during the design stage to prevent failures discussed in the Introduction Section.

3.2 Existing Transformer Models

To allow proper modelling of the transient behaviour of the transformer winding, the mathematical modelling can generally be divided into the following three categories [48], [49], [50]:

1. **Black Box model:** The model's structure and parameters are based on information gathered by external input and output measurements performed on the test transformer. The obtained parameters yield a mathematical equation that describes the model output with the observed data. However, it should be noted that the mathematical expression bares no physical meaning or relationship with the transformer's physical construction [4]. The advantages of this model is that no prior knowledge of the intricate design details of the transformer is needed. Use of this model is constrained to the computation of external stresses impinging on the transformer terminals. Hence this model finds application in studying the high-frequency interaction between a transformer and the external supply network, analysis of transferred over-voltages between the HV or LV winding and incorporating it into insulation coordination studies of a power system. The

disadvantages of course is that it cannot be applied to computation of internal stresses within the windings.

2. **White Box model:** In simple terms, the White Box models the transformer as consisting of components such as resistances, capacitances, conductance's, self and mutual inductances to build the model structure [4]. A particular frequency range is usually of particular interest when this model is used. The advantages of the model is that it can be used for analysing transient events that occur within the transformer. In addition, it can be constructed to represent either all parts of the transformer in greater detail. The disadvantages of the model is that it does not depend on measurement data but actual parameters that have a direct relationship to the transformers physical structure. Such information is usually considered proprietary information that the manufacturer may not be willing to disclose.

3. **Gray Box:** This model is a result of a combination of both the White Box model and the Black Box model. Extraction of the model is based on prior system knowledge of the transformer and additional model parameters are estimated from measurement data [4]. The application of this model is commonly used in computation of the distribution and propagation of an incident electromagnetic transient along the transformer windings [51].

The above constitute the most commonly used models for transformer modelling. High frequency modelling of power transformers presents several challenges that have to be addressed. Transformers are characterized by several resonance points due to inductive and capacitive effects from the windings, tank, and core [1]. This behaviour should be accurately modelled to enable overvoltage studies where the high-frequency transient interaction of the transformer needs to be known i.e. transferred overvoltages between windings and resonant overvoltages within the windings. As previously mentioned, the goal is to be able to address the failure mechanisms of the reviewed Brazilian and South African cases. In addition, an appropriate model that can be integrated within the EMTP type of software and that can be used by transformer manufacturers is preferred.

3.3 Black Box Model

As previously mentioned, the Black Box model is used to reproduce the terminal behaviour of the transformer as seen from the transformer terminals [52], [53], [54], [55], [56]. The model formulated in the frequency domain is described by Equation 3.1 in terms of its admittance

matrix.

$$I_T(s) = Y_T(s)V_T(s) \tag{3.1}$$

Equation 3.1 defines the relationship between the terminal voltages and terminal currents [1], [51]. Considering a case where a transformer has n terminals, Y_T is the admittance matrix of size n x n which relates the terminal voltages and the terminal currents expressed by vectors V_T and I_T respectively. Note that the vectors describing the terminal voltages and currents are all of length n. Extraction of the admittance matrix **Y** in Equation 3.1 can be obtained either by direct measurements on a transformer or from analytical calculations of the transformer's detailed geometrical data [4].

3.3.1 Admittance Matrix by Measurements

If a 1 p.u. voltage is used to excite the transformer terminal node j while zero voltage (short circuit condition) is applied to the remaining terminals, it follows from Equation 3.1 that the jth column of Y_T will be equivalent to the currents Y_{ij} flowing from ground to each terminal i [1]. This allows the measurement setup in Figure 3.1 for direct measurement of Y due to different terminal conditions (i.e. open or short circuited winding).

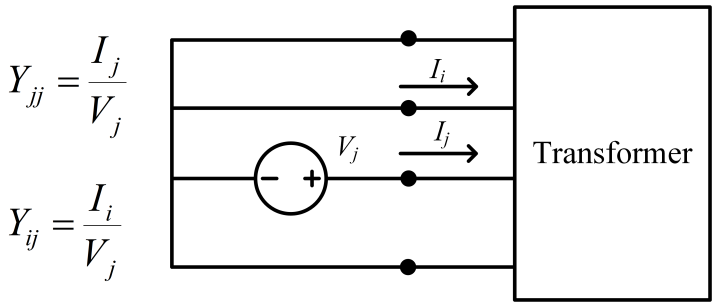

Figure 3.1: Black Box model of a transformer (measurement procedure for the jth column of the admittance matrix from [1])

As such the developed model has to be valid for different terminal conditions. Hence again a case is considered where the transformer terminals are divided into two groups, denoted by A and B, to represent the different terminal conditions. Equation 3.2 can be partitioned as follows [1], [51]:

$$\begin{bmatrix} I_A \\ I_B \end{bmatrix} = \begin{bmatrix} Y_{AA} & Y_{AB} \\ Y_{BA} & Y_{BB} \end{bmatrix} \begin{bmatrix} V_A \\ V_B \end{bmatrix} \tag{3.2}$$

If again another case is considered where the terminals of set A are open-circuited, such that I_A = 0, the following voltage ratio results [1], [51]:

$$V_{AB} = -Y_{AA}^{-1} Y_{AB} \tag{3.3}$$

From Equation 3.3, considering a three phase, two winding transformer where all terminals of one winding are open-circuited, the transferred overvoltages (voltage ratios) between windings can be computed as shown in Equation 3.4 and Equation 3.5:

$$V_{HL} = -Y_{HH}^{-1} Y_{HL} \tag{3.4}$$

$$V_{LH} = -Y_{LL}^{-1} Y_{LH} \tag{3.5}$$

where where H and L are the HV and LV windings respectively. V_{HL} and V_{LH} are matrices of size 3 x 3.

3.3.2 Black Box model admittance matrix derived from White Box model

According to the CIGRE WG (B2/C4.39) the transformer manufacturer may provide a computed Black Box admittance matrix $Y(w)$ derived from the White Box model [4]. This can then be integrated within the Equation 3.2. The merit is that any proprietary information about the transformer design is not revealed.

3.4 White Box models

The most commonly used White Box models are the RLC ladder model and the Multi-Transmission line (MTL)model. Both have their own advantages and disadvantages depending on particular frequency range of interest and application.

3.4.1 RLC ladder Network model

The RLC ladder network model uses a lumped network of cascaded connections (ladder network) of n equal segments, as shown in Figure 3.2. Figure 3.2 shows a basic element for representation of a disc type of transformer winding. Each double disk in the Ladder Network model, is modelled by three parallel branches consisting of a capacitor, resistors and inductors with additional capacitors $(C_1) \cdots (C_1)$ to ground. The resistance and the inductance of each double disk are represented by r_i and L_{ii} respectively.

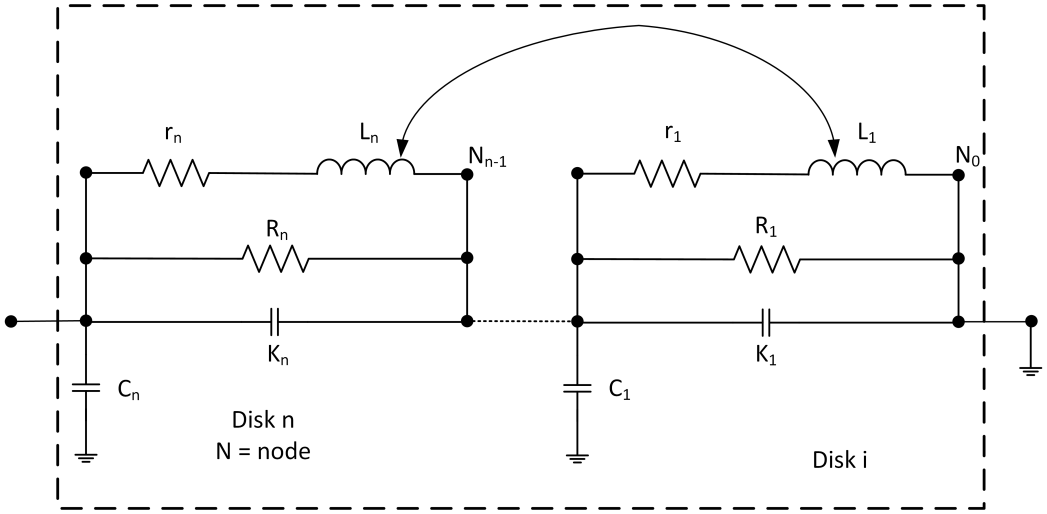

Figure 3.2: RLC ladder network model of transformer winding from [2]

The series capacitance of the i_{th} double disk is modelled by K_i and its dielectric losses represented by R_i. The mutual inductance between adjacent double disks is modelled by L_{ij}. The model can be described by the following equation:

$$\hat{C}\frac{d^2\hat{v}(t)}{dt^2} + \hat{G}\frac{d\hat{v}(t)}{dt} + \hat{\Gamma}\hat{v}(t) = 0 \tag{3.6}$$

where $\hat{C}$ is the nodal capacitance matrix, $\hat{G}$ is the nodal conductance matrix and $\hat{\Gamma}$ is the inverse nodal inductances matrix. $\hat{v(t)}$ is the output vector of node voltages. Equation 3.6 can be reduced by extracting the input node k of known voltage $u(t)$. This results in Equation 3.7 [51].

$$C\frac{d^2v(t)}{dt^2} + G\frac{dv(t)}{dt} + \Gamma v(t) = -C_k\frac{d^2u(t)}{dt^2} - G_k\frac{du(t)}{dt} - \Gamma_k u(t) \tag{3.7}$$

where C is the nodal capacitance matrix, G is the nodal conductance matrix and Γ is the inverse nodal inductances matrix. $v(t)$ is the output vector of the (k-1) node voltages that are unknown [51]. C_k, G_k and Γ_k are the kth columns of $\hat{C_k}$, $\hat{G_k}$ and $\hat{\Gamma}$ respectively without the kth row. Expressed in the Laplace domain, Equation 3.7 yields Equation 3.8:

$$sCV(s) + GV(s) + \frac{\Gamma}{s}V(s) = -sC_kU(s) - G_kU(s) - \frac{\Gamma_k}{s}U(s) \tag{3.8}$$

Re-arranging Equation 3.8 can yield Equation 3.9 [2]:

$$[I(s)] = [Y(s)] \cdot [U(s)] \tag{3.9}$$

where

$$[Y(s)]_{nxn} = \frac{1}{s}\{[\Gamma] + s \cdot [G] + s^2 [C]\} \tag{3.10}$$

$I(s)$ and $U(s)$ are the node current and the node voltage vectors respectively. In this case, the surge input is only applied at node n hence the only non-zero element of $I(s)$ would be the element in the last row. From Equation 3.9, solving for the voltages results in Equation 3.11:

$$\frac{U_j(s)}{U_n(s)} = \frac{1}{Z_{in}(s)} \cdot [Y(s)]^{-} 1_{j,n} \quad for \quad j = 1,2,...,n \tag{3.11}$$

where $Z_{in}(s)$ is the input impedance of the winding [57].

3.4.2 Multi-transmission Line (MTL) model

Analysis of the voltage distribution within the transformer windings can be represented by a group of interconnected and coupled transmission lines as shown Figure 3.3 [44], [58], [59].

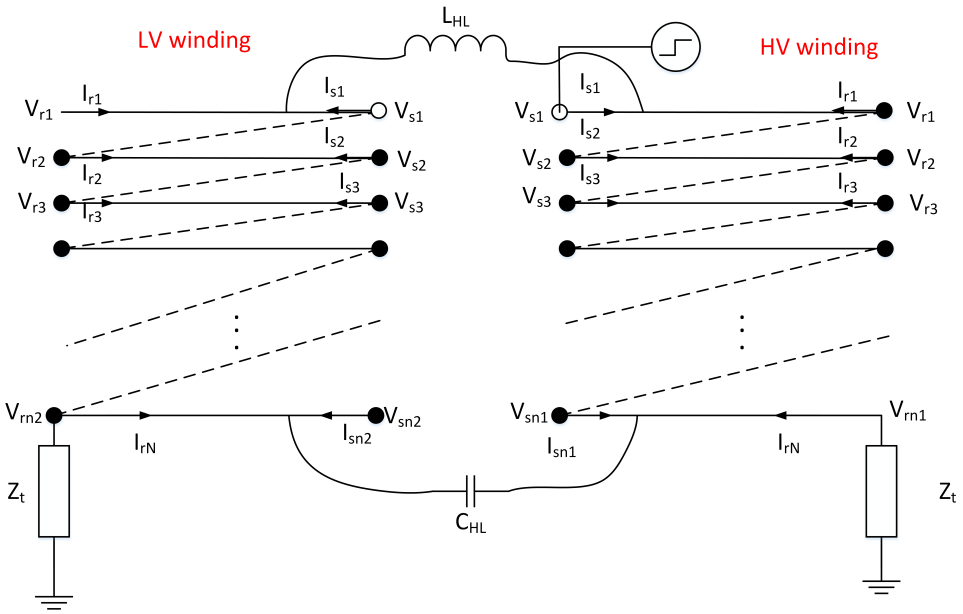

Figure 3.3: Multi-conductor Transmission Line model

Figure 3.3 shows application of the model to a two winding transformer. With reference to IEC 60076-3, transferred voltages have both a capacitive and inductive character which have been presented by C_{HL} and L_{HL} respectively in Figure 3.3. The coupled transmission lines can be described by: Equation 3.12 and Equation 3.13:

$$\frac{d^2\mathbf{V}}{d\mathbf{x}^2} = -[Z][Y] \tag{3.12}$$

$$\frac{d^2\mathbf{I}}{d\mathbf{x}^2} = -[Z][Y] \tag{3.13}$$

where **V** and **I** are the incident voltage and current vectors respectively. **Z** and **Y** are the impedance and admittance matrices of the line respectively. The transmission line equations can be solved by applying a two port network as follows: find the voltages and currents at a distance x as shown in Equation 3.14 and Equation 3.15 [60].

$$V_x = V_1 e^{-[P]x} + V_2 e^{[P]x} \tag{3.14}$$

$$I_x = Y_o \left(V_1 e^{-[P]x} - V_2 e^{[P]x} \right) \tag{3.15}$$

Applying boundary conditions to the solution of Equation 3.14 and Equation 3.15 it is possible to express the sending end $(_S)$ voltage and receiving end $(_R)$ voltage as shown in Equation 3.16 [5], [25]:

$$\begin{bmatrix} I_S \\ I_R \end{bmatrix} = \begin{bmatrix} A & -B \\ -B & A \end{bmatrix} \begin{bmatrix} V_S \\ V_R \end{bmatrix} \tag{3.16}$$

Where:

$$A = YS\gamma^{-1} \coth(\gamma l) S^{-1} \tag{3.17}$$

$$B = YS\gamma^{-1} cosech(\gamma l) S^{-1} \tag{3.18}$$

And in Equation 3.17 and 3.18:

V_R, V_S	voltage vectors at the receiving and sending end of the winding (transmission line)
I_R, I_S	current vectors at the receiving and sending end of the winding (transmission line)
S	matrix of eigenvectors of the matrix ZY
γ^2	eigenvalues of matrix ZY
l	total length of the winding

As mentioned in Chapter 1, the model must compute the voltages in each layer such that the transformer manufacturer can easily identify which disc or layer poses a risk of failure when subjected to steep transients. This being the case, application of the MTL model to describe

each winding turn as a separate transmission line will result in large matrices such that the simulations take too long to process. A more practical solution that will benefit the transformer manufacturer is to present the voltage distribution in each layer or disc. This can be achieved by using the matrix reduction techniques employed in [61], [62]. Hence by grouping the number of turns in each layer to represent a single transmission line as in Figure 3.3, the information at the end of the line remains unchanged as would be the case if separate transmission lines representing separate turns had been used [28]. Applying Equation 3.16 to either the HV or LV winding of Figure 3.3 results in Equation 3.19

$$\begin{bmatrix} I_{S1} \\ I_{S2} \\ . \\ . \\ . \\ I_{Sn} \\ I_{R1} \\ I_{R2} \\ . \\ . \\ . \\ I_{Rn} \end{bmatrix} = \begin{bmatrix} A' & -B' \\ -B' & A' \end{bmatrix} \begin{bmatrix} V_{S1} \\ V_{S2} \\ . \\ . \\ . \\ V_{Sn} \\ V_{R1} \\ V_{R2} \\ . \\ . \\ . \\ V_{Rn} \end{bmatrix} \tag{3.19}$$

By examining Figure 3.3, the following identities hold true [28], [63].

I_{R1} = -I_{S2} $\quad I_{R2}$ = -I_{S3} $\quad \cdots \quad -I_{Rn} = \frac{V_{Rn}}{Z}$

$V_{R1} = V_{S2} \quad V_{R2} = V_{S3} \quad \cdots \quad V_{Rn-1} = V_{Sn}$

By making use of above mentioned identities and matrix operations described in [63] results in Equation 3.20.

$$\begin{bmatrix} I_{S1} \\ 0 \\ . \\ . \\ 0 \\ 0 \end{bmatrix} = \begin{bmatrix} \\ Y \\ \\ \end{bmatrix} \begin{bmatrix} V_{S1} \\ V_{S2} \\ . \\ . \\ V_{Sn} \\ V_{Rn} \end{bmatrix} \tag{3.20}$$

Further manipulation of Equation 3.20 results in Equation 3.21. As the transformer winding is

grounded V_{Rn} = 0 hence the last row can be removed as it is a redundant equation.

$$\begin{bmatrix} V_{S1} \\ V_{S2} \\ \cdot \\ \cdot \\ V_{Sn} \end{bmatrix} = \begin{bmatrix} \\ YY \\ \\ \end{bmatrix} \begin{bmatrix} I_{S1} \\ 0 \\ \cdot \\ \cdot \\ 0 \end{bmatrix} \tag{3.21}$$

Where YY is the inverse matrix of the matrix Y. From Equation 3.21, the voltages at the sending end of the winding between layer 2 and 1 are defined by: $V_{S1} = YY_{(1,1)}I_{S1}$ and $V_{S2} = YY_{(2,1)}I_{S1}$, hence the resonance voltage ratio is defined as:

$$H_1 = \frac{V_{S2}}{V_{S1}} = \frac{YY_{(2,1)}}{YY_{(1,1)}} \tag{3.22}$$

Equation 3.22 can be generalized to calculate the resonance voltage ratio at any arbitrary turn, layer, disc (k) as shown by Equation 3.23

$$H_k = \frac{V_{S(k+1)}}{V_{S1}} = \frac{YY_{(k+1,1)}}{YY_{(1,1)}} \quad k = 1,2,\cdots,n-1 \tag{3.23}$$

It should be noted that $YY_{(1,1)}$ in Equation 3.23 is the terminal admittance of the transformer. Computation of the voltage at the end of each layer can be calculated when the input voltage is known and by making use of the transfer function in Equation 3.23. The time domain is calculated as shown in Equation 3.24

$$V_{Si}(t) = \frac{1}{2\pi}\int_{-\Omega}^{\Omega} \frac{\sin(\pi\omega/\Omega)}{\pi\omega/\Omega} V_{Si}(b+jw)e^{(b+jw)t}d\omega \;\; for\; i = 2,3,\cdots,n \tag{3.24}$$

where

$$V_{Si}(b+j\omega) = H_{i-1}(b+j\omega)V_{S1}(b+j\omega) \;\; for\; 1 = 2,3,\cdots,n. \tag{3.25}$$

From Equation 3.25, the choice of the integral limits must be chosen appropriately such that the computations result in an accurate time-domain response [44], [64].

3.5 Grey Box models

The Grey Box model is a mathematical representation of the complex electromagnetic relationships that exist within the transformer [4]. Modelling of the transformer using the Grey Box approach does not require any knowledge of the transformer's internal geometry nor its material properties.

Rather extraction of the model parameters is obtained directly from the transformer's frequency response measurements. Other parameters may also be obtained from the data on the transformer nameplate, and tank dimensions. Model construction can also be implemented by using typical assumed manufacturing values [3].

3.5.1 Generic Phase Model of the Transformer

A common approach of implementing the Grey Box model of the transformer is to incorporate a ladder network model shown in Figure 3.4 [4].

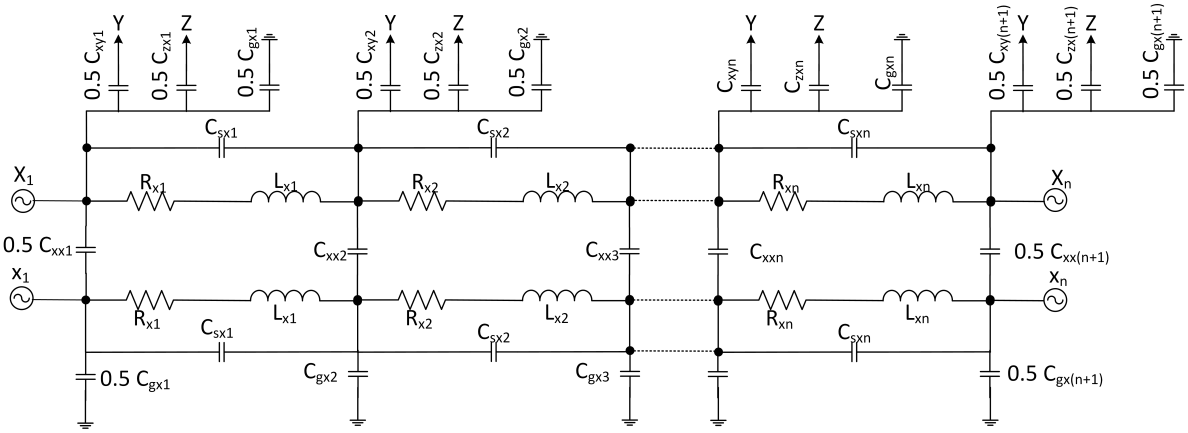

Figure 3.4: Generic phase model of a transformer adapted from [3]

The ladder network is made up of frequency dependent resistors (R), inductors (L) and capacitors (C). The generic phase references X, Y and Z are used to reference the three phase model of a transformer. To estimate the model parameters, Frequency Response Analysis (FRA) can be used. We note that in using the FRA method you need both the amplitude and phase information. This is well documented in [65] with particular application in power transformers. Hence FRA is normally used as a diagnostic tool for detecting changes in the transformer frequency response. Any change in the frequency response from the spectral fingerprint can yield information on winding deformation as well as other electrical and structural problems [3]. However FRA can also be used in model parameter extraction [4], [3]. This can be done by applying the transformer model transfer function to the corresponding FRA terminal spectral fingerprint. The results are well documented in [3], where several FRA signatures were incorporated during the transformer model parameter extraction. To deduce the transfer function of the Grey Box model, the test setup of a transformer being subjected to a series of FRA tests can be considered as represented by a layered model as shown in Figure 3.5. The

aim being to develop a flexible model which will take into account the different transformer vector groups and the different types of FRA tests that can be conducted [3].

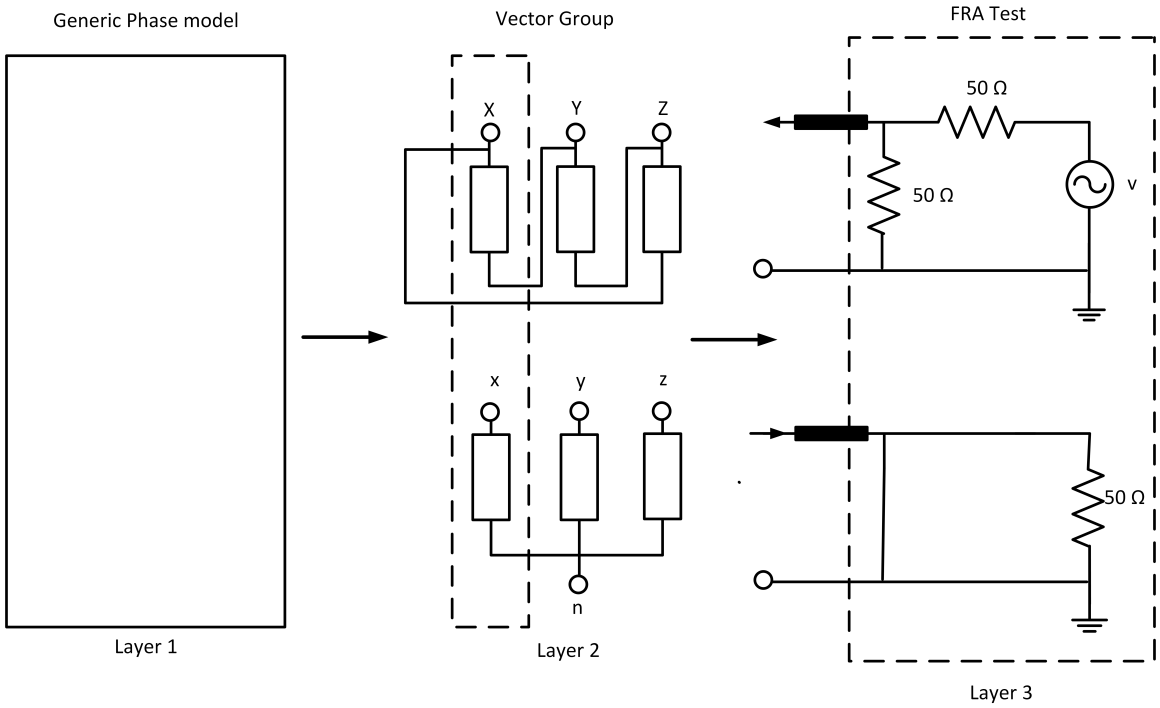

Figure 3.5: Grey box test set-up layered modelling approach adapted from [4]

In Figure 3.5, the first layer is the generic phase model of the transformer shown in Figure 3.4. Layer 2 is the vector group topology of the transformer. Layer 3 is the FRA test connection. The proposed layered model can be presented in the normal tree form [66]. System analysis can be done by using state space equations for a network tree which are defined by:

$$\dot{x}(t) = A(u(t))x(t) + B(u(t))u(t) \tag{3.26}$$

$$y(t) = C(u(t))x(t) \tag{3.27}$$

where x is the state variable vector, u is the input variable vector, t is the time and y is the output variable vector. A, B and C are time-dependent matrices defined in [3]. The resulting transfer function is

$$\hat{H}(s) = \frac{Y(s)}{X(s)} = \mathbf{W}C^{-1}\left[P_q^T - F_{cs}C_sF_{vs}^T\right] \tag{3.28}$$

The derivation of the transfer function is well explained in [3] as well as the model parameter

estimation from FRA.

3.6 Discussion on appropriate model to address the research questions and Conclusion

This chapter has reviewed some of the common models used in transformer modelling. As previously highlighted in the Chapter 1, the model has to allow the investigation into the failure mode occurring within the transformer and address the research questions set out in Chapter 1. Table 3.1 shows the selection criteria used to choose the appropriate model.

Table 3.1: Selection criteria used to pick the proper model

	Models considered			
Selection Criteria	RLC	MTL	Black Box	Grey Box
Research question 1	✓	✓	✓	✓
Computation of inter-turn or inter-layer voltages	x	✓	✓	x
Voltage propagation along the winding	✓	✓	x	x
Frequency range of up to 10 MHz	?	✓	?	x
Transferred overvoltages HV to LV winding	✓	✓	✓	✓
Terminal stresses impinged on the transformer terminals	✓	✓	✓	✓
Construction of model to represent winding geometry	?	✓	x	?

As previously discussed the different models have their own advantages and disadvantages which were explained. The chosen model is the MTL model discussed in Chapter 3.4.2 cause it meets the selection criteria in Table 3.1. The model also provides the insight that is needed to understand the resonance behaviour and overvoltages occurring within each winding. Hence in this research, the MTL model will be used for the computation of the voltage distributions within the winding.

Chapter 4

Parameter Determination

4.1 Chapter Overview

This chapter deals with the determination of the transformer parameters needed for the MTL model. Firstly the per-unit length parameters of the transformer winding are calculated. Then the required capacitance, inductance, resistance and conductance matrices are then computed. Two transformer prototypes were investigated: the transformer with the split MV winding and the transformer with the non-split MV winding. The determination of the transformer parameters for the two prototypes will be explained in this chapter.

4.2 MTL Model flowchart

The impedance **Z** and admittance **Y** matrix of the MTL Equations are expressed as shown in Equation (4.1) and Equation (4.2) from [5] and [25].

$$Z = [j\omega\mathbf{L} + R_S] \tag{4.1}$$

$$Y = (j\omega * C + \omega tan\delta * C) = (j\omega + G) * \mathbf{C} \tag{4.2}$$

The derivation of the resistance (R_s), capacitance (C), conductance (G) and inductance (L) matrices shown in the above equations is explained in Chapter 4.3. As can be seen from Figure 4.1 of the MTL algorithm flow chart, successful computation of the transfer function depends on proper definition of the L , C, G and R_s matrices at different frequencies.

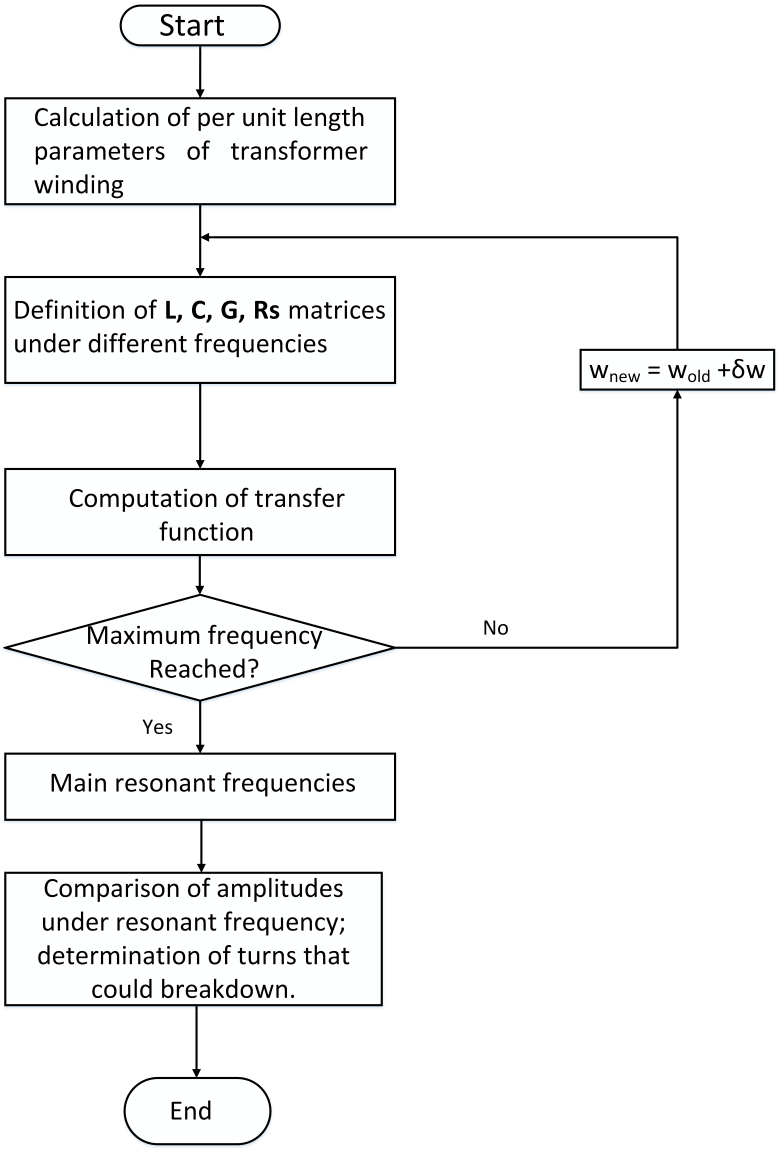

Figure 4.1: MTL model flow chart adapted from [5]

4.3 Parameter extraction

The capacitance, conductance, resistance and inductance matrices were calculated as follows:

4.3.1 Calculation of the C (capacitance) matrix

Figure 4.2 show the capacitances inside a transformer that are needed for computation of fast transients within the winding. For calculating the inter-turn voltages, capacitance C_S is important and must be calculated [28]. For the computation of transferred overvoltages between the HV and LV windings, surge capacitor C_{HL} must be calculated. The capacitive overvoltage transfer brought about by the surge capacitance capacitor C_{HL} will depend on the steepness of the transient. The effect of the surge capacitor will become more marked with a transient that has a high du/dt [44].

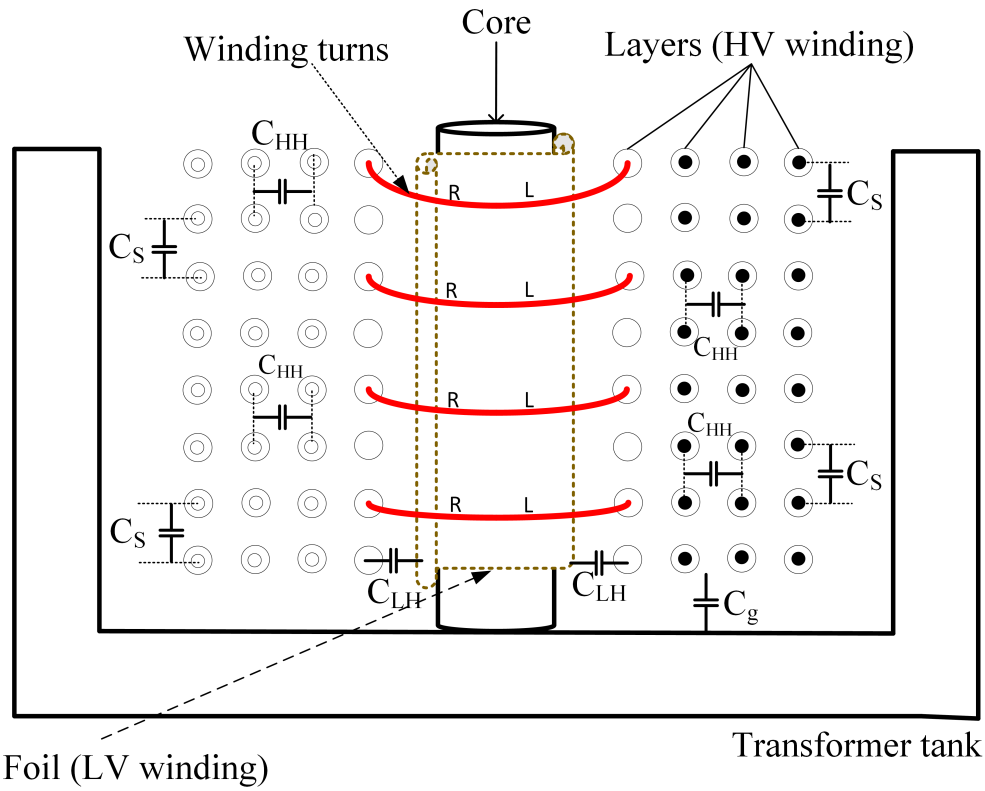

Figure 4.2: Parameters needed for computation of fast transients

The capacitance matrix **C** was formed as follows from [28]:

$C_{i,i}$ capacitance of layer i to ground and the sum of all other capacitances connected to layer i i.e. the diagonal elements of the capacitance matrix

$C_{i,j}$ capacitances between layers i and j taken with negative sign $(i \neq j)$ i.e. These form the off-diagonal elements of the capacitance matrix.

The procedure for the construction of the capacitance matrix is explained in [67], [26]. The formulas for calculating the capacitance were calculated from the basic formulas of cylindrical and plate capacitors shown by Equations 4.3, 4.4 and 4.5 [51].

$$C_S = \frac{\varepsilon_o \varepsilon_r h}{d_s} \tag{4.3}$$

$$C_g = \frac{\varepsilon_o \varepsilon_r \omega}{dg} \tag{4.4}$$

$$C_{ij} = \frac{2\pi\varepsilon_o L}{In\left(\frac{b}{a}\right)} \tag{4.5}$$

where C_s is the turn to turn capacitance, C_g is the turn to earth capacitance and C_{ij} is the capacitance between layer i and j. ε_r is the relative permittivity of the dielectric material between the turns, ε_o is the permittivity of free space. h is the rectangular conductor's height. d_s and d_g are the distance between the turns and distance between turn and ground plane respectively. L is the length of the winding and ω is the rectangular conductor's width. a and b are the inner and outer radius of the winding respectively.

As previously mentioned, in the research question, the application of matrix reduction methods will have to be employed. The goal is to reduce the size of the matrices by grouping the number of turns in each layer to represent a single transmission line. According to the MTL model, the voltages at the end of the line remains unchanged as would be the case if separate transmission lines representing separate turns had been used. The matrix reduction technique explained in [61] and [62], can be applied such that the order of matrices corresponds not to a single turn but to a group of turns. The modified matrix reduction expression is shown in Equation 4.6 and 4.7.

$$C^{layer}_{ii\,node} = \sum_{i=i_i}^{li}\sum_{j=i_i}^{li} C^{turn}_{ij} + \frac{1}{2}\sum_{i=i_i}^{li} C^{turn}_{i,m} + \frac{1}{2}\sum_{j=i_i}^{li} C^{turn}_{m,j} + \frac{1}{2}C^{turn}_{m,m} \tag{4.6}$$

$$C^{layer}_{ij\,node} = \sum_{i=i_i}^{li}\sum_{j=i_i}^{li} C^{turn}_{ij} + \frac{1}{2}\sum_{i=i_i}^{li} C^{turn}_{i,m} + \frac{1}{2}\sum_{j=i_i}^{li} C^{turn}_{m,j} \tag{4.7}$$

where $li = li + (w_k - 1)/2 - 1$, wk is the number of lumped turns in layer k, li is the first turn in layer i and m is the turn in the centre of the layer. The same reduction method can be applied to a group of turns such that they represent the total number of turns in half a layer of the MV winding.

4.3.2 Calculation of the G (conductance) matrix

The conductance (G) is due to the insulation between turns and windings and will result in capacitive losses in the insulation [60], [67]. It is expressed as:

$$G_{ij} = \omega \, tan\delta \, C_{ij} \tag{4.8}$$

The G matrix is calculated as for the C matrix. The diagonal elements of the G matrix are formed by the sum of the conductance connected to each layer. Whilst the off diagonal elements are all negative and equal to the conductance between the layer and adjacent layers. It should be noted that tan δ is frequency, moisture and temperature dependent and will influence the admittance matrix greatly at higher frequencies [67]. As such an appropriate equation that best describes the capacitive losses within the insulation should be applied in-order to get accurate results. Equations 4.9, 4.10, 4.11, 4.13 and 4.12 are some of the equations that describe the variation of tan δ with frequency. Note that the variable c is part of a heaviside function used to model a step function. Hence for frequency values less than a specific value of c the function assumes a value of zero. For frequency values above c the function takes a value of 1.

$$u_c(f) = \begin{cases} 0 & \text{if} \quad f\,[MHz] < c \\ 1 & \text{if} \quad f\,[MHz] > c \end{cases} \tag{4.9}$$

$$tan(\delta) = 0.005\,[u(f-0.01) - u(f-0.04)] + 0.015\,[u(f-0.04) - u(f-1)] \tag{4.10}$$

$$tan(\delta) = 0.005\,[u(f-0.01) - u(f-0.04)] + (5.3 \cdot 10^{-9}x + 0.0047)\,[u(f-0.04) - u(f-1)] \tag{4.11}$$

The step and ramp type variation of tan δ for oil impregnated cellulose paper is described by Equation 4.10 and Equation 4.11 [2]. In [67], an approximated equation described by Equation 4.12 was used to describe the tan δ behaviour of the insulation between the LV foil winding, the insulation between the LV and the HV winding, the insulation between LV to ground and HV to ground and also the inter-turn insulation between the turns of the HV winding. For Nomex paper insulation the variation is satisfied by Equation 4.13 [60].

$$tan(\delta) = (1.082 \times 10^{-8}) \cdot 2\pi f + 5.0 \times 10^{-3} \tag{4.12}$$

$$tan(\delta) = 0.07 \left(1 - \frac{6}{7} \times e^{-(0.308 * fx10^{-6})} \right); \tag{4.13}$$

The variation of tan δ for the above equations is shown in Figure 4.3. Analysis of Figure 4.3, shows that for Equation 4.12 in the frequency range of 10 kHz $< f <$ 1 MHz, tan δ does not

change with frequency. However Equations 4.10, 4.11 and 4.13 approximate the frequency dependent behaviour of tan δ.

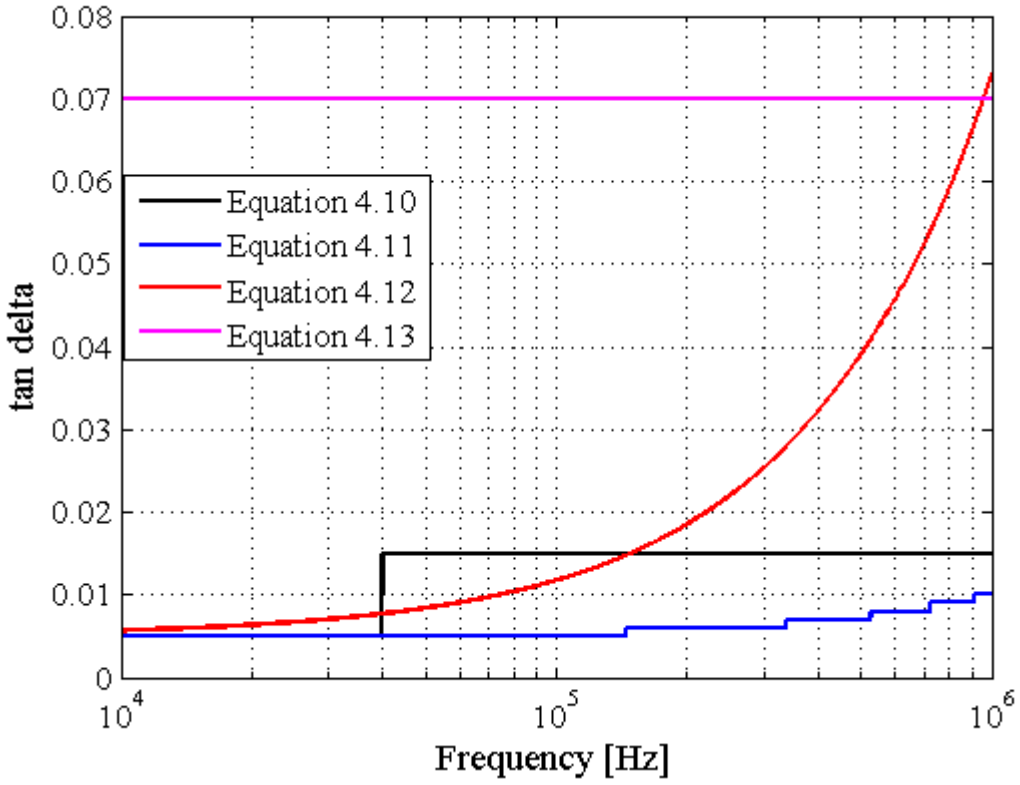

Figure 4.3: tan δ versus frequency (10 kHz $< f <$ 1 MHz)

Most commonly used insulation paper in transformers is Krempel DPP [68], [69] and PUCARO DPP [70]. The transformer press paper is commonly made of unbleached sulphate cellulose with diamond dotted reactive resin coating [69], [70]. Hence as the transformer press paper is mainly made up of cellulose material, Equation 4.10 and 4.11 would best describe the frequency dependent behaviour of the oil impregnated cellulose paper.

4.3.3 Calculation of the R (resistance) matrix

The resistance matrix is calculated by taking into account the skin effect at high frequencies as shown by Equation 4.14 [71], [72].

$$R_s = \left(\frac{1}{2\,(d_1 + d_2))} \right) \cdot \sqrt{\frac{\pi f \mu}{\sigma}} \tag{4.14}$$

where d_1 and d_2 are the length and width dimensions of the conductor. μ and σ are the permeability and conductivity of the conductor respectively. f is the frequency. The above resistance calculation takes into account skin effect considerations. To take into account the proximity effects Equation 4.15 may be applied [44].

$$R_s = \sqrt{\frac{2\omega}{\mu\sigma_o d^2}} \tag{4.15}$$

where d is the distance between the layers [28]. It should be noted that proximity effects will affect the resistance matrix above a certain frequency. Ignoring the proximity effect in the model and only accounting for the skin effect as shown by the analytical formula in Equation 4.14 may result in overestimation at some resonance frequencies as shown in [67].

4.3.4 Calculation of the L (inductance) matrix

The inductance matrix can be expressed as a sum of two component matrices. The first component is obtained directly from the capacitance matrix **C** if the following assumptions are made [63]:

1. High frequency magnetic flux penetration into the iron laminations and transformer core is negligible.

2. The magnetic flux will be constrained within the paths of the insulation.

The above assumptions are meant to simplify calculations with regards to a fundamental problem in evaluating the winding parameters. As opposed to determining the parameters of capacitive elements which are pretty much straightforward as calculations are based on geometry and relative permittivity. Inductance calculations are a bit more difficult as they involve magnetic flux penetration in laminated iron structures at high frequencies. To simplify calculations the following assumptions are made [63]:

- Magnetic flux does not penetrate the iron laminations at all

- The iron acts as a boundary within which the flux is constrained.

The first component inductance matrix can then be obtained using Equation 4.16:

$$L_n = \frac{\varepsilon_r}{v^2} \cdot \mathbf{C}^{-1} \tag{4.16}$$

where v is the velocity of light in vacuum and ε_r is the relative permittivity of the insulation (in this case equivalent relative permittivity of the air and paper combination). The second

component of the inductance matrix takes into account the flux internal to the conductor [5], [25]. It is given by:

$$L_i = \frac{R_s}{f} \tag{4.17}$$

where R_s is from the resistance matrix expressed in Equations 4.14 and 4.15. The total inductance matrix can then be expressed as:

$$\mathbf{L} = L_n + L_i \cdot E_n \tag{4.18}$$

where E_n is a unit matrix of size n x n. n represents the total number of turns in a given winding. It should be noted that the inductance matrix can also be calculated by using the basic formulas for self and mutual inductances of the turns from Maxwell's equations as shown in [28].

4.4 Conclusion

This chapter has elaborated on the determination of the parameters in the MTL model. An in-depth step by step derivation of each individual parameter is explained in the appendix section. The short-comings brought about by approximating the tan δ will become more apparent in Chapters 5 and 6 when the results are analysed. However as highlighted in this chapter, there is no single equation that properly models the tan δ behaviour of the insulation under investigation. Hence any of the approximated equations that will yield the results closest to the measured results will be used.

Chapter 5

Model Verification

5.1 Chapter Overview

This chapter is concerned with verification of the proposed high frequency model of the transformer. As previously mentioned in Chapter 3, the MTL model will be used as the high frequency model of the transformer. The model verification is done by comparing results of a disc type of winding that had been modelled using transmission lines in [5], [25] against the developed MTL model by the author. The results of the comparison indicate that the developed high frequency model of the transformer can be used for estimation of resonant overvoltages within transformer windings.

5.2 Parameters of the transformer winding

In [5] and [25], Sun et al showed how to model transformer windings for the analysis of resonant overvoltages. The author made use of the MTL model as a high frequency model of a transformer. A core-type transformer with a disc type of winding was used. The main parameters of the transformer winding are shown in Table 5.1 [5], [25]. The winding parameters in Table 5.1 were used as input parameters of the MTL model. As can be seen from Table 5.1, the total number of turns would be 180. Specific measuring points were installed along certain points of the winding. The results of measurements obtained from the installed measuring points were compared with the computed results of the MTL model. The procedures for the determination of the capacitance, inductance, resistance and conductance matrices was as explained in Chapter 4. The layout of the transformer under test is shown in Figure 5.1. The measurements are done at the ends of each specific disc as outlined in Section 5.3. It should be noted that the winding makes use of rectangular copper conductors.

Table 5.1: Main Parameters of the winding

Number of discs	18
Turns per disc	10
Conductor width [mm]	6.95
Conductor height [mm]	11.2
Average turn length [m]	1.4828
Thickness of inter-turn insulation [mm]	3.00
Relative permittivity of inter-turn insulation	3.5
Conductor conductance [s $\cdot m^{-1}$]	$3x10^7$
Inter-turn capacitance (C_k) [pF $\cdot m^{-1}$]	120
Inter-section capacitance (C_s) [pF $\cdot m^{-1}$]	10
Turn to core capacitance (C_g) [pF $\cdot m^{-1}$]	15

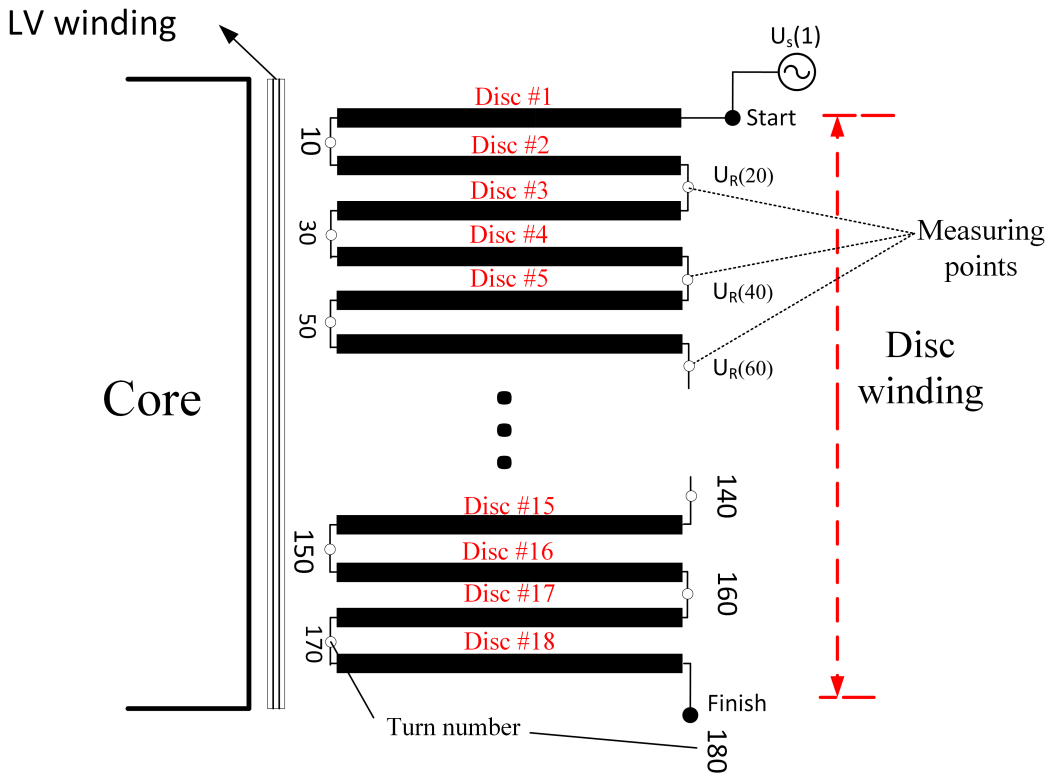

Figure 5.1: Measurement setup of a core-type transformer winding adapted from [5].

Hence conductor width and height refer to the dimensions of the coil used in winding the MV winding. The total length of the winding is found by taking the product of the average turn length and the total number of turns (i.e. number of discs $\times$ turns per disc).

5.3 Model comparison and verification

Resonance calculation was done by computing the transfer function from Equation 3.23. A plot of the amplitude frequency response of the transfer function was calculated using the developed MTL model. The results of the computation were compared with graphs obtained in [5], [25]. The comparison was done by comparing the computed results corresponding to the same measurement points as used in the experimental setup of Sun et. al in [5], [25]. Note that in [5], a comparison of calculated versus measured results in the paper was done. Hence in this Chapter we compare the results of the developed MTL model against the model developed by Liang which had been verified through experimental work as outlined in [5] and [25]. The turns at which measurements were made are turn 20, turn 40 and turn 60 as shown in Figure 5.1. It should be noted that these specific turns were chosen since failure at the end-turns is quite common for transformers exposed to transient overvoltages.

5.3.1 Sweep Frequency response of turn 20, turn 40 and turn 60

The sweep frequency response for turn 20, turn 40 and turn 60 are shown in Figures 5.2, 5.3, 5.4 respectively. A comparison of the results obtained by Sun et. al in [5], [25] is done with the results obtained using the developed MTL model of the author. The comparison is achieved by overlaying the frequency plots together as can be seen in Figures 5.2, 5.3, 5.4. The idea being to observe how closely the results obtained from the developed MTL model match with the results of the Sun et. al MTL model. Equation 5.1 describes the amplitude transfer function at an arbitrary turn k, relative to the input [5], [25]. In Equation 5.1, U_S is the input signal, $U_R(k)$ is the output voltage measured at an arbitrary turn k. Derivation of Equation 5.1 is explained in [5], [25] and bares the same meaning as Equation 3.23 explained in Chapter 3.4.2.

$$A(k) = \frac{U_R(k)}{U_S(1)} = \frac{T(k+1,1)\,T(N+1,N+1) - T(k+1,N+1)\,T(N+1,1)}{T(1,1)\,T(N+1,N+1) - T(N+1,1)\,T(1,N+1)} \tag{5.1}$$

Reference of Equation 5.1 which describes the amplitude transfer function will be made in Figures 5.2, 5.3 and 5.4 to give a comparison between the developed MTL model by the author and Sun et al. MTL model.

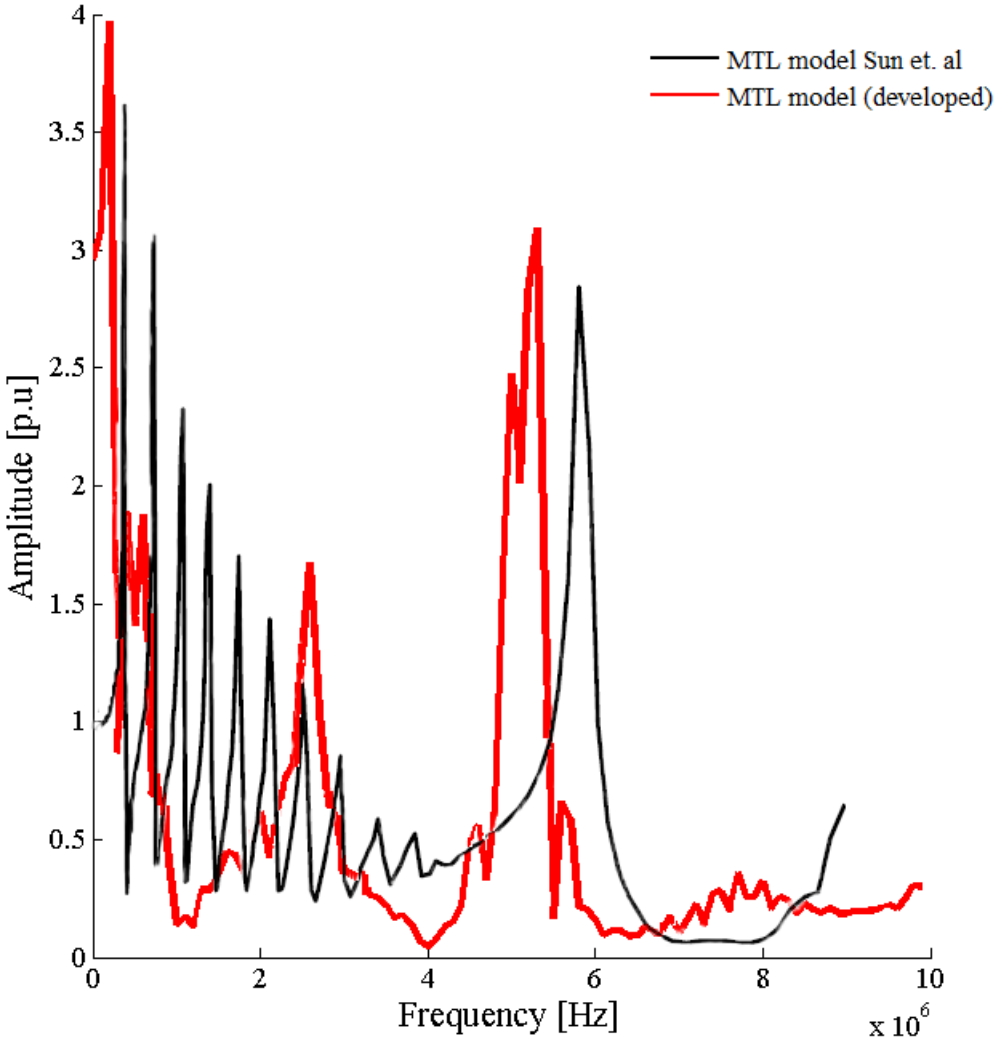

Figure 5.2: Comparison between developed MTL model and Sun et. al MTL model (adapted from [5]) : Amplitude of transfer function between turn 20 of Figure 5.1 and input.

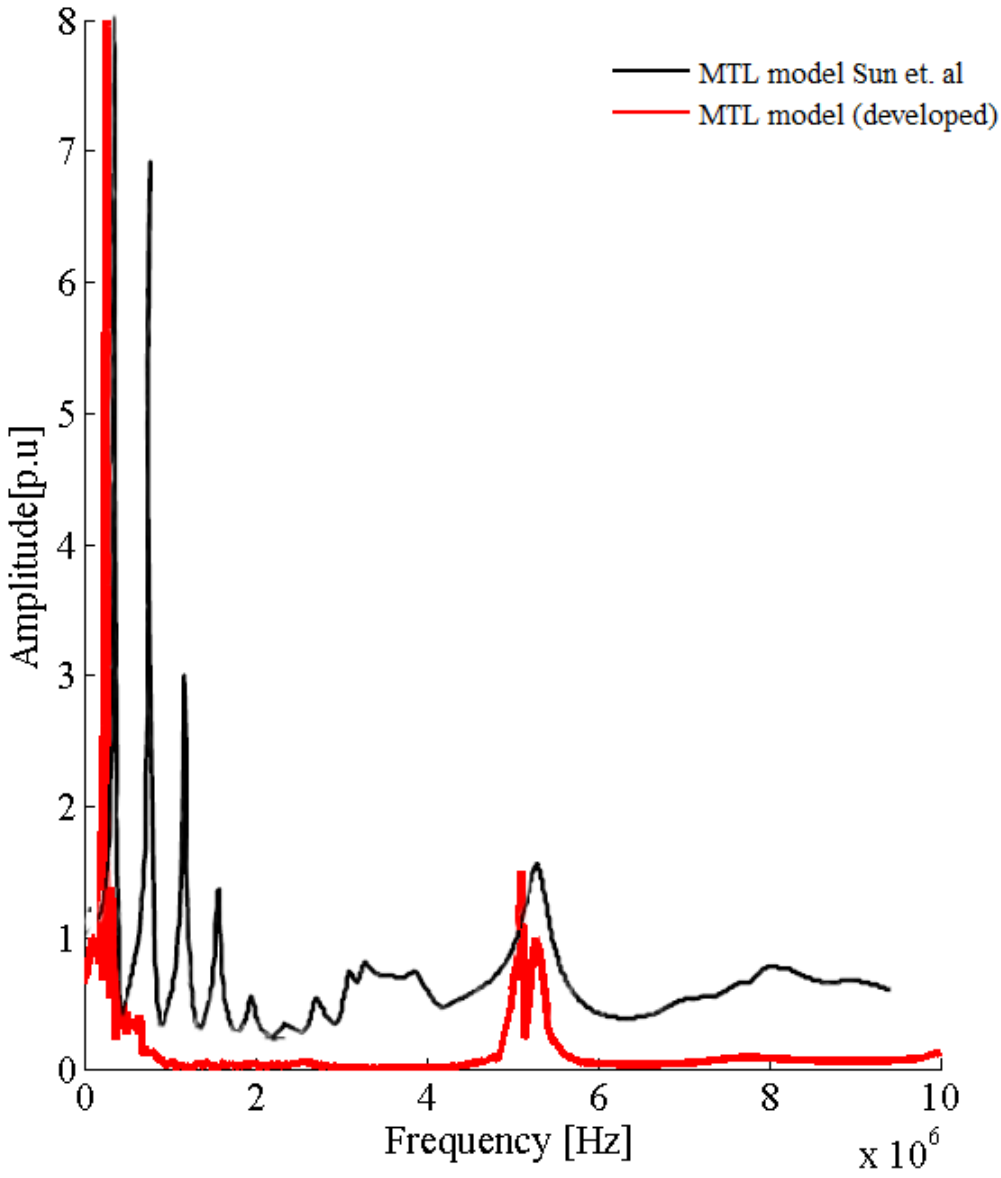

Figure 5.3: Comparison between developed MTL model and Sun et. al MTL model (adapted from [5]) : Amplitude of transfer function between turn 40 of Figure 5.1 and input.

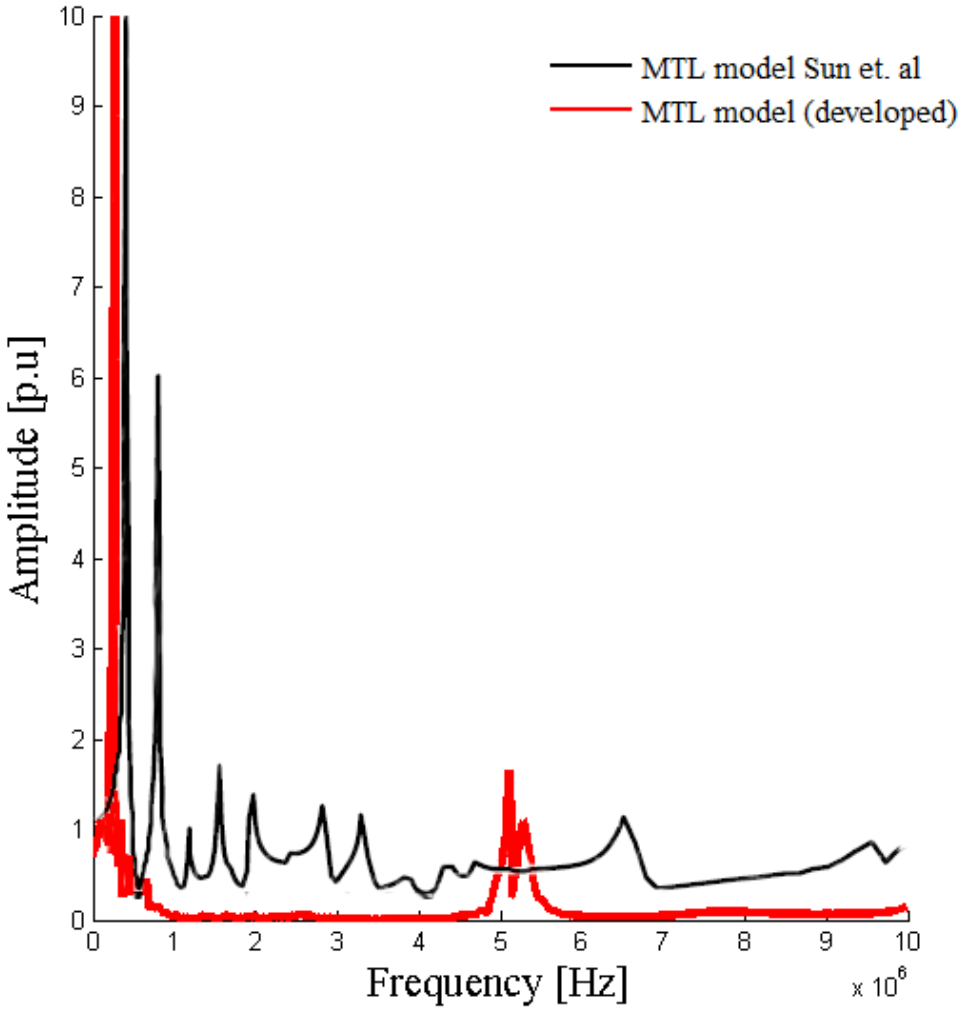

Figure 5.4: Comparison between developed MTL model and Sun et. al MTL model (adapted from [5]) : Amplitude of transfer function between turn 60 of Figure 5.1 and input.

Analysis of Figures 5.2, 5.3, 5.4 reveals that some of the frequency components are not well represented with the developed MTL model. This can be seen by the deviation between 1 to 3 MHz for the frequency plot of turn 40 and turn 60.

5.4 Discussion

The discrepancy off the results obtained by the developed MTL model versus the MTL model by Sun et al. can be explained as:

1. The mismatch between some frequency components could be as a result of the approximated equation for tan δ which was used. Equation 4.11 was used to approximate the frequency dependency of the loss factor of the transformer insulation. Improper approximation of the loss factor will affect the damping magnitude of the frequency components. No tanδ approximation was stated in the work of Sun et. al [5], [25]. The approximated equation used may not yield a clear representation of the tan δ used by Sun et. al. In addition as previously highlighted in Chapter 4, tan δ can be expressed by many equations as shown in Figure 4.3. As such no single equation can be applied for universal modelling of the dissipation factors of the transformer insulation.

2. The importance of the termination impedance shown in Figure 3.3 also plays a role. According to [44], to eliminate the divergence of the computations, a small impedance of $Z_t = 10^{-9}$ Ω must be used. The value used by Sun et. al in [5], [25] is unknown as it was not specified in the paper and may have been different from the one used during the computations.

However the main frequency component around 5 to 6 MHz termed as the dangerous frequency in [5], [25] is relatively well estimated. Analysis of the sweep frequency response of the turns reveals an important characteristic. The magnitude of the high frequency components can be seen decreasing as the number of turns increase down the transformer winding. The same behaviour can be annotated for the magnitude of the low frequency components which increase with an increase in turn number. This behaviour can explain why failure in transformer windings usually occur in the first two and the last two discs or layers. When extended to the time domain, high du/dt surges can cause development of large inter-turn transient voltages at the end turns/ discs/ layers. Hence the failures shown in Figures 1.1, 1.2, 1.3 and 1.4.

The next issue which warrants a discussion is the resistance calculation. In [5] and [25], Sun et al. calculated the resistance by taking into account the skin effect at high frequencies as

shown by Equation 4.14. However, another way of calculating the resistance as previously discussed is by using Equation 4.15 which takes into account proximity effects. Analysing the work done by Soloot et. al in [67], the total resistance is predominantly affected by the proximity effect for frequencies above 4 MHz. Neglecting the proximity effects as done by Sun et. al in [5],[25] and only taking into account the skin effect in the resistance calculation could result in resonant frequencies below 4 MHz with quite high amplitudes [67] as shown in Figures 5.2, 5.3 and 5.4. To illustrate this, the magnitude of the transfer function at turn 20 is re-calculated by taking into account proximity effect. The results of the MTL model with the impedance Equation 4.15 is shown in Figure 5.5. Analysis of Figure 5.5 shows that the magnitude of the resonance frequencies below 4 MHz which had quite high amplitudes have diminished considerably compared to the original waveform in Figure 5.2. Not taking into account the proximity effects can lead to calculated results which have a poor agreement with measurements as demonstrated by Soloot in [67].

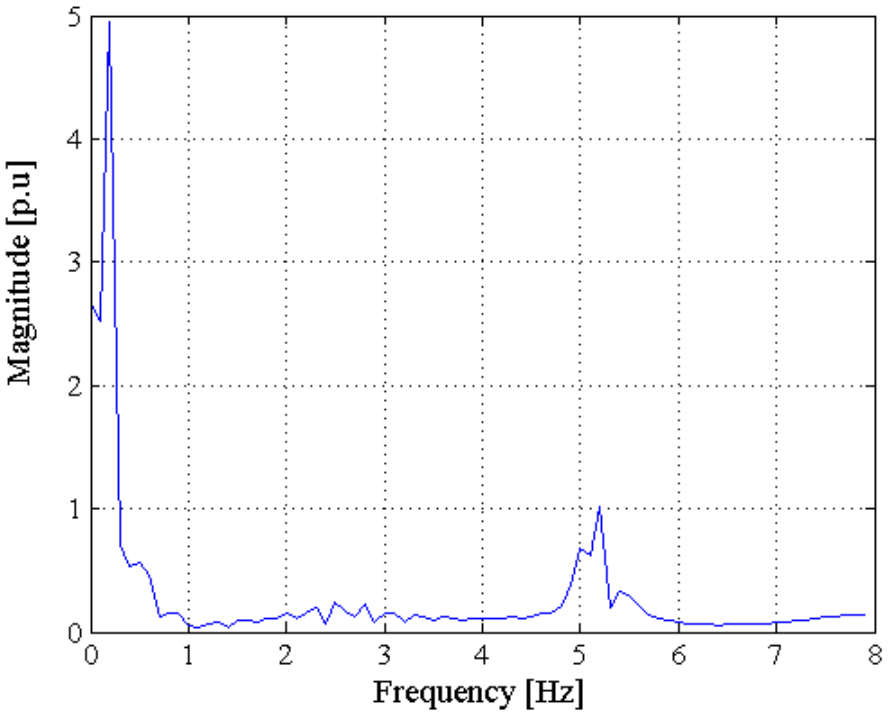

Figure 5.5: Magnitude of transfer function of turn 20 relative to the input (taking into account proximity effects)

5.5 Conclusion

In this chapter verification of the MTL model was done by using published work of Sun et. al [5], [25]. The developed MTL model by the author was compared with the results obtained by Sun et. al [5], [25]. The comparison reveals a relatively good agreement between the two models. However as highlighted in this chapter, several concerns were raised which could explain the discrepancies between the two models. Further work on an actual transformer prototype will be needed to validate the model and expose the short-comings.

Chapter 6

Resonance Analysis: Verification of High Frequency Model of Transformer

6.1 Chapter Overview

In the previous chapter the high frequency model of the transformer was applied to a disc type winding. Further application of the MTL model will now be applied to a layer type of winding. As previously mentioned in Chapter 1, the aim is to address the causes of the failed 2.7 MVA, 0.690 / 33 kV step-up transformer. This was done by investigating the resonant performance of two prototype transformers. The two prototype transformers had the same rating as the failed unit and both used a stacked core as opposed to the failed unit which had a wound core. However they differed in the winding arrangement as one had split round windings and the other had single round windings. Analytical calculations were done using the MTL model and results were compared with measurements. The calculated results using the MTL model showed a relatively good agreement and followed the trend of the measured results for a frequency range of 1 kHz to 10 MHz.

6.2 Test Equipment and Measurement of Resonance

The test equipment consisted of a Krohn-Hite Power Amplifier 7602 M series, a 20 MHz Agilent 3320A waveform generator and a Tektronix (DPO 3032) 300 MHz Oscilloscope as shown in Figure 6.1. A block diagram of the test setup is shown in Figure 6.2 whilst a snapshot at the Transformer Manufacturer test bay is shown in Figure 6.3. The signal generator was connected to the power amplifier to keep the voltage across transformer winding constant as the frequency was varied. The oscilloscope channels displayed the measured voltages at the

measuring taps as follows (i) measure and display the voltage across the whole winding (Start and Finish as in Figure 6.2) (ii) measure and display the output voltage (Voltage at turn k to ground as shown in Figure 6.2).



Figure 6.1: Test equipment used

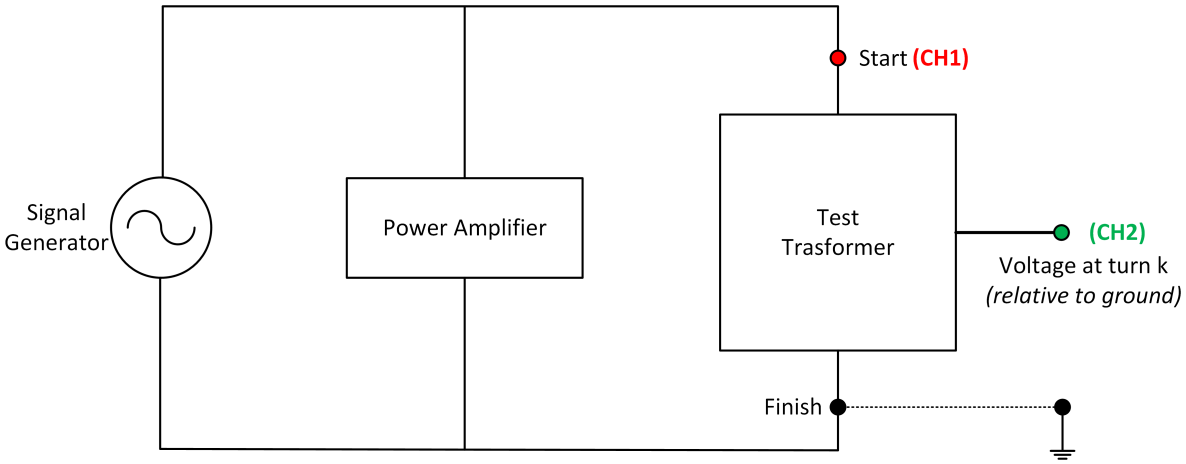

Figure 6.2: Test Setup



Figure 6.3: Test equipment setup

In the literature two methods are outlined for the determination of the frequency response of a transformer: the impedance versus frequency plot using Frequency Response Analysis (FRA) equipment and the amplification factor versus frequency using a signal generator and an oscilloscope. The amplification factor or gain function is defined generally for all cases as [73]:

$$N_{1m,j} = \frac{Voltage\ between\ point\ 1\ and\ m\ at\ frequency\ w_i}{Voltage\ applied\ at\ frequency\ w_i\ to\ node\ j} \tag{6.1}$$

Using FRA equipment Equation 6.1 can be further expanded to Equation 6.2 [32]:

$$N_{1m,j} = \frac{Z_{ij}(j\omega) - Z_{mj}(j\omega)}{Z_{jj}(j\omega)} \tag{6.2}$$

The Resonance Voltage Ratio (RVR) can be derived from the generalized amplification factor in Equation 6.1 to give Equation 6.3.

$$RVR = \frac{Voltage\ between\ point\ 1\ and\ m\ at\ frequency\ w_i}{Voltage\ between\ point\ 1\ and\ m\ at\ 50Hz} \tag{6.3}$$

In Equation 6.3 the RVR is now defined as the voltage between points at the resonant frequency divided by the voltage between the same points when a 50 Hz voltage with the same amplitude is applied to the winding.

6.3 Stacked core transformer prototypes

The design of the stacked core transformer is such that the inner winding is the LV winding whilst the outer winding is the HV (MV) winding. This differs from the wound core transformer as it had the HV winding sitting inside the LV winding with a static screen between the two windings.

6.3.1 Split round winding prototype transformer

The stacked core transformer prototype with split round winding was installed with measuring taps at the ends of each layer as shown in Figure 6.4. Note that the stacked core transformer prototypes only differ in the core structure with the wound core transformer. Both upper and lower coils consisted of a total of 16 layers separated by an oil gap through the use of wooden spacers shown in Figure 6.4. The constructed prototype is shown in Figure 6.5.

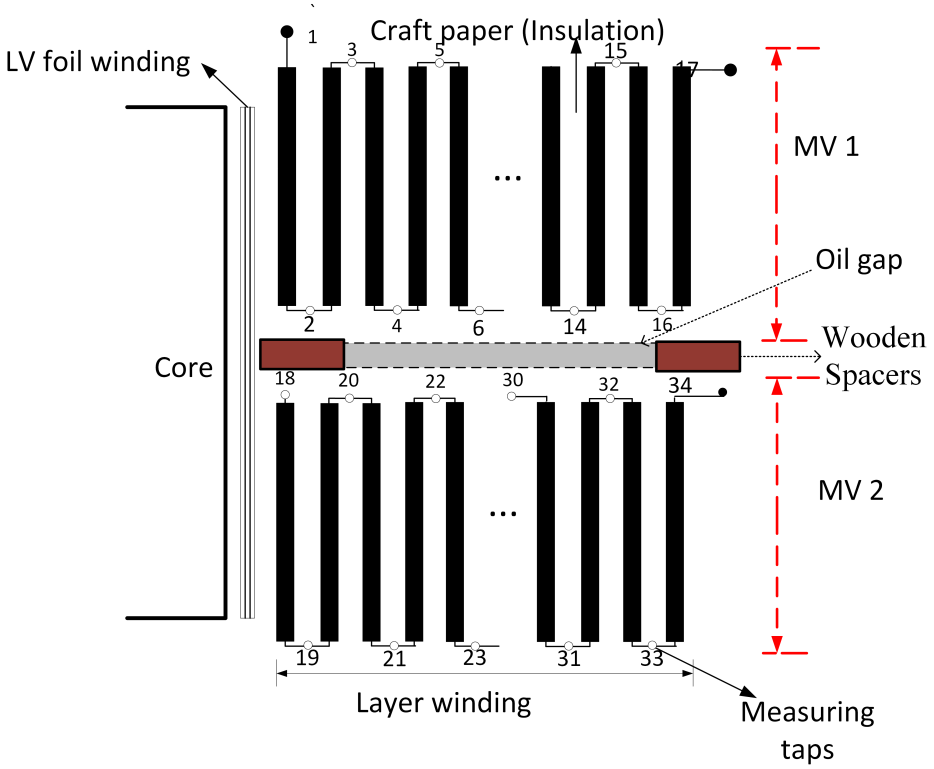

Figure 6.4: Axisymmetric view of the first prototype transformer.

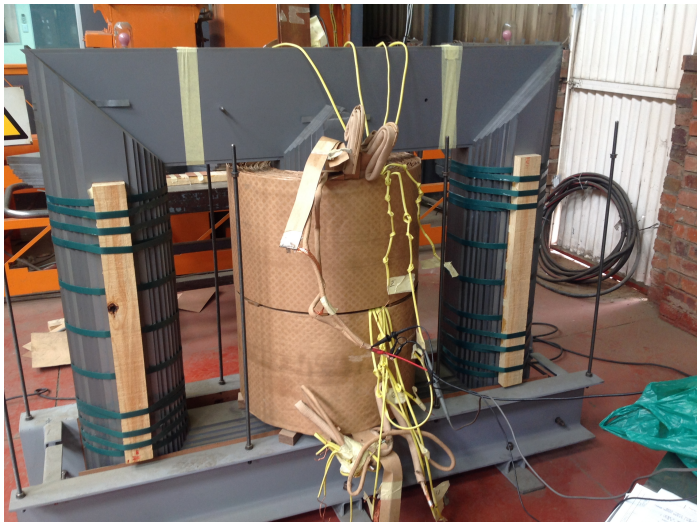

Figure 6.5: Split round winding prototype transformer.

6.3.2 Single round winding prototype transformer

A second prototype transformer was constructed with the same stacked core as in Figure 6.5 but with a single round winding.

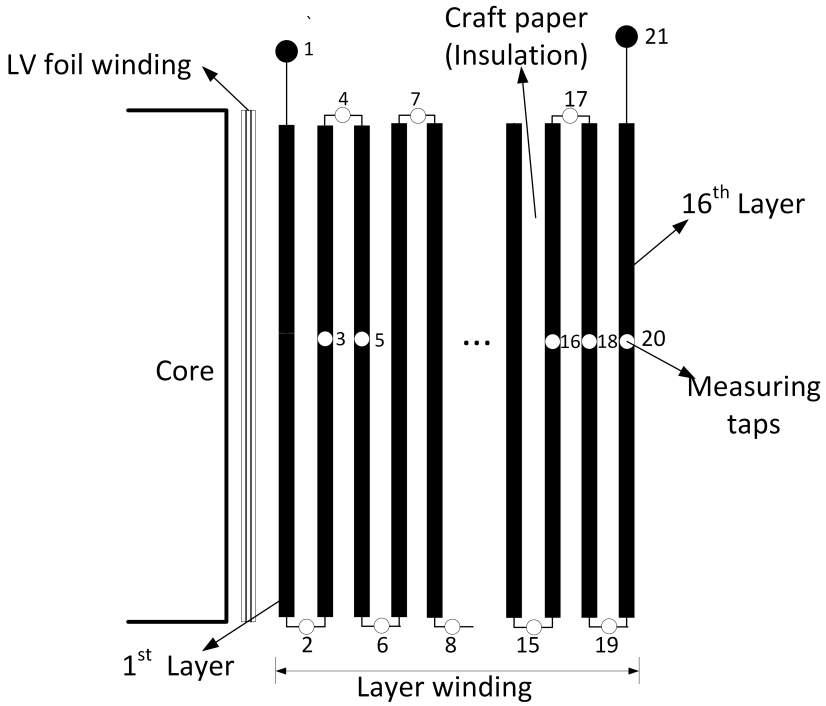

Figure 6.6: Axisymmetric view of the second prototype transformer



Figure 6.7: Non-split round winding prototype transformer

Measuring taps were installed at the start and ends of each layer and also in between the layers as shown in Figure 6.6. The second constructed prototype is shown in Figure 6.7. Both stacked and wound core transformers had the same number of layers.

6.4 Comparison of Measured and Calculated Results

6.4.1 Split round winding prototype transformer

As previously mentioned, resonance can be classified as either internal or external resonance. It is worth noting that internal resonance can be further defined as "internal voltage maximum" and internal anti-resonance can be defined as "internal voltage minimum" [32]. This relationship will be crucial in the analysis of measured and calculated results. Comparison will not be done for all 16 layers, however only critical results will be revealed in this paper.

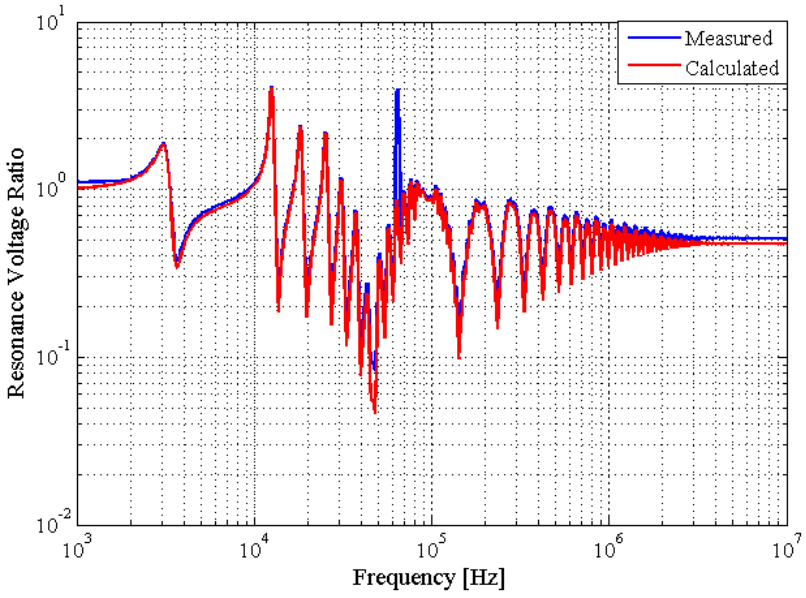

Figure 6.8: Resonance voltage ratio across Layer 1 [measured between tap 1 and tap 2 of Figure 6.4] versus calculated.

In Figures 6.8, 6.9 and 6.10 it can be seen that there is a relatively good agreement between the calculated and measured results. The calculated results follow the profile of the measured results although there is a frequency shift between 1 kHz and 10 kHz for layer 15 and layer 16 (measured between the taps as indicated in Figures 6.9 and 6.10. Analysis of the measured results in Figures. 6.8, 6.9 and 6.10 show that above 500 kHz the resonance voltage ratio decreases almost approaching zero above 1 MHz.

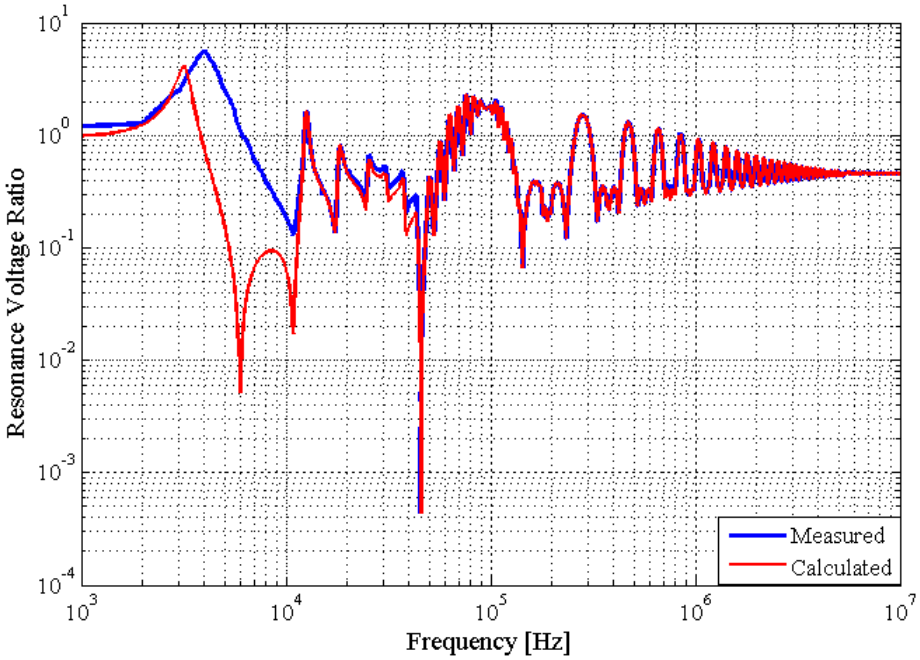

Figure 6.9: Resonance voltage ratio across Layer 15 [measured between tap 32 and tap 33 of Figure. 6.4] versus calculated.

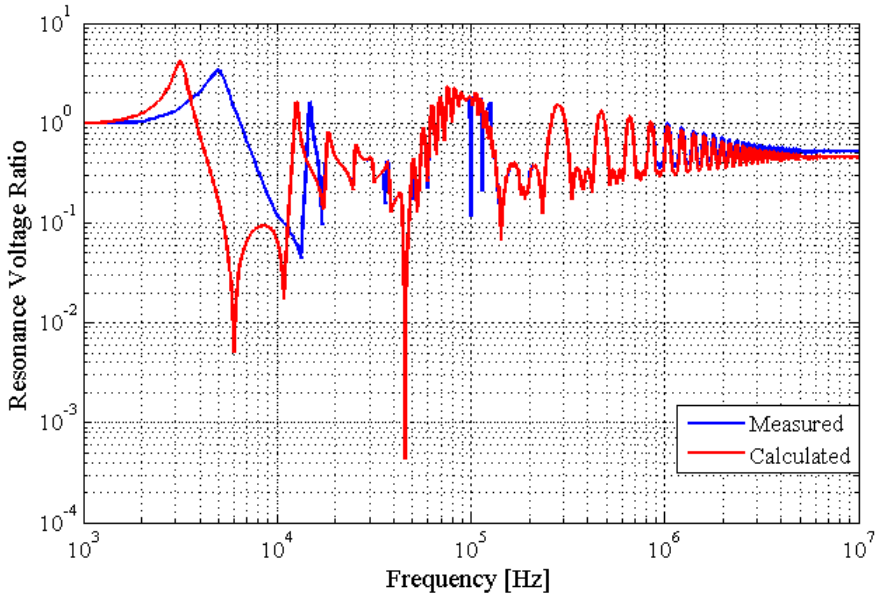

Figure 6.10: Resonance voltage ratio across Layer 1 [measured between tap 33 and tap 34 of Figure. 6.4] versus calculated.

The general trend of the resonance voltage ratio is shown in Figures. 6.11, 6.12, 6.13 and 6.14. It is interesting to note that the magnitude of the resonant voltage ratio increases as you approach the break i.e. layer 1 to layer 5. Then the magnitude starts to decrease for layers 9 to layer 16.

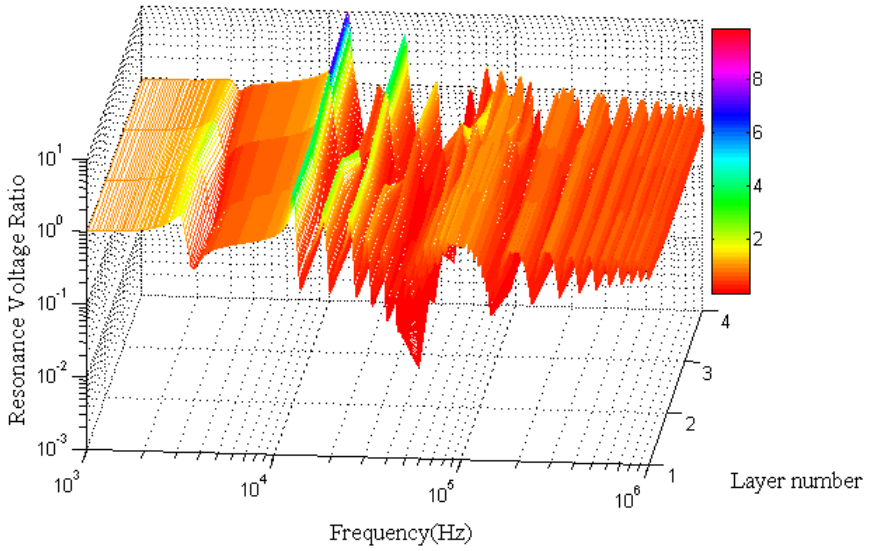

Figure 6.11: Resonance Voltage Ratio (RVR) distribution in layers 1 - 4

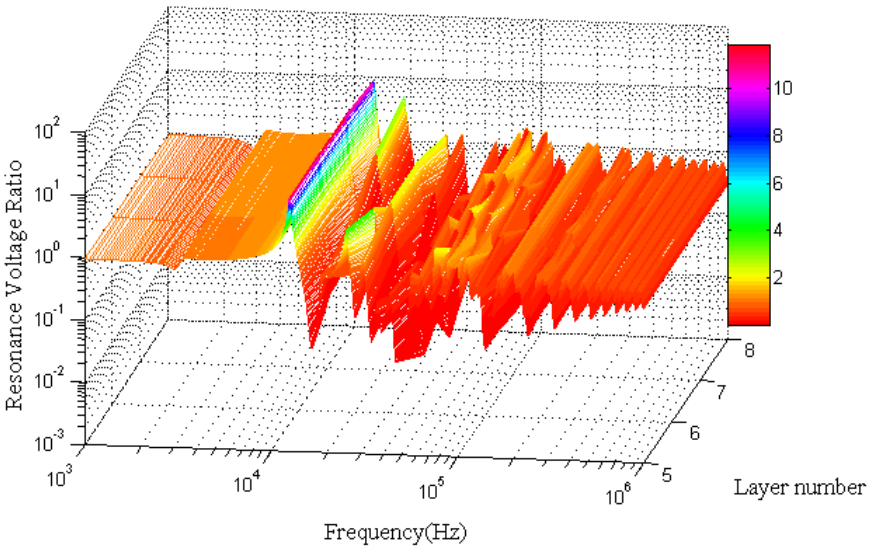

Figure 6.12: Resonance Voltage Ratio (RVR) distribution in layers 5 - 8

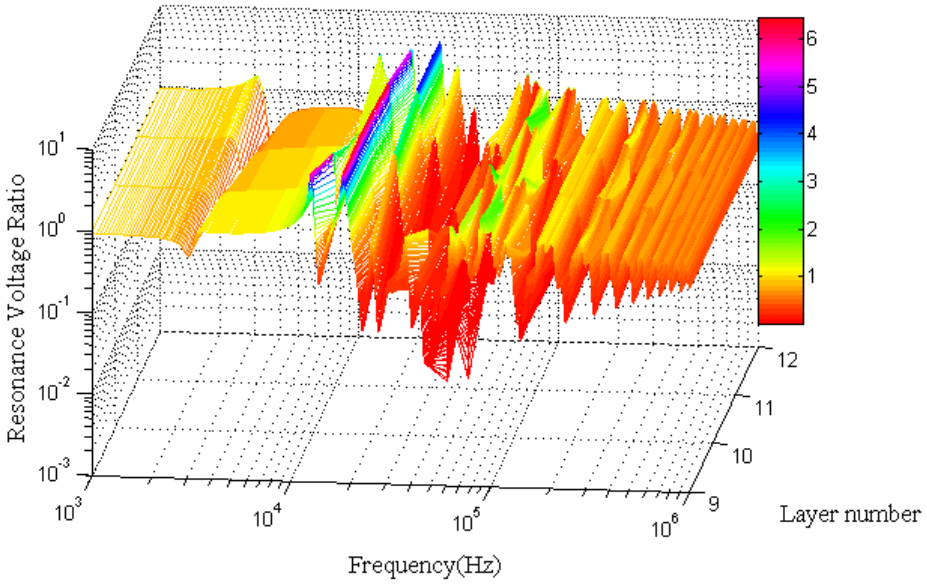

Figure 6.13: Resonance Voltage Ratio (RVR) distribution in layers 9 -12

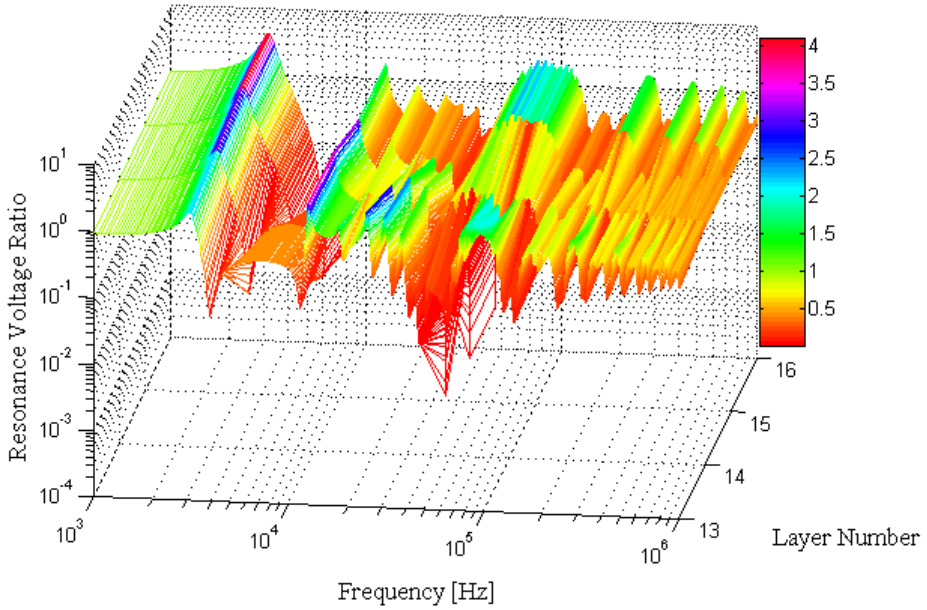

Figure 6.14: Resonance Voltage Ratio (RVR) distribution in layers 13 - 16

6.4.2 Non-split round winding prototype transformer

6.4.2.1 Full layer measurements

For the second prototype, comparison of the measured vs calculated results shown in Figures. 6.15, 6.16, 6.17, 6.18, and 6.19. Analysis of the comparison results for the non-split MV windings reveals that between 1 kHz and 10 kHz the results do not agree. There is also a mismatch of the calculated results with the measured for frequencies between 1 MHz and 2 MHz. However the calculated results using the MTL model do approximate the measured results for frequencies above 30 kHz. The differences in the magnitude will be explained in the discussion section.

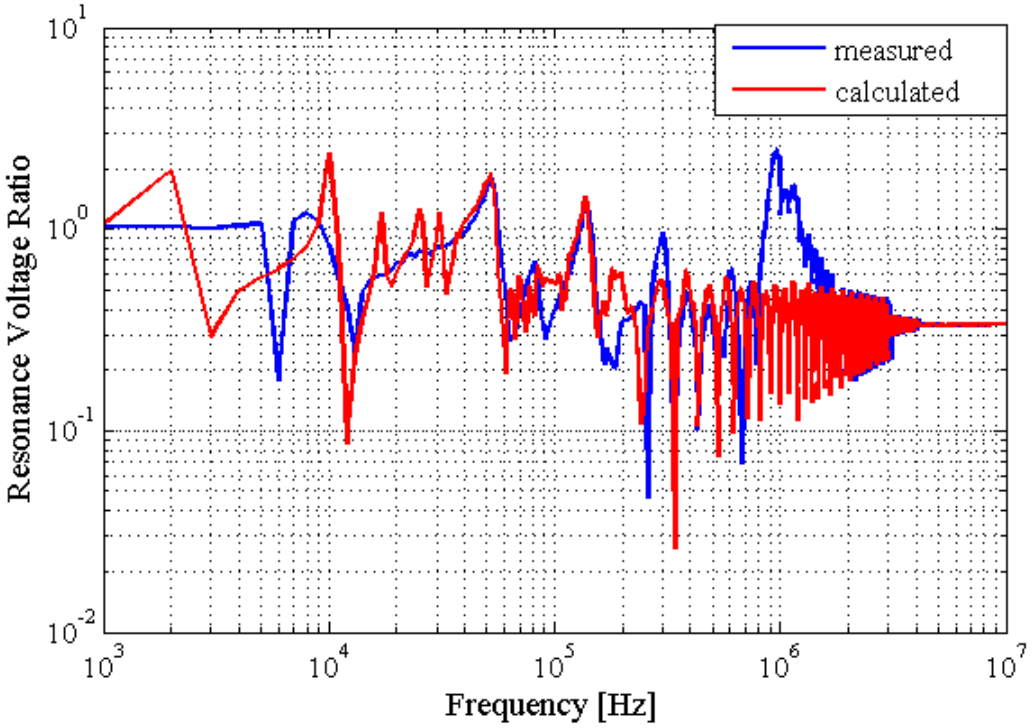

Figure 6.15: Resonance voltage ratio (RVR) across layer 4 [measured between tap 6 and tap 7 of Figure. 6.6] versus calculated.

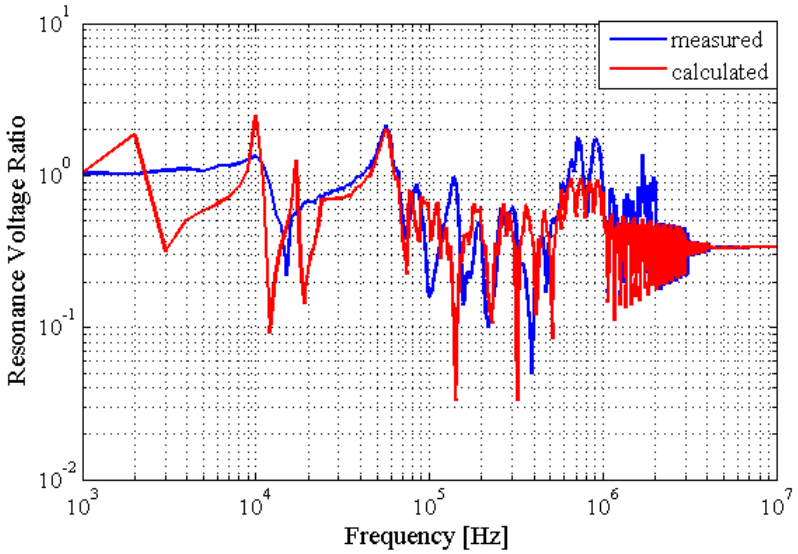

Figure 6.16: Resonance voltage ratio (RVR) across layer 5 [measured between tap 7 and tap 8 of Figure. 6.6] versus calculated.

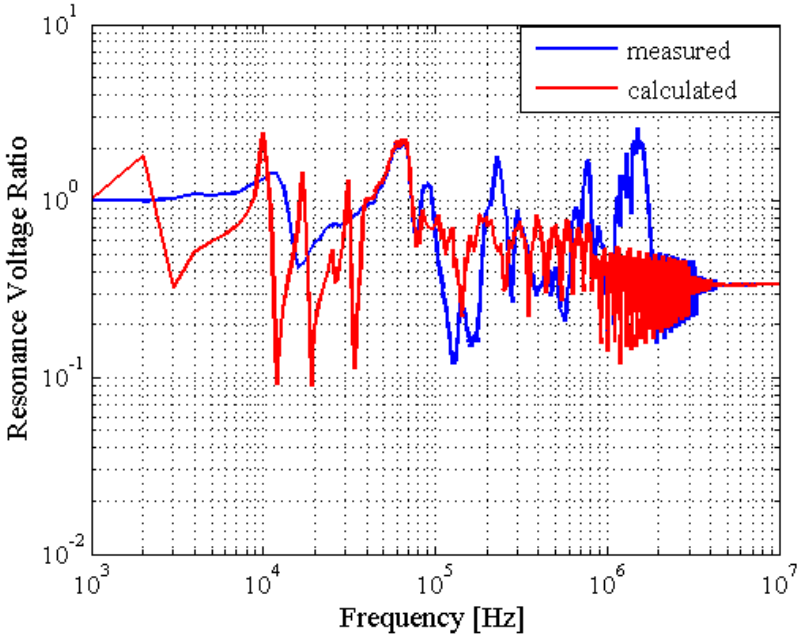

Figure 6.17: Resonance voltage ratio (RVR) across layer 6 [measured between tap 8 and tap 9 of Figure. 6.6] versus calculated.

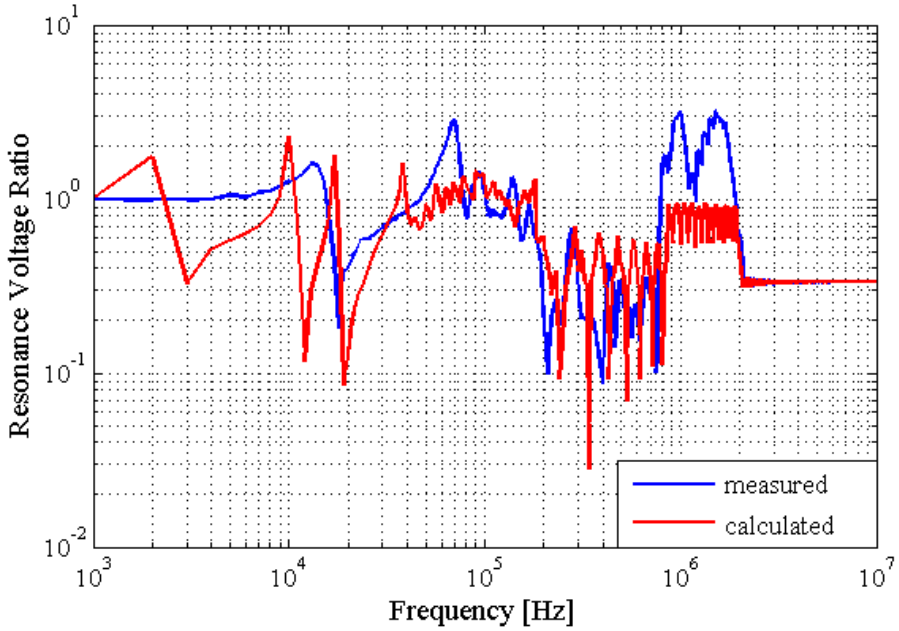

Figure 6.18: Resonance voltage ratio (RVR) across layer 7 [measured between tap 9 and tap 10 of Figure. 6.6] versus calculated.

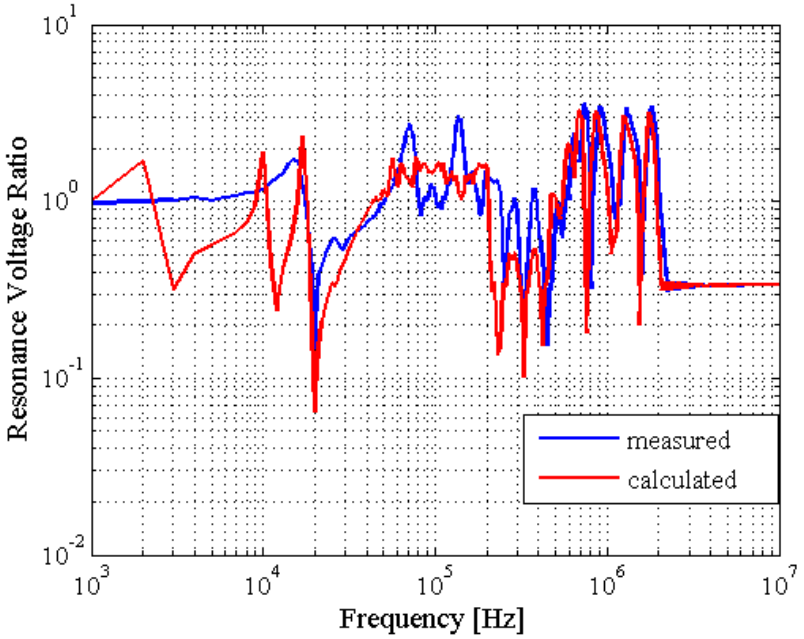

Figure 6.19: Resonance voltage ratio (RVR) across layer 8 [measured between tap 10 and tap 11 of Figure. 6.6] versus calculated.

6.4.2.2 Start to middle of winding measurements

The investigation of the voltage distribution in the middle of the layer has been investigated in [67], [74]. This was done by measuring the voltage drops using FRA equipment. However can the same be investigated using the MTL model and what are the constraints? As previously highlighted by Equations 4.6 and 4.7, matrix reduction is a technique used to reduce the size of matrices by grouping a number of turns in each layer to represent a single transmission line. To test the limitations of this reduction technique when applied to the MTL model, the same Equations 4.6 and 4.7 were applied to represent the total number of turns in half a layer. Hence each group of turns from the start of a layer to the middle of the layer was presented by a single transmission line. The results of the comparison are shown Figures. 6.20 and 6.21. Analysis of these figures reveal that there are limitations of the model within the frequency ranges: 1 kHz to 30 kHz and 1 MHz to 2 MHz.

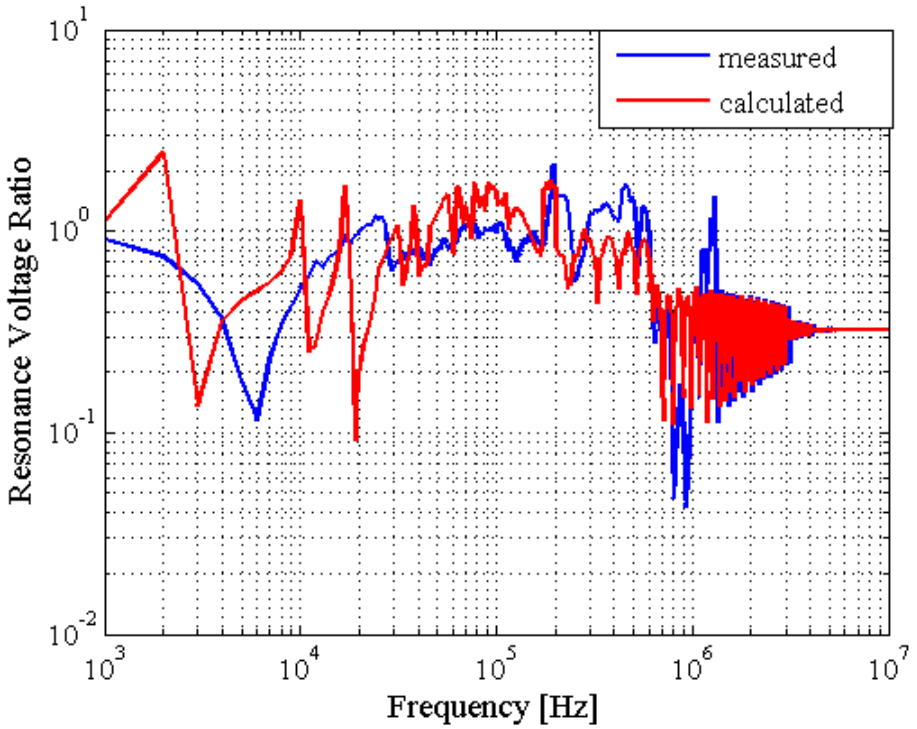

Figure 6.20: Resonance voltage ratio (RVR) across the start to middle of layer 2 [measured between tap 2 and tap 3 of Figure. 6.6] versus calculated.

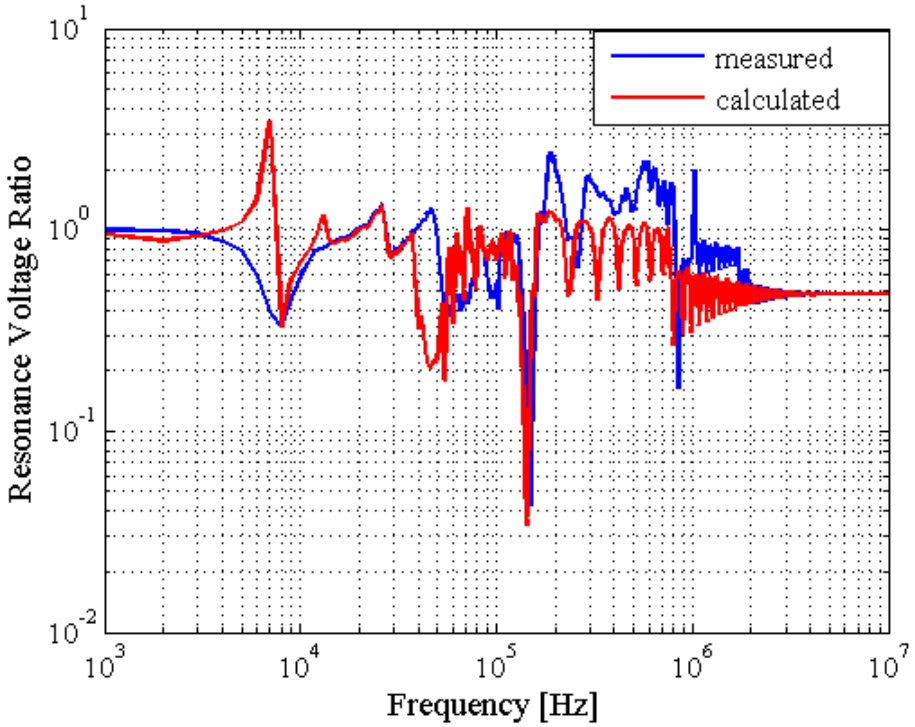

Figure 6.21: Resonance voltage ratio (RVR) across the start to middle of layer 3 [measured between tap 4 and tap 5 of Figure. 6.6] versus calculated.

6.5 Comparison of the Resonance Performance of Split and Non-Split MV Windings

As previously mentioned wind turbine transformers are frequently subjected to repetitive fast transients. These fast transients usually consist of a spectrum of different frequency components that could excite one of the natural resonant frequencies of the winding, resulting in the development of high internal voltages. The measured results for certain layers with high potential risk of failure as discussed in Chapter 1 are going to be discussed by analysing the results of the sweep frequency response measurements of the two designs. Hence a comparison will be made between the transformer with a split MV winding of Figure 6.5 and a non-split MV winding shown in Figure 6.7. As previously highlighted in Chapter 1, the first two layers and the last two layers are usually more prone to failure due to fast transients. Hence a comparison will be done for these specific layers which are layer 1, layer 15 and layer 16. The results are shown in Figures 6.22, 6.23 and 6.24. Comparison of the sweep frequency response for the two transformer winding designs reveals an important result.

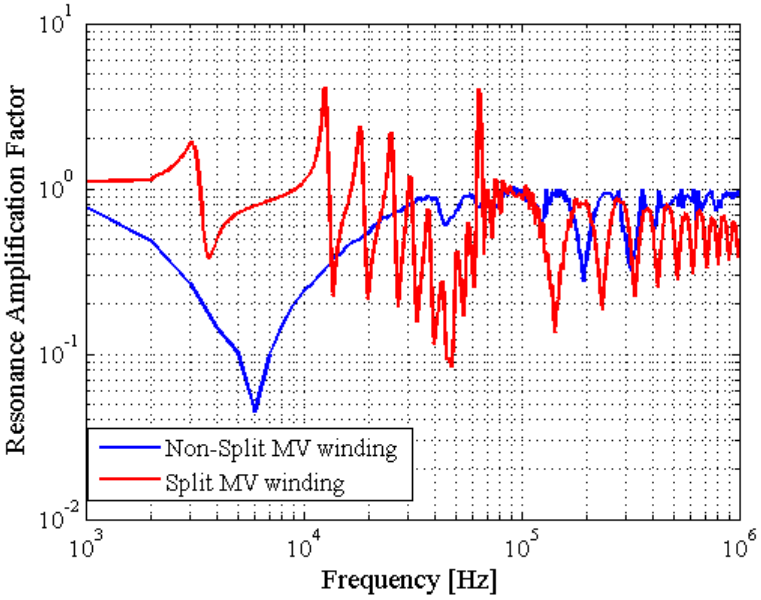

Figure 6.22: Comparison of the sweep frequency response of layer 1 for the transformers in Figures 6.5 and 6.7.

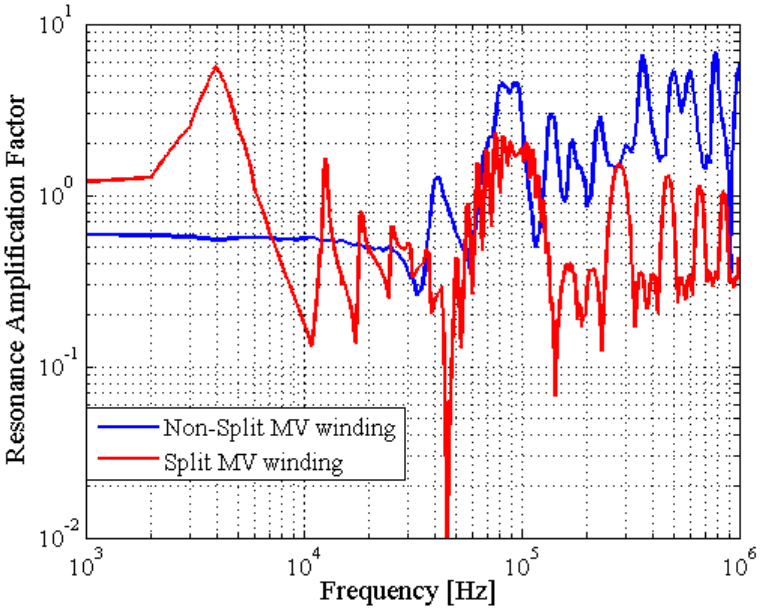

Figure 6.23: Comparison of the sweep frequency response of layer 15 for the transformers in Figures 6.5 and 6.7.

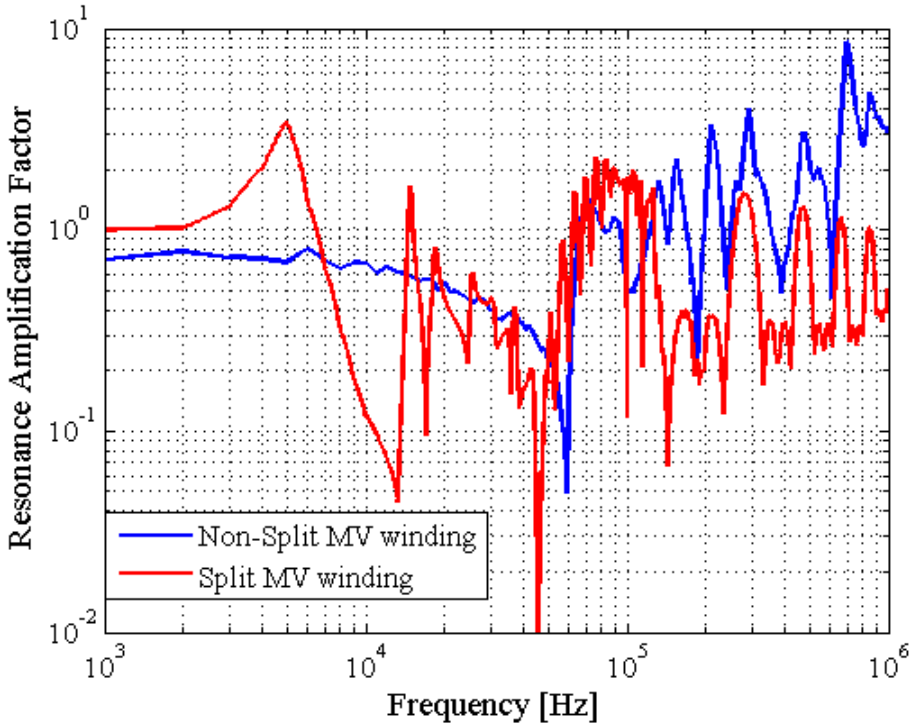

Figure 6.24: Comparison of the sweep frequency response of layer 16 for the transformers in Figures 6.5 and 6.7.

The transformer with the split MV winding has a high resonant amplification factor below 200 kHz. In contrast the transformer with a non-split MV winding has a high resonant amplification factor above 200 kHz. Having gained insight about the resonant performance of the two prototype designs, an appropriate design will have to be chosen. However since the magnitude of the frequency components is unknown at this point, Chapter 7 investigates the measurement of switching surges. Knowledge of the frequency spectrum of the switching surges can help in choosing an appropriate design that is less prone to the effects of internal resonance.

6.6 Discussion and Conclusion

In this chapter modelling of two prototype transformers using the MTL model was investigated. The calculated results using the MTL model were compared with results obtained by measurements. Comparison of the two revealed a relatively good agreement within certain frequency ranges. The major benefit is the insight that the MTL model provided into the resonance performance of the different winding designs considered. Such purpose can find applicability during the

transformer design process. It is important to note that application of a design safety factor will have to be applied to counteract the discrepancies observed during the comparison of calculated and measured results. The resonant performance of the two winding designs revealed that it is possible to shift the resonant frequencies to occur either earlier or later in the frequency spectrum.

Chapter 7

Switching Surges and Severity Factors

7.1 Chapter Overview

In this chapter an investigation into the measurement of switching surges on an actual wind turbine transformer is presented. Since the measurements are made in a wind farm with associated collector cable system, there is a high probability that the generated waveforms due to system interaction may contain oscillatory voltage transients which will be impinged on the transformer terminals. The frequency spectrum of these transients may be such that one of the frequency components may coincide with the transformer's winding natural resonant frequency. Such a case can lead to the development of resonant overvoltages within the windings. Therefore studying the transients generated during switching will be important to assess if they pose a risk to the transformer insulation. If the switching waveforms consist of repetitive transient overvoltages, accelerated ageing of the insulation could occur. This will most likely lead to a reduction of the insulation withstand capability and if not recognized during the design stage, could result in early insulation failure. An analysis technique for assessment of transformer voltage stresses will be done using the CIGRE proposed severity factors [4]. Since the distribution of electric stresses within the transformer are different with each switching event, the severity factors takes into account the voltage stress distribution within the transformer insulation structure for all the different types of standardized tests. The aim being to provide an assessment tool that can be used to evaluate the stresses impinged on the transformer terminals and also locally within the windings.

7.2 Measurement of Switching Transients

Measurements of switching transients at the transformer terminals were conducted at a wind turbine step-up transformer. The tests involved the following:

1. Energizing the transformer on no-load.
2. Disconnecting the transformer on no-load.

Measurement of the three MV phase-to-earth voltages were made by use of a capacitive voltage divider on each phase. The MV bushing screen had a measured capacitance of 32 pF and a 10 nF capacitor was externally mounted in series with the bushing screen terminal and the transformer tank to form a capacitive voltage divider. The resulting voltage division ratio was 313. Measurements were made on the MV side because the MV VCB was constantly switched. The aim of the tests was to investigate the switching transients i.e. pre-strikes (on energizing) and re-strikes and re-ignitions on disconnection. Figure 7.1 shows the measurement setup with the FLUKE 1750 recorder connected to the bushing voltage dividers. A simple block diagram of the test setup is shown in Figure 7.2.

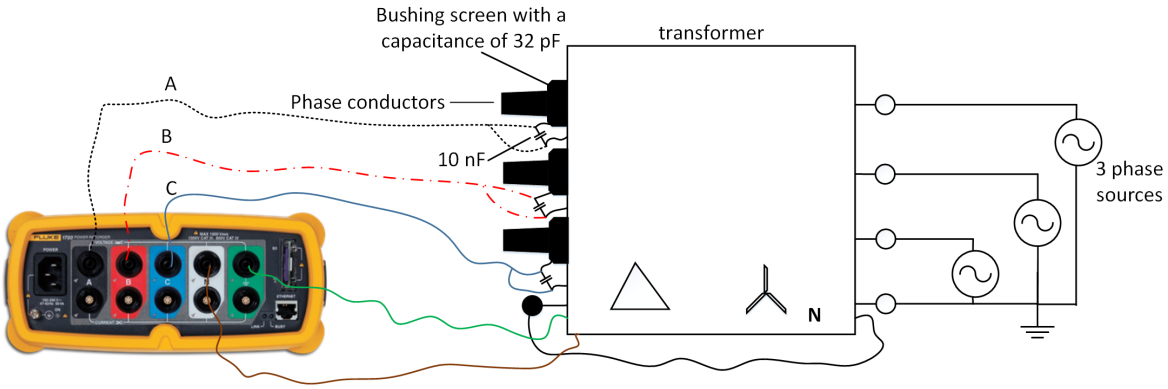

Figure 7.1: Measurement setup on a wind turbine transformer (Pad-mounted Transformer).

7.2.1 Energizing the transformer on no-load

Energization of the transformer always results in at least one pre-strike per phase [75]. During contact closing, generation of high du/dt transients can occur at the transformer terminals [14]. This behaviour can be observed from the measured transients in Figures. 7.3, 7.4, 7.5, 7.6, 7.7 and 7.8. The measurement setup explained in Figure 7.1 was used and the tests were conducted on one step-up wind turbine transformer at a particular wind farm. Analysis of the measured waveforms showed that the pre-strikes are different for each switching event. However they

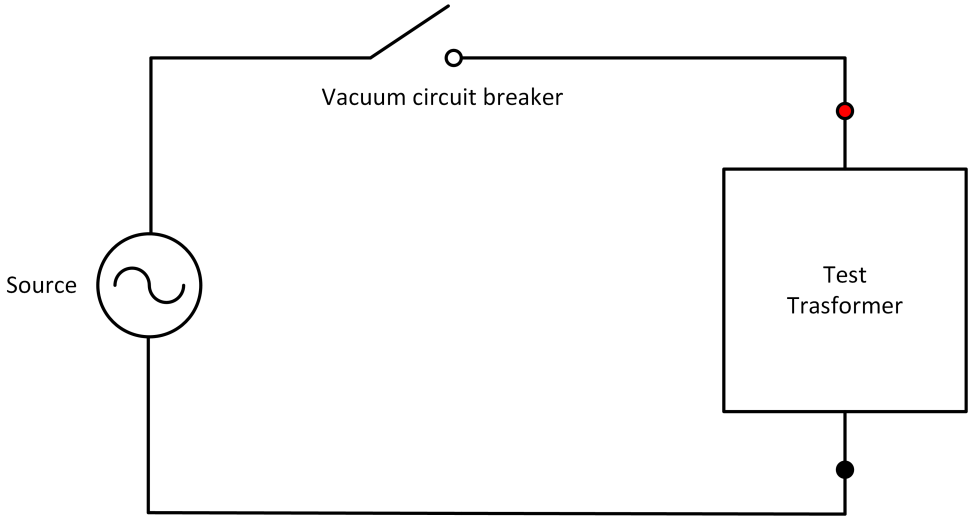

Figure 7.2: Block diagram of test setup.

all exhibit the basic characteristics i.e. they are repetitive in nature and have high du/dt values. Energizing a transformer onto the highly capacitance collector cable network presents voltage transient problems. As the cable connections are short, the speed of the transformer input capacitance charging from the network capacitance is limited in practise only by the cable resistance and the value of the phase to ground capacitance of the transformer. This type of low surge impedance connection has a low du/dt limiting effectiveness [14]. Hence the high du/dt values and the high frequency transients observed in Figures. 7.3, 7.4, 7.5, 7.6, 7.7 and 7.8. It should be noted that the sampling frequency for FLUKE 1750 is 5 MHz with analogue to digital resolution of 14 bits under transient conditions.

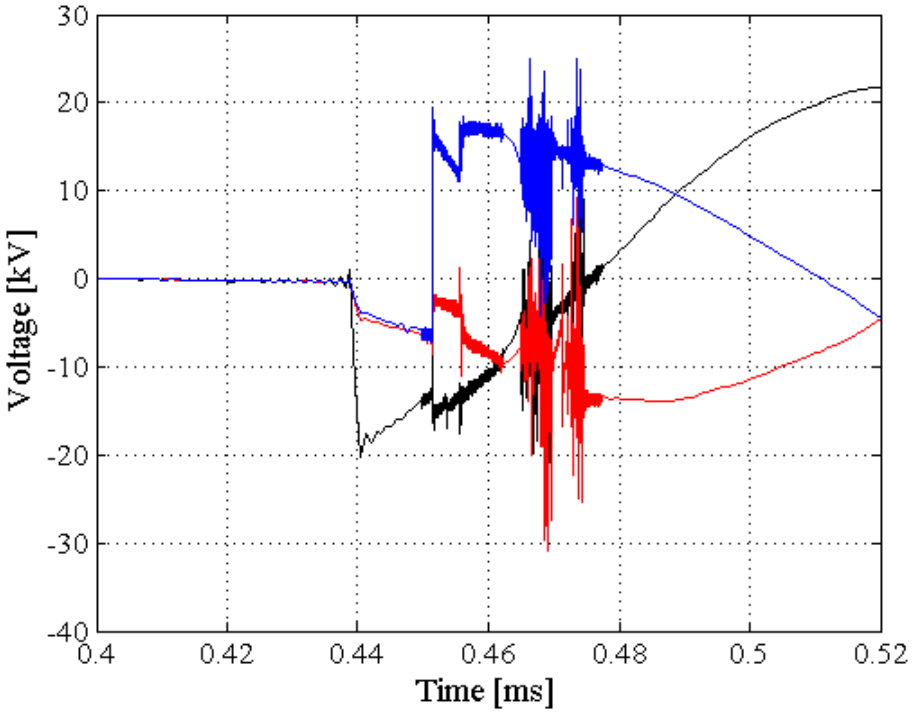

Figure 7.3: Measured pre-strike behaviour at 12:45

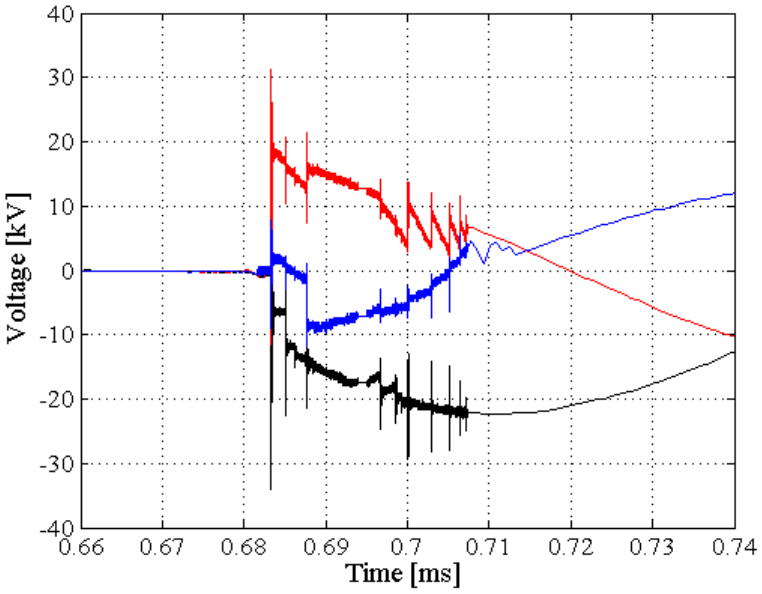

Figure 7.4: Measured pre-strike behaviour at 13:13

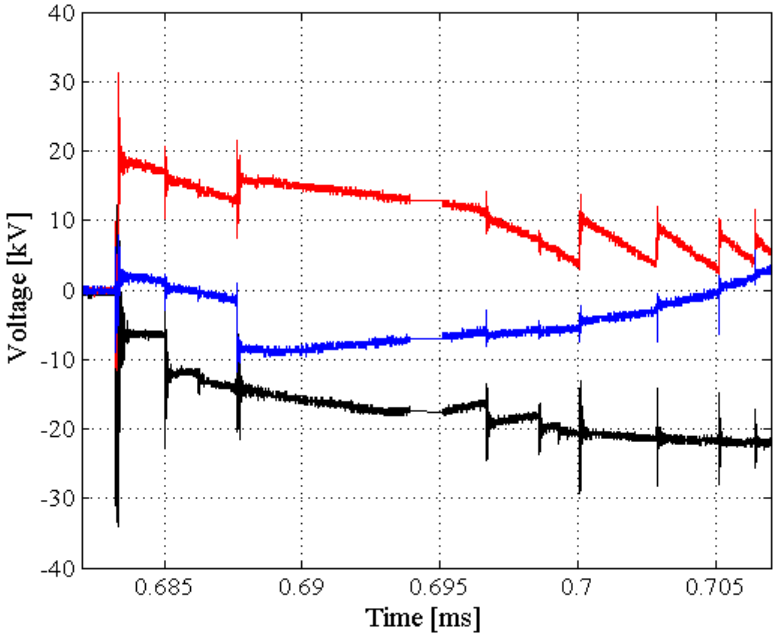

Figure 7.5: Time expansion of measured pre-strike behaviour at 13:13

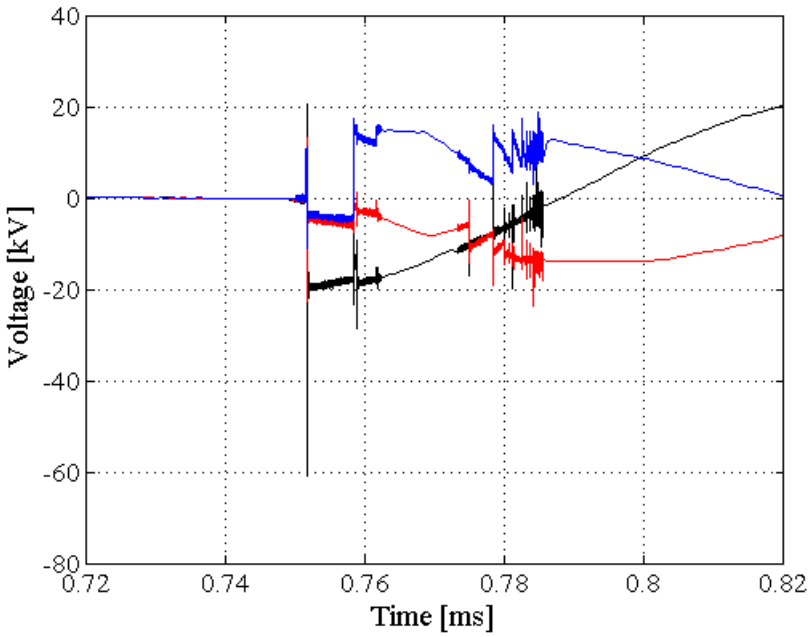

Figure 7.6: Measured pre-strike behaviour at 13:15

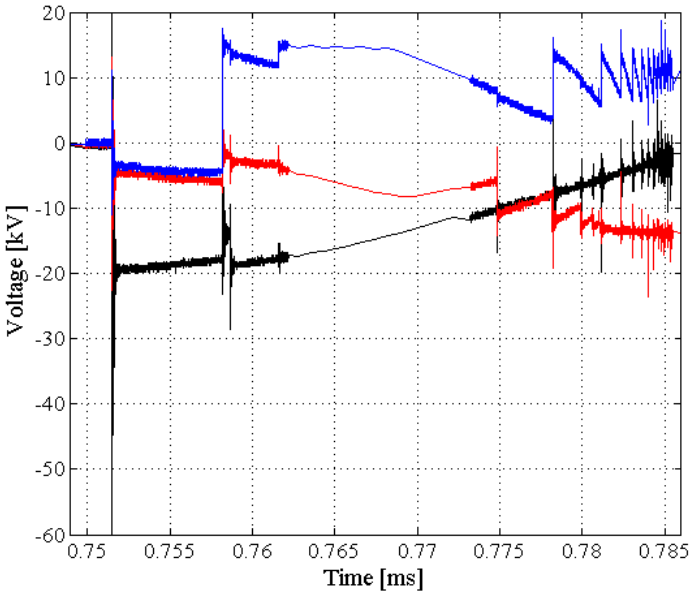

Figure 7.7: Time expansion of measured pre-strike behaviour at 13:15

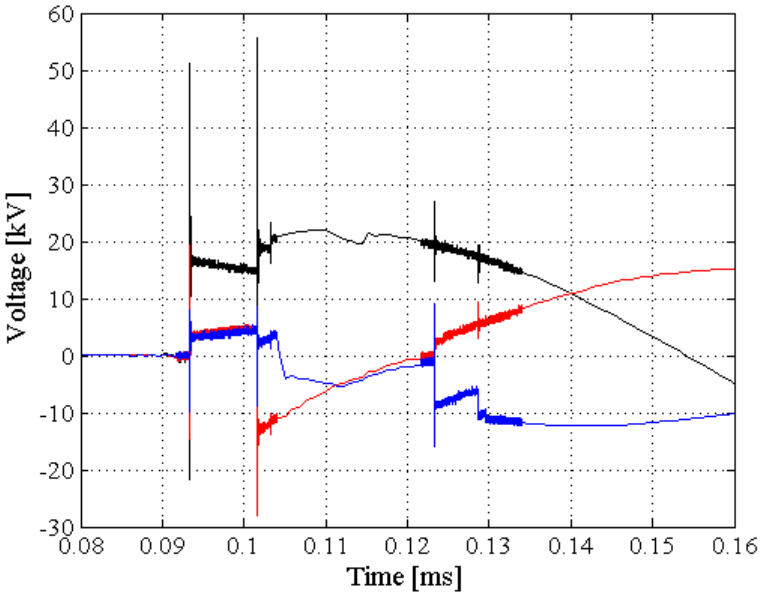

Figure 7.8: Measured pre-strike behaviour at 13:26

7.2.2 Disconnection of the transformer on no-load

On disconnection by the VCB, higher over-voltages can occur if the arc re-ignites after the first current interruption [76]. If the VCB is not able to quench the arc, multiple re-ignitions can occur and with each re-ignition, the voltage escalates resulting in higher over-voltages. No significant over-voltages were measured on disconnection of the transformer. A sample of the waveforms measured during disconnection is shown in Figure 7.9.

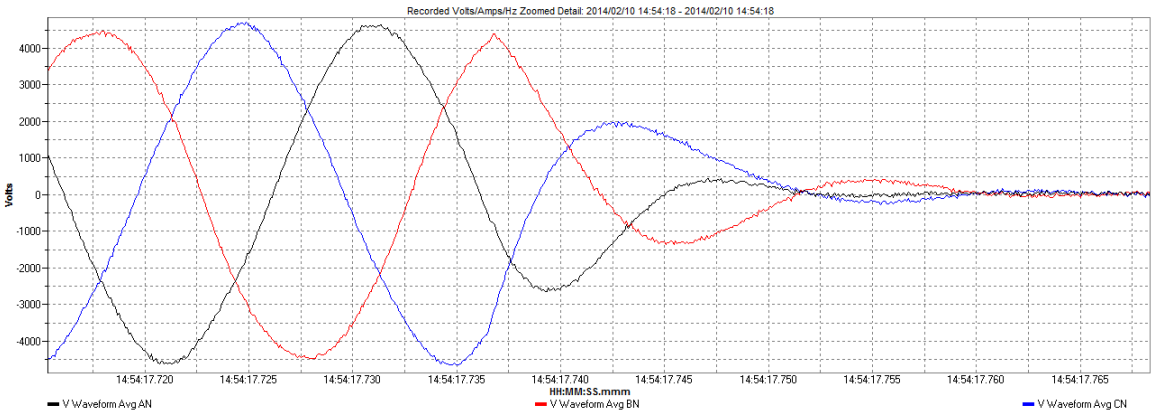

Figure 7.9: Measured waveform during transformer disconnection

7.2.3 Frequency domain analysis

Analysing the measured transients in the frequency domain can give a better perspective than time domain analysis. Hence Fast Fourier Transform (FFT) analysis was performed on the measured transients. In [77] the frequency content of the recorded transient was analysed using the FFT. Analysis of the results yielded the amplitude of the different frequency components. The amplitude spectra for the measured transients are shown in Figures 7.10, 7.11, 7.12 and 7.13. It should be noted that in the frequency domain, a steep front transient is identified by its higher frequency components [4]. The frequency domain results in Figures 7.10, 7.11, 7.12 and 7.13 show higher frequency components which would represent the steep, repetitive transients in the time domain. However there are no frequency components of amplitude significantly larger than the others.

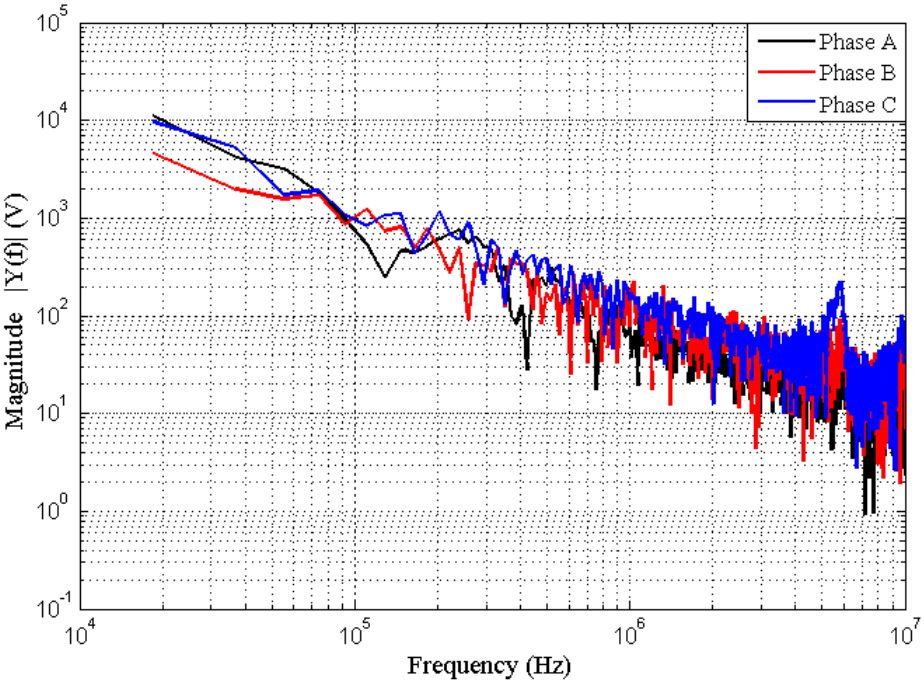

Figure 7.10: FFT analysis for the measured transient at 12:45

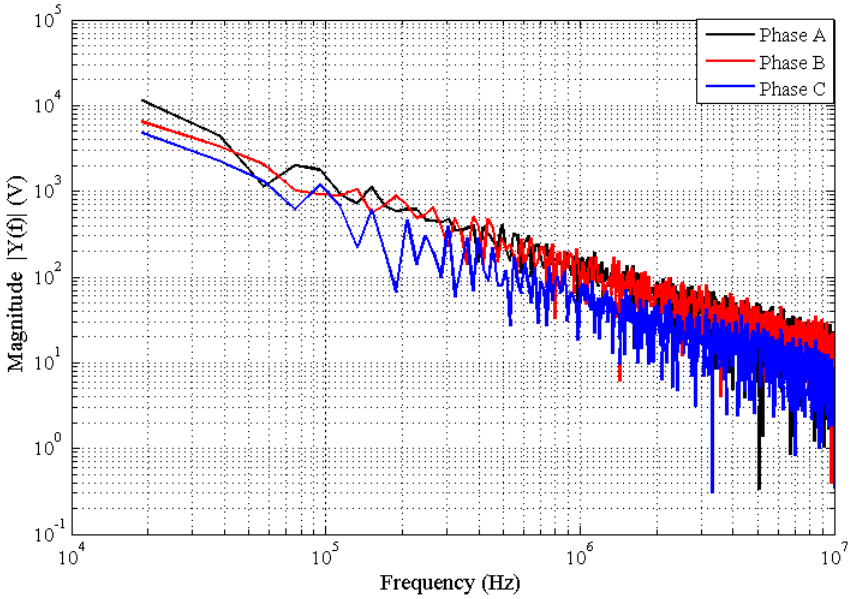

Figure 7.11: FFT analysis for the measured transient at 13:13

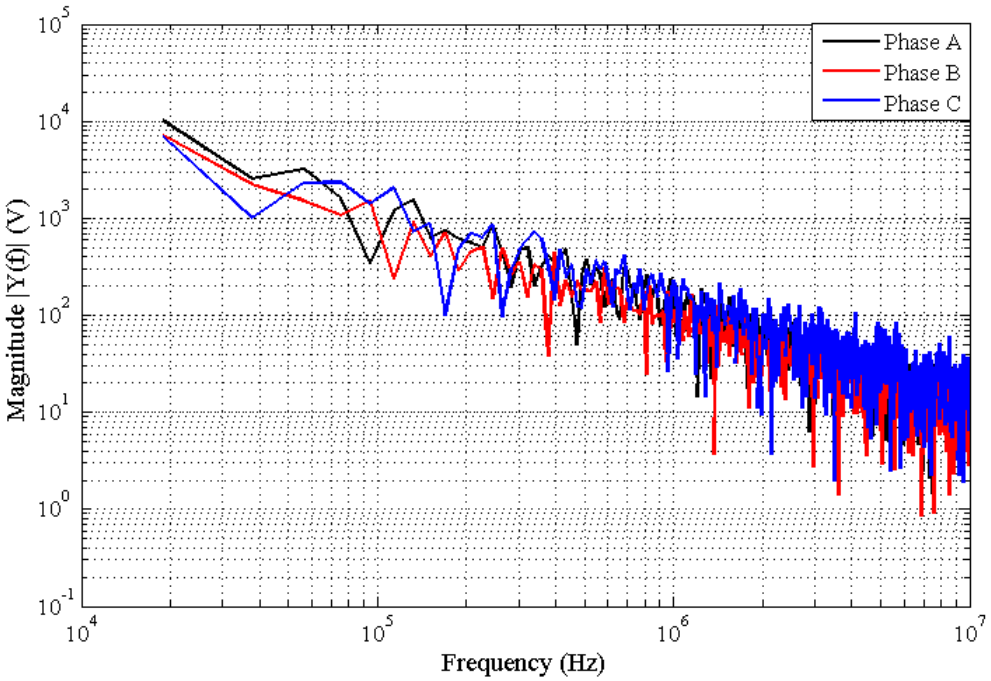

Figure 7.12: FFT analysis for the measured transient at 13:15

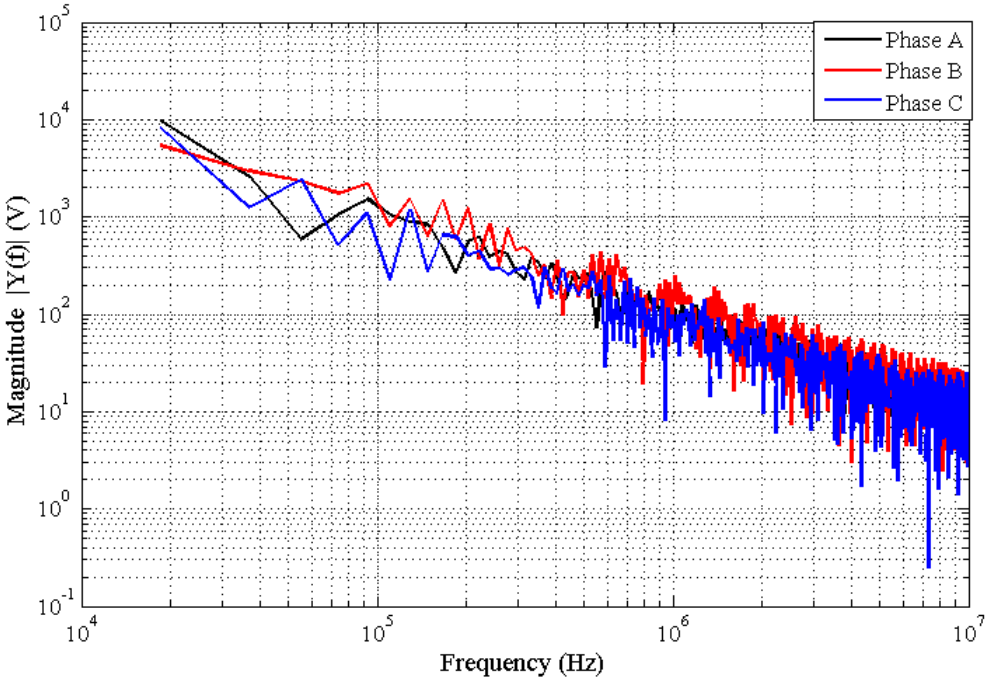

Figure 7.13: FFT analysis for the measured transient at 13:26

7.3 Severity Factor

As previously highlighted voltage stress assessment is important to ensure proper design of the transformer insulation structure. In service, the transformer insulation structure is constantly exposed to normal 50 Hz operating voltages and transient overvoltages such as those due to lightning. Because of these future voltage stresses, the insulation system is subjected to voltage impulse tests in the factory in accordance with specific standards. The BIL rating of a transformer is a measure of a transformer's insulation withstand capability when exposed to a voltage surge of a certain magnitude and duration [4]. However even when proper insulation coordination studies have been conducted, transformers still fail when exposed to transient conditions as discussed in Chapter 1. For this reason, the transformer manufacturer can implement severity factors which may be analysed in either the frequency domain or time domain [4]. These help in establishing an acceptable insulation design that caters for the voltage stress (kV) and the electric field strength of the supporting dielectric in (kV/mm).

7.3.1 Implementation and analysis of the Frequency Domain Severity Factor (FDSF)

A severity factor is defined as a coefficient that can be used in the assessment of the stress applied to a transformer winding insulation by the incoming transient overvoltage [18]. It determines a safety margin that can be used during the design stage with regards to the standard acceptance tests either in the frequency or time domain. The acceptance tests include the lightning impulse test which checks the BIL, switching impulse test to check the Switching Impulse Level (SIL), the short duration power frequency test at 50 Hz and the long duration power frequency test with partial discharge measurement [4]. The wind turbine transformers are tested with a 170 kV lightning impulse according to SANS 60076-3 [8]. Additional waveforms such as the 200 kV lightning impulse test, the chopped 187 kV impulse at 2 μs, 3 μs, 4 μs, 5 μs and 6 μs will also be considered in this report. However according SANS 60076 no switching wave tests should be done for MV distribution transformers hence it will not be considered in the analysis [8]. The chopped wave test is considered the more important than the lightning impulse test since it has a higher peak value and contains higher frequency components [4]. To compute the Frequency Domain Severity Factor (FDSF) knowledge of the frequency components of the incoming surge and the standard waveforms is needed. This was done by computing the FFT and the Energy Spectral Density (ESD) of the waveforms as shown in Equation 7.1 [18].

$$FDSF(\omega) = \frac{ESD_{sw}(\omega)}{ESD_{env}(\omega)} = \frac{|F_{sw}(\omega)|^2}{|F_{env}(\omega)|^2} \tag{7.1}$$

where ω is the angular frequency, $ESD_{sw}(\omega)$ is the maximum energy spectral density of the measured transient at the transformer terminals, and $ESD_{env}(\omega)$ is the energy spectral density envelope for all standards' dielectric tests at the terminals. $F(\omega)$ is the FFT of the signal. To ensure that the measured switching transients are covered by the standard impulse waves, the FDSF should be less than unity [18]. It is important to note that the inter-disk or inter-layer spacing is decided by impulse stresses (i.e. LI, SI, CI) hence to avoid the inter-layer failures due to fast transients shown in Figure 1.4 suitable safety factors should be applied during the insulation design stage [7]. Figure 7.14 shows the magnitude spectrum for the standardized

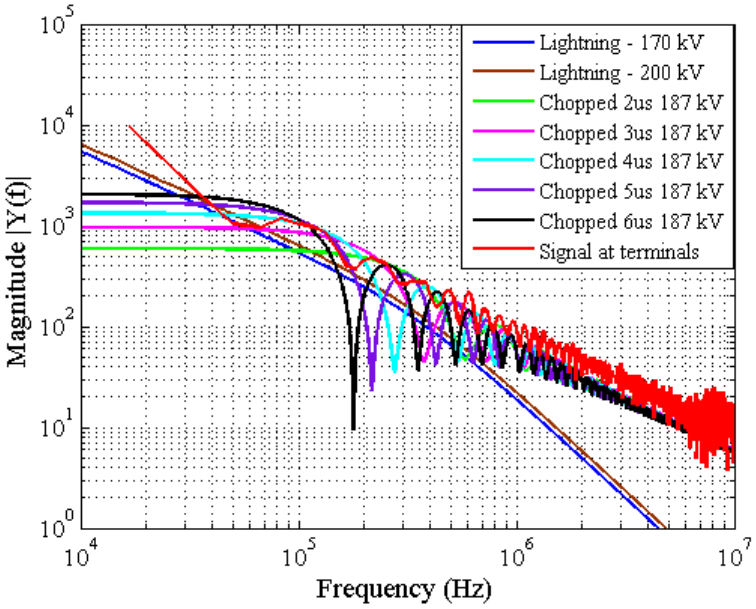

Figure 7.14: Magnitude spectrum for transient signal in Figure 7.8 and standard lightning and chopped lightning waveforms.

waveforms and an FFT of the measured transient in Figure 7.8. By analysing the results in Figure 7.14 it is possible to have a severity factor that takes the maximum value of the standard waveforms to form an envelope of acceptance. This is shown in Figure 7.15. This can then be compared to the ESD of the transient at the transformer terminals as explained by Equation 7.1. Hence any frequency component above the red line will pose a risk to the transformer insulation by winding resonance. The results of the FDSF plots calculated using Equation 7.1 for the transients in Figures 7.4, 7.6 and 7.8 are shown in Figures 7.16, 7.17 and 7.18.

The results of the FDSF for the three different switching events show that the majority of the frequency components are above unity for most of the spectrum symbolising a potential

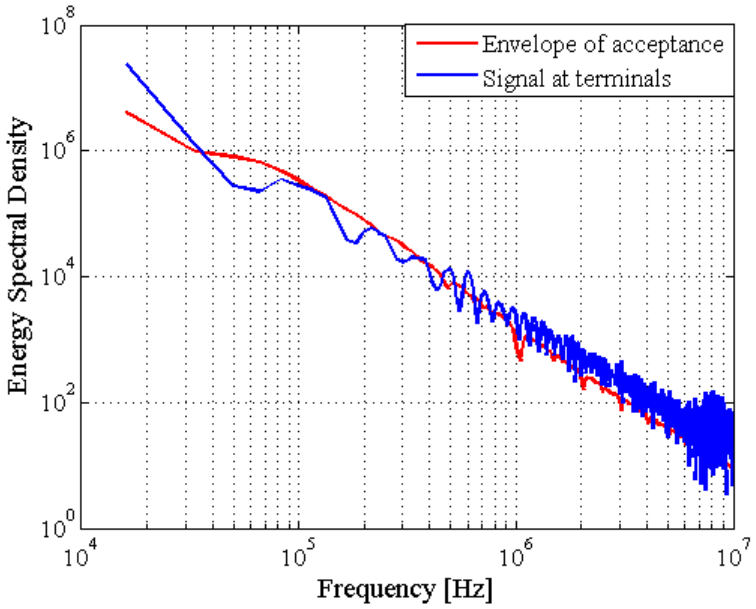

Figure 7.15: Comparison of ESD for transient signal in Figure 7.8 and ESD for standard test waveforms in Figure 7.14

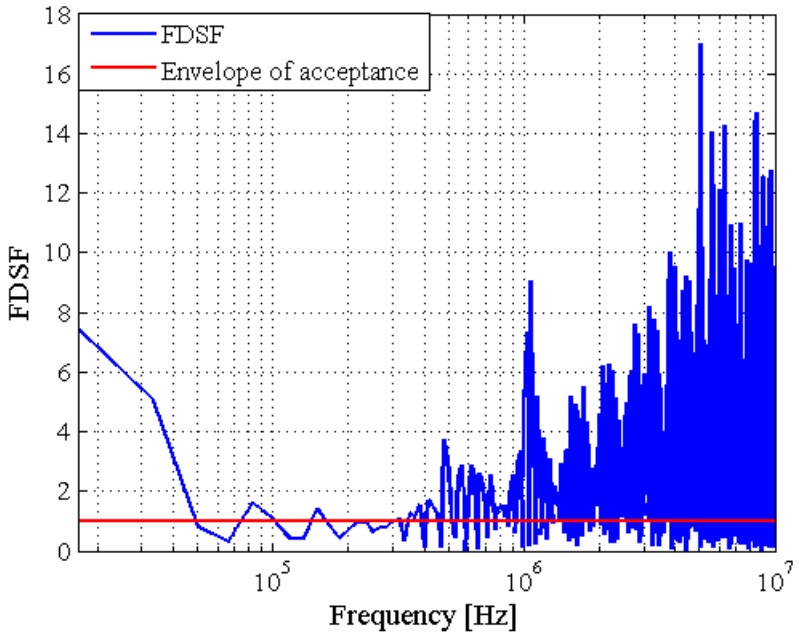

Figure 7.16: FDSF for the measured transient in Figure 7.4.

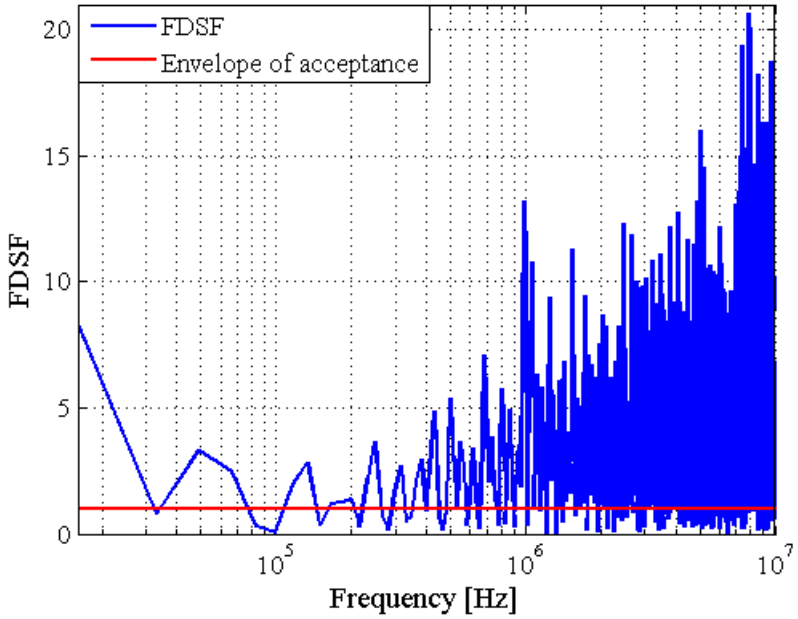

Figure 7.17: FDSF for the measured transient in Figure 7.6.

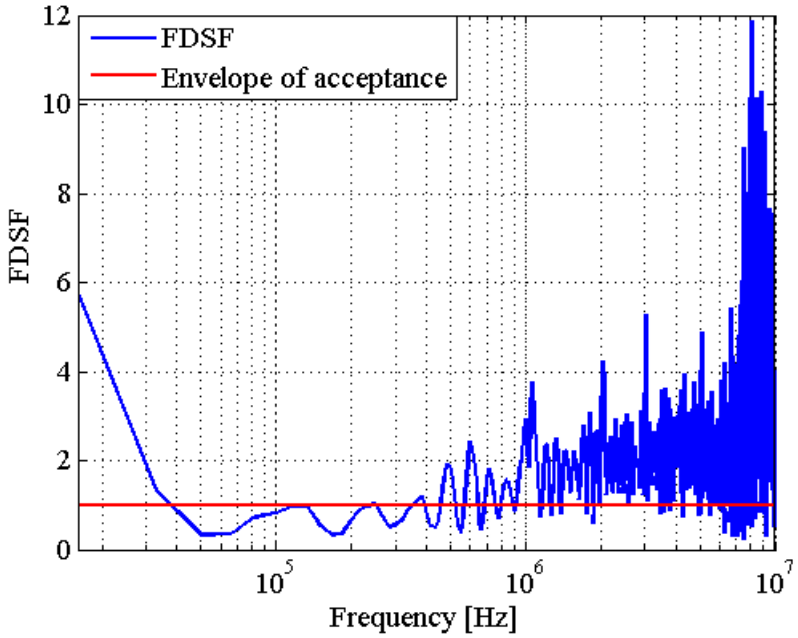

Figure 7.18: FDSF for the measured transient in Figure 7.8.

risk. Hence internal winding resonance could occur when either of the frequency components match a resonant frequency of the transformer winding. The FDSF results also reveal that the transients generated during switching of wind turbine step-up transformers are not well represented by any of the standard wave tests. Also it is worth mentioning that FDSF analysis has several limitations including that it does not take into account damping effects and hence might over-estimate the over-voltages produced at resonance especially for transients with frequency components above 1 MHz shown in Figures 7.16, 7.17 and 7.18. However in light of the FDSF results that were obtained and how severe they are, the transformer manufacturer gains knowledge of the spectral fingerprint during switching transients events and proper protection or safety factors can be implemented to wind turbine transformer designs such that proper protection is taken into account regardless of what the transformer is exposed to. Hence a look at two wind turbine transformer designs will now be investigated.

7.4 Discussion and Conclusion

This can be analysed by looking at the current analysis tool, FDSF. Although FDSF is a powerful analysis tool, it has a limitation in that it does not take into account the severity along the windings to localize dielectrically the weak points as it only describes the terminal response of the transformer [6].

1. In implementing FDSF a comparison of the energy involved during a transient event with the energy involved in the standard test waveforms is made but effects of damping are not taken into account. For transformers the damping ratio (R/X) increases at higher frequencies because of skin effect as well as increased stray losses [13]. Hence some damping should be expected at higher frequencies which may reduce the amplitude of the internal overvoltages.

2. Although FDSF does provide insight in the different frequency components the transient signal has, it does not take into account the phase angle which may over-estimate resonant overvoltages. The FDSF results have indicated that the existing tests waveforms contained in the standards do not completely address all the types of transient events that could occur in the field. The frequency response of the two windings has revealed that the transformer with non-split MV winding could be a better option.

Chapter 8

Insulation Co-ordination

8.1 Chapter Overview

This chapter gives a general discussion of the results obtained. A review of fundamental insulation coordination concepts is also presented. Comparison of insulation design is performed by looking at different values of Design Insulation Level (DIL) of the transformer. Different mitigation techniques for protecting wind turbine transformers against very fast transients are investigated. Finally recommendations and possibilities for future work are also outlined.

8.2 Insulation coordination

As previously mentioned in previous chapters, transformers in service are constantly exposed to operating voltages and in some instances overvoltages. The overvoltages can be caused by a number of phenomena but in this research focus is on overvoltages due to the operation of circuit breakers. To ensure proper operation of the transformer under different conditions it is essential to perform proper insulation coordination studies during the design process. The insulation coordination will be looked at from two different aspects. The first being during the design stage. What sort of insulation coordination practices need to be in place to ensure that a transformer exposed to frequent switching does not result in dielectric failure? The second aspect focuses on the mitigation techniques that can be applied to alleviate the overvoltages caused by circuit breaker switching. Hence the insulation coordination studies will be to coordinate the different protection measures with the insulation level of the transformer.

8.3 Design Insulation Level (DIL)

It is a well-known technique that transformer insulation is tested according to the standard test waveforms specified in SANS 60076-3 [8] which are the lightning impulse, chopped impulse and switching impulse. A common consensus within the transformer manufacturing industry is the representation of the transformer performance using breakdown strength curves which are functions of both amplitude and duration [4]. Hence to take into account these characteristic during the design process, manufacturers apply what is termed as the DIL. The DIL specifies the maximum equivalent one-minute power frequency voltage level based on the three different tests which are BIL, SIL and the long duration (one hour) power frequency voltage. Hence at any given time inside the transformer there is one DIL value that specifies the maximum equivalent AC one-minute r.m.s. value (under various tests) that the transformer insulation can withstand [4], [7]. Typical values of DIL values are shown in Table 8.1 [7].

Table 8.1: Factors for conversion to one-minute (r.m.s.) power frequency level adapted from [7].

Standard voltage test waveforms	**Multiplication factor (D.I.L)**
Lightning Impulse Level (BIL) 1.2/50 Full Wave Impulse	(1/2.30) = 0.44
Switching Impulse Level (SIL) 250/2500	(1/1.80) = 0.55
Short duration power frequency voltage (1 minute)	1.00
Long duration power frequency voltage (60 minutes)	(1/0.80)=1.25

Table 8.2: Test voltage levels and the impulse ratios adapted from [7], [8].

Voltage class [kV]	Full Wave Lightning Impulse [kV]	(LTAC) [kV]	Impulse ratio
36	170	70	2.43
132	550	230	2.39
220	950	395	2.40
400	1300	570	2.28

The DIL specifies a threshold withstand value for the insulation and the resultant voltage is expressed as $V_{DIL-Test}$ in kVrms [7]. This approach is widely used by transformer manufacturers to simplify the insulation design process. To obtain the DIL value, the multiplication factor is defined as the inverse of the impulse ratio. The impulse ratio is found by taking the ratio of full wave lightning impulse to the line terminal AC (LTAC) withstand voltage shown in Table 8.2. The impulse ratio defines an average correction factor that can be applied for voltage impulses within a duration of 10 μs to 100 μs [7]. From the information in Table 8.2 it is clear that the

impulse ratios for different voltage classes ranges between 2.3 to 2.5 which form commonly used values within the industry [78], [79].

However the limitations of applying the DIL becomes apparent when dealing with transients whose duration may be less than 10 μs. As previously shown by the transients in Figures 7.3, 7.4, to Figure 7.8 these overvoltages which will be imposed on the inter-layer or turn to turn insulation may be shorter than 10 μs. In this case the application of the above mentioned correction factors in Table 8.1 and Table 8.2 becomes a bit more conservative. In [80], an impulse ratio of 2.68 was calculated for a 1.5/40 μs impulse resulting in a DIL value of 0.37 for the design of the inter-winding and inter-turn insulation. In contrast if it had been assumed as a normal lightning impulse the DIL value of 0.44 in Table 8.1 would have been used rather than the corrected DIL value of 0.37 which is much lower. A lower DIL value means a lower withstand value for the insulation and opens up avenues for insulation optimization since new designs will have to be considered [7]. With this in mind, special consideration will have to be applied when dealing with transients. It becomes risky to use impulse ratios in the range of 2.3 to 2.5 as suitable correction factors for transformers exposed to transient impulses. Hence the calculated impulse ratios should have a lower value [7]. The only difficult in assessing transients by calculating using the DIL method is the wave shape of transients is random and does not follow the profile of a lightning impulse. Hence in [4], a new assessment tool known as the Time Domain Severity Factor (TDSF) was proposed that can be used when dealing with transients imposed on transformer terminals. The TDSF is discussed in later sections.

8.4 Mitigation techniques against fast transients

As previously mentioned, high frequency components present an undesirable risk in the power system networks. They pose a risk to the electrical equipment as internal resonant phenomena can occur resulting in the local amplification of voltage which degrades the thin insulation between layers or turns [6]. This section investigates suitable protection measures that are commonly used within the industry to suppress the overvoltages and HF oscillations brought about by the switching of vacuum circuit breakers.

8.4.1 Traditional methods of suppressing fast transients

In medium voltage network, there exists several mitigation methods of suppressing the overvoltages imposed on the transformer terminals. The following are amongst the commonly used:

8.4.1.1 RC Snubbers

Figure 8.1 shows the implementation of resistor capacitor (RC) snubber. The resistor acts in the following [73]: (i) By reducing the amplitude factor of the Transient Recovery Voltage (TRV) (ii) By limiting capacitive inrush currents. (iii) By terminating wave reflections at the cable end.

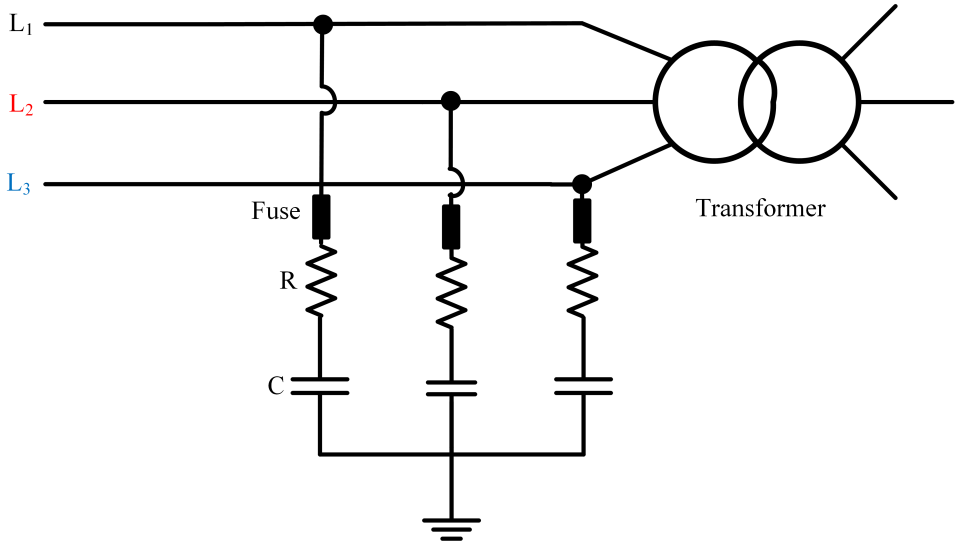

Figure 8.1: RC Snubber network

The capacitor (C) in Figure 8.1 functions by decreasing the frequency of the load side TRV. This is achieved by modifying the frequency components of the incoming transient such that it becomes lower than one of the resonant frequencies of the transformer [73]. Effectively this minimizes the problem of high internal voltage amplification due to internal winding resonance. Typical capacitance values in the range of 0.1 μF to 0.5 μF are suggested in [73]. However proper determination of the exact capacitance values can still be deduced if knowledge of the resonant performance of the transformer and its system parameters are known. The fuse in Figure 8.1 acts by providing secondary protection in the event of RC snubber failure. However it must be ensured that the fuse is rated to withstand both inrush and outrush currents, withstand steady state current and any harmonics which may be generated during system operation [73]. The drawbacks of such an arrangement are:

- The snubber arrangement will most likely contribute to some level of harmonics although this can be counteracted by increasing the current rating by a factor of 1.3 [73].
- Typical resistance values in the range of 5 Ω to 50 Ω have been suggested in [73]. It should be noted a low value of resistance may impact the switching device capabilities

as the TRV amplitude factor can exceed beyond the interrupting threshold level of the switching device. Furthermore, a very large value of resistance may result in high resistive losses and an over-damped TRV [73].

- A too high value of the snubber capacitance can potentially result in capacitive currents imposing high power requirements on the snubber resistor [6].

8.4.1.2 Surge Capacitors

Surge capacitors are normally employed with surge arresters as protective devices. The realization of suppressing the VFT is achieved since the cable surge impedance and the capacitor combine to form a low pass filter [6]. A large capacitance value is normally recommended since the impedance of the cable will be very small. However the introduction of a large value of capacitance presents several problems which are [6]: (i) A large value of a surge capacitor can contribute to the formation of inrush currents during energization of a transformer. (ii) Surge capacitors may form a resonant circuit with the impedance of the connected cable which can potential result in the generation of overvoltages.

8.4.1.3 Surge Arresters

In MV distribution networks, surge arresters are common protection devices installed at the transformer terminals. They are mainly used to mitigate the effects of lightning strikes. However with regards to transients overvoltages, surge arresters only work by providing protection against overvoltages but fail to suppress the rate of change of voltage (du/dt). Hence in most cases the high du/dt values imposed by transients are not affected by the surge arresters as their amplitudes are usually lower than the protection level [14]. Furthermore surge arresters are incapable of filtering the HF oscillations or to eliminate wave reflections occurring at the transformer terminals [14].

8.4.2 RL Choke device

The approach is to employ a series impedance upstream of the protected equipment which would be a transformer in this study [6]. Figure 8.2 shows the implementation of a choke device on a transformer. The choke device consists of a resistor and an inductor connected in parallel as shown in Figure 8.2. The aim of implementing the choke device is to reduce the repetitive nature of transients shown in Figures 7.3, 7.4, 7.6, 7.8 and the amplitude built up that results due to a lack of appropriate termination at the end of the cable [14]. In order to allow suppression of overvoltages and HF oscillations brought about by the switching operation

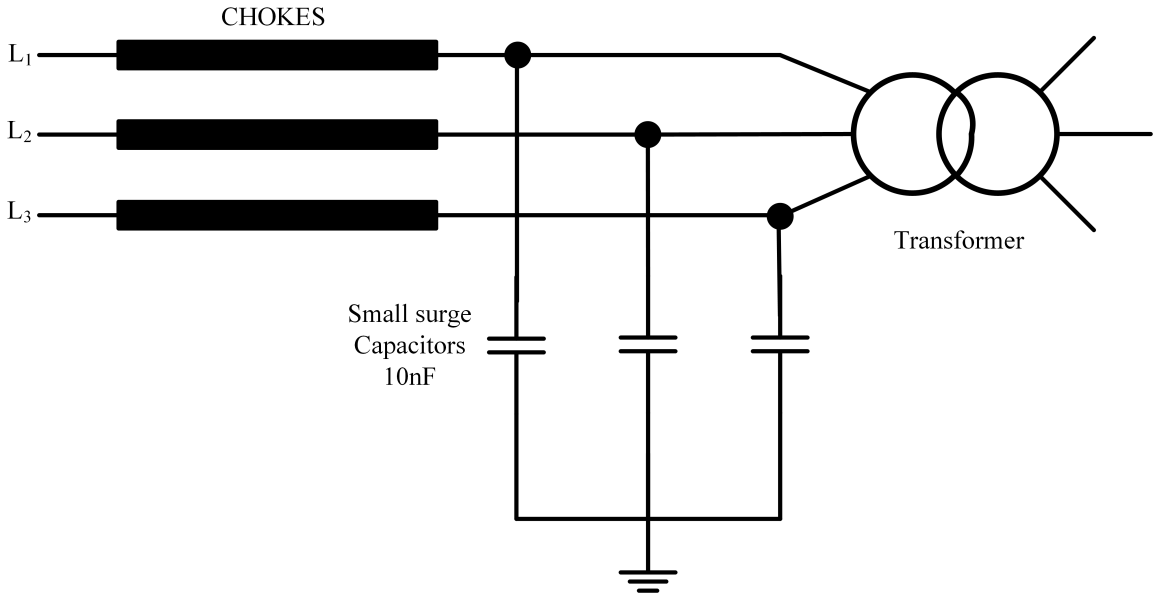

Figure 8.2: Physical realization of VFT suppressing devices installed on a transformer

whilst being able to maintain normal operation of the transformer, the RL choke device should meet the following criteria [6]:

- The RL choke device should not be saturated by the load current.
- The RL choke device should exhibit a small voltage drop under 50 Hz operation.
- The RL choke device should exhibit a significant impedance below 1 MHz to allow reduction of high dU/dt values (the resistive character of the choke and the phase to ground capacitor form a low pass filter).
- The RL choke device should be able to restrict the overvoltages to within safe levels that coordinate with the insulation co-ordination of the transformer.
- At high frequencies the RL choke device should limit the wave reflections by terminating any reflections at its terminals due to its high impedance.

An RL choke device meeting the above mentioned criteria was designed and manufactured by the authors in [6]. The frequency response of the RL choke device is shown in Figure 8.3. Simulations were performed in the frequency domain to assess the suppression effects of the RL choke device . A surge capacitor with a capacitance value of 0.1 μF was used. The circuit in Figure 8.7 was analysed in the frequency domain together with the measured time waveforms in Figures 7.3, 7.4 and 7.6 acting as the input. A comparison of the FDSF results obtained

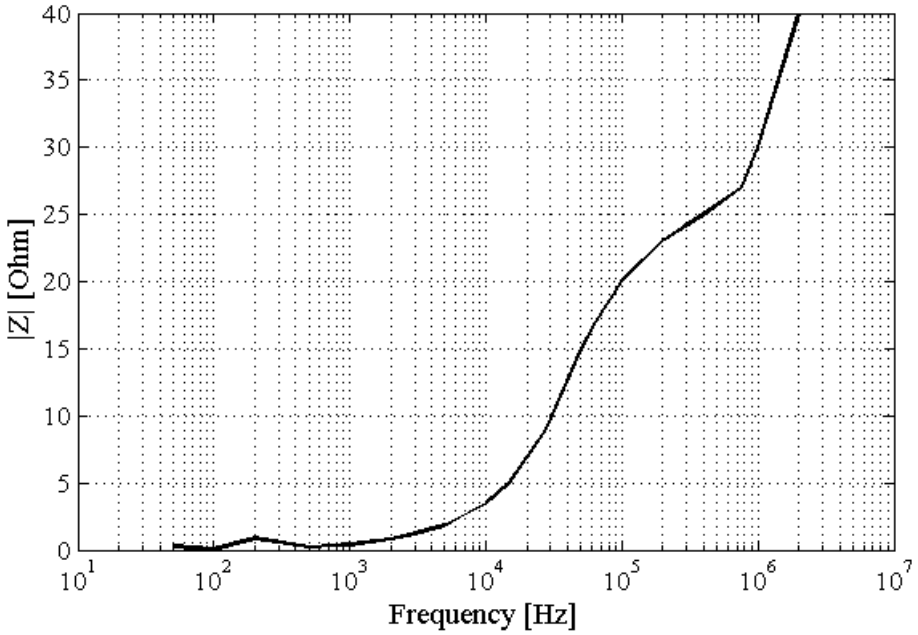

Figure 8.3: Impedance vs Frequency plot of RL choke device adapted from [6]

before and after installing an RL choke device on all phases of the transformer are shown in Figures 8.4, 8.5 and 8.6. It should be noted that the methods to obtain the FDSF were explained in Section 7.31: Implementation and analysis of FDSF. The introduction of an RL choke device has drastically reduced the magnitude of the frequency components to within safe levels. As previously mentioned in Chapter 7 , the FDSF should be less than unity to ensure that the transformer is properly protected. This is shown by the results in Figures 8.4, 8.5 and 8.6 after RL choke device installation. It is important to note that analysis of the RL choke device was only performed in the frequency domain due to the published impedance vs frequency plot characteristics in [6].

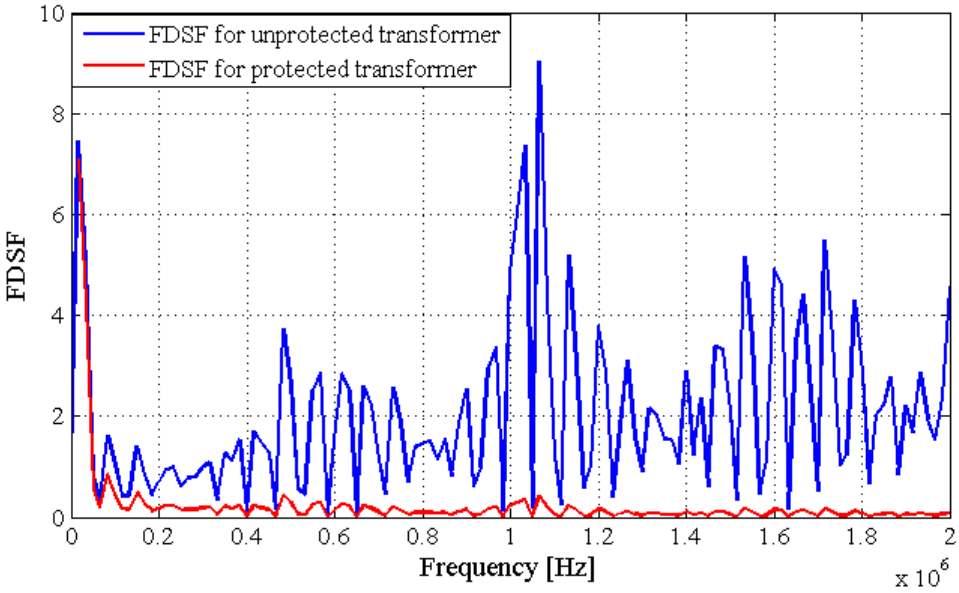

Figure 8.4: FDSF for the measured transient in Figure 7.4 before and after RL choke device installation.

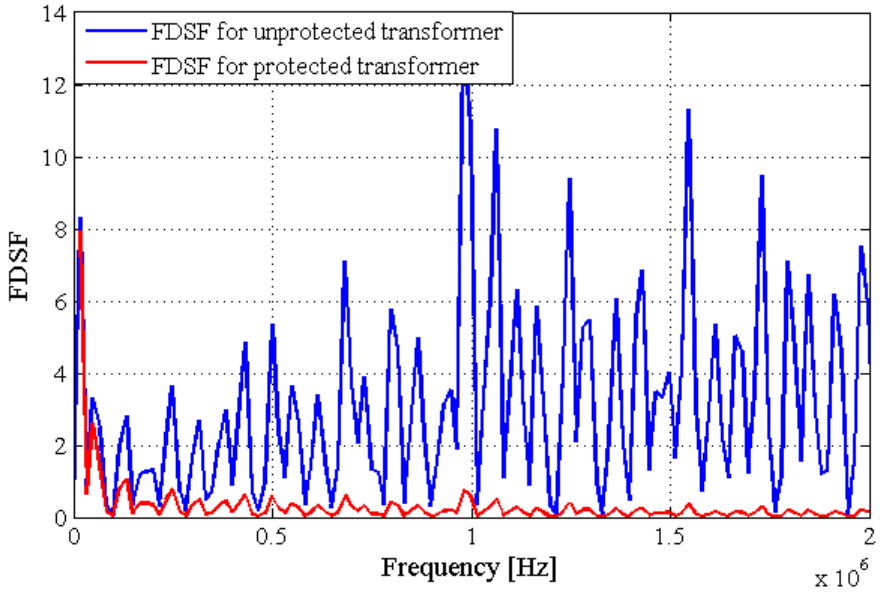

Figure 8.5: FDSF for the measured transient in Figure 7.6 before and after RL choke device installation.

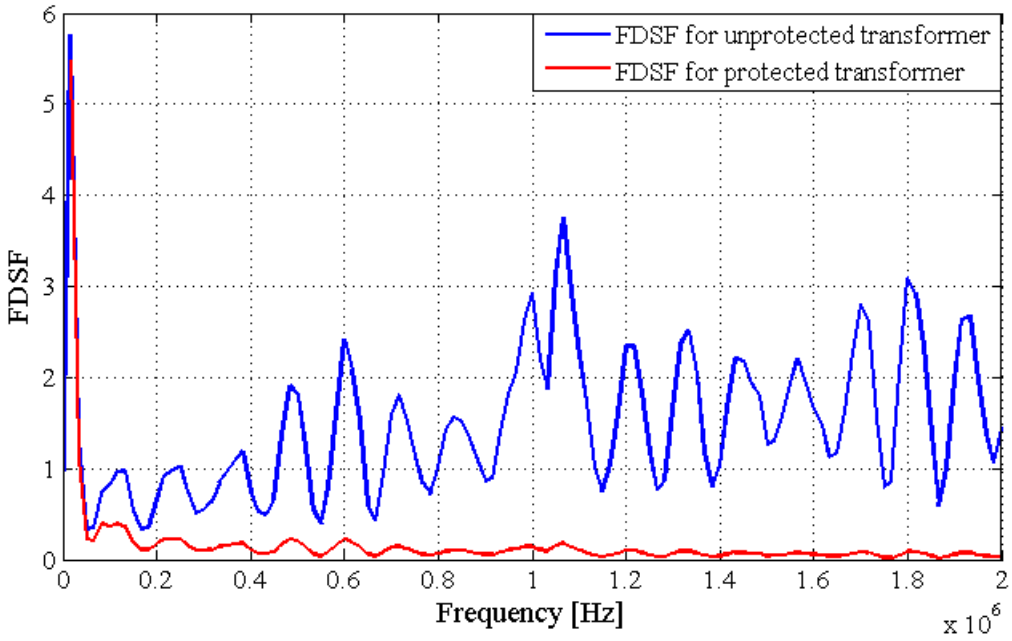

Figure 8.6: FDSF for the measured transient in Figure 7.8 before and after RL choke device installation.

Figure 8.7 shows the simulated circuit in ATP DRAW. The design of the RL choke was done from the impedance plot shown in Figure 8.3. The resistance in parallel with the choke device was chosen to be 50 Ω and the inductance of the choke was chosen to be 13.9 mH. This resulted in a low impedance choke device with an impedance of 0.25 Ω at 50 Hz.

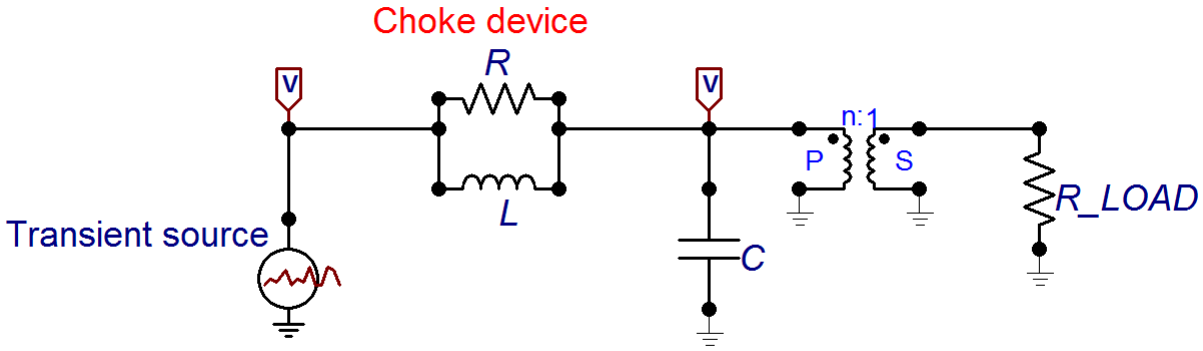

Figure 8.7: RL choke device implementation in ATP DRAW

As previously mentioned on the design criteria of the choke device, it should be able to exhibit

a small voltage drop under power frequency whilst being able to suppress overvoltages brought about by the switching operation. To investigate the transparency of the choke device under power frequency operation, a signal with an amplitude of 2 V_{pp} and frequency of 50 Hz was generated by the transient source and the output waveform measured across the capacitor.

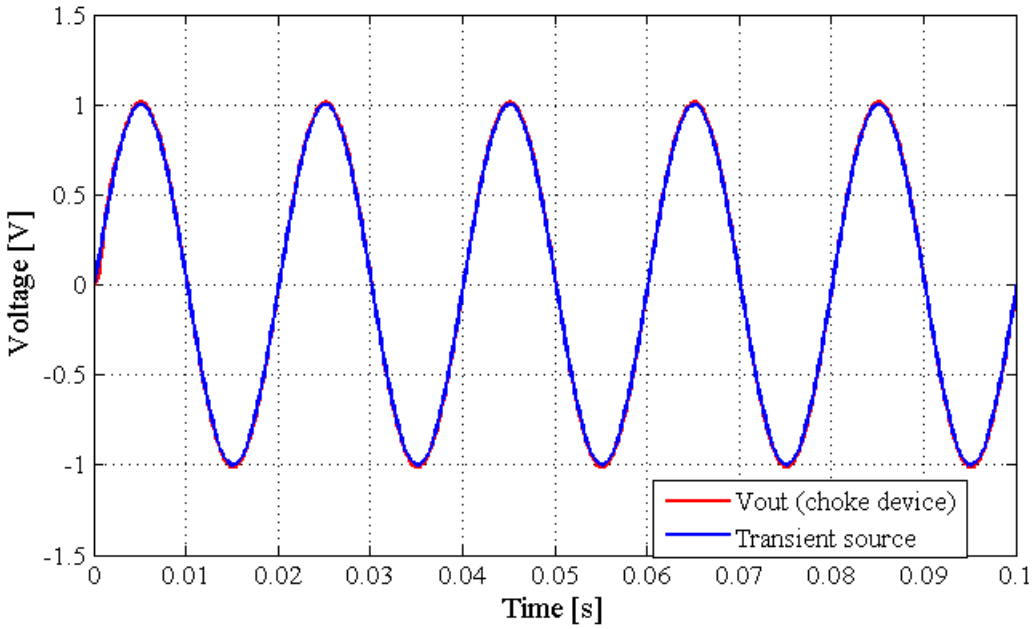

Figure 8.8: 50 Hz transparency of RL choke device

As seen in Figure 8.8, there is a close correlation between the transient source and Vout from the choke device. This shows the transparency of the choke device under power frequency operation. Furthermore to investigate the suppression effects of the designed choke device when there are transients as previously shown in Figures 7.3, 7.4 and 7.6 the empirical source in Figure 8.7 was used to generate these transient waveforms. Hence the empirical source in Figure 8.7 acts to replicate the transient waveforms that were measured on the transformer terminals for the investigated wind farm. The results of the waveforms at the transformer terminals for an unprotected transformer are shown in Figures 8.9, 8.11 and 8.13. Subsequently the resulting waveforms after choke device implementation are shown in Figures in 8.10, 8.12 and 8.14.

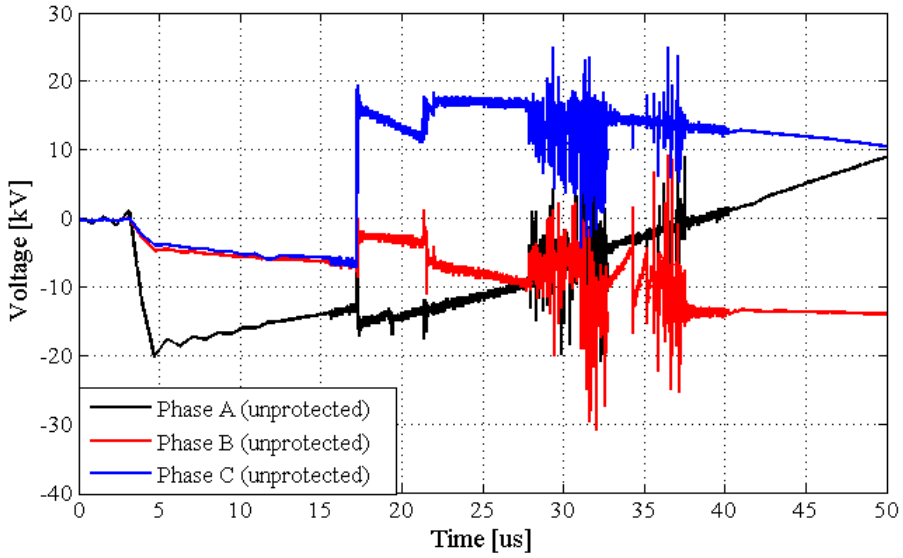

Figure 8.9: Unprotected terminal phase voltages measured using the setup in Figure 7.1

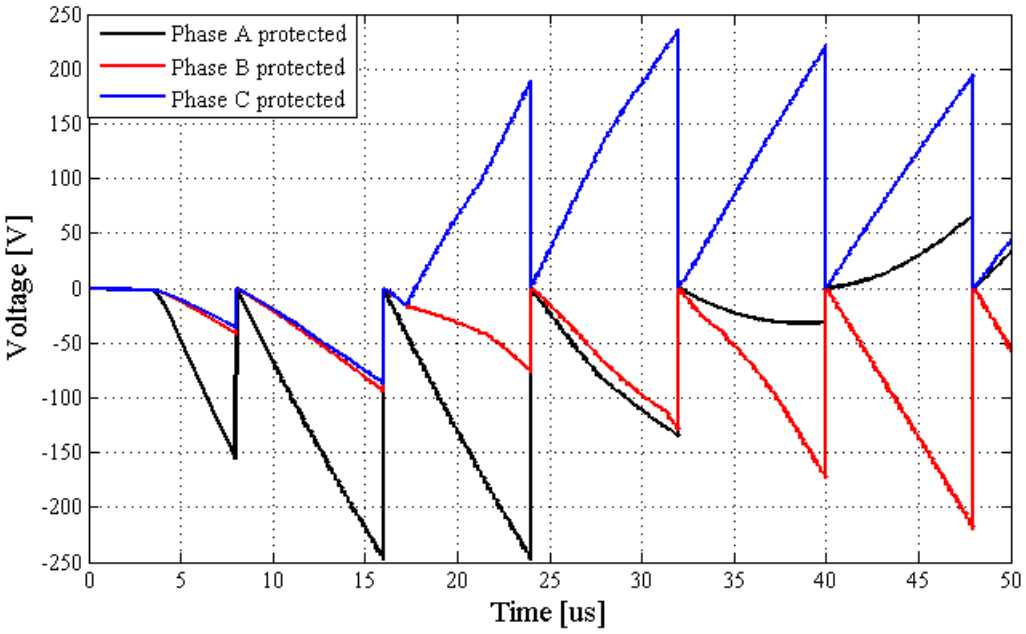

Figure 8.10: Protected terminal phase voltages using choke device to suppress the measured transients in Figure 8.9

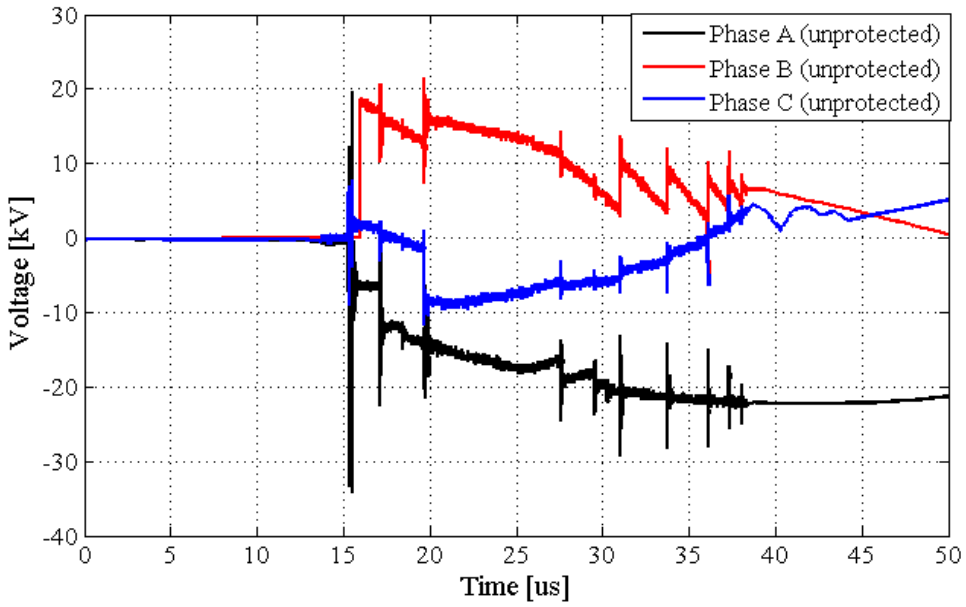

Figure 8.11: Unprotected terminal phase voltages measured using the setup in Figure 7.1

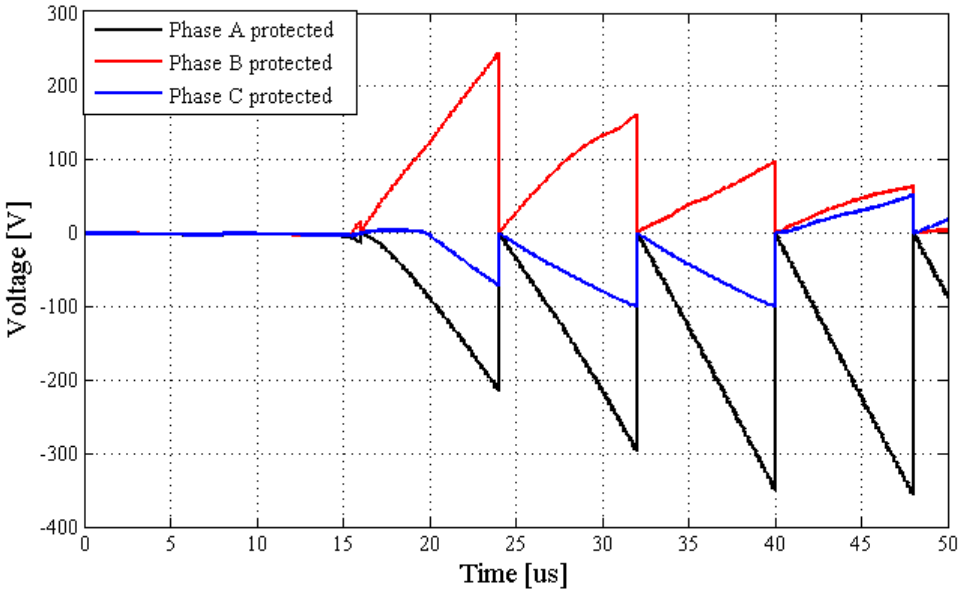

Figure 8.12: Protected terminal phase voltages using choke device to suppress the measured transients in Figure 8.11

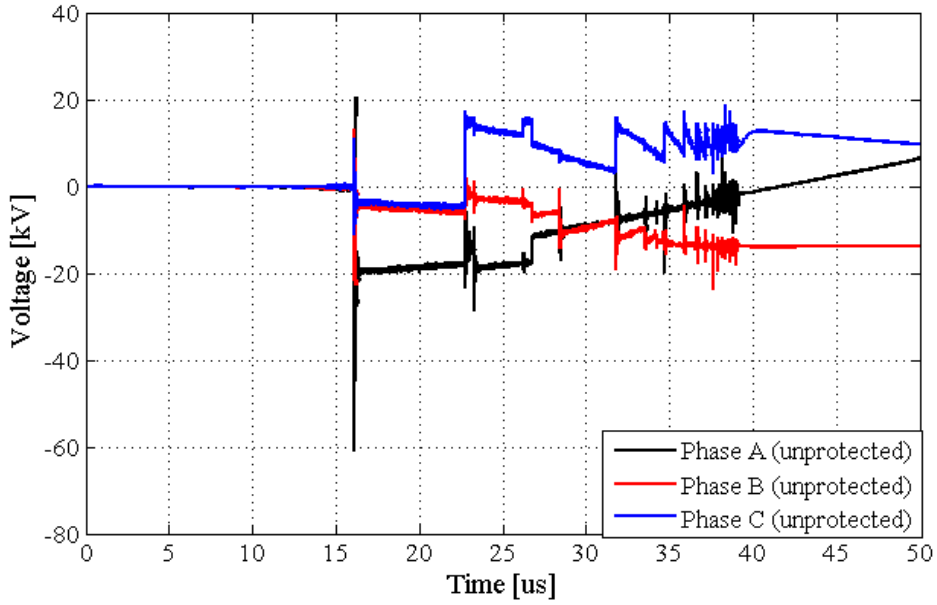

Figure 8.13: Unprotected terminal phase voltages measured using the setup in Figure 7.1

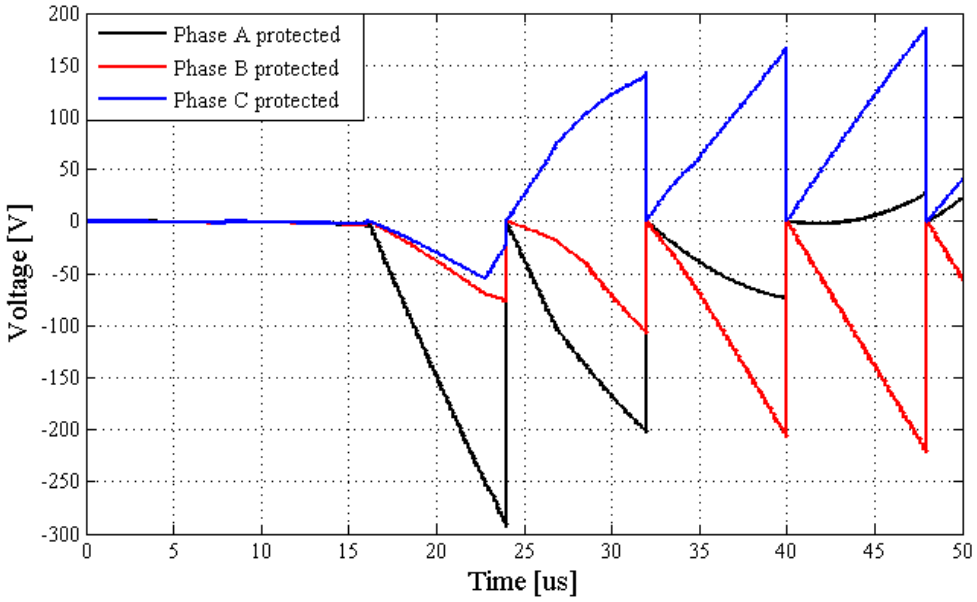

Figure 8.14: Protected terminal phase voltages using choke device to suppress the measured transients in Figure 8.13

Analysis of the measured waveforms in Figures in 8.10, 8.12 and 8.14 show that the output wave has been attenuated by the choke device. The high du/dt values have been reduced to within safe levels which the transformer insulation should be able to withstand. It should be noted that it has been assumed that the pre-strike waveforms in Figures 8.9, 8.11 and 8.13 will remain the same even after RL choke device installation. However in practice, the nature of these repetitive transients will differ due to the termination provided by the choke device. Hence the waveforms may not exhibit the pre-strike nature shown in Figures 8.9, 8.11 and 8.13.

8.5 Special winding designs

In Chapter 6, the resonance performance of two different wind turbine step-up transformers were investigated. A comparison of transformers with a split MV winding versus a transformer with a non-split MV winding was also investigated. The two designs revealed that the resonant frequencies of the winding can be shifted to occur either early within 1 kHz to 20 kHz or later after 200 kHz. This is an important characteristic and can be used to coordinate with the protection of the RL choke device. As shown in Figures 6.22, 6.23 and 6.24, the transformer with the non-split MV winding would be the best option to integrate with the RL choke device. This is because it has high resonant overvoltages above 200 kHz and any incoming transient with frequency range above 200 kHz can damped out by the RL choke device.

Another well-known technique within the transformer industry is to apply a specialized design with an increased insulation level so as to equalize the initial voltage distribution [81]. Hence for the investigated wind turbine step up transformer it would have its insulation level rated for 66 kV instead of the 33 kV. However several challenges arise with regards to pursuing complicated designs. Reinforcing the insulation can help in minimizing inter-turn and inter-layer faults. However this presents further uncertainties as it changes the impedance of the transformer and subsequently its frequency response. This can be a major problem for customers who usually require a low impedance unit.

8.6 Discussion and Conclusion

This chapter has reviewed the fundamental principles of insulation co-ordination from the design of the insulation within the windings to external mitigation techniques that can be used to suppress the effect of very fast transients.

Chapter 9

Conclusions, Future Work and Recommendations

9.1 Chapter Overview

This chapter concludes the thesis by reviewing how the research questions mentioned in Chapter 1 have been addressed in this research. Possibilities of extending this research are also proposed under the section of Future Work. Recommendations on improving the current work are also proposed in this chapter.

9.2 Assessment of the outcome of the research questions

The research questions mentioned in Chapter 1.3 set the research objectives and defined goals that the author had to meet. A review of these research questions and their main findings will be crucial in concluding this research. The research questions and their main findings were:

9.2.1 Research Question 1

What are the methods available in the literature that can be used to formulate a high frequency model of a transformer?

Several methods can be used to characterise the high frequency behaviour of a transformer. Different methods exist and an in-depth investigation was presented in Chapter 3. In this research the MTL model was chosen as the appropriate model for the prediction of resonant overvoltages in transformer windings. The MTL model represents the transformer windings as

coupled transmission lines. The procedure for the determination of the MTL model is discussed in Chapter 3.4.2.

9.2.2 Research Question 2

In the literature the Multi-conductor Transmission Line (MTL) model is used for the computation of the inter-turn voltages. Can the model be extended for the computation of inter-layer or layer voltages using appropriate matrix reduction techniques? i.e. grouping the total number of turns in a layer winding to represent the voltage distribution in that layer?

The extension of the MTL model was successfully applied to include the computation of inter-layer voltage stresses as shown in Chapter 6. Using matrix reduction techniques discussed in Chapter 4.3.1 the MTL model was extended to include voltage stresses from the start of the layer to the middle of the layer as shown in Chapter 6.4.2.2.

9.2.3 Research Question 3

The MTL model is a commonly used model for the calculation of voltage distribution within transformer windings. Can the MTL model be applied for any transformer winding geometry? i.e. either split MV winding or non-split MV winding?

Modelling of any transformer geometry, topology and its electrical behaviour during normal and transient conditions is an important characteristic that the chosen model should be able to successfully replicate. The MTL model was successful applied to two transformer prototypes which had the same power rating but differed in the design of the MV winding. One of the prototypes used a split MV winding whilst the other used a non-split MV winding. The application of the MTL model was successfully applied to the two prototypes and the results of the analytical solutions were verified against measurements. The main findings are reported in Chapter 6.

9.2.4 Research Question 4

In the literature different methods are proposed for the mitigation of fast transients brought about by transformer circuit breaker interaction. The protection methods range from the use of RC snubbers, surge capacitors and surge arrestors, to RL choke devices. Hence, what are the limitations of using these protection methods to curb the development of resonant overvoltages

inside transformer windings? What appropriate protection methods can be used to co-ordinate with the insulation level of the transformer for protection against switching surges?.

The different protection methods that can be used in the suppressing of fast transients brought about by transformer circuit breaker interaction were covered in Chapter 8.4. The limitations of the RC Snubber, Surge Capacitors and Surge Arresters indicated that although these devices can still function in suppressing transients they still have major drawbacks. The RL choke device would be the most ideal protection device to use in suppressing very fast transients. The performance of the RL choke device in suppressing fast transients were validated by comparing its du/dt limiting effectiveness with actual recorded on-site transients waveforms as shown in Chapter 8.4.2. The results indicated that RL choke device can reduce the transient overvoltages to safe levels that would match with the insulation co-ordination of the transformer.

9.3 Future work and recommendations

The research has presented important findings which addressed resonance in transformer windings and several techniques which can be used in the mitigation of very fast transients. However certain concerns arise if too much emphasis is placed on the results of the frequency domain and time domain analysis is neglected. As previously mentioned in Chapter 7, FDSF is a powerful tool for assessing the severity supported by the transformer when subjected to steep transients. However the biggest limitation is the failure to identify the dielectrically weak points that could pose a risk of failure when steep transients are imposed at the transformer terminals. The following is the current work being done by the author to try and address the shortfalls.

9.3.1 Time Domain Severity Factor (TDSF)

The TDSF complements the shortfalls of the FDSF by providing more insight into the severity supported by the transformer along the windings. It is defined by Equation 9.1.

$$TDSF = \frac{\Delta V_{max_{switching}}(t)}{\Delta V_{max_{envelope}}(t)} \tag{9.1}$$

The TDSF assesses the stress imposed on the transformer insulation when subjected to a transient event ($V_{max_{switching}}$) emanating from the power system in comparison to an internal response due to standardised dielectric tests ($V_{max_{envelope}}$) which form the envelope of acceptance in the time domain [18]. If the calculated values of TDSF along the windings are less than unity, then the transformer insulation structure will be well coordinated to withstand such a

particular switching event [4]. A prototype transformer has been constructed for the purpose of measuring the voltage distribution within the windings shown in Figure 9.1.



Figure 9.1: Prototype transformer to be tested

The final constructed prototype transformer will resemble that shown in Figure 9.2.

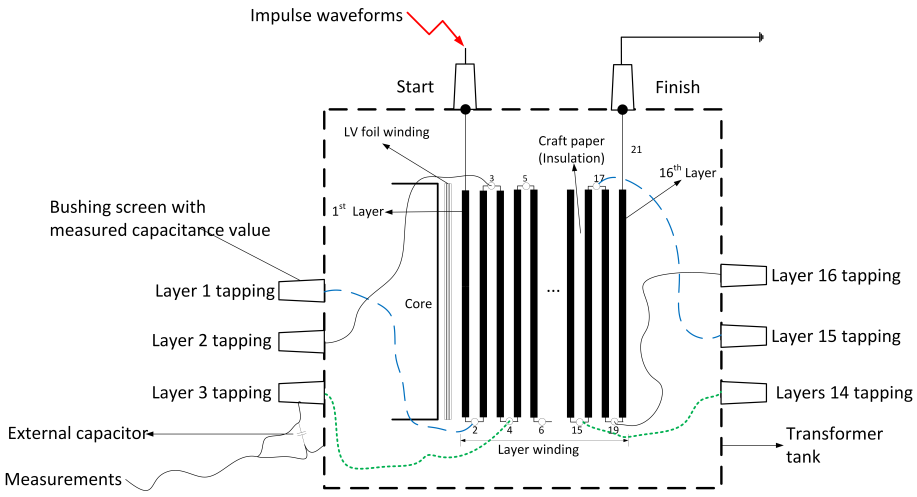

Figure 9.2: Final prototype transformer

The transformer is a step-up wind turbine transformer rated at 1.8 MVA, 690 V to 33 kV. To predict the transformer response to the measured switching surges in Figures 7.3, 7.4 and 7.6, the current high frequency model would have to be extended to the time domain.

The procedures have been depicted in Chapter 3 where the extension of the current model in the frequency domain is Equation 3.23 to the time domain equation which is Equation 3.24. However to prove the accuracy of the model certain measurements will need to be done. Hence from Figure 9.2, lightning impulse and chopped impulse waves will be applied across the whole winding. The goal being to obtain the response of the winding for the first three layers and last three layers which have been the dielectrically weak areas that suffered insulation failures as reviewed during the Brazilian and South African case studies. If the measured waveforms agree with the calculated model of Equation 3.24, when the winding is excited by the impulse waveforms then the effect of switching surges on those specific layers can then be investigated. The above constitute what the author is currently investigating with an abstract for the paper already having been accepted for the CIGRE "International Colloquium on EMC, Lightning and Power Quality Considerations for Renewable Energy Systems" in Curitiba, Brazil 2016.

9.3.2 Condition monitoring

A new area that could be used in extending the lifetime of transformers is to employ condition monitoring of the insulation structure. Several techniques exist in the literature which are used in the assessment of the transformer health index. Amongst the several techniques, Dissolved Gas Analysis (DGA) and Furan Analysis (FA) are the most common. DGA is used to diagnose faults within transformers such as thermal faults, arcing and partial discharges [82]. Furan analysis addresses the shortfalls of DGA since DGA cannot estimate the remaining life of transformer insulation. FA is a method of determining the amount of "furans" which are the organic compounds produced by the degradation of transformer insulation paper [82]. The concentration levels of furan compounds in the oil can give a clear estimation of the remaining life of the transformer insulation structure. The integration of traditional condition monitoring techniques with Artificial Neural Networks (ANNs) has been investigated in [82], [83]. The use of ANNs is possible due to their unique ability to learn directly from different measurement data and can be programmed to give diagnosis of the transformer insulation based on several case studies. Hence ANN can be used with DGA or FA to achieve a more enhanced and efficient real time monitoring system of the transformer insulation structure as outlined in [82]. The main challenges of such a complicated system are the high set-up costs.

Appendix A - (Supplement of Chapter 4)

This Appendix supplements more information that was not provided in Chapter 4.

.1 Calculation of Capacitance Matrix

The capacitance needed for computation in the MTL model where shown in Figure 4.2. Figure 3 shows the cross-sectional view of the capacitance represented in Figure 4.

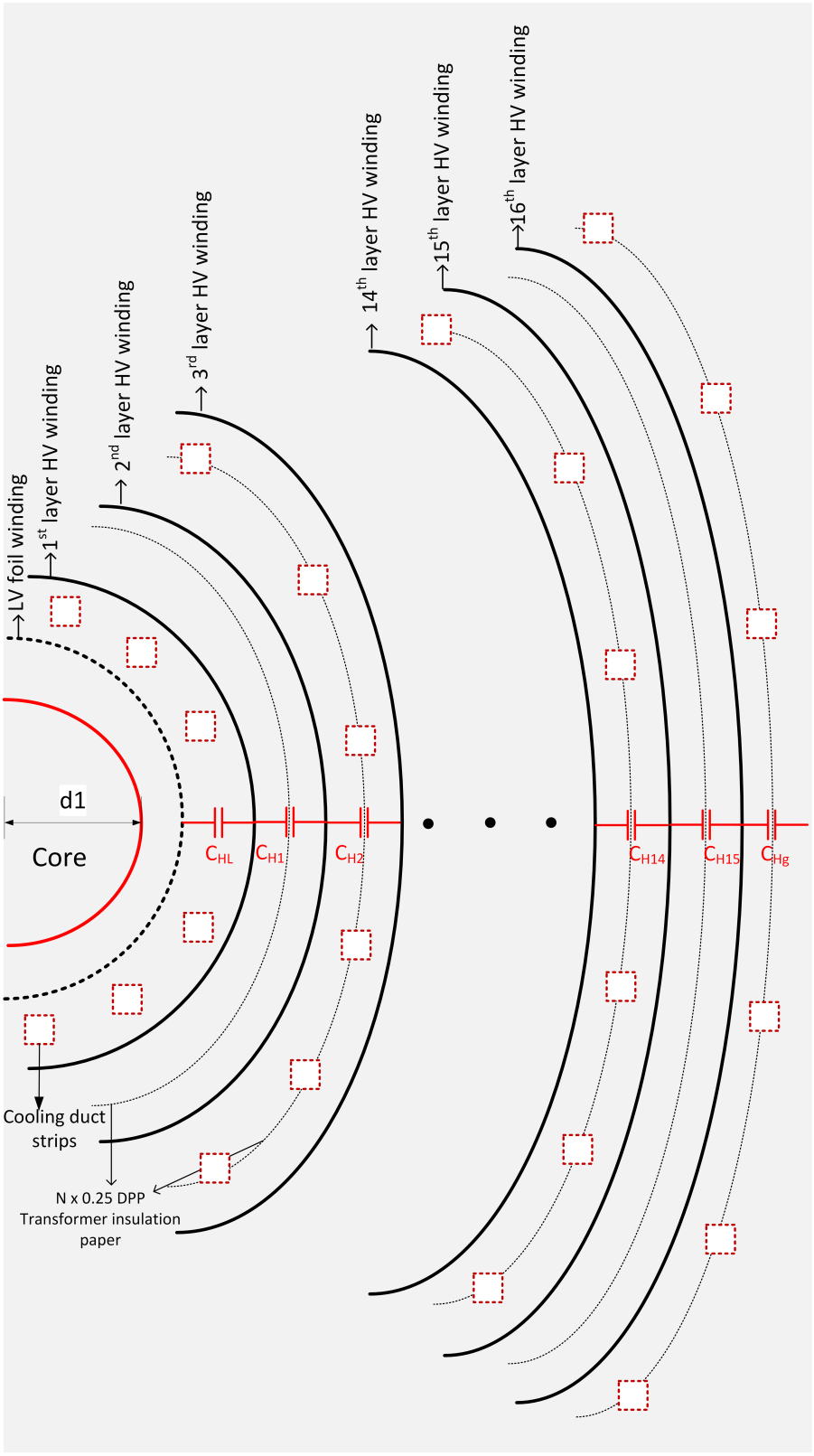

Figure 3: Capacitance top view

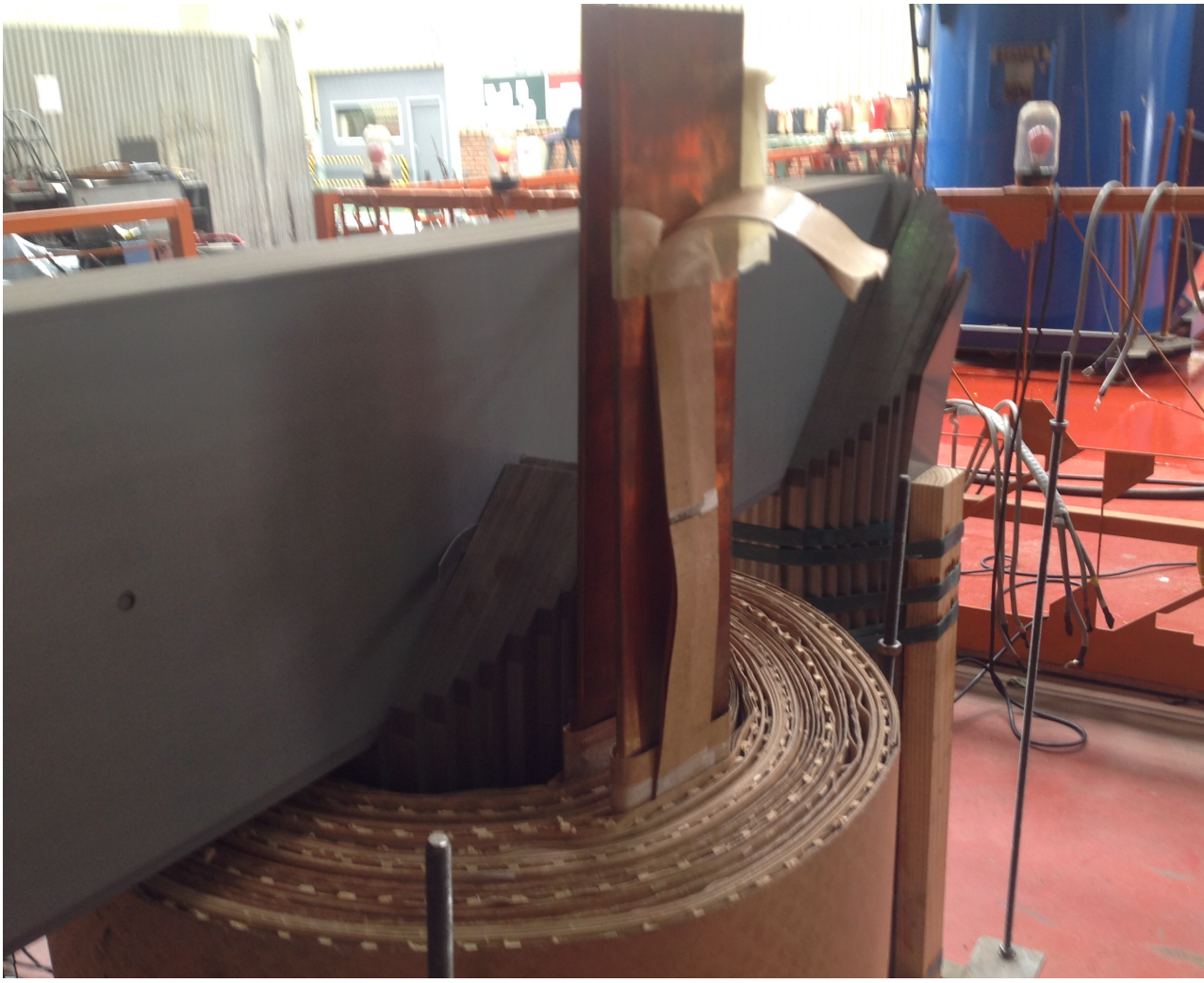

Figure 4: Prototype transformer

Table 1: Calculated Capacitors for Transformer with split MV winding shown in Figure 6.5 in Chapter 6.3.1

Capacitor	**Capacitance value**
C_{HH1}	2.59E-09
C_{HH2}	2.67E-09
C_{HH3}	2.76E-09
C_{HH4}	2.84E-09
C_{HH5}	2.92E-09
C_{HH6}	3.00E-09
C_{HH7}	3.09E-09
C_{HH8}	3.17E-09
C_{HH9}	3.25E-09
C_{HH10}	3.34E-09
C_{HH11}	3.42E-09
C_{HH12}	3.50E-09
C_{HH13}	3.58E-09
C_{HH14}	3.67E-09
C_{HH15}	3.75E-09
$C_{layer\ layer}$	1.00E-10
C_{ss}	4.43E-08
C_{gg}	1.44E-12
C_{HL}	6.95E-10

Table 2: Calculated Capacitors for Transformer with non-split MV winding shown in Figure 6.7 in Chapter 6.3.2

Capacitor	**Capacitance value**
C_{HH1}	2.16E-08
C_{HH2}	2.18E-08
C_{HH3}	2.20E-08
C_{HH4}	4.22E-08
C_{HH5}	4.24E-08
C_{HH6}	4.25E-08
C_{HH7}	4.27E-08
C_{HH8}	4.29E-08
C_{HH9}	4.30E-08
C_{HH10}	4.32E-08
C_{HH11}	4.34E-08
C_{HH12}	2.28E-08
C_{HH13}	2.30E-08
C_{HH14}	2.32E-08
C_{HH15}	2.33E-08
$C_{HH\,16g}$	3.69E-08
C_{ss}	4.43E-08
C_{HL}	1.40E-09

.2 Parameters of Split MV winding Transformer

Due to a non-disclosure agreement between the Author and Actom Distribution transformers the transformer geometry and any associated drawings will not be included in this section. However the following should suffice for any derivations that may be needed.

Table 3: 2700kVA three phase 33000/690V Dyn11 three limb mitre core transfomer with split MV winding shown in Figure 6.5 in Chapter 6.3.1

Parameter Description	**Parameter Information**
Winding material	Copper / Copper
Type of winding	Layer
Inner Coil	LV
Outer Coil	MV
Power rating	2700 kVA
Voltage Ratio	33000/690 Volts
Tappings	2.5 & 5
Tapping side	MV
Short cct voltage	2310 Volts
Load loss @ Ref temp	17372 Watts
No load Loss	2980 Watts
No Load current	6 Amps
No of layers (N1)	16
Number of Turns/layer	5 x 40t & 11 x 49t
Inner radius of MV winding	227.5 mm
External raduis of MV winding	301 mm
Inner radius of LV winding	166 mm
External raduis of LV winding	227.5 mm
LV conductor	720 x 1.5 Cu Foil
MV conductor	6 x 2.36 Cu Strip
Tripple wire insulation	0.6 mm
Distance between layers	0.52 mm
Coil height	MV_1 and MV_2 at 375 mm
Top / Bottom distance to core	32.5 mm
Dielectric permitivity of oil	2.3
Dielectric permitivity of wire insulation	4
Number of Foils (N2)	1
Dielectric permitivity of foil insulation	3
Foil insulation	0.25 mm

.3 Parameters of Non-split MV winding Transformer

Table 4: 2700kVA three phase 33000/690V Dyn11 three limb mitre core transfomer with non-split MV winding shown in Figure 6.7 in Chapter 6.3.2

Parameter Description	**Parameter Information**
Winding material	Copper / Copper
Type of winding	Layer
Inner Coil	LV
Outer Coil	MV
Power rating	2700 kVA
Voltage Ratio	33000/690 Volts
Tappings	2.5 & 5
Tapping side	MV
Short cct voltage	2310 Volts
Load loss @ Ref temp	17372 Watts
No load Loss	2980 Watts
No Load current	6 Amps
No of layers (N1)	16
Total number of Turns	1478
Inner radius of MV winding	227.5 mm
External raduis of MV winding	301 mm
Inner radius of LV winding	166 mm
External raduis of LV winding	227.5 mm
LV conductor	720 x 1.5 Cu Foil
MV conductor	6 x 2.36 Cu Strip
Tripple wire insulation	0.6 mm
Distance between layers	0.52 mm
Coil height	750 mm
Top / Bottom distance to core	32.5 mm
Dielectric permitivity of oil	2.3
Dielectric permitivity of wire insulation	4
Number of Foils (N2)	1
Dielectric permitivity of foil insulation	3
Foil insulation	0.25 mm

Appendix B - Publications

.4 List of attached publications

The following are the attached list of publications

1. Banda C. A. and Van Coller J. M. Measurement of switching surges and resonance behaviour in transformer windings. **In Proceedings of the 23rd Southern African Universities Power Engineering Conference (SAUPEC 2015)**, pp. 496 - 501. Jan. 2015

2. Banda C. A and Van Coller, J.M, "Investigation into Resonant Overvoltages in Wind Turbine Transformers due to Switching Surges" paper presented at **International Conference on Power Systems Transients (IPST2015) in Cavtat, Croatia June 15-18, 2015**.

3. Banda C. A and Van Coller, J.M, "Resonant Overvoltages in Wind Turbine Transformers" paper presented at **Powertech Conference in Eindhoven, Netherlands 29 June - 2 July 2015**.

4. Banda C. A and Van Coller, J, M, "Measurement of switching surges in onshore windfarms and resonance overvoltages in transfomer windings" paper presented at the 19th **International Symposium on High Voltage Engineering (ISH2015),Pilsen on August, 23-28, 2015**.

5. Banda C. A and Van Coller, J, M "Resonance overvoltages in single and split winding wind turbine step-up transformers" paper presented at **CIGRE/IEC SYMPOSIUM on Development of Electricity Infrastructures in Sub-saharan Africa, CapeTown, South Africa, October 26-30, 2015**.

MEASUREMENT OF SWITCHING SURGES AND RESONANCE BEHAVIOUR IN TRANSFORMER WINDINGS

Cedric. A Banda[a]* **and Dr John M. Van Coller***

* *School of Electrical and Information, Private Bag 3, Wits 2050, South Africa E-mail: cedric.banda@students.wits.ac.za & john.vancoller@wits.ac.za*

Abstract: Internal winding resonance is a phenomenon which can lead to overvoltages within transformer windings. This paper will address resonance behaviour in transformer windings using the Multi-conductor Transmission Line (MTL) model. The aim in using the MTL model is to determine the turns between which insulation breakdown can occur due to internal winding resonances. Since an internal winding resonance can be excited when a frequency component of an incoming surge equals a resonance frequency of the transformer, measurement of the switching surges generated when switching a transformer with a vacuum circuit breaker were conducted. Results of the pre-strike behaviour also indicated high du/dt which could lead to stressing of the end-turn insulation of the transformer.

Key words: MTL model, pre-strike, resonance over-voltage.

1. INTRODUCTION

Switching transients due to vacuum circuit breakers can lead to resonant over-voltages in wind turbine step-up transformers. In medium voltage networks the switching of vacuum circuit breakers [1], [2] can result in re-ignitions and pre-strikes. These can lead to high-frequency oscillations with also high du/dt resulting in stressing of the end-turn insulation of the transformer. A more prominent problem is resonance phenomena in transformer windings which can be classified as either internal resonance or external resonance. External resonance occurs due to cable and transformer interaction such that the natural frequency of the supplying cable matches the natural frequency of the transformer. This is more common in wind turbine transformers where energization may result in cable-transformer resonant transients [3]. Onshore wind farms can have a vast cable network with lengths of up to 600m. If the quarter wave frequency of such cables is in the vicinity of the resonant frequencies of wind turbine transformers, resonant overvoltages may occur on the LV terminal of step-up transformers and inside HV windings [3]. Internal resonance occurs when a frequency component of the incoming surge equals a resonance frequency of the transformer winding. These resonant over-voltages can result in a flashover from the windings to the core or between the turns [4]. However it should be noted that internal winding resonances will not necessarily result in immediate breakdown, but may result in partial discharges, which will further aid in insulation degradation and ultimately failure [1]. Measurement of resonance overvoltages cannot be done at the transformer terminals since they occur inside the windings. Special prototype transformers are usually constructed for the measurement of these overvoltages or through an analytical high frequency model of a transformer. In the literature, two high frequency modelling techniques are usually employed which are the Multi-conductor Transmission Line (MTL) model and the RLC ladder equivalent circuit [5], [6], [7], [8]. The MTL model is usually used for analysis of fast transients with frequency components above 1 MHz whereas the RLC ladder equivalent circuit for transients up to 1 MHz [8]. In [9], a special prototype wind turbine step-down transformer was designed for the purpose of analysis of resonant overvoltages in wind turbine transformers. The special prototype transformer was a 11/0.24 kV 500 kVA transformer with three different winding designs which are pancake, layer and disc winding [3]. Results show that a layer winding is more likely to have a higher transferred overvoltage to the LV terminal than disc and pancake windings. However the layer and pancake windings have lower values with regards to resonance over-voltages inside the windings compared to the disc winding. This paper deals with the calculation of the inter-turn overvoltage using transformer parameters from [6] and the measurement of switching transients obtained at wind farm.

2. BACKGROUND THEORY

Analysis of the voltage distribution within the transformer windings can be represented by a group of interconnected and coupled transmission lines as shown in Figure 1.

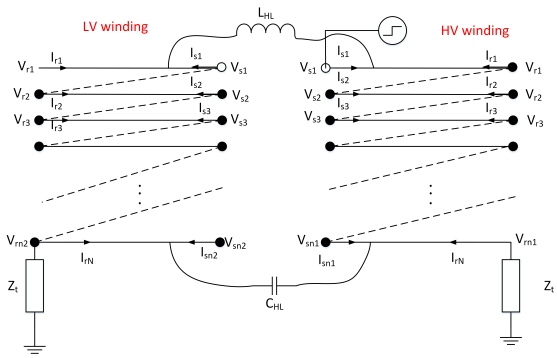

Figure 1: Multi-conductor Transmission Line model

Figure 1 shows a model representation of the HV and LV

windings. With reference to SANS 60076-3, transferred voltages have both a capacitive and inductive character which are presented by C_{HL} and L_{HL} respectively in Figure 1. The coupled transmission lines can be described by the Telegraphers equations: Equation 1 and Equation 2:

$$\frac{d^2\mathbf{V}}{d\mathbf{x}^2} = -[Z][Y] \tag{1}$$

$$\frac{d^2\mathbf{I}}{d\mathbf{x}^2} = -[Z][Y] \tag{2}$$

where **V** and **I** are the incident voltage and current vectors respectively. **Z** and **Y** are the impedance and admittance matrices of the line respectively. The Telegraphers equations can be solved to find the voltages and currents at a distance x as shown in Equation 3 and Equation 4 [10].

$$V_x = V_1 e^{-[P]x} + V_2 e^{[P]x} \tag{3}$$

$$I_x = Y_o\left(V_1 e^{-[P]x} - V_2 e^{[P]x}\right) \tag{4}$$

Applying boundary conditions to the solution of Equation 3 and Equation 4 it is possible to express the sending end $(_S)$ and receiving end $(_R)$ voltages as shown in Equation 5 [6]:

$$\begin{bmatrix} I_S \\ I_R \end{bmatrix} = \begin{bmatrix} A & -B \\ -B & A \end{bmatrix} \begin{bmatrix} V_S \\ V_R \end{bmatrix} \tag{5}$$

where:

$$A = YS\gamma^{-1}\coth(\gamma l)S^{-1} \tag{6}$$

$$B = YS\gamma^{-1}cosech(\gamma l)S^{-1} \tag{7}$$

and I_R and I_S are the current vectors at the receiving and sending end respectively. V_R and V_S are the voltage vectors at the receiving and sending end respectively. In Equation 6 and Equation 7: S is the matrix of eigenvectors and γ^2 is the matrix of eigenvalues of the matrix ZY. l is the length of the line. Further simplification of Equation 5 results in the following:

$$\begin{bmatrix} I_{S1} \\ I_{S2} \\ \cdot \\ \cdot \\ I_{Sn} \\ I_{R1} \\ I_{R2} \\ \cdot \\ \cdot \\ I_{RN} \end{bmatrix} = \begin{bmatrix} A & -B \\ -B & A \end{bmatrix} \begin{bmatrix} V_{S1} \\ V_{S2} \\ \cdot \\ \cdot \\ V_{Sn} \\ V_{R1} \\ V_{R2} \\ \cdot \\ \cdot \\ V_{RN} \end{bmatrix} \tag{8}$$

From Figure 1 it is possible to apply the following identities to Equation 8 [11]:

$I_{r1} = -I_{s2}$ $I_{r2} = -I_{s3}$ $-I_{rn} = V_{rn}/Z_t$ $V_{rl} = V_{s2}$ $V_{r2} = V_{s3}$ ...

This will enable matrix reduction techniques to be applied without altering the system equations. The result is Equation 9.

$$\begin{bmatrix} I_{S1} \\ 0 \\ \cdot \\ \cdot \\ 0 \\ 0 \end{bmatrix} = \begin{bmatrix} \\ Y \\ \\ \end{bmatrix} \begin{bmatrix} V_{S1} \\ V_{S2} \\ \cdot \\ \cdot \\ V_{Sn} \\ V_{Rn} \end{bmatrix} \tag{9}$$

where Y is an n x n matrix. The termination impedance for the transformer winding Z_t in Figure 1 is assumed to be $10^{-}9\ \Omega$ [12]. If the current I_{S1} is eliminated from Equation 9 then Equation 9 can be re-written as shown in Equation 10 to solve for the voltages at any arbitrary turn k.

$$\begin{bmatrix} V_{S2} \\ V_{S3} \\ \cdot \\ \cdot \\ V_{Sn} \end{bmatrix} = \begin{bmatrix} H_1 & & \\ H_2 & & \\ \cdot & & \\ \cdot & & \\ H_{n-1} & & \end{bmatrix} \begin{bmatrix} V_{S1} \\ 0 \\ \cdot \\ \cdot \\ 0 \end{bmatrix} \tag{10}$$

where the magnitude of the transfer function at turn k relative to the input can be calculated as [5]:

$$H_k = \frac{YY_{(k+1,1)}}{YY_{(1,1)}} \qquad k = 1,2,\cdots,n-1 \tag{11}$$

YY is the inverse matrix of the matrix Y in Equation 9 and H is a square matrix of order (n-1) x (n-1). It should be noted that surge transference from HV to LV winding as depicted in Figure 1 will not be the focus in this paper.

3. PARAMETER CALCULATION OF A TRANSFORMER WINDING

In [6] and [13] Liang showed how to model transformer windings for the analysis of resonant overvoltages. A core-type transformer was used and the winding parameters shown in Table 1 will be used in this paper [13].

The impedance **Z = R + j ωL** and admittance **Y = G + jωC** matrix of Equation 1 and Equation 2 are calculated as:

$$Z = \left[j\omega\mathbf{L} + \left(\frac{1}{2(d_1+d_2))}\right)\cdot\sqrt{\frac{\pi f\mu}{\sigma}}\right] \tag{12}$$

$$Y = (j\omega + \omega\tan\delta)\,\mathbf{C} \tag{13}$$

where μ and σ are the permeability and conductivity of the conductor. d_1 and d_2 are the diameter of the conductor.

Table 1: Main Parameters of the winding

Number Of discs	18
Turns per disc	10
Conductor width [mm]	6.95
Conductor height [mm]	11.2
Average turn length [m]	1.4828
Thickness of inter-turn insulation [mm]	3.00
Relative permittivity of inter-turn insulation	3.5
Conductor conductance [s $\cdot m^{-1}$]	$3x10^7$
Inter-turn capacitance (C_k) [pF $\cdot m^{-1}$]	120
Inter-section capacitance (C_s) [pF $\cdot m^{-1}$]	10
Turn to core capacitance (C_g) [pF $\cdot m^{-1}$]	15

In (12) the real part takes into account the skin effect at high frequencies [13]. The real part of Equation 13 represents the dissipation factor (tan δ) or dielectric losses [5], [12]. It should be noted that tan δ is frequency, moisture and temperature dependent and will influence the admittance matrix greatly at higher frequencies. An approximate equation for tan δ (Equation 14) was used to model the frequency dependency of the transformer insulation [3].

$$tan(\delta) = (1.082x10^{-8}) \cdot 2\pi f + 5.0x10^{-3} \qquad (14)$$

The capacitance and inductance matrix were calculated as follows:

3.1 Capacitance

The capacitance matrix **C** was formed as follows in [12]:

$C_{i,i}$ capacitance of layer i to ground and the sum of all other capacitances connected to layer i

$C_{i,j}$ capacitances between layers i and j taken with negative sign $(i \neq j)$

It should be noted that the capacitance matrix is crucial especially for the determination of the transient voltages between the turns.

3.2 Inductance

The inductance matrix is calculated from two parts. The first is directly from the capacitance matrix **C** if the following assumptions are made [11]:

1. High frequency magnetic flux penetration into the iron laminations and transformer core is negligible.
2. The magnetic flux will be constrained within the paths of the insulation.

The first inductance matrix can then be obtained using Equation 15:

$$L_n = \frac{\varepsilon_r}{v^2} \cdot \mathbf{C}^{-1} \qquad (15)$$

where v is the velocity of light in vacuum and ε_r is the relative permittivity of the insulation (in this case equivalent permittivity of the air and paper combination). The second part of the inductance takes into account the flux internal to the conductor [13]. It is given by:

$$L_i = \frac{\mathbf{R}}{f} \qquad (16)$$

where **R** is from the real part of Equation 12. The total inductance matrix can be expressed as:

$$\mathbf{L} = L_n + L_i \cdot E_n \qquad (17)$$

where E_n is a unit matrix of size nxn.

4. COMPARISON WITH PREVIOUS WORK

As previously mentioned, this work was done by Liang in [6] and [13]. The aim of redoing Liang work was to validate the work that was done earlier and test the validity of the developed algorithm. From then on the algorithm will be applied to transformers at a wind farm to try to explain if failure could be caused by resonance behaviour. Resonance phenomena in transformer windings is usually brought about if the frequency components of the switching surges matches one of the resonant frequencies of the transformer winding. The high frequency components lead to destruction of the insulation and breakdown tends to occur in the turns close to the led-in end [13].

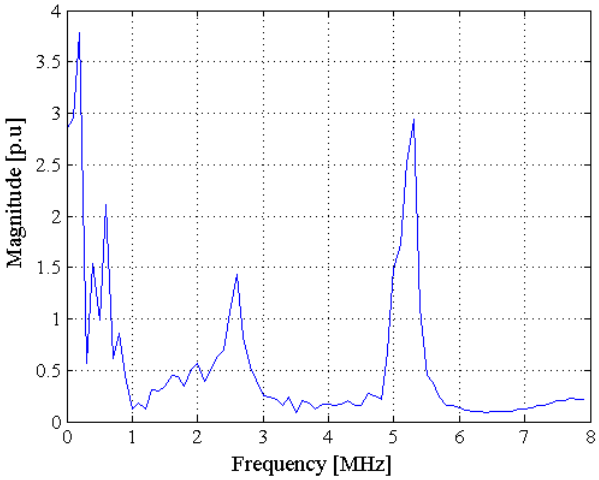

Figure 2: Magnitude of the transfer function of turn 20 relative to the input

Figure 2, Figure 3 and Figure 4 show the magnitude profile at different turns. An important characteristic to note from the waveforms is that the magnitude of the high frequency components decreases as the number of turns increase down the transformer winding. The waveforms

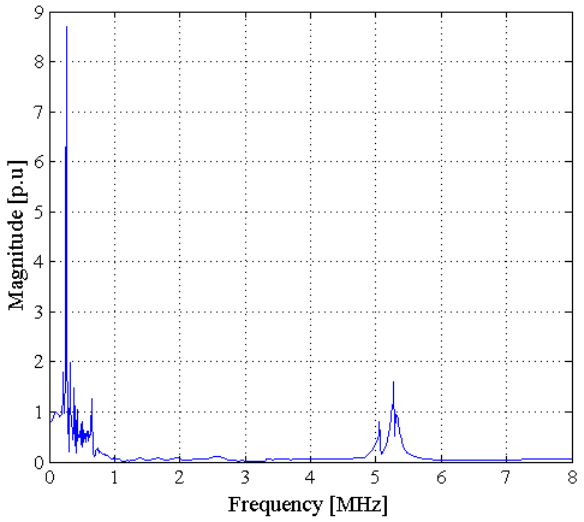

Figure 3: Magnitude of the transfer function of turn 40 relative to the input

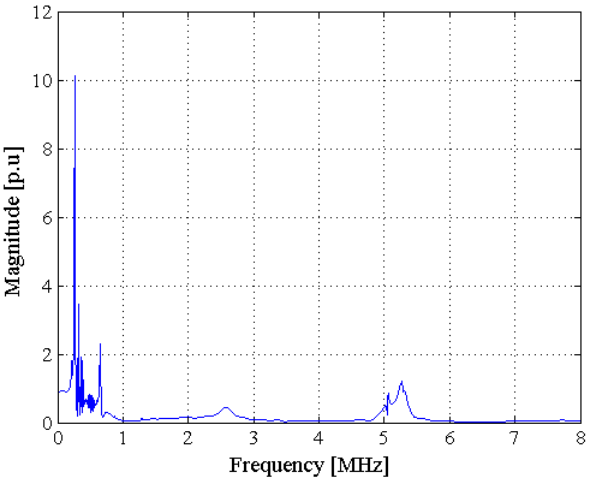

Figure 4: Magnitude of the transfer function of turn 60 relative to the input

produced show a resonant frequency around 5 to 6 MHz. Comparison with the results obtained by Liang in [13] reveal that the waveforms follow the same profile although the magnitude of some frequency components do not correlate. This could be as a result of the approximation for the calculation of $tan(\delta)$ and also the assumed termination impedance of $Z_t = 10^{-9}\Omega$. However the results of Figure 2, Figure 3 and Figure 4 are a good enough approximation to visualize the resonance phenomena in transformer windings and the possible determination of inter-turns breakdown.

4.1 Measurement of switching transients

As discussed earlier, internal resonance occurs when one of the frequency components of the incoming surge equals a resonance frequency of the transformer winding. Switching transients tests were conducted on a Wind turbine transformer. The tests involved the following:

1. Energizing the transformer during no-load.
2. Disconnecting the transformer during no-load.

Measurement of the three MV phase-to-earth voltages were made by use of a capacitive voltage divider on each phase. The MV bushing screen had a measured capacitance of 32 pF and an additional capacitance of 10 nF was externally mounted in series with the bushing screen terminal and the transformer tank which provided local earth. The resulting voltage division ratio was 313. Figure 5 shows the measurement setup with the FLUKE 1750 connected to the phase conductors.

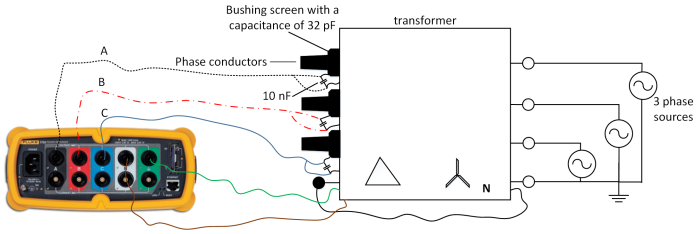

Figure 5: Measurement setup for recording transients

4.2 Energizing the transformer during no-load

Energization of the transformer from always results in at least one pre-strike per phase [14]. During the contact making process of the vacuum circuit breaker, generation of high du/dt transients can occur at the transformer terminals leading to over-voltages within a few milliseconds [15]. This behaviour can be observed from the measured transients in Figure 6. Analysis of the waveform in Figure 6 reveals a pre-strike behaviour with high du/dt which could result in the development of resonance overvoltages within the transformer winding.

4.3 Disconnecting the transformer during no-load

On disconnection of the VCB higher over-voltages can occur if the arc re-ignites after the first current interruption [16]. If the VCB is not able to quench the arc, multiple re-ignitions can occur and with each re-ignition, the voltage escalates resulting in higher over-voltages. No significant over-voltages were measured on de-energizing of the transformer.

5. DISCUSSION

In this paper a study into resonant overvoltages has been presented. White box models such as the MTL model and RLC model require the precise geometry of the transformer windings. In this paper since the actual parameters of the wind turbine transformers were not known, external transformer parameters where chosen to illustrate resonance phenomena in transformer windings. However the model has several limitations. Firstly an

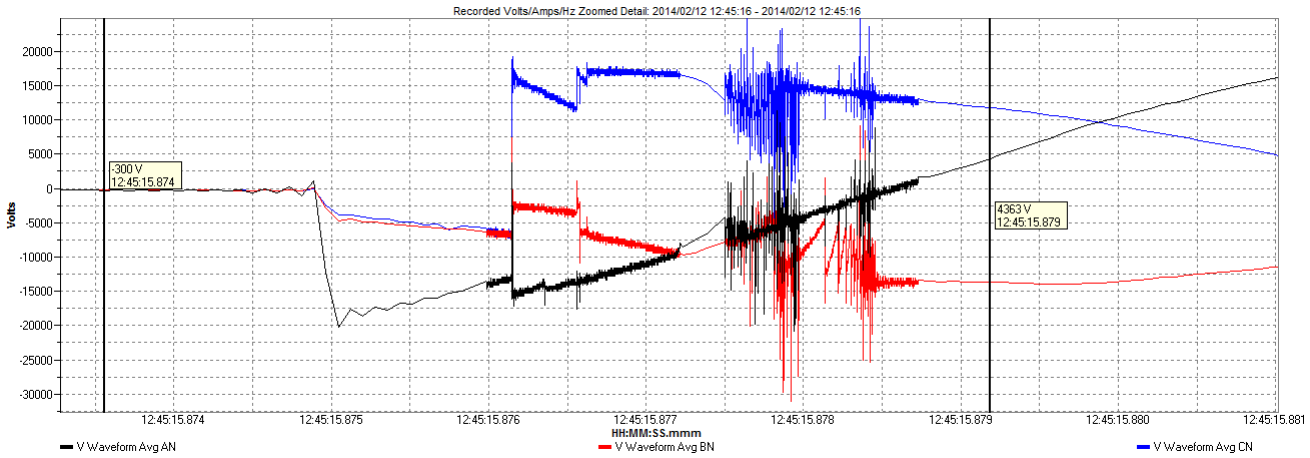

Figure 6: Measured pre-strike behaviour on closing of the vacuum circuit breaker

assumed value of the termination impedance was used. According to [12], to eliminate the divergence of the computations, a small impedance: $Z_t = 10^{-9}\Omega$ must be used. This value may be different from the termination impedance used by Liang in [6], [13].

As previously mentioned $tan(\delta)$ is frequency, moisture and temperature dependent and Equation 14 is an approximate equation. Thus at frequencies above 1 MHz, Equation 14 will not take into account the detailed frequency dependency of the dissipation factors of the transformer insulation, which is crucial for accurate modelling using the MTL model [3].

The next issue which warrants a discussion is the resistance calculation. In [13], Liang calculated the resistance by taking into account the skin effect at high frequencies as shown in Equation 12. However, another way of calculating the impedance is shown in Equation 18.

$$Z = \left(j\omega + \sqrt{\frac{2\omega}{\sigma\mu_o d^2}} \right) \mathbf{L} \qquad (18)$$

where the real part takes into account the skin effect and proximity effects of the conductor and its dependency on frequency [12]. In Equation (18), d is the distance between the layers and σ is the conductivity of the conductor. According to [3], the total resistance is dominantly affected by the proximity effect for frequencies above 4 MHz. Neglecting the proximity effects as done by Liang in [13] and only taking into account the skin effect in the resistance calculation can result in resonant frequencies below 1 MHz with quite high amplitudes [3] as shown in Figures 2, 3 and 4. To illustrate Hans Kristian Hidalen point [3], the magnitude of the transfer function at turn 20 is re-calculated taking into account proximity effect. The results of the MTL model with the impedance Equation (18) is shown in Figure 7. Analysis of Figure 7 shows that the magnitude of the resonance frequencies below 1 MHz which had quite high amplitudes have diminished considerably compared to the original waveform in Figure 2. Not taking into account the proximity effects can lead to calculated results which have a poor agreement with measurements as shown in [3].

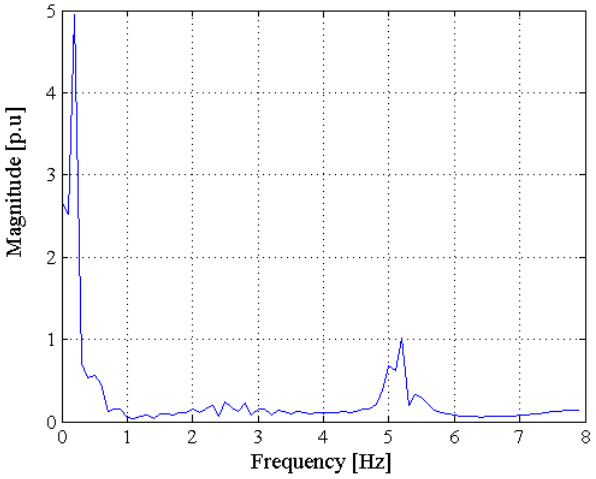

Figure 7: Magnitude of transfer function of turn 20 relative to the input (taking into account proximity effects)

6. CONCLUSION

In this paper, resonance phenomena in transformer windings and the measurement of switching transients have been presented. The MTL model has been used to calculate the magnitude of the resonant over-voltages within the turns and the possibility of breakdown between turns. Although the model has several shortcomings, the qualitatively good agreement of the calculated waveforms with the measured results can help understand the phenomena of internal winding resonance in transformers windings.

ACKNOWLEDGEMENT

This work is in partial fulfilment towards an MSc in Electrical Engineering and the author would like to thank

the Eskom Power Plant Engineering Institute (EPPEI) and Dr John Van Coller for their support and funding of the research program. Also the engineers from the transformer factory and at the wind farm who made all the measurements possible.

REFERENCES

[1] T. Craenenbroek, J. D. Ceuster, J. P. Marly, H. D. Herdt, B. Brouwers, and D. V. Dommelen. "Experimental and numerical analysis of fast transient phenomena in distribution transformers." *in IEEE Power Engineering Society Winter Meeting, Singapore*, vol. 3, no. 1, pp. 2193–2198, Jan. 2000.

[2] M. Popov and L. van der Sluis. "Improved calculations for no-load transformer switching surges." *in IEEE Transactions on Power Delivery*, vol. 16, no. 3, pp. 401–408, Jan. 2001.

[3] A. H. Soloot, H. K. Hidalen, and B. Gustavsen. "Modeling of Wind Turbine Transformers for the Analysis of Resonant Overvoltages." *in International Conference on Power Systems Transients IPST2013 in Vancouver, Canada*, pp. 1–7, Jul. 2013.

[4] M. Popov, L. V. der Sluis, G. C. Paap, and H. D. Herdt. "Computation of Very Fast Transient Overvoltages in Transformer Windings." *in IEEE Transactions on POWER DELIVERY*, vol. 18, no. 4, pp. 1268–1274, Oct. 2003.

[5] M. Popov, L. V. der Sluis, R. P. P. Smeets, and J. L. Roldan. "Analysis of Very Fast Transients in *Layer – Type* Transformer Windings." *in IEEE TRANSACTIONS ON POWER DELIVERY*, vol. 22, no. 1, pp. 238–247, Jan. 2007.

[6] H. Sun, G. Liang, X. Zhang, and X. Cui. "Analysis of Resonance in Transformer Windings under Very Fast Transient Overvoltages." *in 17th International Zurich Symposium on Electromagnetic Compatibility*, vol. 22, no. 1, pp. 432–435, Jan. 2006.

[7] J. Du, G. Liang, H. Sun, X. Liu, and X. Liu. "Lumped Parameter Modeling of Transformer windings under VFTO." *in 17th International Zurich Symposium on Electromagnetic Compatibility*, pp. 258–261, Jan. 2011.

[8] S. Hosseini, M. Vakilian, and G. Gharehpetian. "Comparison of transformer detailed models for fast and very fast transient studies." *in IEEE Transactions on Power Delivery*, vol. 23, no. 2, pp. 733–741, Apr. 2008.

[9] A. H. Soloot, H. K. Hidalen, and B. Gustavsen. "Upon the Improvement of the Winding Design of Wind Turbine Transformers for Safer Performance within Resonance Overvoltages." *in Tenth Deep Sea Offshore Wind Research and Development Seminar*, pp. 1–7, Jan. 2013.

[10] S. N. Hettiwatte, P. A. Crossley, Z. D. Wang, A. Darwin, and G. Edwards. "Simulation of a transformer winding for partial discharge propagation studies." *in IEEE Power Engineering Society Winter Meeting*, vol. 2, no. 1, pp. 95–101, Jun. 2002.

[11] J. Guardado and K. J. Cornick. "A Computer model for calculating Steep-Fronted Surge Distribution in Machine WIndings." *in IEEE TRANSACTIONS ON Energy Conversion*, vol. 4, no. 1, pp. 95–101, Mar. 1989.

[12] M. Popov, L. V. der Sluis, and R. P. P. Smeets. "Evaluation of surge-transferred overvoltages in distribution transformers." *in Electric Power Systems Research 78 (ELSEVIER)*, vol. 78, no. 3, pp. 441–449, May 2007.

[13] H. Sun, G. Liang, X. Zhang, and X. Cui. "Modelling of Transformer Windings under Very Fast Transient Overvoltages." *in IEEE Transactions on Electromagnetic Compatibility*, vol. 48, no. 4, pp. 621–627, Nov. 2006.

[14] L. Liljestrand, E. Lindell, D. Bormann, C. Ray, and E. Dullni. "Vacuum circuit breaker and Transformer interaction in a cable system." *CIRED 22nd International Conference on Electricity Distribution Stockholm*, , no. 0412, pp. 1–4, Jun. 2013.

[15] D. Smugala, W. Piasecki, M. Ostrogorska, M. Florkowski, M. Fulczyk, and P. Kyls. "Distribution transformers protection against High Switching Transients." *Przeglad Elekrotechniczny (Electrical Review)*, pp. 296 – 300, Jan. 2012.

[16] A. Mueller and D. Saemann. "Switching phenomena in Medium Voltage Systems - Good Engineering Practise on the application of Vacuum circuit breakers and contractors." pp. 1–9, Mar. 2011.

Investigation into Resonant Overvoltages in Wind Turbine Transformers due to Switching Surges

Cedric Amittai Banda and John Michael Van Coller

***Abstract*--This paper presents an investigation into resonant overvoltages in wind turbine transformers. The transformers are frequently switched by vacuum circuit breakers depending on the wind speed. Switching surges measured on-site which show repetitive, high du/dt transients where believed to contribute to the development of resonant overvoltages in the transformer windings. Two transformers with different core and winding arrangements but the same MV/LV voltage ratio and power rating where investigated. The transformers where rated 2.7 MVA, 0.690 / 33 kV with the MV side consisting of delta connected layer windings and the LV side consisting of star connected foil windings. A failed transformer had a wound core and used an egg-shaped winding whilst the special prototype transformer had a stacked core with split round windings. Part winding resonance tests carried out on one of the healthy windings of the failed transformer indicated a resonance amplification factor of 2.5 at 660 kHz. Measurements where also performed on the split winding prototype and results indicated that only the top half of the transformer coil had marked resonance effects. Calculations where then done using the Multi-Transmission Line model and results where verified against the measurements. The calculated and measured results had good agreement with the same profile from 1 kHz to 10 MHz.**

***Keywords*: MTL model, resonant overvoltages, split winding design, switching surges and wind turbine transformer.**

I. Introduction

Switching transients due to vacuum circuit breaker operation can lead to the development of resonant over-voltages in wind turbine transformers. In medium voltage networks the switching of vacuum circuit breakers [1], [2] can result in re-ignitions and pre-strikes. These high-frequency transients with high du/dt can lead to stressing of the end-turn insulation of the transformer. Resonance phenomena in transformer windings can be categorized as either internal resonance or external resonance. External resonance occurs due to cable and transformer interaction such that the natural frequency of the supplying cable matches the natural frequency of the transformer. This is more common in wind turbine transformers where energization may result in cable transformer resonant transients [3]. Internal resonance occurs when the frequency of the incoming surge equals a resonant frequency of the transformer winding. These resonant overvoltages can result in a flashover from the windings to the core or between the turns [4]. However it should be noted that internal winding resonances will not necessarily result in immediate breakdown, but may result in partial discharges, which will further aid in insulation degradation and ultimately failure [1]. Transformer failure due to internal resonant overvoltages has been widely reported in [5], [6], and [7]. The increase in transformer dielectric failures led to the initiation of the CIGRE working group (A2/C4.39) and their findings where published in [8]. Although it was concluded that failures are mainly caused by the interaction of the transformer with the network for different cable lengths and loading conditions [9], [10], and [11] some of the expertise in transformer modelling will be applied in this paper. In [12], [13], and [14], the author investigated the frequency response of layer, pancake and disc winding types with the main focus being on resonant overvoltages in wind turbine transformers. A special prototype transformer with the three different winding designs was designed and manufactured. The results indicated that layer windings have a higher transferred overvoltage from LV to MV winding than disc and pancake windings. However the layer and pancake windings have a low voltage distribution further down in the middle of the winding and nearer to ground than the disc winding which keeps the high values of the voltage drops at resonant frequencies. This paper will focus on the layer type of winding with an interest on the resonant performance of split round windings. It should be noted that the analysis of very fast transients in layer- windings has been extensively researched in [4], [15], [16] and the use of the Multi-Transmission Line model for calculation of layer to layer voltage distribution will be used.

II. Wound Core Transformer

Failure of a wound core transformer on-site initiated the investigation into resonant overvoltages in wind turbine transformers and if switching surges could be a contributing factor. The damaged transformer when unwound at the transformer factory showed the inter-turn insulation was severely damaged as shown in Fig. 1. Substantial distortion of the first and second layer of the MV winding was also observed. A burn through the MV to LV barrier was also observed with a puncture through the first layer of the LV foil winding as shown in Fig. 2.

This work was funded by Eskom through the Eskom Power Plant Engineering Institute (EPPEI) program. C. A. Banda is currently with the University of Witwatersrand, Johannesburg, South Africa studying towards an MSc in Electrical Engineering (e-mail: cedric.banda@students.wits.ac.za). J. M. Van Coller is with the University of Witwatersrand and is a Senior Lecturer who has been with University for many years and holds the Eskom Chair of High Voltage (e-mail: john.vancoller@wits.ac.za).

Paper submitted to the International Conference on Power Systems Transients (IPST2015) in Cavtat, Croatia June 15-18, 2015



Fig. 1. Failed winding with inter-turn insulation severely damaged.



Fig. 2. Burning of the first layer of the LV foil winding

Part winding resonance tests were conducted on one of the undamaged windings of the wound core transformer to ascertain if resonance could be a contributing factor to the damage observed in the transformer. A ratio known as the Resonance Voltage Ratio (RVR) was used which is defined as the voltage between points of resonance divided by the 50 Hz voltage at the same point. The method used was to excite the winding with a variable frequency sinusoidal voltage and record the maximum amplitude between two layers for a frequency range of 1 kHz to 2 MHz. The results are shown in Table I.

TABLE I
PART WINDING RESONANCE OF THE TRANSFORMER

Point in Winding	**Frequency**	**RAF**
Start of winding (between 2 layers)	536 kHz	1.15
Middle of winding (between 2 layers)	1.17 MHz	0.67
End of winding (between 2 layers)	181 kHz	0.95
End of winding (between 2 layers)	660 kHz	2.5
End of winding (between 2 layers)	1.32 MHz	0.67

From Table I at 660 kHz the amplification factor of 2.5 was recorded between the last and second last layer of the MV winding. This could result in a resonant overvoltage with a sufficient magnitude to stress the inter-turn insulation when closing transients occur. From Fig. 1, it is difficult to predict if the failure started as an inter-turn or inter-layer fault due to the burning of the oil paper insulation. However the failure mechanism had sufficient magnitude to cause substantial distortion of the first two layers and create a puncture through to the LV foil winding. This paper will seek to address the above mentioned problem by investigating resonant performance of a split MV winding in comparison with the failed transformer that had a non-split MV winding through measurements and an analytical solution.

III. STACKED CORE PROTOTYPE TRANSFORMER

The design of the stacked core transformer is such that the inner winding is the LV winding whilst the outer winding is the MV winding. This differs from the wound core transformer as it had the MV winding sitting inside the LV winding with a static screen between the two windings. The wound core transformer used an egg-shaped winding against the stacked core's split round winding. The stacked core transformer prototype was installed with measuring taps at the end of each layer as shown in Fig. 3.

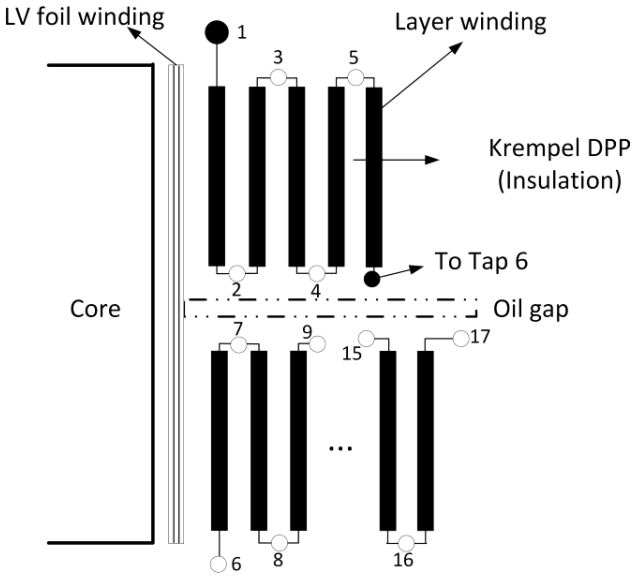

Fig. 3. Axisymmetric view of the prototype transformer

The upper coil consisted of 5 layers whilst the bottom coil consisted of 11 layers separated by an oil gap. It should be noted that both transformers had the same number of layers. The constructed prototype is shown in Fig. 4.

IV. ANALYTICAL MODEL OF THE TRANSFORMER

Analysis of the voltage distribution within the transformer windings can be represented by a group of interconnected and coupled transmission lines. The analytical modelling of the stacked core transformer was done using the Multi-Transmission Line (MTL) model. The MTL equations are described by (1) and (2):

$$\frac{d^2V}{dx^2} = -[Z][Y] \tag{1}$$

$$\frac{d^2I}{dx^2} = -[Z][Y] \tag{2}$$



Fig. 4. Prototype transformer with measuring taps installed.

where V and I are the incident voltage and current vectors respectively. Z and Y are the impedance and admittance matrices of the winding respectively. The solution of the above equation is well documented in [15] and [16] to yield Equation (3).

$$\begin{bmatrix} I_{S1} \\ 0 \\ . \\ . \\ 0 \\ 0 \end{bmatrix} = \begin{bmatrix} & & \\ & Y & \\ & & \end{bmatrix} \begin{bmatrix} V_{S1} \\ V_{S2} \\ . \\ . \\ V_{Sn} \\ V_{Rn} \end{bmatrix} \tag{3}$$

The matrix reduction techniques that are applied to get to equation (3) are best explained in [17]. Further manipulation of (3) results in (4). As the transformer winding is grounded $V_{Rn} = 0$ hence the last row can be removed as it is a redundant equation.

$$\begin{bmatrix} V_{S1} \\ V_{S2} \\ . \\ . \\ . \\ V_{Sn} \end{bmatrix} = \begin{bmatrix} & & \\ & YY & \\ & & \end{bmatrix} \begin{bmatrix} I_{S1} \\ 0 \\ . \\ . \\ . \\ 0 \end{bmatrix} \tag{4}$$

From (4), the voltages at the sending end of the winding between turn 2 and 1 are defined by: $V_{S1} = YY_{(1,1)} I_{S1}$ and $V_{S2} = YY_{(2,1)} I_{S1}$, hence the resonance voltage ratio is defined as:

$$H_1 = \frac{V_{S2}}{V_{S1}} = \frac{YY_{(2,1)}}{YY_{(1,1)}} \tag{5}$$

Equation (5) can be generalized to calculate the resonance voltage ratio at any arbitrary turn k as shown by (6)

$$H_k = \frac{V_{S(k+1)}}{V_{S1}} = \frac{YY_{(k+1,1)}}{YY_{(1,1)}} \quad \text{k = 1, 2,…, n-1} \tag{6}$$

where YY is the inverse matrix of the matrix Y in (3). Equation (6) is the analytical expression of the RVR defined in section II and a comparison of the analytical calculation vs measured RVR is done in section VI.

V. DETERMINATION OF THE TRANSFORMER PARAMETERS

The impedance **Z = R + j ωL** and admittance **Y = G + jωC** matrix of the MTL equations were calculated as shown in (7) and (8) from [5] and [6].

$$Z = \left[j\omega L + \left(\frac{1}{2(d_1 + d_2)} \right) \right] \sqrt{\frac{\pi f \mu}{\sigma}} \tag{7}$$

$$Y = \left(j\omega + \omega \tan\delta \right) \cdot C \tag{8}$$

where μ and σ are the permeability and conductivity of the conductor. d_1 and d_2 are the diameters of the conductors. In (7) the real part takes into account the skin effect at high frequencies [6]. The real part of (8) represents the dissipation factor (tan δ) or dielectric losses [15], [16]. It should be noted that tan δ is frequency, moisture and temperature dependent and will influence the admittance matrix greatly at higher frequencies. An approximate equation for tan δ shown in (9) was used to model the frequency dependency of the transformer insulation [3].

$$\tan(\delta) = \left(1.082 \times 10^{-8}\right) \cdot 2\pi f + 5.0 \times 10^{-3} \tag{9}$$

The capacitance and inductance matrix were calculated as follows:

A. Capacitance

The capacitance matrix **C** was formed as follows from [16]:

Cii — Capacitance of layer i to ground and the sum of all capacitances connected to layer i.

Cij — Capacitance between layers i and j taken with the negative sign (i≠j)

The formulas for calculating the capacitance were calculated from the basic formulas of cylindrical and plate capacitors in [18] and are shown in (10), (11) and (12).

$$C_s = \frac{\varepsilon_o \varepsilon_r h}{d_S} \tag{10}$$

$$C_g = \frac{\varepsilon_o \varepsilon_r \omega}{d_g} \tag{11}$$

$$C_{ij} = \frac{2\pi\varepsilon_o L}{In\left(\frac{b}{a}\right)} \tag{12}$$

where C_s is the turn to turn capacitance, C_g is the turn to earth capacitance and C_{ij} is the capacitance between layer i and j. ε_r is the relative permittivity of the dielectric material between the turns, ε_o is the permittivity of free space. h is the rectangular conductor's height. ds and dg are the distance between the turns and distance between turn and ground plane respectively. L is the length of the winding and w is the rectangular conductor's width. a and b are the inner and outer radius of the winding respectively.

The procedure for the construction of the capacitance matrix is explained in [19]. A matrix reduction technique explained in [20], [21] can be applied such that the order of matrices corresponds not to a single turn but to a group of turns. In this paper the group of turns will represent each layer of the MV winding.

B. *Inductance*

The inductance matrix is calculated from two parts. The first is directly from the capacitance matrix **C** if the following assumptions are made [17]:

1. High frequency magnetic flux penetration into the iron laminations and transformer core is negligible.
2. The magnetic flux will be constrained within the paths of the insulation.

The first inductance matrix can then be obtained using (13):

$$L_n = \frac{\varepsilon_r}{v^2} \cdot C^{-1} \tag{13}$$

where v is the velocity of light in vacuum and ε_r is the relative permittivity of the insulation (in this case equivalent permittivity of the air and paper combination). The second part of the inductance takes into account the flux internal to the conductor [6]. It is given by:

$$L_i = \frac{R}{f} \tag{14}$$

where R is from the real part of (7) and f is the frequency. The total inductance matrix can be expressed as:

$$L = L_n + L_i \cdot E_n \tag{15}$$

where E_n is a unit matrix of size n x n. It should be noted that the MTL model has also been applied for a disc winding in [22].

VI. MEASUREMENTS AND SIMULATIONS

A. *Test Equipment*

The equipment used included a Krohn-Hite Power Amplifier 7602 M series, 20 MHz Agilent 3320A waveform generator and Tektronix DPO 3032 Oscilloscope 300 MHz, 2.5 GS/s. The power amplifier is connected after the signal generator to keep the input voltage fairly constant. The amplifier energizes the whole winding whilst the oscilloscope measures the layer voltages from the measuring taps shown in Fig. 3 as the output. The RVR ratio was used to ascertain if resonance had occurred or not.

B. *Comparison of measured and calculated results*

As previously mentioned, resonance can be classified as either internal or external resonance. It is worth noting that internal resonance can be further defined as internal voltage maximum and internal anti-resonance as internal voltage minimum [23]. This relationship will be crucial in the analysis of measured and calculated results. Comparison will not be done for all 16 layers, however only crucial results will be revealed in this paper. In Figs. 5, 6 and 7 it can be seen that there is a relatively good agreement between the calculated and measured results.

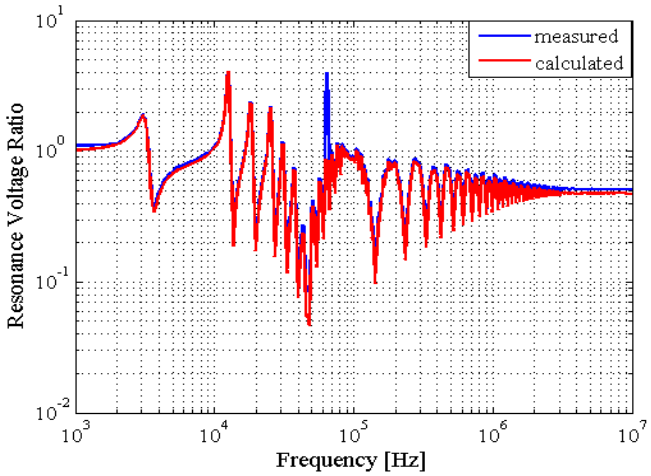

Fig. 5. Resonance voltage ratio across layer 1 – measured (across lead 1 and 2 in Fig. 3) vs calculated.

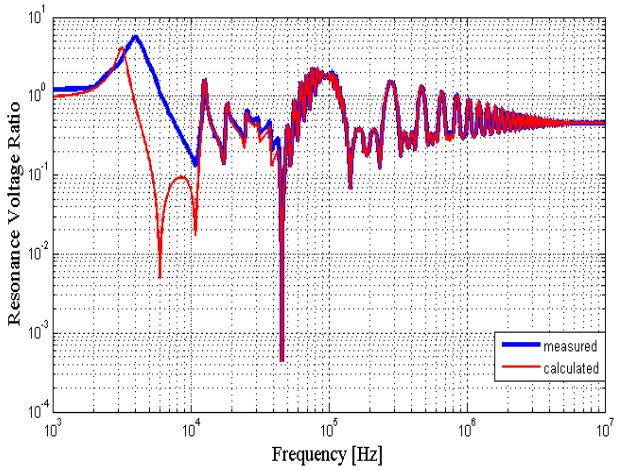

Fig. 6. Resonance voltage ratio across layer 15 – measured (across lead 15 and 16 in Fig. 3) vs calculated.

The calculated results follow the profile of the measured results although there is a frequency shift between 1 kHz and 10 kHz for layers 15 and layer 16. The general trend of the

resonance voltage ratio is shown in Fig. 8, 9, 10 and 11.

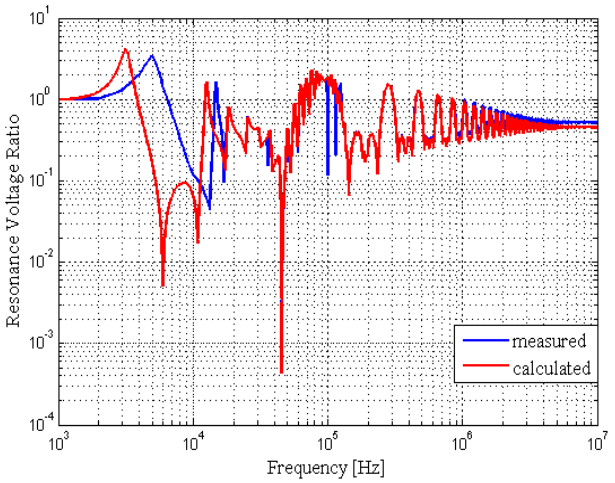

Fig. 7. Resonance voltage ratio across layer 16 – measured (across lead 16 and 17 in Fig. 3) vs calculated.

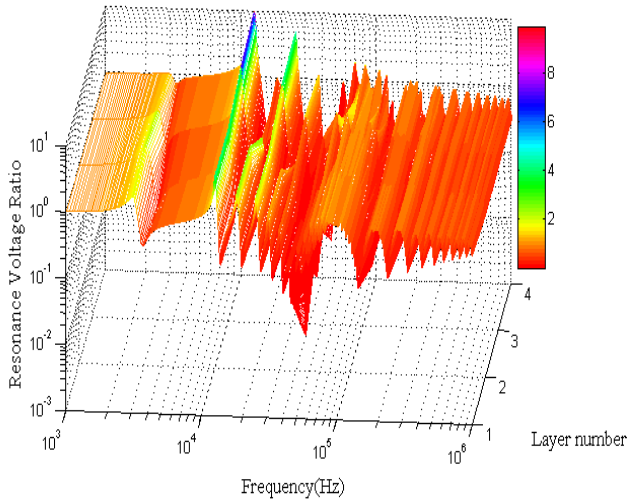

Fig. 8. Measured: resonance voltage distribution in layers 1-4.

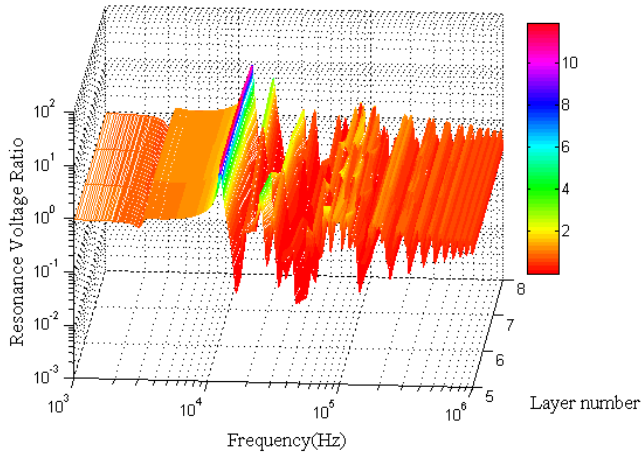

Fig. 9. Measured: resonance voltage distribution in layers 5-8.

It is interesting to note that the magnitude of the resonant overvoltages increase as you approach the break i.e. layer 1 to layer 5. Then the magnitude starts to decrease for layers 9 to layer 16.

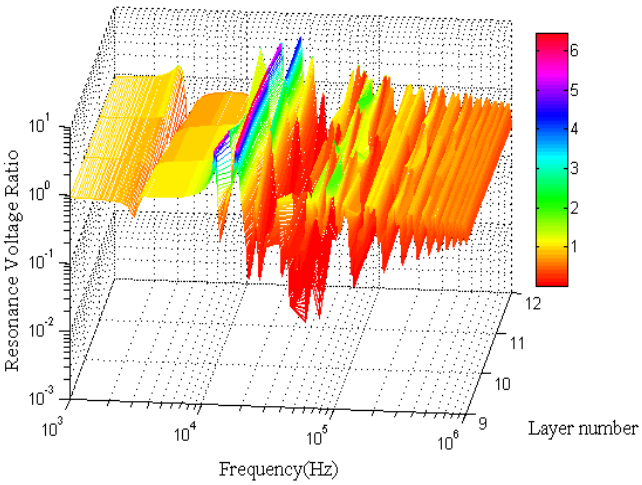

Fig. 10. Measured: resonance voltage distribution in layers 9-12.

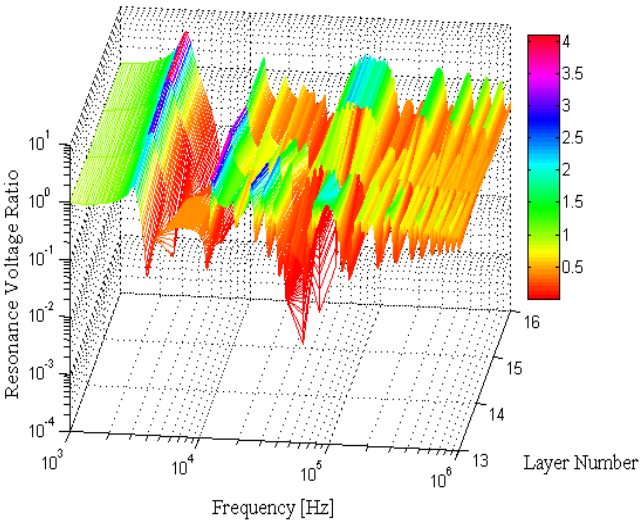

Fig. 11. Measured: resonance voltage distribution in layers 13-16.

VII. Switching Surge Measurement and Analysis

As previously mentioned, internal resonance occurs when a frequency component of the incoming surge equals a resonant frequency of the transformer leading to resonant overvoltages. In order to investigate the impact of switching surges in the development of resonant overvoltages the following tests were performed:

1. Energizing the transformer during no-load.
2. Disconnecting the transformer during no-load.

Measurement of the three MV phase-to-earth voltages was done using a capacitive voltage divider on each phase. The MV bushing screen had a measured capacitance of 32 pF and an additional capacitance of 10 nF was externally mounted in series with the bushing screen terminal and the transformer tank which provided local earth. The resulting voltage division ratio was 313.

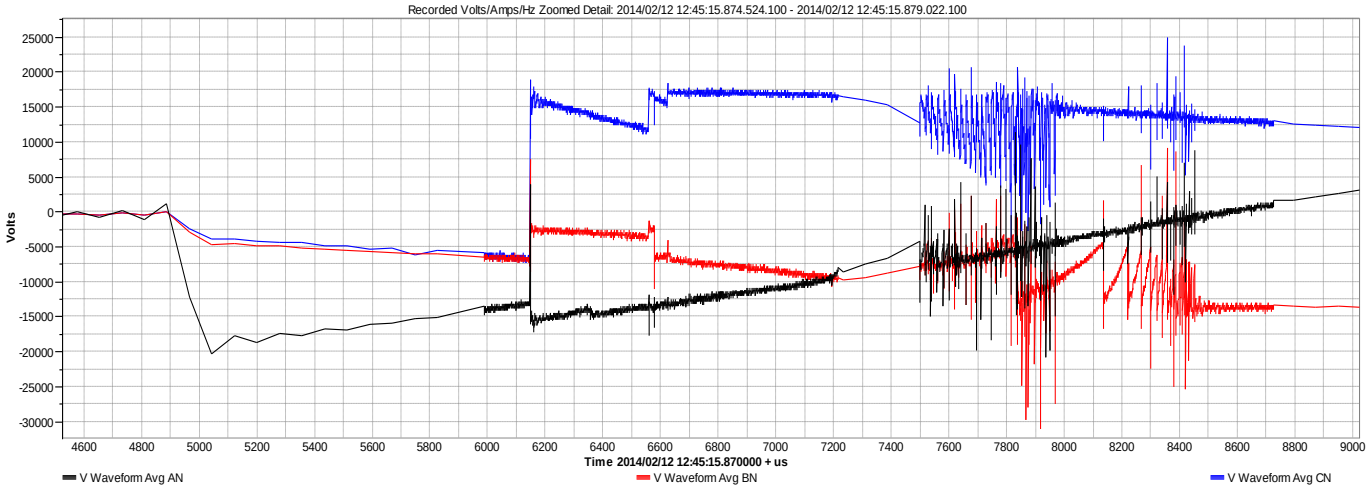

Fig. 13. Measured pre-strikes which show a high du/dt

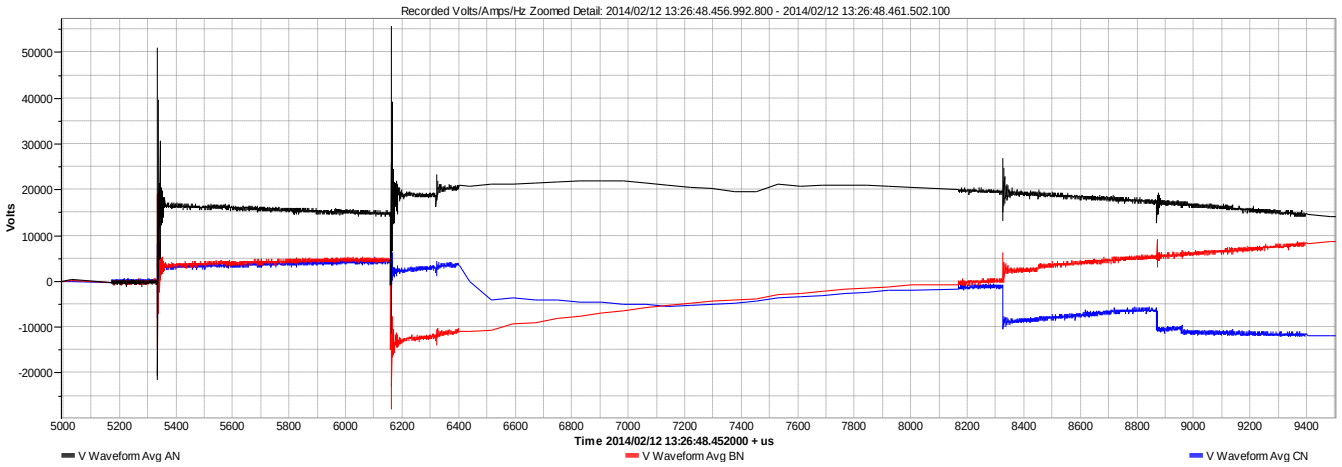

Fig. 14. Measured pre-strikes which show a high du/dt

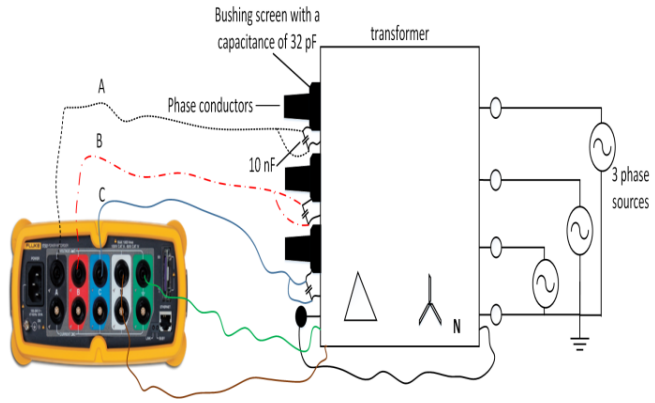

Fig. 12. Measurement setup for recording transient events during switching.

The setup for recording the transient events is shown in Fig. 12. It should be noted that the above setup measures phase to earth voltages on the MV side. Measurement of the voltage waveforms was done using a Fluke 1750 Power Recorder which samples transients at 5 Mega samples per second.

A. Energizing the transformer during no-load

Energization of the transformer always results in at least one pre-strike per phase [24]. During the contact making process of the vacuum circuit breaker, generation of high dU/dt transients can occur at the transformer terminals leading to over-voltages [7]. This behaviour can be observed from the measured transients in Figs. 13 and 14. Analysis of the measured waveforms show that there is substantial overshoot and ringing when the contacts are closed. Also from Figure 14, the peak value of the second peak is almost 2.5 times above the system voltage. Since relatively short cables of small surge impedance exist between the VCB and the transformer, this type of low surge impedance connection has a low du/dt limiting effectiveness [7]. Hence the high value of overvoltages and high frequency transients which were measured.

B. De-energizing the transformer during no-load

On disconnection by the VCB higher over-voltages can occur if the arc re-ignites after the first current interruption [25]. If the VCB is not able to quench the arc, multiple re-ignitions can occur and with each re-ignition, the voltage escalates

resulting in higher overvoltages. No significant over-voltages were measured on de-energizing of the transformer.

VIII. Discussion

In [26], research was conducted on the performance of oil impregnated cellulose paper when subjected to transients with different repetition frequency, rise time and magnitude. It was found that the faster the rise time, the more damage to the insulation that occurs and the quicker the transient reaches its peak value the more profound the damage to the insulation. Most commonly used insulation paper in transformers is Krempel DPP 0.25mm which has a breakdown voltage in oil of 13.5 kV [27]. From the peak values in Figs. 13 and 14, it is possible to design the insulation system such that it is able to withstand the high overvoltages between the layers. However the repetition rate would require damping by series connected choke elements [7]. It should be noted that the insulation system of the wound core transformer withstood the routine induced overvoltage test specified in IEC 60076 and complied with the impulse test in IEC 60076.

Use of the MTL model was possible since precise design information was made available by the transformer manufacturer. However no tan (δ) testing is done for an MV distribution transformers hence an approximated equation was used. As previously mentioned equation (9) will not take into account the detailed frequency dependency of the dissipation factors of the transformer insulation, which are crucial for accurate modelling using the MTL model. This could explain why the model was not able to accurately predict certain resonance frequencies for the transformer winding.

Two transformer designs have been presented. The major difference is the transformer with the split winding has higher resonant overvoltages below 100 kHz whereas the investigated transformer that had a non-split winding had high resonant overvoltages above 500 kHz. The split winding could be the reason why only the top half of the coil participates in resonances as can be seen by the decreasing trend of the resonant voltage ratio in Figs. 8, 9, 10 and 11.

Although the two transformers also differed in the type of core used, where the failed transformer used a wound core as opposed to the constructed prototype which used a stacked core, the focus was on resonance performance between a split MV winding versus a non-split MV winding. Customers usually prefer a transformer with a stacked core over the wound core. This is largely due to difficulties associated with a wound core when compared to a stacked core which are [28] (i) air gaps may diverge due to the tolerances of the machine during the cutting and winding of the sheets and also difficulties in processing of the magnetic material (ii) obtaining accurate dimensions in stacked cores is much easier than in wound cores during cutting (iii) core formation may deteriorate the magnetic material insulation and (iv) homogeneous temperature distribution in a wound core is hard to obtain during the annealing procedure as compared to stacked cores.

The measurement of resonance voltage ratio in this paper was done using the oscilloscope and signal generator. These measured RVR were needed for comparison with the calculated RVR in equation (6) for resonance analysis. However a different technique could have been done using frequency response analysis equipment where the impedance characteristics of the winding are determined. Both analysis techniques have been shown to produce the same results as shown in [29].

IX. Conclusion

In this paper, resonance phenomena in transformer windings and the measurement of switching transients have been presented. The MTL model has been used to calculate the magnitude of the resonant overvoltages within the layers and to determine between which layers breakdown could occur. Different winding designs were also investigated and their effect on part winding resonance was explored. The developed model still has several shortcomings; however it can be used in the prediction of resonances, especially in layer type transformers.

X. Acknowledgment

The author would like to thank the engineers from the transformer factory and the wind farm for allowing us to do measurements and research on different transformer designs.

XI. References

[1] T. Craenenbroek, J. D. Ceuster, J. P. Marly, H. D. Herdt, B. Brouwers, and D. V. Dommelen. “Experimental and numerical analysis of fast transient phenomena in distribution transformers.” *in* IEEE Power Engineering Society Winter Meeting, Singapore, vol. 3, no. 1, pp. 2193–2198, Jan. 2000.

[2] M. Popov and L. van der Sluis. “Improved calculations for no-load transformer switching surges.” *in IEEE Transactions on Power Delivery*, vol. 16, no. 3, pp. 401–408, Jan. 2001.

[3] A. H. Soloot, H. K. Hodalen, and B. Gustavsen. “Modeling of Wind Turbine Transformers for the Analysis of Resonant Overvoltages.” in International Conference on Power Systems Transients IPST2013 in Vancouver, Canada, pp. 1–7, Jul. 2013.

[4] M. Popov, L. V. der Sluis, G. C. Paap, and H. D. Herdt. “Computation of Very Fast Transient Overvoltages in Transformer Windings.” in IEEE Transactions on POWER DELIVERY, vol. 18, no. 4, pp. 1268–1274, Oct. 2003.

[5] H. Sun, G. Liang, X. Zhang, and X. Cui. “Analysis of Resonance in Transformer Windings under Very Fast Transient Overvoltages.” in 17th International Zurich Symposium on Electromagnetic Compatibility, vol. 22, no. 1, pp. 432–435, Jan. 2006.

[6] H. Sun, G. Liang, X. Zhang, and X. Cui. “Modelling of Transformer Windings under Very Fast Transient Overvoltages.” *in IEEE Transactions on Electromagnetic Compatibility*, vol. 48, no. 4, pp. 621–627, Nov. 2006.

[7] D. Smugala, W. Piasecki, M. Ostrogorska, M. Florkowski, M. Fulczyk, and P. Kyls. “Distribution transformers protection against High Switching Transients.” *Przeglad Elekrotechniczny (Electrical Review)*, pp. 296 – 300, Jan. 2012.

[8] CIGRE. “Electrical Transient Interaction between Transformers and the POWER SYSTEM.” In PART 1: EXPERTISE by CIGRE Joint Working Group A2/C4.39, Chapter. 4: Transformer Modelling, CIGRE ISBN: 978-2-85873272-2, pp. 33–56. Apr. 2014.

[9] R. Asano, A. C. O. Rocha, and G. M. Bastos. “Electrical transient interaction between transformers and the power system.” in CIGRE-33 CIGRE Brazil JWG A2/C4-03, pp. 401–408, Jun. 2007.

[10] A. C. O. Rocha. “Electrical transient interaction between transformers and the power system.” in CIGRE C4-104, CIGRE Brazil JWG A2/C4-

03, Paris, France, pp. 1–7, Jun. 2008.
[11] A. Theocharis, M. Popov, R. Seibold, S. Voss, and M. Eiselt. “Analysis of Switching effects of Vacuum Circuit Breaker on *Dry−Type* Foil winding transformers validated by experiments.” in IEEE Transactions on Power Delivery, pp. 1–9, May 2014.
[12] A. H. Soloot, H. K. Hodalen, and B. Gustavsen. “Upon the Improvement of the Winding Design of Wind Turbine Transformers for Safer Performance within Resonance Overvoltages.” in proc. of CIGRE Joint Colloquium - *SC A2/C4*, pp. 1–7, 2013.
[13] A. H. Soloot, H. K. Hodalen, and B. Gustavsen. “The effect of winding design on transformer frequency response with application on offshore wind farm energization.” in proc. Of Intl. Conference on Renewable Energy Research and Applications *(ICRERA)*, pp. 1–7, Nov. 2012.
[14] A. H. Soloot, H. K. HÃ¸idalen, and B. Gustavsen. “Internal Resonant Overvoltage in Wind Turbine Transformers- Sensitivity Analysis of Measurement Techniques.” *in International Conference on Electrical Machines and Systems, Busan, Korea*, pp. 1–7, Oct. 2013.
[15] M. Popov, L. V. der Sluis, R. P. P. Smeets, and J. L. Roldan. “Analysis of Very Fast Transients in *Layer−Type* Transformer Windings.” *in IEEE TRANSACTIONS ON POWER DELIVERY*, vol. 22, no. 1, pp. 238–247, Jan. 2007.
[16] M. Popov, L. V. der Sluis, and R. P. P. Smeets. “Evaluation of surge-transferred overvoltages in distribution transformers.” in Electric Power Systems Research 78 (ELSEVIER), vol. 78, no. 3, pp. 441–449, May 2007.
[17] J. Guardado and K. J. Cornick. “A Computer model for calculating Steep-Fronted Surge Distribution in Machine Windings.” in IEEE TRANSACTIONS ON Energy Conversion, vol. 4, no. 1, pp. 95–101, Mar. 1989.
[18] J. A. Martinez-Velasco. “Power System Transients.” In Parameter Determination, Chapter 4: Transformers, CRC Press Taylor and Francis Group, ISBN 978-1-4200-6529-9 (Hardback), pp. 177–255. 2010.
[19] Y. Shibuya, S. Fujita, and N. Hosokawa. “Analysis of very fast transient overvoltage in transformer winding.” *in IEE Proc.-Gener. Transm. Distrib*, vol. 144, no. 5, pp. 461–468, 1997.
[20] F. de Leon and A. Semlyen. “Reduced order model for transformer transients.” *in IEEE Transactions on Power Delivery*, vol. 7, no. 1, pp. 361–369, Jan. 1992.
[21] F. de Leon and A. Semlyen. “Efficient calculation of Elementary parameters of Transformer.” *in IEEE Transactions on Power Delivery*, vol. 7, no. 1, pp. 376–383, Jan. 1992.
[22] C. A. Banda and J. M. Van Coller, “Measurement of switching surges and resonance behavior in transformer windings,” in Proceedings of the 23rd Southern African Universities Power Engineering Conference, pp 496-501. Jan 2015.
[23] R. C. Degeneff. “A general method for determining resonances in transformer windings.” *in IEEE Transactions on Power Apparatus and Systems*, vol. PAS-96, no. 2, pp. 423–430, Mar. 1977.
[24] L. Liljestrand, E. Lindell, D. Bormann, C. Ray, and E. Dullni. “Vacuum circuit breaker and Transformer interaction in a cable system.” *CIRED 22nd International Conference on Electricity Distribution Stockholm*, no. 0412, pp. 1–4, Jun. 2013.
[25] A. Mueller and D. Saemann. “Switching phenomena in Medium Voltage Systems - Good Engineering Practise on the application of Vacuum circuit breakers and contractors.” pp. 1–9, Mar. 2011.
[26] T. L. Koltunowicz, R. Kochetov, G. Bajracharya, D. Djairam and J. J. Smit “Repetitive Transient Aging, the Influence of Rise Time” *in* Electrical Insulation Conference, Annapolis, Maryland pp.151-155, Jun 2011
[27] KREMPEL, ‘Technical datasheet KREMPEL DPP.” P. 11/96 Aug. 2012
[28] P.S. Georgilakis, N.D. Hatziargyriou, N.D. Doulamis, A.D. Doulamis and S.D. Kollias, “Prediction of iron losses of wound core distribution transformers based on artificial neural networks” *in* Neurocomputing 23 (ELSEVIER), pp. 15-29, July 1998.
[29] IEEE, “Guide to describe the occurrence and mitigation of switching transients induced by transformers, switching device, and system interaction,” IEEE Std C57.142, pp. 35, Dec. 2010.

Resonant Overvoltages in Wind Turbine Transformers

Cedric Amittai Banda, Student Member, IEEE and Dr. John M. Van Coller Senior Member, IEEE

***Abstract*—In this paper, modelling and measurement of resonant overvoltages in wind turbine step-up transformers is presented. A failed 2.7 MVA, 0.690 / 33 kV step-up transformer with the MV side consisting of delta connected layer windings and the LV side consisting of star connected foil windings is presented as a case study. The failed transformer showed substantial damage in the first and second layer of the 33 kV winding with a burn through the HV to LV winding barrier. Two different prototype transformers with the same rating as the failed unit were constructed for the purpose of investigating resonant overvoltages. Both transformers used a stacked core but differed in the winding arrangement where one had split round windings and the other had single round windings. Analytical calculations were done using the Multi-conductor Transmission Line (MTL) model and results were compared with measurements. The calculated results using the MTL model showed a relatively good agreement and followed the trend of the measured results for a frequency range of 1 kHz to 10 MHz. The significance of this work is that it was shown that the MTL model can be used for the determination of the inter-layer stresses and hence can assist during the transformer design stage.**

***Index Terms*—MTL model, resonance, wind turbine transformer.**

I. Introduction

RESONANT overvoltages may occur in wind turbine transformers that are exposed to frequent switching. The switching of vacuum circuit breakers in medium voltage networks [1], [2] may result in pre-strikes and re-ignitions. These can lead to high-frequency oscillations with high du/dt resulting in stressing of the end-turn insulation of the transformer. These transients present a more prominent problem in respect to resonance phenomena in transformer windings which may be further classified as either internal resonance or external resonance. External resonance occurs due to cable and transformer interaction such that the natural frequency of the supplying cable matches the natural frequency of the transformer [3]. Internal resonance occurs when a frequency component of the incoming surge equal a resonant frequency of the transformer. These resonant over-voltages can result in a flashover from the windings to the core or in-between the turns [4]. Internal winding resonances will not necessarily result in immediate breakdown, but may result in partial discharges, which will further aid in insulation degradation and ultimately failure [1]. Transformer failure due to internal resonant overvoltages has been widely reported in [5], [6], [7]. The increase in transformer insulation failures led to the initiation of the CIGRE working group (A2/C4.39) and their findings where published in [8]. Although it was concluded that failures are mainly caused by the interaction of the transformer with the network for different cable lengths and loading conditions [9], [10] and [11], some of the methods in transformer modelling will be applied in this paper. In [12], [13] and [14], the author investigated the frequency response of layer, pancake and disc winding types with the main focus being on resonant overvoltages in wind turbine step-up transformers. A special prototype transformer with the three different winding types was designed and manufactured. The results indicated that layer windings have a higher overvoltage from LV to HV winding than the disc and pancake windings. However the layer and pancake windings have a low voltage distribution further down in the middle of the winding and nearer to ground than the disc winding which keeps the high values of the voltage drops at resonant frequencies. This paper will focus on the layer type of winding with an emphasis on the resonant performance of two special prototype transformers. It should be noted that the analysis of very fast transients in layer windings has been extensively researched in [4], [15], [16] and the Multi-Transmission Line (MTL) model for calculation of inter-layer voltages will be used in this paper.

This work was funded by Eskom through the Eskom Power Plant Engineering Institute (EPPEI) program. C. A. Banda is currently with the University of the Witwatersrand, Johannesburg, South Africa studying towards an MSc in Electrical Engineering (e-mail: cedric.banda@students.wits.ac.za). J. M. Van Coller is a Senior Lecturer at the University of Witwatersrand (e-mail: john.vancoller@wits.ac.za).

II. Case study: Wound core transformer

Failure of a wound core step-up transformer initiated the investigation into resonant over-voltages in wind turbine step-up transformers and into whether switching surges could be a contributing factor. The damaged transformer when unwound at the transformer factory showed that the inter-turn insulation had been severely damaged as shown in Fig. 1. Upon further examination of the winding it was observed that substantial distortion of the first and second layer of the MV winding had occurred. A burn through the HV-LV winding barrier was also observed as shown in Fig. 2 with a puncture through the first layer of the LV foil winding as shown in Fig. 3. Part winding resonance tests were conducted on one of the undamaged windings of the wound core transformer to ascertain if resonance could be a contributing factor to the damage observed in the failed transformer.

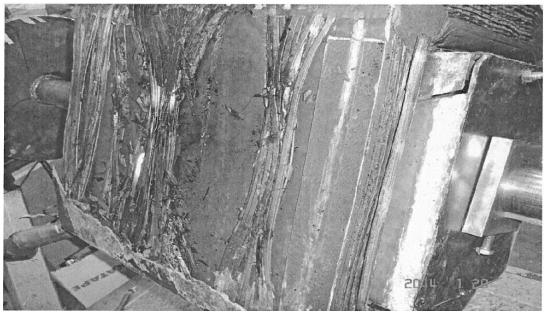

Fig. 1. Failed winding with inter-turn insulation severely damaged

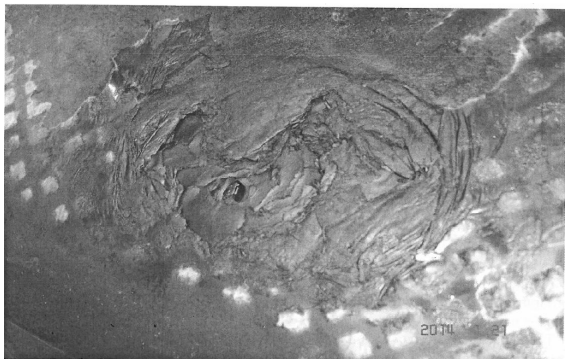

Fig. 2. Burn through the HV-LV barrier



Fig. 3. Burning of first layer of LV foil winding

A ratio known as the Resonance Voltage Ratio (R.V.R) was used which is defined as the voltage between points at the resonant frequency divided by the voltage between the same points when a 50 Hz voltage with the same amplitude is applied to the winding. The method used was to excite the winding with a variable frequency sinusoidal voltage and record the maximum amplitude between between two layers for a frequency range of 1 kHz to 2 MHz. The results are shown in Table I. From Table I at 660 kHz the amplification factor of 2.5 was recorded between the last and second last layer of the HV winding. This could result in a resonant overvoltage with sufficient magnitude to stress the inter-turn insulation when circuit breaker closing transients occur. From

TABLE I
PART WINDING RESONANCE OF THE WINDING

Point in Winding	Frequency	R.A.F
Start of winding (between 2 layers)	536 kHz	1.15
Middle of winding (between 2 layers)	1.17 MHz	0.67
End of winding (between 2 layers)	181 kHz	0.95
End of winding (between 2 layers)	660 kHz	2.5*
End of winding (between 2 layers)	1.32 MHz	0.67

Fig. 1, it is difficult to determine if the failure started as an inter-turn or inter-layer fault due to the extensive damage to the oil-paper insulation. However the failure mechanism had sufficient magnitude to cause substantial distortion of the first two layers and create a puncture through to the LV foil winding.

III. STACKED CORE TRANSFORMER PROTOTYPES

A. Split round winding prototype transformer

The stacked core transformer prototype with split round winding was installed with measuring taps at the ends of each layer as shown in Fig. 4.

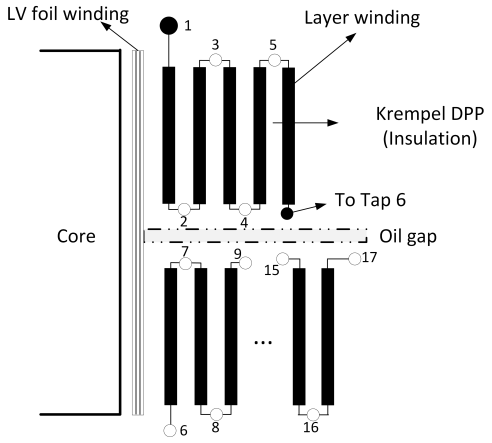

Fig. 4. Axisymetric view of first prototype transformer

The upper coil consisted of 5 layers whilst the bottom coil consisted of 11 layers separated by an oil gap. The constructed prototype is shown in Fig. 5.

B. Single round winding prototype transformer

A second prototype transformer was constructed with the same stacked core as in Fig. 5 but with a single round winding. Measuring taps were installed at the start and ends of each layer and also in between the layers as shown in Fig. 6. The second constructed prototype is shown in Fig. 7. Both stacked and wound core transformers had the same number of layers.

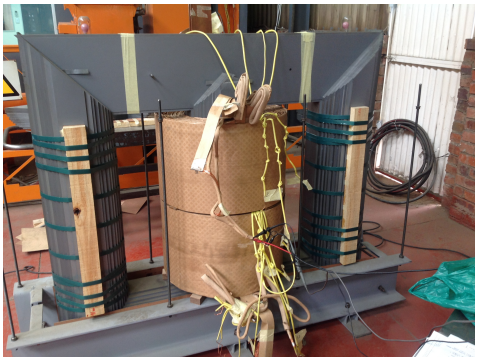

Fig. 5. Split round winding prototype transformer

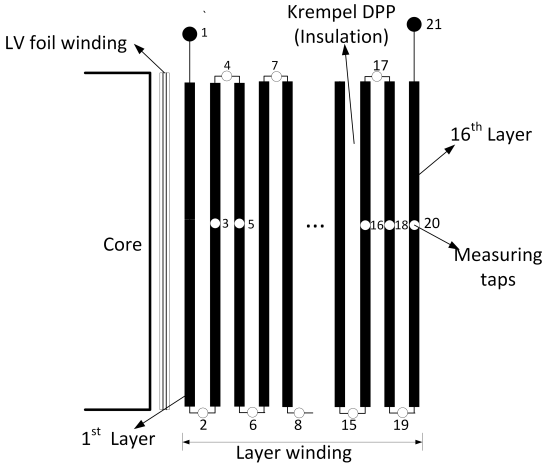

Fig. 6. Axisymetric view of second prototype transformer

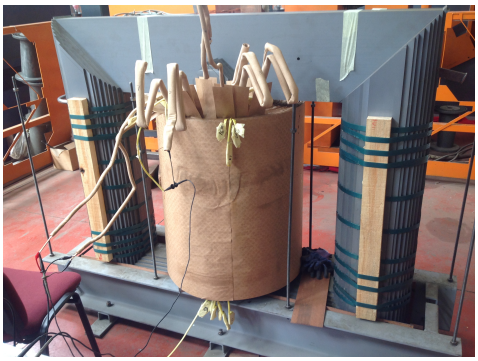

Fig. 7. Non-split round winding prototype transformer

IV. Analytical Model of the Transformer

The transformer windings can be represented by a group of interconnected and coupled transmission lines [16]. These coupled transmission lines can be described by (1) and (2).

$$\frac{d^2\mathbf{V}}{d\mathbf{x}^2} = -[Z][Y] \tag{1}$$

$$\frac{d^2\mathbf{I}}{d\mathbf{x}^2} = -[Z][Y] \tag{2}$$

where **V** and **I** are the voltage and current vectors respectively. **Z** and **Y** are the impedance and admittance matrices of the winding respectively. The solution of the above equation is well documented in [15] and [16]. The magnitude of the transfer function at turn k relative to the input can be calculated as [15]:

$$H_k = \frac{YY_{(k+1,1)}}{YY_{(1,1)}} \qquad k = 1, 2, \cdots, n-1 \tag{3}$$

where YY is the inverse of the matrix Y in [15] and H is a square matrix of order (n-1) x (n-1). Surge transference from HV to the LV winding will not be discussed in this paper.

V. Determination of the Transformer Parameters

The impedance (**Z = R + j** ω**L**) and admittance (**Y = G +** **j**ω**C**) matrix of the MTL equations were calculated as shown in (4) and (5) from [5] and [6].

$$Z = \left[j\omega\mathbf{L} + \left(\frac{1}{2\,(d_1 + d_2)} \right) \cdot \sqrt{\frac{\pi f \mu}{\sigma}} \right] \tag{4}$$

$$Y = (j\omega + \omega \tan\delta)\,\mathbf{C} \tag{5}$$

where μ and σ are the permeability and conductivity of the conductor. d_1 and d_2 are the diameters of the conductors. In (4) the real part takes into account the skin effect at high frequencies [6]. The real part of (5), represents the dissipation factor (tan δ) or dielectric losses [15], [16]. tanδ is frequency, moisture and temperature dependent and as such will influence the admittance matrix greatly at higher frequencies. The tanδ equation was obtained from the figures in [17] which describe the frequency dependent behaviour of the loss factor for oil impregnated cellulose paper.

A. Capacitance

Construction of the capacitance matrix **C** was as was done in [16] for $C_{i,i}$ and $C_{i,j}$. The formulas for calculating the capacitance were calculated from the basic formulas of cylindrical and plate capacitors in [18]. The procedure for the construction of the capacitance matrix is explained in [19]. A modified matrix reduction technique explained in [20] and [21], can be applied such that the group of turns will represent the total number of turns in each layer of the MV winding as shown in (6) and (7).

$$C_{ii\,node}^{layer} = \sum_{i=i_i}^{li} \sum_{j=i_i}^{li} C_{ij}^{turn} + \frac{1}{2} \sum_{i=i_i}^{li} C_{i,m}^{turn} + \frac{1}{2} \sum_{j=i_i}^{li} C_{m,j}^{turn} + \frac{1}{2} C_{m,m}^{turn} \tag{6}$$

$$C_{ij\ node}^{layer} = \sum_{i=i_i}^{li} \sum_{j=i_i}^{li} C_{ij}^{turn} + \frac{1}{2} \sum_{i=i_i}^{li} C_{i,m}^{turn} + \frac{1}{2} \sum_{j=i_i}^{li} C_{m,j}^{turn} \quad (7)$$

where $li = li + (w_k - 1)/2 - 1$, wk is the number of lumped turns in layer k, li is the first turn in layer i and m is the turn in the center of the layer. The same reduction method can be applied to a group of turns such that they represent the total number of turns in half a layer of the MV winding.

B. Inductance

The inductance matrix can be expressed as a sum of two component inductance matrices. The first component inductance matrix is obtained directly from the capacitance matrix C if the assumptions from [22] are made which are: (a) High frequency magnetic flux penetration into the iron laminations and transformer core is negligible (b) The magnetic flux will be constrained within the paths of the insulation. The first component inductance matrix can then be obtained using (8):

$$L_n = \frac{\epsilon_r}{v^2} \cdot \mathbf{C}^{-1} \quad (8)$$

where v is the velocity of light in vacuum and ϵ_r is the relative permittivity of the insulation (in this case equivalent permittivity of the air and paper combination). Adding the second component inductance matrix that takes into account the flux internal to the conductor [6] the total inductance is given by (9):

$$\mathbf{L} = L_n + \frac{\mathbf{R}}{f} \cdot E_n \quad (9)$$

where $\mathbf{R}$ is the real part of (4), E_n is a unit matrix of size nxn. The inductance matrix can also be calculated using the basic formulas for self and mutual inductances of the turns from Maxwell equations as shown in [15]. However as shown by the impedance characteristics in [15], both inductance calculation methods yield the same results.

VI. Measurements and Simulations

A. Test Equipment

The test equipment consisted of a Krohn-Hite Power Amplifier 7602 M series, 20 MHz Agilent 3320A waveform generator and Tektronix (DPO 3032) 300 MHz Oscilloscope. The signal generator connected to the amplifier energized the whole winding while the oscilloscope measured the voltages at the measuring taps as shown in Figs. 4 and 6. The RVR ratio was used to ascertain if resonance had occurred.

B. Comparison of Measured and Calculated Results: First prototype transformer

In Figs. 8, 9 and 10 it can be seen that there is a relatively good agreement between the calculated and measured results. The calculated results follow the profile of the measured results although there is a frequency shift between 1 kHz and 10 kHz for layer 15 and layer 16. After 500 kHz the resonance voltage ratio decreases almost approaching zero after 1 MHz.

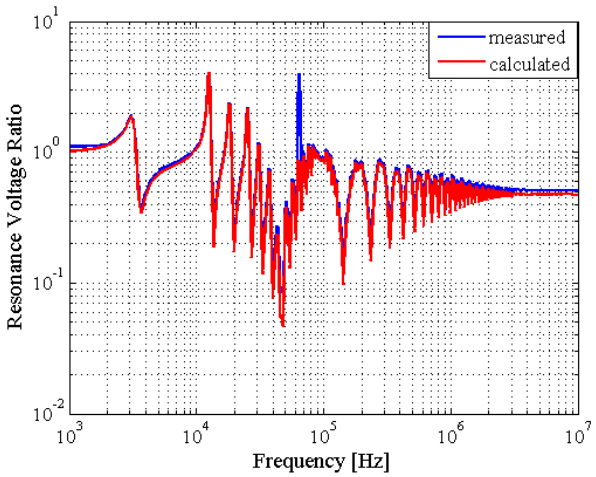

Fig. 8. Resonance voltage ratio across Layer 1 [measured (across tap 1 and tap 2 of Fig. 4) vs calculated]

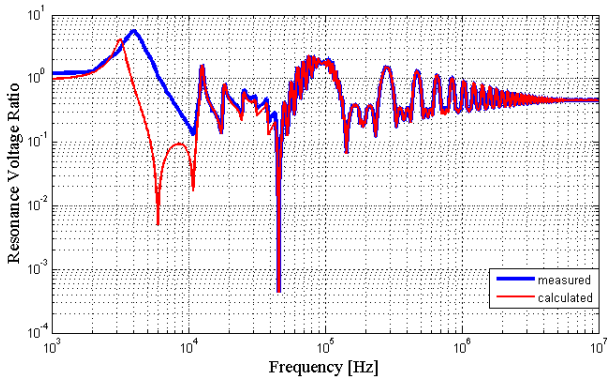

Fig. 9. Resonance voltage ratio across Layer 15 [measured (across tap 15 and tap 16 of Fig. 4) vs calculated]

C. Comparison of Measured and Calculated Results: Second prototype transformer

For the second prototype, comparison of the measured vs calculated results shown in Figs. 11, 12 and 13 reveal that between 1 kHz and 10 kHz the results do not agree. Although the calculated results relatively approximates the measured results for frequencies above 30 kHz the differences in the magnitude will be explained in the discussion section.

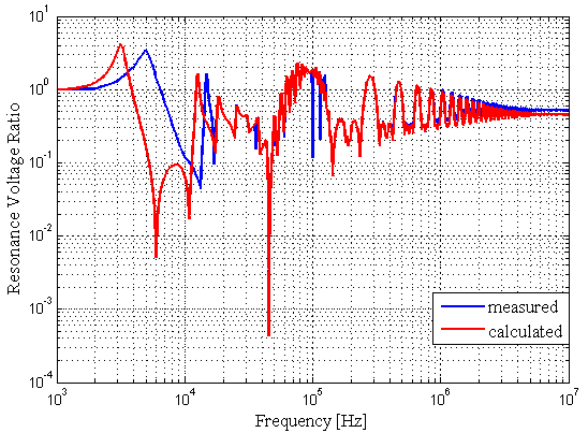

Fig. 10. Resonance voltage ratio across Layer 16 [measured (across tap 16 and tap 17 of Fig. 4) vs calculated]

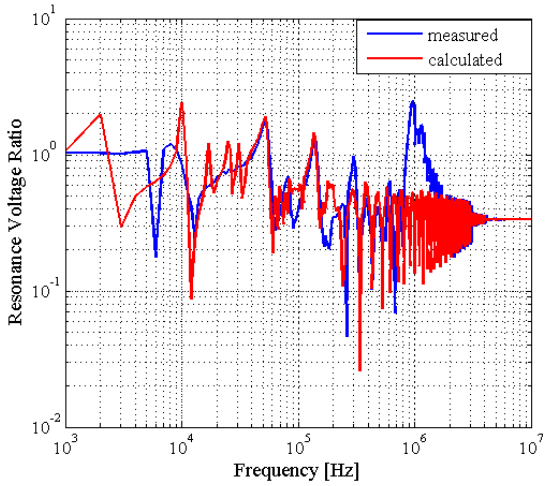

Fig. 11. Resonance voltage ratio across Layer 4 [measured (across tap 6 and tap 7 of Fig. 6) vs calculated]

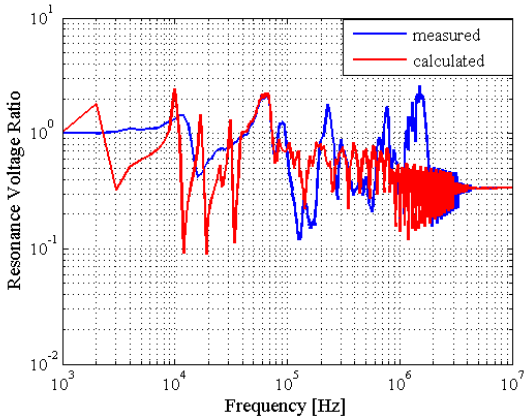

Fig. 12. Resonance voltage ratio across Layer 6 [measured (across tap 8 and tap 9 of Fig. 6) vs calculated]

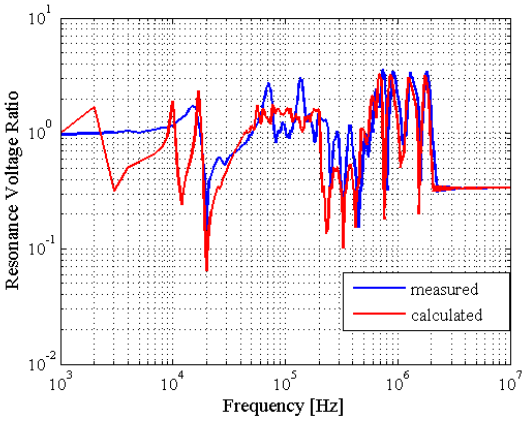

Fig. 13. Resonance voltage ratio across Layer 8 [measured (across tap 10 and tap 11 of Fig. 6) vs calculated]

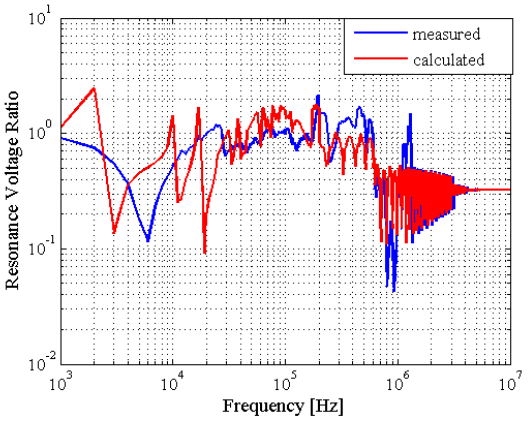

Fig. 14. Resonance voltage ratio across the start to middle of Layer 2 [measured (between tap 2 and tap 3 of Fig. 6) vs calculated]

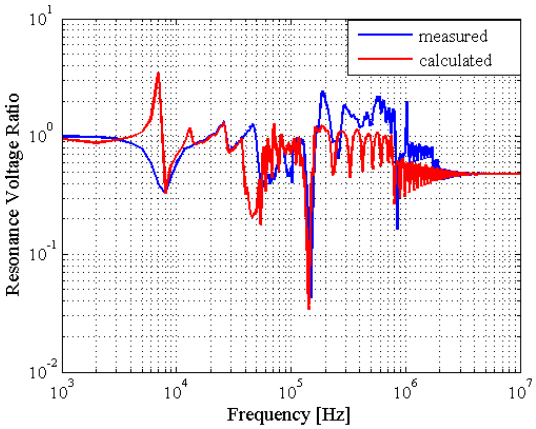

Fig. 15. Resonance voltage ratio across the start to middle of Layer 3 [measured (between tap 4 and tap 5 of Fig. 6) vs calculated]

Using the matrix reduction techniques discussed in section IV the calculated results can be scaled to represent resonance

voltage ratio from the start to the middle of the layer as shown by Figs. 14 and 15. Analysis of these figures reveal there is good agreement between measured and calculated results.

VII. DISCUSSION

The effect of different tan(δ) values on the MTL model can be shown in [23]. The approximated equation of ramp and step discussed in [17] will not necessarily take into account the detailed frequency dependency of transformer insulation needed for accurate modelling. It should be noted that the split winding has a higher magnitude of resonance from 1 kHz to 200 kHz whilst the single winding has higher magnitudes above 200 kHz. Hence depending on the magnitude of the frequencies of the incoming surge, an appropriate design can be chosen that has low resonance for a specific frequency range.

VIII. CONCLUSION

In this paper the frequency response of two layer type stacked transformers prototypes has been investigated. It has been shown that the MTL model can be used to quantify internal resonance phenomena in layer type windings using appropriate matrix reduction techniques. This analysis method may be crucial to transformer designers during the design stage of transformers which are exposed to frequent switching.

IX. ACKNOWLEDGEMENT

The authors gratefully acknowledge the contributions of all the engineers at the transformer factory for the design and manufacturing of the prototype transformers.

REFERENCES

[1] T. Craenenbroek, J. D. Ceuster, J. P. Marly, H. D. Herdt, B. Brouwers, and D. V. Dommelen. "Experimental and numerical analysis of fast transient phenomena in distribution transformers." *in IEEE Power Engineering Society Winter Meeting, Singapore*, vol. 3, no. 1, pp. 2193–2198, Jan. 2000.

[2] M. Popov and L. van der Sluis. "Improved calculations for no-load transformer switching surges." *in IEEE Transactions on Power Delivery*, vol. 16, no. 3, pp. 401–408, Jan. 2001.

[3] A. H. Soloot, H. K. Hidalen, and B. Gustavsen. "Modeling of Wind Turbine Transformers for the Analysis of Resonant Overvoltages." *in International Conference on Power Systems Transients IPST2013 in Vancouver, Canada*, pp. 1–7, Jul. 2013.

[4] M. Popov, L. V. der Sluis, G. C. Paap, and H. D. Herdt. "Computation of Very Fast Transient Overvoltages in Transformer Windings." *in IEEE Transactions on POWER DELIVERY*, vol. 18, no. 4, pp. 1268–1274, Oct. 2003.

[5] H. Sun, G. Liang, X. Zhang, and X. Cui. "Analysis of Resonance in Transformer Windings under Very Fast Transient Overvoltages." *in 17th International Zurich Symposium on Electromagnetic Compatibility*, vol. 22, no. 1, pp. 432–435, Jan. 2006.

[6] H. Sun, G. Liang, X. Zhang, and X. Cui. "Modelling of Transformer Windings under Very Fast Transient Overvoltages." *in IEEE Transactions on Electromagnetic Compatibility*, vol. 48, no. 4, pp. 621–627, Nov. 2006.

[7] D. Smugala, W. Piasecki, M. Ostrogorska, M. Florkowski, M. Fulczyk, and P. Kyls. "Distribution transformers protection against High Switching Transients." *Przeglad Elekrotechniczny (Electrical Review)*, pp. 296 – 300, Jan. 2012.

[8] CIGRE. "ELECTRICAL TRANSIENT INTERACTION BETWEEN TRANSFORMERS AND THE POWER SYSTEM." In *PART 1: EXPERTISE by CIGRE Joint Working Group A2/C4.39,Chapt. 4: Transfomer Modelling, CIGRE ISBN : 978-2-85873272-2*, pp. 33–56. Apr. 2014.

[9] R. Asano, A. C. O. Rocha, and G. M. Bastos. "Electrical transient interaction between transformers and the power system." *in CIGRE-33 CIGRE Brazil JWG A2/C4-03*, pp. 401–408, Jun. 2007.

[10] A. C. O. Rocha. "Electrical transient interaction between transformers and the power system." *in CIGRE C4-104, CIGRE Brazil JWG A2/C4-03, Paris, France*, pp. 1–7, Jun. 2008.

[11] A. Theocharis, M. Popov, R. Seibold, S. Voss, and M. Eiselt. "Analysis of Switching effects of Vacuum Circuit Breaker on $Dry-Type$ Foil winding transformers validated by experiments." *in IEEE Transactions on Power Delivery*, pp. 1–9, May 2014.

[12] A. H. Soloot, H. K. Hidalen, and B. Gustavsen. "Upon the Improvement of the Winding Design of Wind Turbine Transformers for Safer Performance within Resonance Overvoltages." *in proc. of CIGRE Joint Colloquium - SC A2/C4*, pp. 1–7, 2013.

[13] A. H. Soloot, H. K. Hidalen, and B. Gustavsen. "The effect of winding design on transformer frequency response with application on offshore wind farm energization." *in proc. Of Intl. Conference on Renewable Energy Research and Applications (ICRERA),*, pp. 1–7, Nov. 2012.

[14] A. H. Soloot, H. K. Hidalen, and B. Gustavsen. "Internal Resonant Overvoltage in Wind Turbine Transformers- Sensitivity Analysis of Measurement Techniques." *in International Conference on Electrical Machines and Systems, Busan, Korea*, pp. 1–7, Oct. 2013.

[15] M. Popov, L. V. der Sluis, R. P. P. Smeets, and J. L. Roldan. "Analysis of Very Fast Transients in $Layer-Type$ Transformer Windings." *in IEEE TRANSACTIONS ON POWER DELIVERY*, vol. 22, no. 1, pp. 238–247, Jan. 2007.

[16] M. Popov, L. V. der Sluis, and R. P. P. Smeets. "Evaluation of surge-transferred overvoltages in distribution transformers." *in Electric Power Systems Research 78 (ELSEVIER)*, vol. 78, no. 3, pp. 441–449, May 2007.

[17] S. M. H. Hosseini, M. Vakilian, and G. B. Gharehpetian. "Comparison of Transformer Detailed Models for Fast and Very Fast Transient Studies." *in IEEE TRANSACTIONS ON POWER DELIVERY*, vol. 23, no. 2, pp. 733–741, Apr. 2008.

[18] J. A. Martinez-Velasco. "Power System Transients." In *Parameter Determination, Chaptr 4: Transfomers, CRC Press Taylor and Francis Group, ISBN 978-1-4200-6529-9 (Hardback)*, pp. 177–255. 2010.

[19] Y. Shibuya, S. Fujita, and N. Hosokawa. "Analysis of very fast transient overvoltage in transformer winding." *in IEE Proc.-Gener. Transm. Distrib*, vol. 144, no. 5, pp. 461–468, 1997.

[20] F. de Leon and A. Semlyen. "Reduced order model for transformer transients." *in IEEE Transactions on Power Delivery*, vol. 7, no. 1, pp. 361–369, Jan. 1992.

[21] F. de Leon and A. Semlyen. "Efficient calculation of Elementary parameters of Transformer." *in IEEE Transactions on Power Delivery*, vol. 7, no. 1, pp. 376–383, Jan. 1992.

[22] J. Guardado and K. J. Cornick. "A Computer model for calculating Steep-Fronted Surge Distribution in Machine WIndings." *in IEEE TRANSACTIONS ON Energy Conversion*, vol. 4, no. 1, pp. 95–101, Mar. 1989.

[23] S. M. H. Hosseini, M. Vakilian, and G. B. Gharehpetian. "An Improved MTL Modeling of Transformer Winding." *in International Conference on Power Systems Transients*, pp. 1–5, Jun. 2007.

MEASUREMENT OF SWITCHING SURGES IN ONSHORE WINDFARMS AND RESONANCE VOLTAGES IN TRANSFORMER WINDINGS

C. A. Banda[1*] and J. M. Van Coller[1]
[1]School of Electrical & Information Engineering
University of the Witwatersrand, Johannesburg, Private Bag 3, Wits, 2050, South Africa
*Email: <cedric.banda@students.wits.ac.za >

Abstract: In this paper, measurement of switching surges during energization of a step-up transformer at an onshore wind farm is presented. Wind turbine transformers may be frequently switched into and out of the collector grid depending on the wind profile. Fast transients are generated during the opening or closing of the circuit breakers. The measured transients during energizing of the transformer showed a pre-strike behaviour with fast, repetitive, high du/dt values. FFT analysis was performed on the measured waveforms to understand the magnitude of the frequency components. As with internal resonance, if a frequency component of the incoming surge equals a resonant frequency of the transformer winding, internal winding resonance can occur. A prototype transformer was then manufactured with taps at the winding ends for part-winding resonance testing. A discussion of part winding resonance tests and possible implications of these fast transients on internal winding resonance is presented.

1 INTRODUCTION

Transformers operating in onshore wind farms are exposed to frequent switching through the action of circuit breakers. Most of these MV circuit breakers are Vacuum Circuit Breakers (VCB) [1]. In MV networks the switching of VCB [2],[3] can result in pre-strikes. These switching transients have high du/dt values which can pose a significant risk to the transformers due to the following [4]: i) Highly non-uniform initial voltage distribution ii) Internal resonant phenomena resulting in local amplification of the voltage. Over the years different study committees and working groups have been set up to explain transformer insulation failures. The statistics of transformer failures provided by IEEE in [5] indicate that of the 23% of the failures, the root cause could not be clearly identified [6]. The CIGRE A2-A3-B3.21 joint working group [7] refer to the numbers in [5] and suggest that failures can be categorized as 10% being design related and 17 % being to the contribution of very fast transients. Recently the CIGRE working group (A2/C4.39) of 2014 were tasked with investigating a number of transformer dielectric failures attributed to transient overvoltages, even when good practices for insulation design and insulation coordination had been applied. The findings were published in [8]. Of the several conclusions the following apply to this paper: (i) For certain network configuration e.g. (wind farms), there is a high probability that system-initiated transients may contain oscillatory voltage waveforms at the transformer's terminals which may coincide with the transformer winding's natural frequencies. These internal voltages can exceed the insulation withstand capability of the transformer by resonant voltage build-up. (ii) Repetitive transient overvoltages and ageing reduces the insulation withstand capability and must be recognized in the design of the transformer insulation system. This paper will investigate internal resonant voltage build-up in transformer windings. As such a definition of internal resonance with respect to transformers is necessary. It is defined as occurring when a frequency component of the incoming surge equal a resonant frequency of the transformer winding. The build-up of resonant over-voltages can result in flashovers from the windings to the core or in-between the turns [9]. However it should be noted that internal winding resonances will not necessarily result in immediate breakdown, but may result in partial discharges, which will further aid in insulation degradation and ultimately failure [2]. The measurement of switching transients will also be discussed and their contribution to internal resonance phenomena on a constructed prototype wind turbine step-up transformer.

2 EXPERIMENTAL METHODOLOGY

2.1 Measurement of switching transients

As mentioned earlier, internal resonance occurs when a frequency component of the incoming surge equals a resonant frequency of the transformer winding. Switching transient measurements were conducted at a wind turbine step up transformer. The tests involved the following:

1. Energizing the transformer during no-load.
2. Disconnecting the transformer during no-load.

Measurement of the three MV phase-to-earth voltages were made by use of a capacitive voltage divider on each phase. The MV bushing screen had a measured capacitance of 32 pF and an additional capacitance

of 10 nF was externally mounted in series with the bushing screen terminal and the transformer tank which provided local earth. The resulting voltage division ratio was 313. Figure 1 shows the measurement setup with the FLUKE 1750 connected to the bushing voltage dividers.

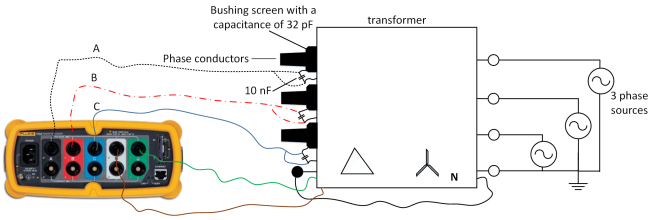

Figure 1: Measurement setup for recording transients

2.2 Measurement of resonance

In literature two methods are outlined for the determination of the frequency response of a transformer. The impedance versus frequency plot using frequency response analysis (FRA) equipment and the amplification factor versus frequency using the usual signal generator and oscilloscope. The amplification factor or gain function is defined generally for all cases as [10]:

$$N_{1m,j} = \frac{Voltage\ between\ point\ 1\ and\ m\ at\ frequency\ w_1}{Voltage\ applied\ at\ frequency\ w_i\ to\ node j} \quad (1)$$

Using FRA equipment Equation 1 can be further expanded to Equation 2 [11]:

$$N_{1m,j} = \frac{Z_{ij}\,(j\omega) - Z_{mj}\,(j\omega)}{Z_{jj}\,(j\omega)} \quad (2)$$

The resonance voltage ratio (RVR) can be derived from the generalized amplification factor in equation 1 to give equation 3.

$$RVR = \frac{Voltage\,between\,point\,1\,and\,m\,at\,frequency\,w_i}{Voltage\,between\,point\,1\,and\,m\,at\,50Hz} \quad (3)$$

In Equation 3 the RVR is now defined as the voltage between points at the resonant frequency divided by the voltage between the same points when a 50 Hz voltage with the same amplitude is applied to the winding.

2.2.1 Single round winding prototype transformer

A prototype wind turbine step-up transformer was constructed for the purpose of RVR measurements. The transformer was rated 2700 kVA, 690 V/ 33 kV. The MV side consisted of a delta-connected layer winding whilst the LV side consisted of star connected foil winding. Measuring taps were installed at the start and ends of each layer and also in between the layers as shown in Figure 2. The constructed prototype is shown in Figure 3.

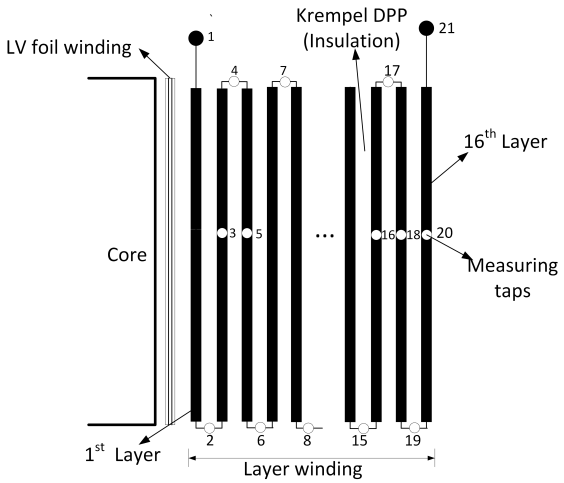

Figure 2: Axisymetric view of prototype transformer

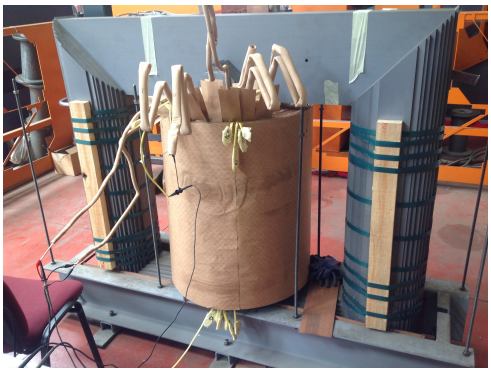

Figure 3: Prototype step-up wind turbine transformer

3 SWITCHING TRANSIENTS

3.1 Energizing the transformer during no-load

Energization of the transformer always results in at least one pre-strike per phase [12]. During contact closing, generation of high du/dt transients can occur at the transformer terminals [13]. This behaviour can be observed from the measured transients in Figures. 4, 5, 6, 7, 8 and 9. The measurement setup explained in Figure 1 was used and the tests were conducted on one wind turbine transformer at a particular wind farm. Analysis of the measured waveforms show that the pre-strikes are different for each switching event. However they all exhibit the basic characteristics i.e. they are repetitive in nature and have high dU/dt values. Energizing a transformer onto a high capacitance collector cable network in this case a wind farm presents voltage transient problems. As the cable connections are short, the speed of the transformer input capacitance charging from the network capacitance is limited in practise only by the cable resistance and the value of the phase to ground capacitance of the transformer. This type of low surge impedance connection has a low du/dt limiting effectiveness [13]. Hence the high dU/dt values and

the high frequency transients observed in Figures. 4, 5, 6, 7, 8 and 9.

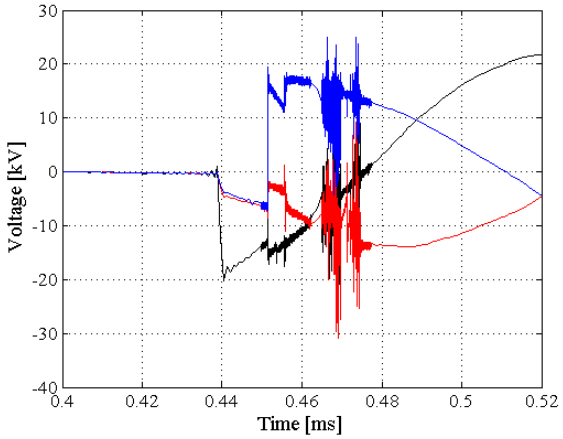

Figure 4: Measured pre-strike behaviour at 12:45

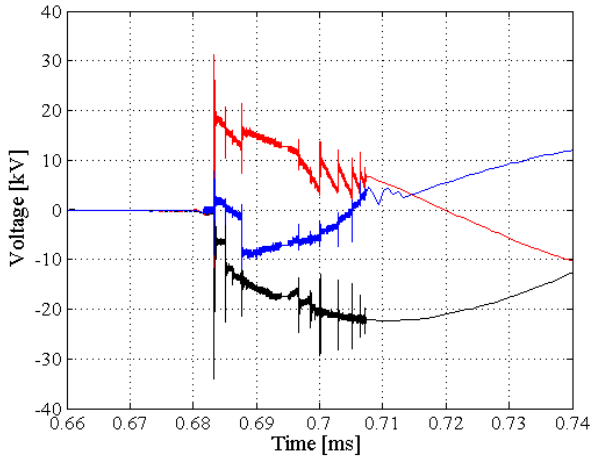

Figure 5: Measured pre-strike behaviour at 13:13

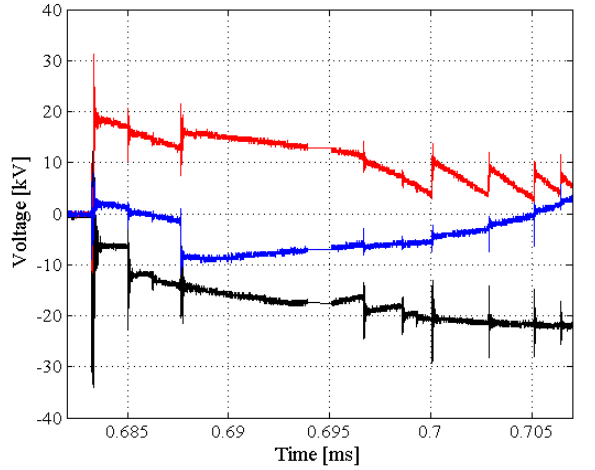

Figure 6: Time expansion of measured pre-strike behaviour at 13:13

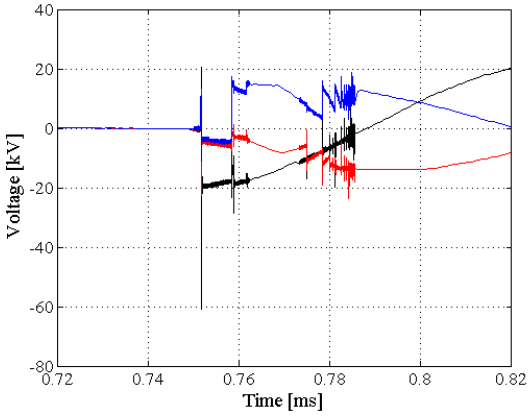

Figure 7: Measured pre-strike behaviour at 13:15

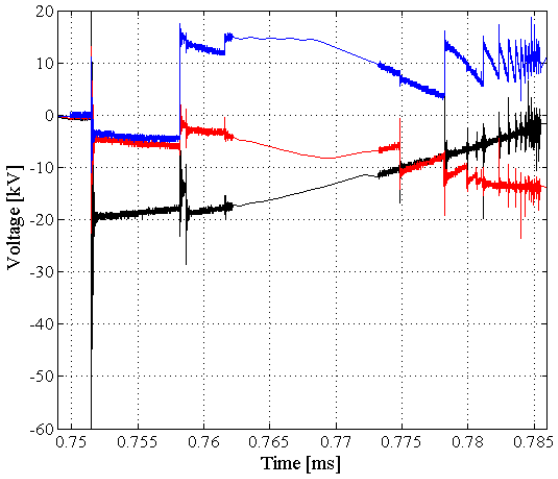

Figure 8: Time expansion of measured pre-strike behaviour at 13:15

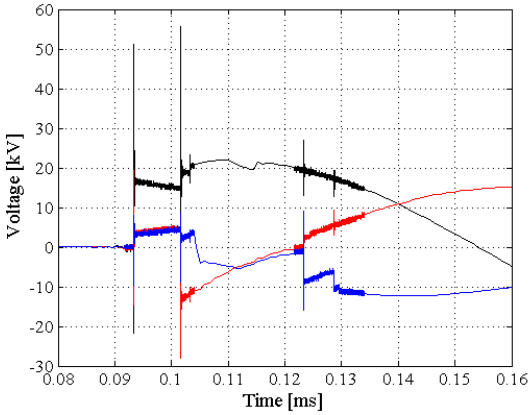

Figure 9: Measured pre-strike behaviour at 13:26

3.2 De-energizing the transformer during no-load

On disconnection by the VCB higher over-voltages can occur if the arc re-ignites after the first current interruption [14]. If the VCB is not able to quench the arc, multiple re-ignitions can occur and with

each re-ignition, the voltage escalates resulting in higher over-voltages. No significant over-voltages were measured on de-energizing of the transformer.

3.3 Frequency domain analysis

Analyzing the measured transients in the frequency domain can give a better perspective than time domain analysis. Hence FFT analysis was performed on the measured transients. In [15] the frequency content of the recorded transient was analyzed using the FFT. Analysis of the results yielded the amplitude of the different frequency components. The amplitude spectra for the measured transients are shown in Figures 10, 11, 12 and 13. It should be noted that in the frequency domain, a steep front transient is identified by its higher frequency components [8]. The frequency domain results in Figures 10, 11, 12 and 13 show higher frequency components which would represent the steep, repetitive transients in the time domain.

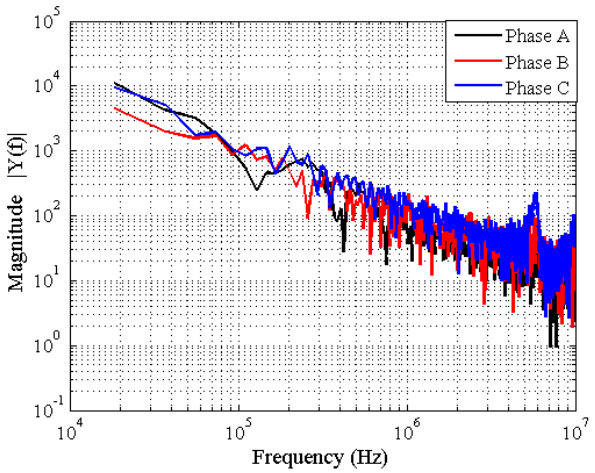

Figure 10: FFT analysis for the measured transient at 12:45

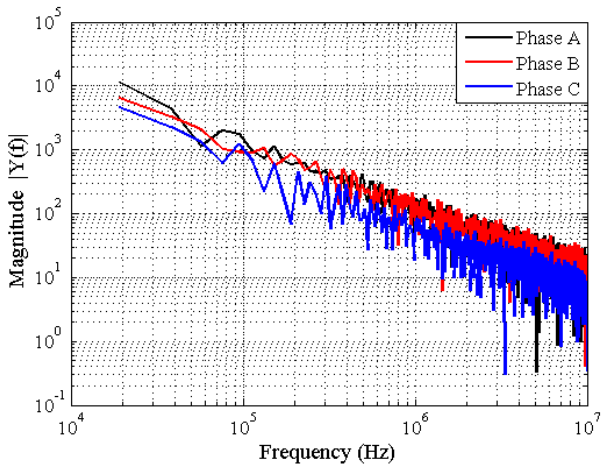

Figure 11: FFT analysis for the measured transient at 13:13

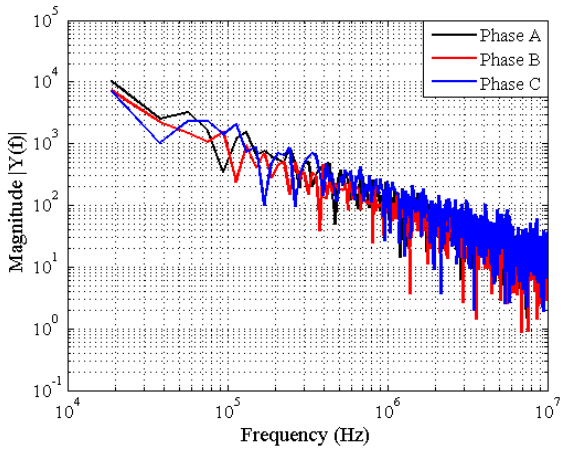

Figure 12: FFT analysis for the measured transient at 13:15

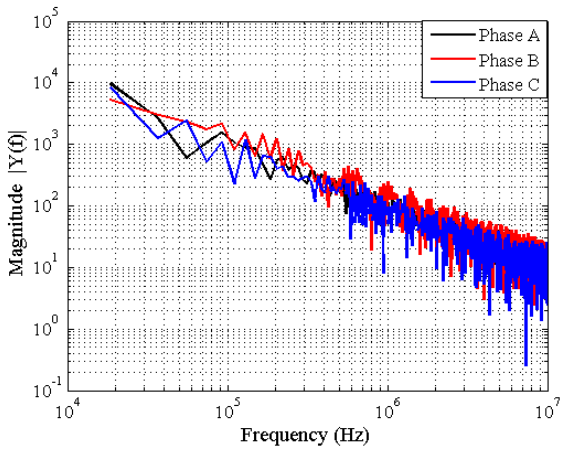

Figure 13: FFT analysis for the measured transient at 13:26

4 RESONANCE ANALYSIS AND MEASUREMENTS

4.1 Test Equipment

The test equipment consisted of a Krohn-Hite Power Amplifier 7602 M series, 20 MHz Agilent 3320A waveform generator and Tektronix (DPO 3032) 300 MHz Oscilloscope. The signal generator connected to the amplifier energized the whole winding while the oscilloscope measured the voltages at the measuring taps as shown in Figure 2.

4.2 Measured results

For obtaining the frequency response of each layer, Equation 3 was used. As previously mentioned internal winding resonance occurs when a frequency component of the incoming surge equal a resonant frequency causing resonant voltage build up which can exceed the insulation withstand capability. The frequency response of each layer was measured and the results are shown in Figures 14, 15, 16 and 17.

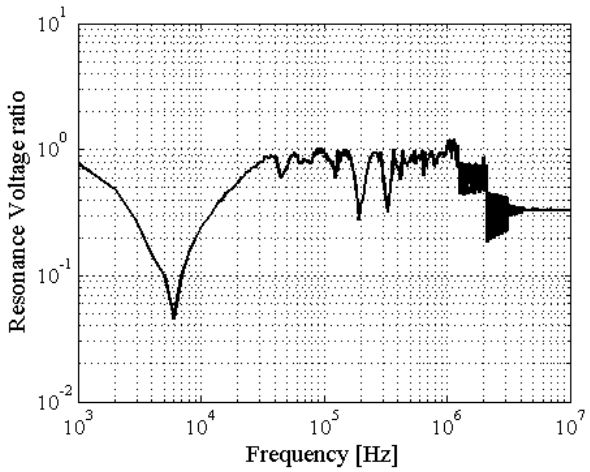

Figure 14: Resonance amplification factor across Layer 1 [measured (across tap 1 and tap 2 of Figure 2)

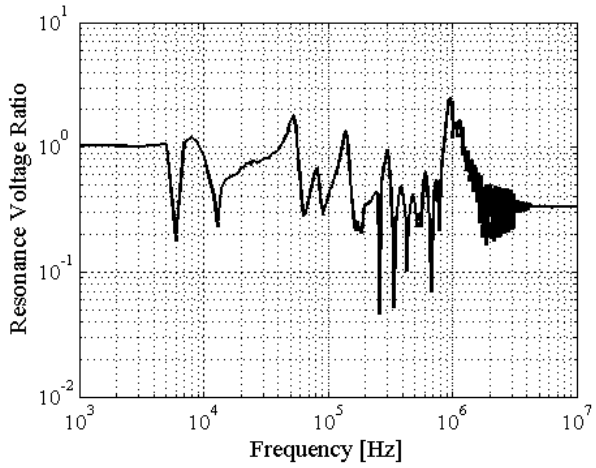

Figure 15: Resonance amplification factor across Layer 4 [measured (across tap 6 and tap 7 of Figure 2)

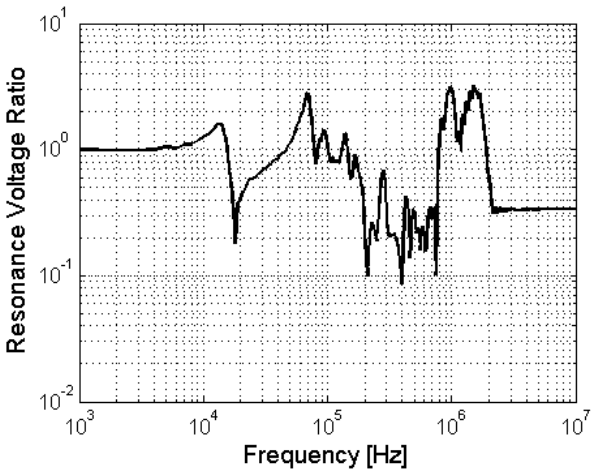

Figure 16: Resonance amplification factor across Layer 7 [measured (across tap 9 and tap 10 of Figure 2)

Analysis of the measured frequency response of each layer revealed that the RVR increases as measurements

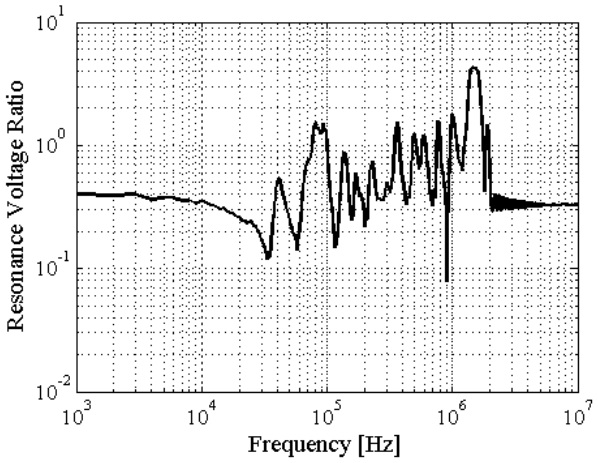

Figure 17: Resonance amplification factor across Layer 15 [measured (across tap 17 and tap 19 of Figure 2)

are made towards the end of the MV winding. Above 1 MHz the higher frequency components have high RVR with amplification gain of above 2. At low frequencies i.e. 1kHz to 100 kHz the amplification is not as severe as at higher frequencies. Comparison of the magnitude of the switching transients in Figures 10, 11, 12 and 13 and the frequency responses of the layer winding reveal that only frequencies from 10 kHz to 100 kHz should be of concern. The magnitude of the frequency components components in this range could excite one of the resonant frequencies of the winding causing local amplification of the voltage which may be above the insulation withstand capability.

5 DISCUSSION

In [16] and [17] research was conducted on the performance of oil impregnated cellulose paper when subjected to transients with different repetition frequency, rise time and magnitude. It was found that the faster the rise time, the more damage to the insulation. In [17] it was found that if the incoming transient has higher frequency components, accelerated ageing of the cellulose paper could result. Also the life time of the insulation paper decreased with the an increase of repetition frequency of the applied transient for a frequency range of 1 kHz to 10 kHz. These findings apply to the insulation system of wind turbine step-up transformers which are frequently exposed to transients with high frequency components as shown in Figures 10, 11, 12 and 13. However more research still needs to be done for repetitive transient overvoltages with frequency components above 10 kHz.

6 CONCLUSION

It is concluded that repetitive pre-strike voltage waveforms with high du/dt values can lead to stressing of the end-turn insulation of the transformer as well as causing damaging resonant over-voltages within the

winding. Hence as discussed in the paper the effect of repetitive transient overvoltages which reduce the insulation withstand capability must be recognized in the design of the transformer insulation system.

ACKNOWLEDGMENTS

This work was funded by Eskom through the Eskom Power Plant Engineering Institute (EPPEI) program. The authors gratefully acknowledge the contributions of all the engineers at the transformer factory for the design and manufacturing of the prototype transformer.

REFERENCES

[1] D. Smugala, W. Piasecki, M. Ostrogorska, M. Florkowski, M. Fulczyk, and O. Granhaug, "New approach to protecting transformers against high frequency transients wind turbine case study," *in PRZEGLAD ELEKTROTECHNICZNY, ISSN 0033-2097, R. 89*, no. 10, pp. 186–190, Apr. 2013.

[2] T. Craenenbroek, J. D. Ceuster, J. P. Marly, H. D. Herdt, B. Brouwers, and D. V. Dommelen, "Experimental and numerical analysis of fast transient phenomena in distribution transformers," *in IEEE Power Engineering Society Winter Meeting, Singapore*, vol. 3, no. 1, pp. 2193–2198, Jan. 2000.

[3] M. Popov and L. van der Sluis, "Improved calculations for no-load transformer switching surges," *in IEEE Transactions on Power Delivery*, vol. 16, no. 3, pp. 401–408, Jan. 2001.

[4] W. Piasecki, M. Ostrogorska, M. Florkowski, M. Fulczyk, and P. Klys, "du/dt protection for distribution transformers," *in International Conference on Power System Transients (IPST), Kyoto, Japan*, pp. 1–5, Jun. 2009.

[5] IEEE, "Guide for reporting failure data for power transformers and shunt reactors on electric utility power systems," *ANSI/IEEE C57.117*, pp. 1–29, Feb. 1986.

[6] W. Piasecki, G. Bywalec, M. Florkowski, M. Fulczyk, and J. Furgal, "New approach towards very fast transients suppression," *in International Conference on Power System Transients (IPST), Lyon, France*, pp. 1–6, Jun. 2007.

[7] CIGRE, "Working group a2-a3-b3.21, electrical environment of transformers: Impact of fast transients," *ELECTRA 208*, Feb. 2005.

[8] $CIGRE$, "Electrical transient interaction between transformers and the power system," in *PART 1: EXPERTISE by CIGRE Joint Working Group A2/C4.39,Chapt. 6 to 7 CIGRE ISBN : 978-2-85873272-2*, Apr. 2014, pp. 81 –104.

[9] M. Popov, L. V. der Sluis, G. C. Paap, and H. D. Herdt, "Computation of very fast transient overvoltages in transformer windings," *in IEEE Transactions on POWER DELIVERY*, vol. 18, no. 4, pp. 1268–1274, Oct. 2003.

[10] IEEE, "Guide to describe the occurrence and mitigation of switching transients induced by transformers, switching device, and system interaction," *IEEE Std C57.142*, pp. 8–58, Dec. 2010.

[11] R. C. Degeneff, "A general method for determining resonances in transformer windings," *in IEEE Transactions on Power Apparatus and Systems*, vol. PAS-96, no. 2, pp. 423–430, Mar. 1977.

[12] L. Liljestrand, E. Lindell, D. Bormann, C. Ray, and E. Dullni, "Vacuum circuit breaker and transformer interaction in a cable system," *CIRED 22nd International Conference on Electricity Distribution Stockholm*, no. 0412, pp. 1–4, Jun. 2013.

[13] D. Smugala, W. Piasecki, M. Ostrogorska, M. Florkowski, M. Fulczyk, and P. Kyls, "Distribution transformers protection against high switching transients," *Przeglad Elekrotechniczny (Electrical Review)*, pp. 296 – 300, Jan. 2012.

[14] A. Mueller and D. Saemann, "Switching phenomena in medium voltage systems - good engineering practise on the application of vacuum circuit breakers and contractors," pp. 1–9, Mar. 2011.

[15] R. Malewski, J. Douville, and L. Lavallee, "Measurement of switching transients in 735-kv substations and assessment of their severity for transformer insulation," *in IEEE Transactions on Power Delivery*, vol. 3, no. 4, pp. 1380 – 1390, Oct. 1988.

[16] T. L. Koltunowicz, R. Kochetov, G. Bajracharya, D. Djairam, and J. J. Smit, "Repetitive transient aging, the influence of rise time," *in Electrical Insulation Conference, Annapolis, Maryland*, pp. 151–155, May 2011.

[17] R. Kochetov, T. L. Koltunowicz, G. Barjracharya, D. Djairam, and J. J. Smit, "Repetitive transient aging, the influence of repetition frequency," *Electrical Insulation Conference, Annapolis, Maryland*, pp. 444–448, May 2011.

21, rue d'Artois, F-75008 PARIS
http : //www.cigre.org

44

SOUTH AFRICA 2015

RESONANCE OVERVOLTAGES IN SINGLE AND SPLIT WINDING WIND TURBINE STEP-UP TRANSFORMERS

Cedric A. Banda [(1)]*, John M. Van Coller [(1)], Jorge del Pozo [(2)], Lee T. Mbenge [(2)]
[(1)]University of Witwatersrand, Johannesburg, South Africa
[(2)]Actom Distribution Transformers, Boksburg, South Africa

SUMMARY

Over the years a number of transformer insulation failures have been attributed to transient overvoltages even when good practices of insulation design and insulation coordination had been followed. This report adds to recent research done by CIGRE JWG A2/C4.39 (2014) by presenting an investigation into resonant overvoltages within wind turbine step-up transformers which are frequently exposed to transient overvoltages. The switching transients which were measured at the transformer terminals showed high du/dt values, were repetitive and oscillatory in nature and differed with each switching event. As has been the norm, the manufacturing industry and transformer purchasers have assumed that the problems associated with transient phenomena are covered by existing voltage impulse test standards. However this is not always the case and to help with assessment, the Frequency Domain Severity Factor (FDSF) will be used in this paper as a design review analysis technique of expected transients. The FDSF was implemented by taking the ratio of the energy spectral density of the transient event with respect to the energy spectral density of standard voltage impulse test waveforms. The obtained results were greater than unity for most of the frequency range signifying that additional measures would have to be considered for protection against the transient overvoltages. Two prototype wind turbine step-up transformers were constructed for the purpose of resonant voltage ratio measurements. The transformers were rated 2.7 MVA, 0.690 kV / 33 kV with the MV side consisting of a delta connected layer winding and the LV side consisting of a star connected foil winding. Both transformers used a stacked core but differed in the winding arrangement. One transformer used a split-winding on the MV side and the other used a non-split winding on the MV side. The results of the sweep frequency response showed that the transformer with the split MV winding has a high resonant amplification factor for frequencies below 100 kHz whereas the transformer with the non-split MV winding has a high resonant amplification factor for frequencies above 200 kHz.

KEYWORDS

Switching, Overvoltages, Transformers, Winding, Resonances, Wind Turbines, Pre-strikes.

cedric.banda@students.wits.ac.za

1. INTRODUCTION

Transformers operating in onshore wind farms are exposed to frequent switching through the action of circuit breakers. Most of these MV circuit breakers are Vacuum Circuit Breakers (VCBs) [1]. The VCB pre-strikes during closing result in transient voltages being applied to the transformer winding [2], [3]. These switching transients have high du/dt values which can pose a significant risk to the transformers due to the following [4]: (i) Highly non-uniform initial transient voltage distribution within winding (ii) Internal resonant phenomena within winding resulting in local amplification of the transient voltage.

Different CIGRE working groups have been setup over the years to understand transformer interaction with the power system [5]. These include the CIGRE WG 12-07 "Resonance Behaviour in HV Transformers" – 1979, CIGRE JWG 33/13,9 "Very fast transient phenomena associated with gas insulated substations" – 1988, CIGRE JWG A2-A3-B3.21 "Electrical environment of transformers – Impact of fast transients" – 2005, CIGRE-Brazil JWG A2/C4.03 "Interaction between transformers and the electrical system with focus on high frequency electromagnetic transients" – 2011, and recently CIGRE WG A2/C4.39 "Electrical Transient Interaction between Transformers and the Power System" – 2014. Of the findings of the different study groups, the findings of CIGRE WG A2/C4.39 apply to this paper.

The working group of 2014 was tasked with investigating a number of transformer dielectric failures attributed to transient overvoltages, even when good practices for insulation design and insulation coordination had been applied. The findings were published in [6]. Of the several conclusions the following apply to this paper:

- For certain network configuration e.g. (wind farms), there is a high probability that system-initiated transients may contain oscillatory voltage waveforms at the transformer's terminals which may coincide with the transformer winding's natural frequencies. These internal voltages can exceed the insulation withstand capability of the transformer by resonant voltage build-up.
- Repetitive transient overvoltage ageing reduces the insulation withstand capability and must be recognized in the design of the transformer insulation.

In this report, measurements of repetitive transient overvoltages will be presented. An analysis of whether the switching surges generated during energizing of the transformer are covered by the standard voltage impulse test waveforms will be done using the Frequency Domain Severity Factor (FDSF). In the literature, the energization of wind turbine transformers in offshore wind farms has been known to cause oscillatory waveforms on the transformer terminals due to reflections from the end of the line and/or from any point of discontinuity [7]. These reflections will result in a disturbed and mostly oscillating waveform with different frequency components. If some frequency components in the transient match the resonant frequencies of a wind turbine transformer winding, it might result in high overvoltages within the winding, presenting a potential risk [7]. This report will also look at the transients generated during switching at an onshore wind farm and what impact these oscillatory waveforms have on the transformer. It should be noted that internal winding resonance occurs when a frequency component of the incoming surge equals a resonant frequency of the transformer winding. The build-up of resonant over-voltages can result in breakdown from the windings to the core or between the turns [8]. However internal winding resonances will not necessarily result in immediate breakdown, but may result in partial discharges, which will further aid in insulation degradation and ultimately failure [2].

2. MEASUREMENT OF SWITCHING TRANSIENTS

Measurement of switching transients at the transformer MV terminals was conducted at a wind turbine step-up transformer. The tests involved the following:

1. Energizing the transformer during no-load (a common condition).
2. Disconnecting the transformer during no-load (another common condition).

Measurement of the three MV phase-to-earth voltages was done using a capacitive voltage divider on each phase. The MV bushing screen had a measured capacitance of 32 pF and an additional capacitance of 10 nF was externally mounted between the bushing screen terminal and the transformer tank which provided local earth. The resulting voltage division ratio was 313. Measurements were made on the MV side because the MV VCB was constantly switched. The aim of the tests was to investigate the phenomena associated with switching transients i.e. pre-strikes (on energizing) and re-strikes and re-ignitions on de-energizing. Figure 1 shows the measurement setup with a FLUKE 1750 connected to the MV bushing voltage dividers.

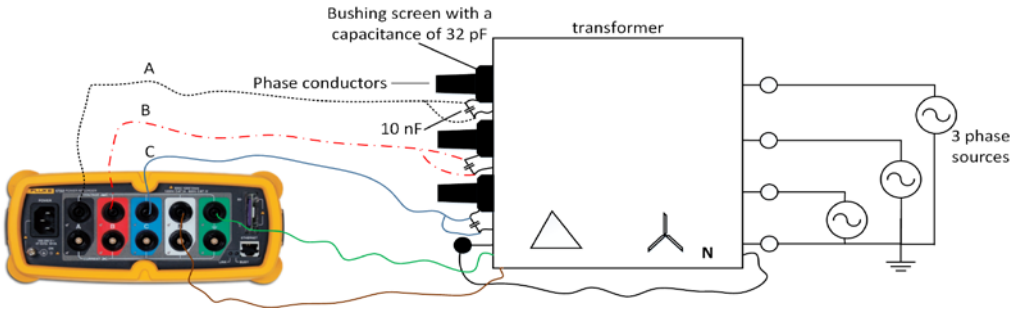

Figure 1: Measurement setup on a wind turbine step-up transformer.

2.1 Energizing the Transformer

The process of closing the contacts of a circuit breaker causes pre-strikes as each pole closes [9]. The pre-strike behaviour can be observed from the measured transients in Figures. 2, 3, and 4.

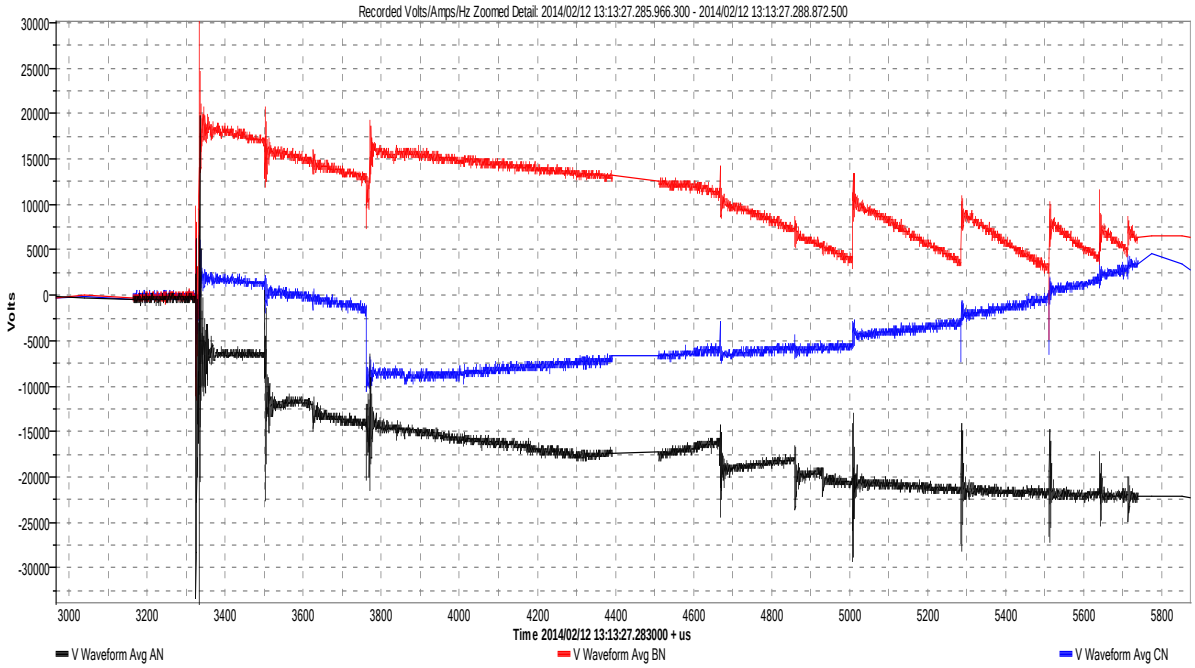

Figure 2: Measured waveform on energizing the step-up transformer from the MV side.

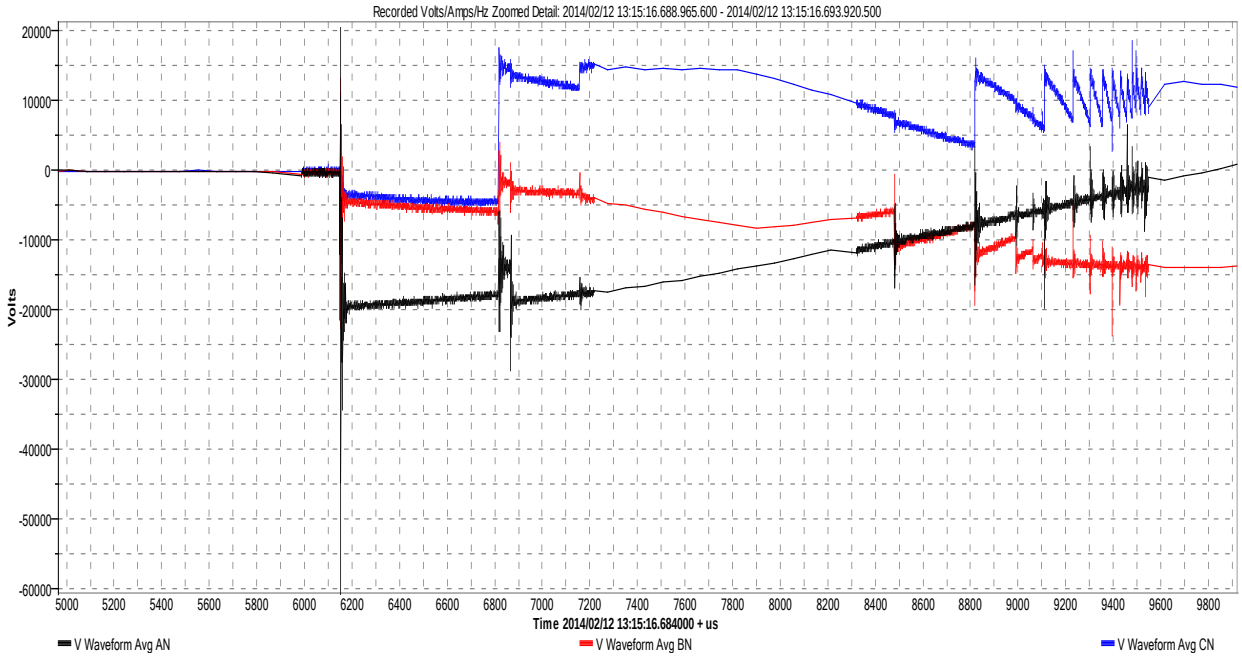

Figure 3: Measured waveform on energizing the step-up transformer from the MV side.

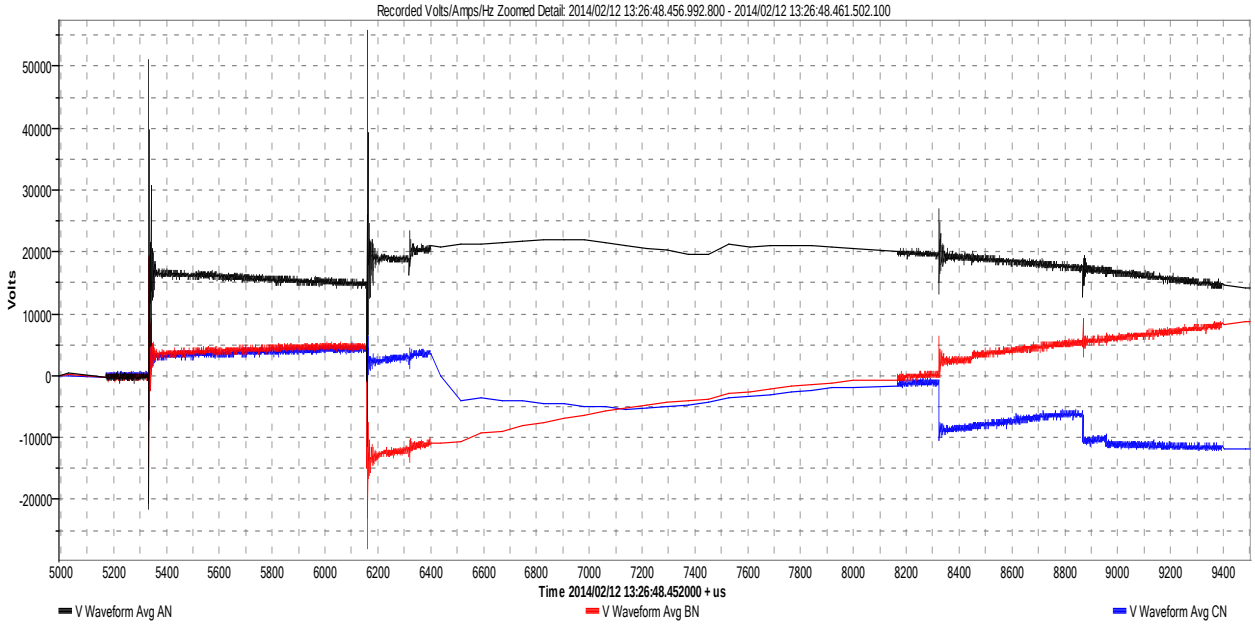

Figure 4: Measured waveform on energizing the step-up transformer from the MV side.

Energizing a transformer onto a high capacitance collector cable network in this case a wind farm presents voltage transient problems. As the cable connections are short, the speed of the transformer input capacitance charging from the network capacitance is limited in practise only by the cable resistance and the value of the phase to ground capacitance of the transformer. This type of low surge impedance connection has a low du/dt limiting effectiveness [1]. Hence the high du/dt values and high frequency transients in Figures 2, 3 and 4. No significant over-voltages were measured on de-energizing of the transformer.

2.2 Implementation and analysis of Frequency Domain Severity Factor

Reference [10] defined a severity factor as a parameter that can be used in the assessment of the severity of an incoming transient overvoltage. It has the form of a safety margin that can

be used during the transformer design stage with regards to the standard acceptance tests either in the frequency domain or in the time domain. The wind turbine step-up transformers are tested with a 170 kV standard lightning impulse voltage according to SANS 60076-3 [11]. Additional test waveforms can be made such as the 200 kV lightning impulse voltage, the 187 kV lightning impulse voltage waveform chopped at 2µs, 3µs, 4µs, 5µs and 6µs according to SANS 60076-16 [12]. These test waves will also be considered in this report. However according SANS 60076-3 no switching wave tests should be done for MV distribution transformers rated at 36 kV hence it will not be considered in the analysis [11]. The chopped wave test is considered the most important since it has a higher peak value and contains higher frequency components [6]. To compute the FDSF, knowledge of the amplitude of the frequency components of the incoming surge and the standard test waveforms is needed. This was done by computing the FFT and the Energy Spectral Density (ESD) of the waveforms as shown in Equation 1 [10].

$$FDSF(\omega) = \frac{ESD_{SW}(\omega)}{ESD_{ENV}(\omega)} \tag{1}$$

where ω is the angular frequency, $ESD_{SW}(\omega)$ is the maximum energy spectral density of the actual transient as measured at the transformer terminals, and $ESD_{ENV}(\omega)$ is the energy spectral density for the dielectric tests in the standards as measured at the transformer terminals. To ensure that the actual measured switching transients are covered by the standard impulse waveforms, the FDSF(ω) should be less than unity [10].

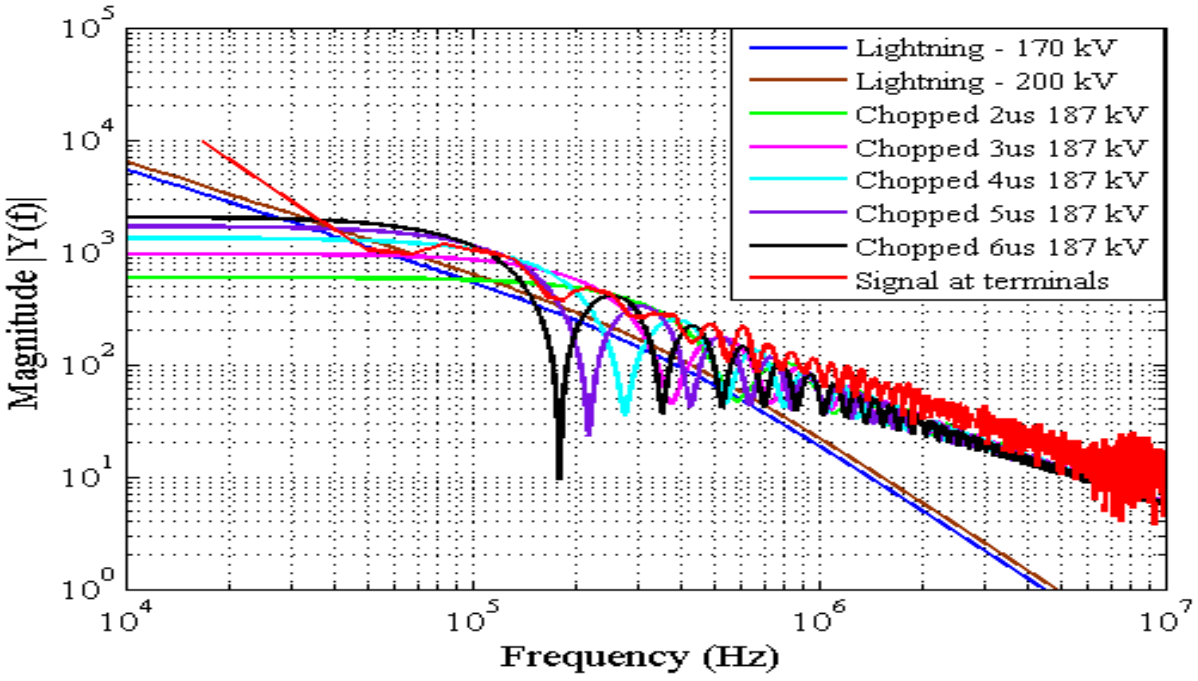

Figure 5: Magnitude spectrum for transient waveform in Figure 4 and standard waveforms.

Figure 5 shows the FFT of the standard waveforms and the FFT of the actual measured transient in Figure 4. By analysing the results in Figure 5 it is possible to have a severity factor that takes the envelope of all standard waveforms to compare with the FFT of the transient measured at the transformer terminals as explained by Equation 1. The results of the FDSF plots calculated using Equation 1 for the transients in Figures 2, 3, 4 are shown in Figures 6, 7 and 8.

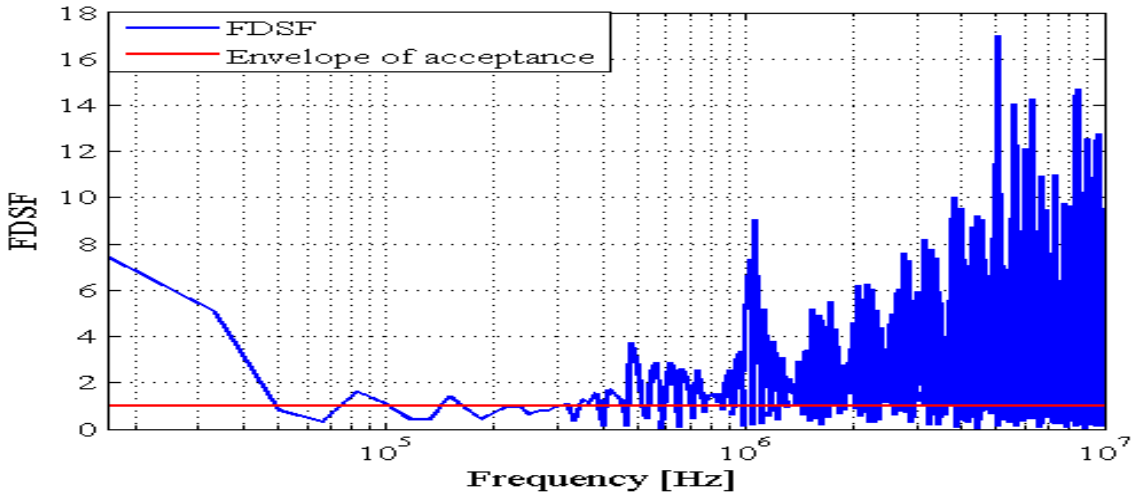

Figure 6: FDSF for the measured transient in Figure 2

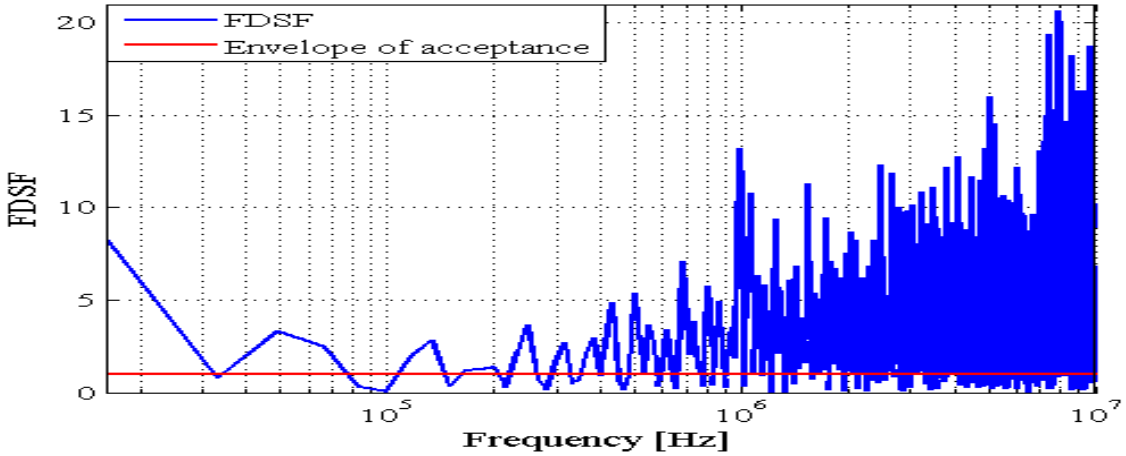

Figure 7: FDSF for the measured transient in Figure 3

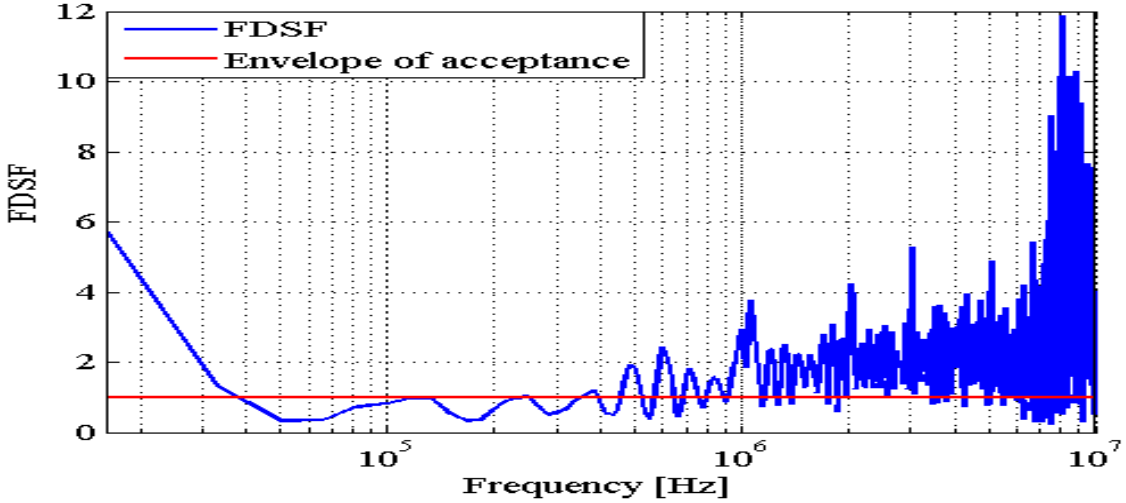

Figure 8: FDSF for the measured transient in Figure 4

The results of the FDSF for the three different switching events show that the majority of the values are above unity for most of the spectrum symbolising a potential risk. Hence internal winding resonance could occur when any of the frequency components match a resonant frequency of the transformer winding. The FDSF results also reveal that the transients

generated during switching of wind turbine transformers are not well represented by any of the standard transient voltage waveform tests. Also it is worth mentioning that the FDSF analysis has several limitations including that it does not take into account damping effects and hence might over-estimate the over-voltages produced at resonance especially for transients with frequency components above 1 MHz as shown in Figures 6, 7 and 8. However in light of the FDSF results that were obtained and how severe they are, the transformer manufacturer gains knowledge of the spectral fingerprint during switching transients and proper protection or safety factors can be selected. Two wind turbine step-up transformer designs will now be investigated.

3. RESONANCE PERFORMANCE OF SPLIT AND NON-SPLIT MV WINDING

Two prototype wind turbine step-up transformers were constructed for the purpose of checking part-winding resonance. As previously mentioned, both transformers had the same rating but differed in the winding arrangement. One prototype transformer had a split round winding shown in Figure 9a with two MV coils made up of 16 layers each and separated by an oil gap. The other had a non-split round windings as shown in Figure 9b. Both transformers were installed with measuring taps at the ends of each layer or in between the layers.

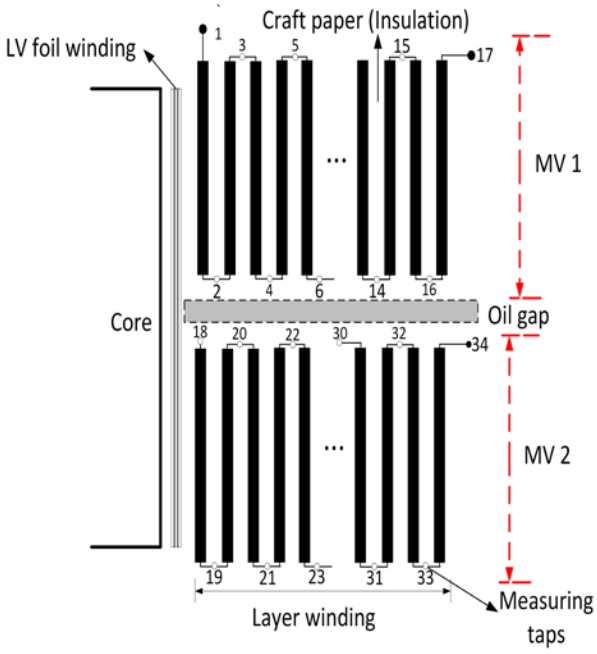

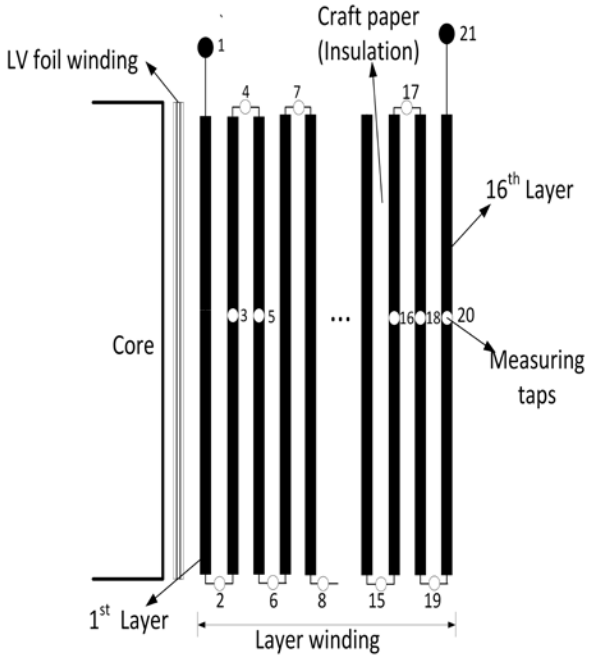

Figure 9a: Split MV winding transformer **Figure 9b: Non-split MV winding transformer**

The constructed prototypes are shown in Figures 10a and Figure 10b. The test equipment consisted of a Krohn-Hite Power Amplifier 7602 M series, 20 MHz Agilent 3320A waveform generator and Tektronix (DPO 3032) 300 MHz Oscilloscope. The signal generator was connected to the input of the amplifier and the output of the amplifier energized the whole winding. The oscilloscope measured the tap voltages.

3.1 Measured results

The measured results for certain layers with high potential risk for breakdown are discussed by analysing the results of the sweep frequency response measurements. The measured results for Layer 1 (measuring between taps 1 and 2) for both designs, Layer 15: (measuring between



Figure 10a: Split MV winding transformer



Figure 10b: Non-split MV winding transformer

taps 32 and 33 of Figure 9a) for the split MV winding transformer and (measuring between taps 17 and 19 of Figure 9b) for the transformer with the non-split MV winding. For Layer 16 (measuring between taps 33 and 34 of Figure 9a) and (measuring taps 19 and 21 of Figure 9b). The results of the measurements are shown in Figures 11, 12 and 13.

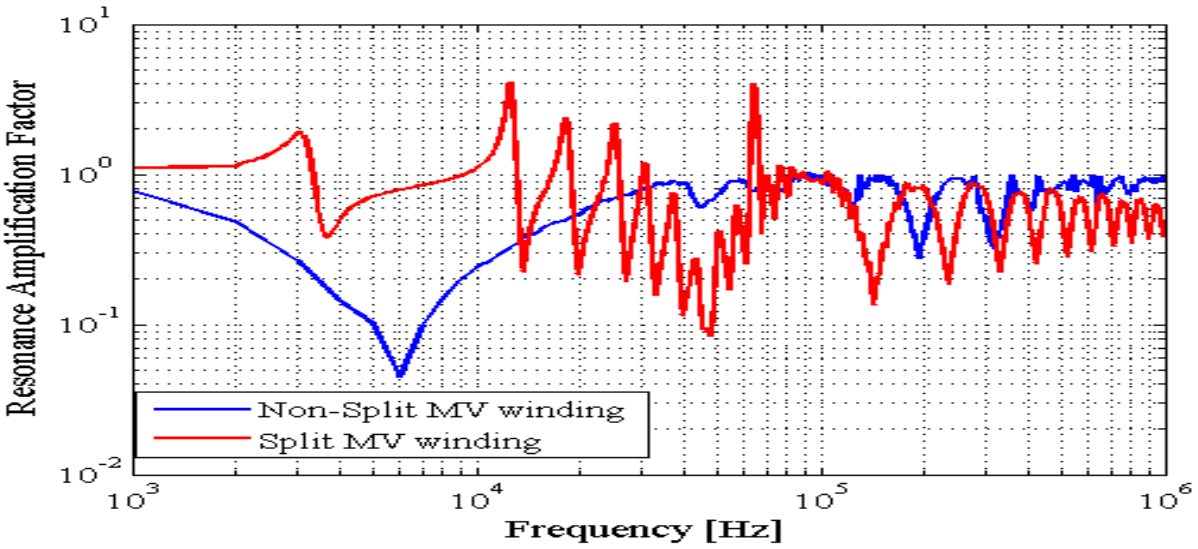

Figure 11: Frequency response for Layer 1

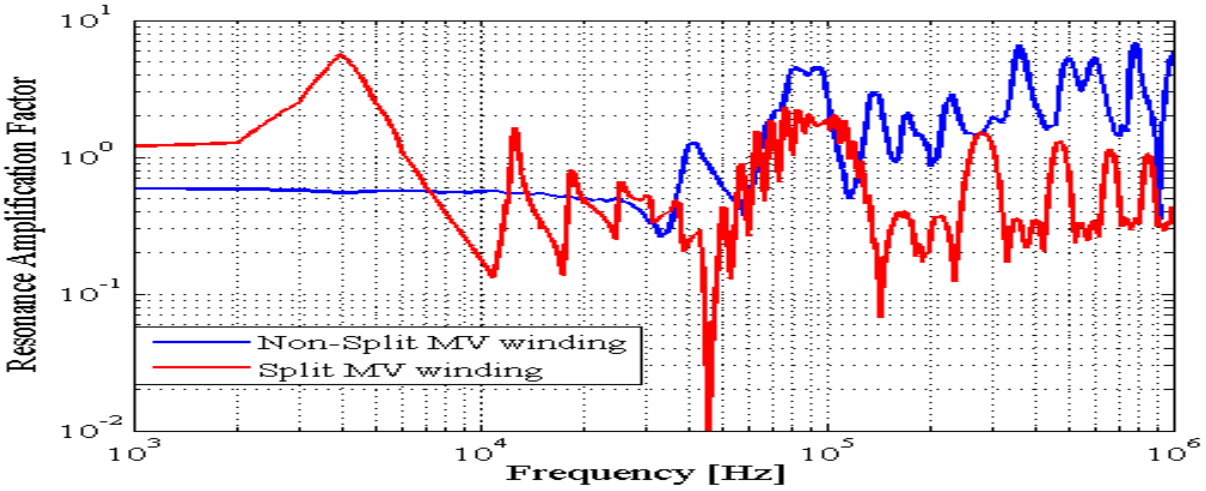

Figure 12: Frequency response for Layer 15

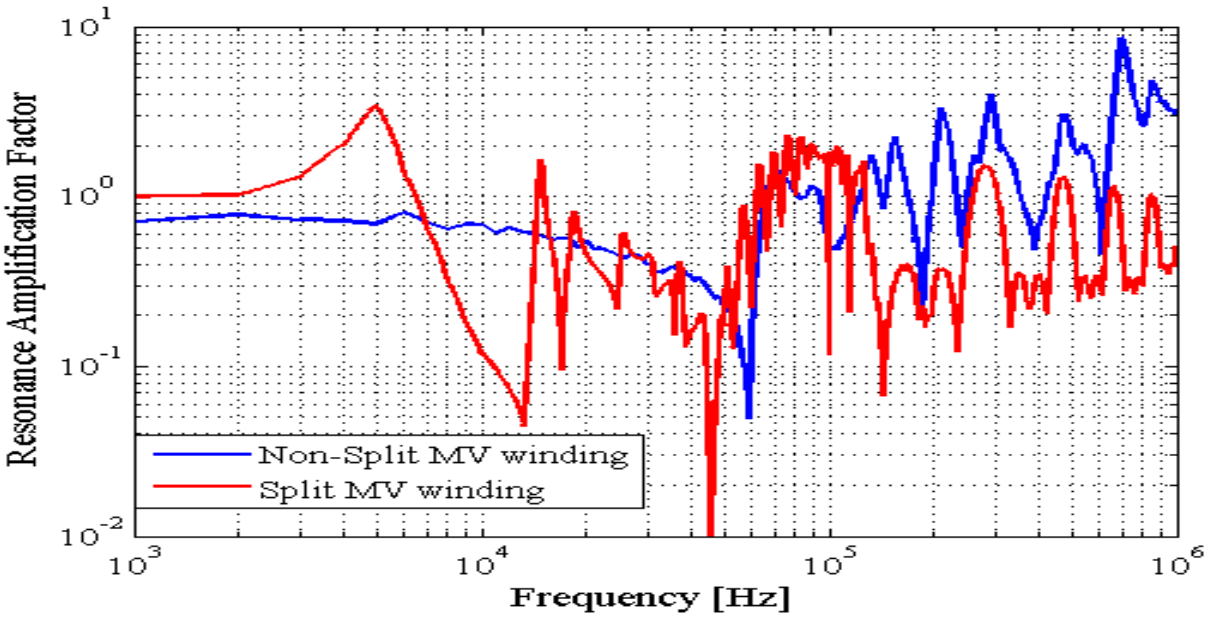

Figure 13: Frequency response of layer 16

Comparison of the sweep frequency response for the two transformer designs reveals an important result. The transformer with the split MV winding has a high resonant amplification factor below 200 kHz. In contrast, the transformer with a non-split MV winding has a high resonant amplification factor above 200 kHz. When compared to the results of FDSF, there is a high probability that internal winding resonance could occur and potentially the transformer is at risk. However as analysis of the waveforms was done in the frequency domain, several limitations of FDSF should be noted:

- FDSF does not take into account the severity along the windings to localize dielectrically the weak points as it only describes the terminal response of the transformer [6].
- In implementing FDSF a comparison of the energy involved during a transient event with the energy involved in the standard test waveforms is made but effects of damping are not taken into account. For transformers the damping ratio (R/X) increases at higher frequencies because of skin effect as well as increased stray losses [13]. Hence some damping should be expected at higher frequencies which may reduce the amplitude of the internal overvoltages.
- Although FDSF does provide insight in the different frequency components the transient signal has, it does not take into account the phase angle which may over-estimate resonant overvoltages.

The FDSF results have indicated that the existing tests waveforms contained in the standards do not completely address all the types of transient events that could occur in the field. The frequency response of the two windings has revealed that the transformer with non-split MV winding could be a better option.

4. CONCLUSION

Repetitive prestrikes with high du/dt values brought about by switching of vacuum circuit breakers threaten the insulation system of the transformer. By analysing the frequency components of the measured waveforms using FDSF, appropriate protection measures or insulation design changes can be implemented to protect the transformer.

ACKNOWLEDGEMENTS

The authors wish to acknowledge the contributions of the engineers from Actom Distribution Transformers for the design and manufacturing of the different prototype transformers and conducting measurements at the wind turbine transformer. Also the funding of the research by Eskom through the Eskom Power Plant Engineering Institute (EPPEI) program is acknowledged.

BIBLIOGRAPHY

[1] D. Smugala, W. Piasecki, M. Ostrogorska, M. Florkowski, M. Fulczyk, and O. Granhaug, “New approach to protecting transformers against high frequency transients wind turbine case study,” in PRZEGLAD ELEKTROTECHNICZNY, ISSN 0033-2097, R. 89, no. 10, pages. 186–190, Apr. 2013.

[2] T. Craenenbroek, J. D. Ceuster, J. P. Marly, H. D. Herdt, B. Brouwers, and D. V. Dommelen, “Experimental and numerical analysis of fast transient phenomena in distribution transformers,” in IEEE Power Engineering Society Winter Meeting, Singapore, vol. 3, no. 1, pp. 2193–2198, Jan. 2000.

[3] M. Popov and L. van der Sluis, “Improved calculations for no-load transformer switching surges,” in IEEE Transactions on Power Delivery, vol. 16, no. 3, pp. 401–408, Jan. 2001.

[4] W. Piasecki, M. Ostrogorska, M. Florkowski, M. Fulczyk, and P. Klys, “du/dt protection for distribution transformers,” in International Conference on Power System Transients (IPST), Kyoto, Japan, pp. 1–5, Jun. 2009.

[5] G. Simioli, "WEIDMANN: Transformers and electric grid transient interactions – The phenomena and some topics to consider in insulation design" in Transformer Life Management Conference pages 1-30, 2014.

[6] Working Group A2/C4.39 - CIGRE, “Electrical transient interaction between transformers and the power system,” in PART 1: EXPERTISE, CIGRE ISBN: 978-2-85873272-2, pages 1 –175. Apr. 2014.

[7] A, Holdyk, J. Holboell, I. Arana, A. Jensen, "Switching operation simulations in a large offshore wind farm with use of parametric variation and Frequency Domain Severity Factor" in Universities Power Engineering Conference (UPEC), 2012 47th International, pages 1-6, Sept 2012.

[8] M. Popov, L. V. der Sluis, G. C. Paap, and H. D. Herdt, “Computation of very fast transient overvoltages in transformer windings,” in IEEE Transactions on POWER DELIVERY, vol. 18, no. 4, pp. 1268–1274, Oct. 2003.

[9] L. Liljestrand, E. Lindell, D. Bormann, C. Ray, and E. Dullni, “Vacuum circuit breaker and transformer interaction in a cable system,” CIRED 22nd International Conference on Electricity Distribution Stockholm, no. 0412, pp. 1–4, Jun. 2013.

[10] X.M. Lopez-Fernandez, C. Alvarez-Marino, "Induced Transient Voltage Performance Between Transformers and VCB. Severity Factors and Case Studies" in Power Delivery, IEEE Transactions on Vol:PP ,Issue: 99 pages 1-8 Jan. 2015

[11] SANS 60076-3 “Power transformers Part 3: Insulation levels, dielectric tests and external clearances in air” 2014.

[12] SANS 60076-16: "Power transformers Part 16: Transformers for wind turbine applications, Edition 1" 2011.

[13] IEEE Std C57.142 "Guide to Describe the Occurrence and Mitigation of Switching Transients Induced by Transformers, Switching Device, and System Interaction" pages 1-46 Apr. 2010

References

[1] Gustavsen, "Wide band modeling of power transformers," *in IEEE TRANSACTIONS ON POWER DELIVERY*, vol. 19, no. 1, pp. 414–422, Jan. 2004. ix, 13, 17, 18, 19

[2] S. M. H. Hosseini, M. Vakilian, and G. B. Gharehpetian, "Comparison of transformer detailed models for fast and very fast transient studies," *in IEEE TRANSACTIONS ON POWER DELIVERY*, vol. 23, no. 2, pp. 733–741, Apr. 2008. ix, 20, 32

[3] S.D.Mitchell and J.S.Welsh, "Modelling power transformers to support the interpretation of frequency response analysis," *in IEEE Transactions on Power Delivery*, vol. 4, no. 26, pp. 2705 – 2717, Oct. 2011. ix, 25, 26

[4] *CIGRE*, "Electrical transient interaction between transformers and the power system," in *PART 1: EXPERTISE by CIGRE Joint Working Group A2/C4.39,Chapt. 6 to 7 CIGRE ISBN : 978-2-85873272-2*, Apr. 2014, pp. 81 –104. ix, 2, 7, 16, 17, 18, 19, 24, 25, 26, 63, 69, 72, 78, 79, 94

[5] H. Sun, G. Liang, X. Zhang, and X. Cui, "Analysis of resonance in transformer windings under very fast transient overvoltages," *in 17th International Zurich Symposium on Electromagnetic Compatibility*, vol. 22, no. 1, pp. 432–435, Jan. 2006. ix, x, 12, 14, 22, 28, 29, 35, 36, 37, 38, 39, 40, 41, 42, 43, 44

[6] W. Piasecki, G. Bywalec, M. Florkowski, M. Fulczyk, and J. Furgal, "New approach towards very fast transients suppression," *Presented at the International Conference on Power Systems Transients (IPST) in Lyon, France on June 4-7.* xi, 79, 81, 82, 83

[7] S. Kulkarni and S. Khaparde, "Transformer engineering design and practice," *Marcel Dekker, Library of Congress Cataloging in Publication Data, ISBN 0-8247-5653-3*, pp. 348–351, Jul. 2004. xiii, 73, 78, 79

[8] SANS, "60076-3:power transformers," *Part 3: Insulation levels, dielectric tests and external clearances in air*, pp. 1–59, Jan. 2014. xiii, 72, 78

[9] "Renewable energy independent power producer procurement programme - first window, south africa," *Engineering News Magazine*, pp. 1–9, Aug. 2013. 1

[10] W. Piasecki, G. Bywalec, M. Florkowski, M. Fulczyk, and J. Furgal, "New approach towards very fast transients suppression," *in International Conference on Power System Transients (IPST), Lyon, France*, pp. 1–6, Jun. 2007. 1

[11] T. Craenenbroek, J. D. Ceuster, J. P. Marly, H. D. Herdt, B. Brouwers, and D. V. Dommelen, "Experimental and numerical analysis of fast transient phenomena in distribution transformers," *in IEEE Power Engineering Society Winter Meeting, Singapore*, vol. 3, no. 1, pp. 2193–2198, Jan. 2000. 1, 2

[12] M. Popov and L. van der Sluis, "Improved calculations for no-load transformer switching surges," *in IEEE Transactions on Power Delivery*, vol. 16, no. 3, pp. 401–408, Jan. 2001. 1

[13] D. Smugala, W. Piasecki, M. Ostrogorska, M. Florkowski, M. Fulczyk, and O. Granhaug, "New approach to protecting transformers against high frequency transients wind turbine case study," *in PRZEGLAD ELEKTROTECHNICZNY, ISSN 0033-2097, R. 89*, no. 10, pp. 186–190, Apr. 2013. 1

[14] D. Smugala, W. Piasecki, M. Ostrogorska, M. Florkowski, M. Fulczyk, and P. Kyls, "Distribution transformers protection against high switching transients," *Przeglad Elekrotechniczny (Electrical Review)*, pp. 296 – 300, Jan. 2012. 1, 64, 65, 81

[15] Gustavsen, "Study of transformer resonant overvoltages caused by cable-transformer high-frequency interaction," *in IEEE TRANSACTIONS ON POWER DELIVERY*, vol. 25, no. 2, pp. 770–779, Apr. 2010. 2

[16] M. Popov, L. V. der Sluis, G. C. Paap, and H. D. Herdt, "Computation of very fast transient overvoltages in transformer windings," *in IEEE Transactions on POWER DELIVERY*, vol. 18, no. 4, pp. 1268–1274, Oct. 2003. 2, 12

[17] A. H. Soloot, H. K. Hoidalen, and B. Gustavsen, "Internal resonant overvoltage in wind turbine transformers- sensitivity analysis of measurement techniques," *in International Conference on Electrical Machines and Systems, Busan, Korea*, pp. 1–7, Oct. 2013. 2

[18] X. Lopez-Fernandez and C. Alvarez-Marino, "Induced transient voltage performance between transformers and vcb. severity factors and case studies," *in IEEE Transactions on Power Delivery*, vol. PP, no. 99, pp. 1–8, Jan. 2015. 2, 72, 73, 93

[19] A. da Costa Oliveira Rocha, "Electrical transient interaction between transformers and the power system: on behalf of cigre-brazil joint working group a2/c4.03 brazil," *in CIGRE 2008 Paris Session, France*, no. C4-104, pp. 1–10, Jun. 2008. 2

[20] A. Rocha, "Electrical transient interaction between transformers and the power system cigre joint working group a2/c4.39 technical brochure," *in II seminario internacional gestion de activos de transformadores, CIER 2014*, pp. 1–57, Jun. 2014. 2

[21] M. Popov, G. C. Paap, L. V. der Sluis, and H. D. Herdt, "Analysis of voltage distribution in transformer windings during circuit breaker prestrike," *in International Conference on Power Systems Transients (IPST2009) in Kyoto, Japan*, no. 8, pp. 1–6, Jun. 2009. 11, 12

[22] R. E. Pretorius, "The generation of travelling waves in cable connected motor circuits and the effect there upon of rc surge suppressor circuits," *CSIR Special Report ELEK90*. 11

[23] R. Pretorius, "Optimised surge suppression on high voltage vacuum contractor controlled motors," *IEEE 3rd International Conference on Sources and effects of Power System Disturbances, London*. 11

[24] R. E. Pretorius and A. Eriksson, "A basic guide to rc surge suppression to medium voltage motors and transformers," *SAIEE*. 11

[25] G. Liang, H. Sun, X. Zhang, and X. Cui, "Modeling of transformer windings under very fast transient overvoltages," *in IEEE TRANSACTIONS ON ELECTROMAGNETIC COMPATIBILITY*, vol. 48, no. 4, pp. 621–627, Nov. 2006. 12, 14, 22, 28, 35, 36, 38, 42, 43, 44

[26] Y. Shibuya, S. Fujita, and N. Hosokawa, "Analysis of very fast transient overvoltage in transformer winding," *in IEE Proc.-Gener. Transm. Distrib*, vol. 144, no. 5, pp. 461–468, 1997. 12, 31

[27] A. Theocharis, M. Popov, and V. Terzija, "Computation of internal voltage distribution in transformer windings by utilizing a voltage distribution factor," *in International Conference on Power Systems Transients (IPST2015) in Cavtat, Croatia*, no. 27, pp. 1–6, Jun. 2015. 12, 13

[28] M. Popov, L. van der Sluis, R. P. P. Smeets, and J. L. Roldan, "Analysis of very fast transients in layer-*type* transformer windings," *in IEEE Transactions on Power Delivery*, vol. 22, no. 1, pp. 238–245, Jan. 2007. 12, 23, 30, 34, 35

[29] M. Popov, V. Terzija, R. Smeets, J. Roldan, and L. van der Sluis, "Modelling simulation and measurement of very transients in transformer windings with consideration of frequency-dependent losses," *in IET Electr. Power Appl.*, vol. 1, no. 1, pp. 29–35, Jan. 2007. 12, 14

[30] Y. Shibuya, E. Tamaki, and S. Fujita, "Analysis of very fast transient in transformers," *in IEE Proc.-Gener. Transm. Distrib*, vol. 148, no. 5, pp. 377–383, 2001. 12

[31] M. M. Kane and S. V. Kulkarni, "Mtl-based analysis to distinguish high-frequency behavior of interleaved windings in power transformers," *in IEEE Trans. Power Delivery*, vol. 28, no. 4, pp. 2291–2299, Oct. 2013. 12

[32] R. C. Degeneff, "A general method for determining resonances in transformer windings," *in IEEE Transactions on Power Apparatus and Systems*, vol. PAS-96, no. 2, pp. 423–430, Mar. 1977. 12, 48, 51

[33] J. H. McWhirter, C. D. Fahrnkopf, and J. H. Steele, "Determination of impulse stresses within transformer windings by computer," *in AIEE Trans.*, pp. 1267–1274, 1957. 12

[34] P. I. Fergestad and T. Henriksen, "Transient oscillations in multiwinding transformers," *in IEEE Trans. Power App. Syst*, pp. 500–509, 1974. 12

[35] A. Miki, T. Hosoya, and K. Okuyama, "A calculation method for pulse voltage distribution and transferred voltage in transformer windings," *in IEEE Trans. Power App. Syst*, pp. 930–939, 1978. 12

[36] W. J. McNutt, T. J. Blalock, and R. A. Hinton, "Response of transformer windings to system transient voltages," *in IEEE Trans. Power App. Syst*, pp. 457–467, 1974. 12

[37] T. Teranishi, M. Ikeda, M. Honda, and T. Yanari, "Local voltage oscillation in interleaved transformer windings," *in IEEE Trans. Power App. Syst*, pp. 973–881, 1981. 12

[38] Y. Shibuya and S. Fujita, "High-frequency model of transformer winding," *in Elct. Eng. Japan*, pp. 8–15, 2004. 12

[39] R. P. P. Smeets, M. Popov, L. van der Sluis, H. de Herdt, and J. Declercq, "Experimental and theoretical analysis of vacuum circuit breaker prestrike effect on a transformer," *IEEE Trans. Power Delivery*, vol. 24, no. 3, pp. 1266–1274, Jul. 2009. 12

[40] R. C. Degeneff, W. J. Mcnutt, W. Neugebauer, J. Panck, J. M. E. McCallum, and C. C. Honey, "Transformer response to system switching voltages," *IEEE Trans. Power App. Syst*, vol. 101, no. 6, pp. 1457–1470, Jul. 1982. 12

[41] R. Dugan, R. Gabrick, J. Wright, and K. Pattern, "Validated techniques for modeling shell-form ehv transformers," *IEEE Trans. Power App. Syst*, vol. 4, no. 2, pp. 1070–1078, Apr. 1989. 12

[42] Y. Yang, Z. J. Wang, X. Cai, and Z. D. Wang, "Improved lumped parameter model for transformer fast transient simulations," *IET Electr. Power Appl*. 12

[43] B. Jurisic, I. Uglesic, A. Xemard, F. Paladian, and P. Guuinic, "Difficulties in high frequency transformer modelling," *in International Conference on Power Systems Transients (IPST2015) in Cavtat, Croatia*. 13, 14

[44] M. Popov, L. van der Sluis, R. P. P. Smeets, and J. L. Roldan, "Evaluation of surge-transferred overvoltages in distribution transformers," *in Electric Power Systems Research (Elsevier)*, vol. 22, no. 1, pp. 441–449, May 2007. 14, 21, 24, 30, 34, 42

[45] B. Gustavsen and A. Portillo, "A black-box approach to interfacing white-box transformer models with electromagnetic transients program," *presented at the IEEE PES General meeting, Washington, DC, USA, 2014*. 14

[46] A. Portillo and B. Gustavsen, "A black-box approach to interfacing white-box transformer models with electromagnetic transients program," *in PES General Meeting, Conference and Exposition*. 14

[47] A. Holdyk and B. Gustavsen, "External and internal overvoltages in a 100 mva transformer during high-frequency transients," *presented at International Conference on Power Systems Transients (IPST2015) in Cavtat, Croatia*. 14

[48] L. Ljung, "System identification, theory for the user, university of linkoping, sweden," *2nd ed. P T R Prentice Hall, Englewood Cliffs, New Jersey 07632*, pp. 1–255, 1999. 16

[49] P. Bosh, P. J. V. Den, and A. C. V. der Klauw, "Modeling, identification and simulation of dynamical systems," *CRC Press, Library of Congress Cataloging in Publication Data, ISBN 9780849391811*, pp. 43–59, Jul. 1994. 16

[50] O. Nelles, "Nonlinear system identification from classical approaches to neural networks and fuzzy models," *Springer, Library of Congress Cataloging in Publication Data, ISBN 978-3-642-08674-8*, p. 15, Jul. 1994. 16

[51] J. A. Martinez-Velasco, “Power system transients,” in *Parameter Determination, Chaptr 4: Transfomers, CRC Press Taylor and Francis Group, ISBN 978-1-4200-6529-9 (Hardback)*, 2010, pp. 177–255. 17, 18, 19, 20, 31

[52] B. Gustavsen, “Frequency-dependent modelling of power transformers with ungrounded windings,” *in IEEE TRANSACTIONS ON POWER DELIVERY*, vol. 19, no. 3, pp. 1328–1334, Jul. 2004. 17

[53] ——, “A hybrid measurement approach for wide-band characterization and modelling of power transformers,” *in IEEE TRANSACTIONS ON POWER DELIVERY*, vol. 25, no. 3, pp. 1932–1939, Jul. 2010. 17

[54] A. Morched, L. Marti, and J. Ottevangers, “A high frequency transformer model for the emtp,” *in IEEE TRANSACTIONS ON POWER DELIVERY*, vol. 8, no. 3, pp. 1615–1626, Jul. 1993. 17

[55] M. Manyahi and R. Thottappillil, “Transfer of lightning transients through distribution transformers,” *in Proceedings of International Conference on Lightning Protection, Cracow*, pp. 435–440, Sep. 2002. 17

[56] M. Tiberg, D. Bormann, B. Gustavsen, and C. Heitz, “Generic and automated simulation modelling based on measurements,” *in Proceedings of International Conference on Power System Transients, Lyon, France*, pp. 1–6, Jun. 2007. 17

[57] H. M. G. B. Gharehpetian and K. Moller, “Hybrid modeling of inhomogeneous transformer windings for very fast transient overvoltage studies,” *in IEEE TRANSACTIONS ON POWER DELIVERY*, vol. 13, no. 1, pp. 157–163, Jan. 1998. 21

[58] G. Liang, X. Zhu, and H. Dong, “Calculation of very fast transient in transformer windings based on transmission line theory,” *in Automation Congress, 2008. WAC 2008. World*, pp. 1 – 5, Oct. 2008. 21

[59] L. Ruan, C. Zhao, Z. Du, J. Ruan, W. Deng, and Y. Shen, “Solution for voltage distribution in transformer winding based on the model of multi-conductor transmission line,” *in International Conference on Computer and Electrical Engineering,Phuket, ICCEE 2008.*, pp. 87 – 91, Dec. 2008. 21

[60] S. N. Hettiwatte, P. A. Crossley, Z. D. Wang, A. Darwin, and G. Edwards, “Simulation of a transformer winding for partial discharge propagation studies,” *in IEEE Power Engineering Society Winter Meeting*, vol. 2, no. 1, pp. 95–101, Jun. 2002. 22, 32

[61] F. de Leon and A. Semlyen, "Reduced order model for transformer transients," *in IEEE Transactions on Power Delivery*, vol. 7, no. 1, pp. 361–369, Jan. 1992. 23, 31

[62] A. Semlyen and F. de Leon, "Efficient calculation of elementary parameters of transformer," *in IEEE Transactions on Power Delivery*, vol. 7, no. 1, pp. 376–383, Jan. 1992. 23, 31

[63] J. Guardado and K. J. Cornick, "A computer model for calculating steep-fronted surge distribution in machine windings," *in IEEE TRANSACTIONS ON Energy Conversion*, vol. 4, no. 1, pp. 95–101, Mar. 1989. 23, 34

[64] J. Bickford, N. Mullineux, and J. Reed, "Computation of power system transients," in *IEE, Peter Peregrinus Ltd., 1976, ISBN 0901223859*. 24

[65] A. Kraetge, M. Krger, and J. L. Velsquez, "Experiences with the practical application of sweep frequency response analysis (sfra) on power transformers," *Proceedings of the 16th International Symposium on High Voltage Engineering*. 25

[66] R. A. Rohrer, "Circuit theory: An introduction to the state variable approach," in *New York: McGraw-Hill, 1970*. 26

[67] H. K. Hoidalen, B. Gustavsen, and A. H. Soloot, "Modeling of wind turbine transformers for the analysis of resonant overvoltages," *in International Conference on Power Systems Transients IPST2013 in Vancouver, Canada*, pp. 1–7, Jul. 2013. 31, 32, 34, 43, 58

[68] F. Kubler, "Cellulose based insulation materials for oil immersed transformers," *pp. 1-29. [Online] Availabe: www.highvolt.de/XparoDownload.ashx?raid=52997*. 33

[69] KREMPEL, "Technical data $krempel - dpp$," p. 11/96, Aug. 2012. 33

[70] PUCARO, "Pucaro transformer presspaper," *DDP, Type 4.1, Technical Data*, pp. 1–3. 33

[71] C. Paul, "Analysis of multi-conductor transmission lines," *NewYork: Wiley, 1994*. 33

[72] G. Lupo, C. Petrarca, M. Vitelli, and V. Tucci, "Multiconductor transmission line analysis of steep-front surge in machine windings," *IEEE transactions on Dielectrics and Electrical Insulation*, vol. 9, no. 3, pp. 467–478, Jun. 2002. 33

[73] IEEE, "Guide to describe the occurrence and mitigation of switching transients induced by transformers, switching device, and system interaction," *IEEE Std C57.142*, pp. 8–58, Dec. 2010. 48, 80, 81

[74] A. H. Soloot, H. K. Hoidalen, and B. Gustavsen, "Upon the improvement of the winding design of wind turbine transformers for safer performance within resonance overvoltages," *in proc. of CIGRE Joint Colloquium - SC A2/C4*, pp. 1–7, 2013. 58

[75] L. Liljestrand, E. Lindell, D. Bormann, C. Ray, and E. Dullni, "Vacuum circuit breaker and transformer interaction in a cable system," *CIRED 22nd International Conference on Electricity Distribution Stockholm*, no. 0412, pp. 1–4, Jun. 2013. 64

[76] A. Mueller and D. Saemann, "Switching phenomena in medium voltage systems - good engineering practise on the application of vacuum circuit breakers and contractors," pp. 1–9, Mar. 2011. 69

[77] R. Malewski, J. Douville, and L. Lavallee, "Measurement of switching transients in 735-kv substations and assessment of their severity for transformer insulation," *in IEEE Transactions on Power Delivery*, vol. 3, no. 4, pp. 1380 – 1390, Oct. 1988. 69

[78] D. Tschudi, C. Krause, H. Kirch, M. Franchek, and R. Malewski, "Strength of transformer paper-oil insulation expressed by the weidmann oil curves," *CIGRE WG 33.03*. 79

[79] J. Nelson, "An assessment of the physical basis for the application of design criteria for dielectric structures," *in IEEE Transactions on Electrical Insulation*. 79

[80] A. Lokhanin, T. Morozova, I. Voevodin, Z. Beletsky, G. Kuchinsky, and D. Kaplan, "Problems of coordination of dielectric strength of extra high-voltage power transformer major insulation," *CIGRE*. 79

[81] W. Piasecki, M. Ostrogorska, M. Florkowski, M. Fulczyk, and P. Klys, "du/dt protection for distribution transformers," *Presented at the International Conference on Power Systems Transients (IPST) in Kyoto, Japan on June 3-6*. 90

[82] P. H. Mukti, F. A. Pamuji, and B. S. Munir, "Implementation of artificial neural networks for determining power transfomer condition," *Presented at the 5th International Symposium on Advanced Control of Industrial Processes (ADCONIP 2014), Hiroshima*. 95

[83] E. Husain, M. M. Mohsin, and Satyaprakash, "Transformer insulation condition monitoring using artificial neural network," *2001 IEEE 7th International Conference on Solid Dielectrics, June 25-29,2001, Eindhoven, the Netherlands*. 95